



International Conference on Multi-Disciplinary Research
Studies and Education
(ICMDRSE-19)

Hyderabad, Telangana
28th - 29th June 2019

Institute For Engineering Research and Publication (IFERP)

www.iferp.in

Publisher: IFERP Explore

©Copyright 2019, IFERP-International Conference, Hyderabad, Telangana

No part of this book can be reproduced in any form or by any means without prior written
Permission of the publisher.

This edition can be exported from India only by publisher

IFERP-Explore

PREFACE

We cordially invite you to attend the ***International Conference on Multi-Disciplinary Research Studies and Education (ICMDRSE-19)*** which will be held at ***Hotel Quality Inn Residency, Hyderabad, Telangana*** on ***June 28th -29th, 2019***. The main objective of ***ICMDRSE-19*** is to provide a platform for researchers, engineers, academicians as well as industrial professionals from all over the world to present their research results and development activities in relevant fields of Multi-Disciplinary Research Studies and Education. This conference will provide opportunities for the delegates to exchange new ideas and experience face to face, to establish business or research relationship and to find global partners for future collaboration.

These proceedings collect the up-to-date, comprehensive and worldwide state-of-art knowledge on cutting edge development of academia as well as industries. All accepted papers were subjected to strict peer-reviewing by a panel of expert referees. The papers have been selected for these proceedings because of their quality and the relevance to the conference. We hope these proceedings will not only provide the readers a broad overview of the latest research results but also will provide the readers a valuable summary and reference in these fields.

The conference is supported by many universities, research institutes and colleges. Many professors played an important role in the successful holding of the conference, so we would like to take this opportunity to express our sincere gratitude and highest respects to them. They have worked very hard in reviewing papers and making valuable suggestions for the authors to improve their work. We also would like to express our gratitude to the external reviewers, for providing extra help in the review process, and to the authors for contributing their research result to the conference.

Since April 2019, the Organizing Committees have received more than 62 manuscript papers, and the papers cover all the aspects in Multi-Disciplinary Research Studies and Education. Finally, after review, about 21 papers were included to the proceedings of ***ICMDRSE-19***

We would like to extend our appreciation to all participants in the conference for their great contribution to the success of ***ICMDRSE-19*** We would like to thank the keynote and individual speakers and all participating authors for their hard work and time. We also sincerely appreciate the work by the technical program committee and all reviewers, whose contributions made this conference possible. We would like to extend our thanks to all the referees for their constructive comments on all papers; especially, we would like to thank to organizing committee for their hard work.

Acknowledgement

IFERP is hosting the ***International Conference on Multi-Disciplinary Research Studies and Education (ICMDRSE-19)*** this year in month of June. The main objective of ICMDRSE is to grant the amazing opportunity to learn about groundbreaking developments in modern industry, talk through difficult workplace scenarios with peers who experience the same pain points, and experience enormous growth and development as a professional. There will be no shortage of continuous networking opportunities and informational sessions. The sessions serve as an excellent opportunity to soak up information from widely respected experts. Connecting with fellow professionals and sharing the success stories of your firm is an excellent way to build relations and become known as a thought leader.

I express my hearty gratitude to all my Colleagues, staffs, Professors, reviewers and members of organizing committee for their hearty and dedicated support to make this conference successful. I am also thankful to all our delegates for their pain staking effort to travel such a long distance to attain this conference.



Ankit Rath
Chief Scientific Officer
Institute for Engineering Research and Publication (IFERP)



044-42918383



Email: info@iferp.in
www.iferp.in



Girija Towers, Arumbakkam, Chennai - 600106

Keynote Speaker



Dr. Sangeeta Ahuja

Senior Scientist
IASRI (CAR),
Ministry of Agriculture and Farmers Welfare,
Govt of India,
New Delhi

I am delighted to be a part of “International Conference on Multi-Disciplinary Research Studies and Education(ICMDRSE-19)” and to interact with enthusiastic scientists and technologists gathering at Hyderabad, India from June 28th-29th, 2019.

The present-day world is the result of pursuits for novel scientific and technical innovations by the intellectual scientific societies. Burgeoning research has resulted in remarkably enhanced and comfortable human life. However, the urbanization, industrial developments and other anthropogenic activities have resulted in the environmental catastrophe. In spite of breakthrough inventions in engineering and technology, we are facing numerous challenges like climate change, global warming, carbon emission, rising sea level and the environmental deterioration.

New scientific ideas and innovative technology can only help us to cope up with such challenges. The need of hour is that, the contemporary scientist and technologists should find solutions to these problems by continuous progressive efforts, dedication and determination. The interdisciplinary approach combining engineering sciences, basic sciences and social sciences seems to be much effective to address these problems by integrating different novel ideas and technologies.

Further, for the success of new findings and novel technologies, the concerted efforts and trials are needed at global level. This conference is an appropriate platform that can provide an arena to achieve such feats by giving the chance to scientist and technologists to interact, plan and to move together even working at different places.

I hope researchers from different fields will learn from each other and discuss their issues well. I express heartily thanks to organizing committee and wish for the great successful, fruitful and joyous ICMDRSE-19.



Dr. Chitra Kiran.N

Professor & Head Dept of ECE

Alliance College of Engineering & Design

Alliance University, Anekal, Bangalore

I congratulate IFERP for its sustained work towards multidisciplinary Engineering Research and Publication. IFERP is playing a magnificent role by conducting Conferences, Workshops, Seminars across the globe in association with other esteemed organizations.

I congratulate all the authors , members of the program committee , the external referees, Reviewers, organizers, members of editorial board with their valuable opinion and expertise, ensured a very high quality program. I wish that the proceedings will serve as a useful reference for research. I wish this International conference on Multi-Disciplinary Research Studies and Education (ICMDRSE) to be held on 28th - 29th June 2019, Hyderabad would be a remarkable bench mark event across the globe. Wishing you a great success.

ICMDRSE-19

International Conference on Multi-Disciplinary Research Studies and Education

Hyderabad, Telangana, June 28th - 29th, 2019

Organizing Committee

DR. A. MALLIKARJUNA REDDY

Assoc. Professor
Department of CSE, Anurag Group of Institutions (AGI)
Venkatapur, Telangana

DR.V.VENKATESWARA REDDY

Vice Principal and Professor
Department of Civil Engineering
JNTUH College of Engineering,
Sultanpur

DR. ANAND KISHORE KOLA

Professor & Former HoD
Department of Chemical Engineering
National Institute of Technology,
Warangal

DR. P. NARAHARI SASTRY

Professor
Department of ECE, Chaitanya Bharathi Institute of Technology
Gandipet, Hyderabad

DR. Y RAMA DEVI

Professor
Department of CSE, Chaitanya Bharathi Institute of Technology,
Gandipet, Hyderabad

DR. N. V. SRINIVASULU

Professor
Department of Civil Engineering
Chaitanya Bharathi Institute of Technology,
Gandipet, Hyderabad

DR.K.KRISHNAVENI

Professor
Department of EEE
Chaitanya Bharathi Institute of Technology
Gandipet, Hyderabad

DR. RAMACHANDRA C. G

Professor
Department of Mechanical Engineering
School of Engineering, Presidency University
Bengaluru

DR. G. CHANDRA MOHAN REDDY

Professor
Department of Mechanical Engineering
Chaitanya Bharathi Institute of Technology
Gandipet, Hyderabad

DR.B.SURESH KUMAR

Associate Professor
Department of EEE
Chaitanya Bharathi Institute of Technology
Gandipet, Hyderabad

S.SUNDARA MAHALINGAM

Assistant Professor
Department of EEE
Mepco Schlenk Engineering College
Sivakasi

SRI KALYANA RAMA J

Assistant Professor
Department of Civil Engineering
BITS Pilani
Hyderabad

DR.-ING. PAVAN KUMAR P

Assistant Professor
Department of Mechanical Engineering
Birla Institute of Technology & Science,
Telangana, Hyderabad

PILLA RAVI KISHORE

Assistant Professor & HOD
Civil Engineering
Aditya Engineering College, Surampalem,
Andhra Pradesh

ADARI SATISH KUMAR

Assistant Professor
Civil Engineering
Aditya Engineering College, Surampalem,
Andhra Pradesh

CONTENTS

SL.NO	TITLES AND AUTHORS	PAGE NO
1.	Expert System for Patchouli Species ➤ <i>Dr. Sangeeta Ahuja</i>	1 - 5
2.	A Model for Estimation of Capacity and Critical Gap at Unsignalized Intersections in Hyderabad city ➤ <i>M.Satya Deepthi</i> ➤ <i>A. Ramesh</i>	6 - 12
3.	Design and Verification of Serial Peripheral Interface Protocol using QuestaSim ➤ <i>P. Naga Gayathri</i> ➤ <i>Sri. K. Naga Koushil Reddy</i>	13 - 17
4.	Design and Verification of Advanced High-Performance Bus Lite Protocol using QuestaSim ➤ <i>B. Chinna Munaiah</i> ➤ <i>Dr. S.M. Shamsheer Daula</i>	18 - 23
5.	Performance Evaluation of Pox Controller for Software Defined Networks ➤ <i>Elfreda Albert</i> ➤ <i>Adarsh V Srinivasan</i> ➤ <i>Mr. N. Saritakumar</i> ➤ <i>Dr. S. Subha Rani</i>	24 - 31
6.	An Experimental Investigation on Mechanical Properties of Mixed Synthetic Fiber Reinforced Concrete ➤ <i>G.Gopala Krishna</i> ➤ <i>A.S. Swetha Sri</i> ➤ <i>P. Ravi Kishore</i>	32 - 36
7.	Experimental Study of Geopolymer Concrete by Addition of Nano-Silica and Steel Fiber ➤ <i>Nitesh Kumar Yadav</i> ➤ <i>A. Satish Kumar</i> ➤ <i>P. Ravi Kishore</i>	37 - 41
8.	Comparative Study of the Strength Properties of the Concrete with Partial Replacement of the Coarse Aggregate with Pumice and Over Burnt Bricks ➤ <i>S.Anka Rao</i> ➤ <i>A. Satish Kumar</i> ➤ <i>P. Ravi Kishore</i>	42 - 47
9.	Influence of Sisal Fibers on the Properties of Rammed Earth ➤ <i>P. Vinay Kumar</i> ➤ <i>M.Eswar Kumar Yadav</i>	48 - 53

CONTENTS

SL.NO	TITLES AND AUTHORS	PAGE NO
10.	Performance Analysis of Spectrum Sensing Techniques <ul style="list-style-type: none"> ➤ <i>Anitha Bujunuru</i> ➤ <i>Prof.Srinivasulu Tadisetty</i> 	54 - 58
11.	Accelerated PVT analysis of UCM architecture using Cadence ADE-XL <ul style="list-style-type: none"> ➤ <i>Rajkumar Sarma</i> ➤ <i>Cherry Bhargava</i> ➤ <i>Shruti Jain</i> 	59 - 65
12.	Text Detection and Recognition for Calorie-conscious Life style <ul style="list-style-type: none"> ➤ <i>Mr Aran Nash</i> ➤ <i>Ms Swathika R</i> ➤ <i>Ms N Radha</i> 	66 - 71
13.	Investigation of temperature dependent DC conductivity and frequency dependent dielectric property of polysiloxane - TiO ₂ nanocomposites <ul style="list-style-type: none"> ➤ <i>Md Nasir Ali</i> ➤ <i>Dr S Chakradhar Goud</i> 	72 - 78
14.	Multi – Level Wavelet and Curvelet based Video Watermarking for Copyright Protection <ul style="list-style-type: none"> ➤ <i>M. Selvaganapathy</i> ➤ <i>Dr. R. Kayalvizhi</i> 	79 - 86
15.	An Intelligent Model for Residual life Prediction of Thyristor <ul style="list-style-type: none"> ➤ <i>Cherry Bhargava</i> ➤ <i>Jagdeep Singh</i> ➤ <i>Pardeep Kumar Sharma</i> 	87 - 91
16.	Experimental Study on Performance and Emission Characteristics of Country Borage Methyl Ester - Diesel Blend In a Compression Ignition Engine <ul style="list-style-type: none"> ➤ <i>Anbarasan B</i> ➤ <i>Venkatesh J</i> ➤ <i>Jamunarani M</i> 	92 - 97
17.	Investigation of frequency dependent dielectric property of polysiloxane – TiO ₂ nanocomposites <ul style="list-style-type: none"> ➤ <i>Md Nasir Ali</i> ➤ <i>Mir Safiulla</i> 	98 - 103
18.	Electronic Toll Collection System Using RF Transceiver and IoT <ul style="list-style-type: none"> ➤ <i>Dr. Chitra kiran N</i> ➤ <i>Abhilash reddy S</i> ➤ <i>Diliipgowda B.M</i> ➤ <i>Bhargav saiTeja GS</i> ➤ <i>Meghana.A</i> 	104 - 105

CONTENTS

SL.NO

TITLES AND AUTHORS

PAGE NO

19.	Wang Landau - Adaptive Monte Carlo Approach to Monomodal Brain Image Registration ➤ <i>D.Sasikala</i> ➤ <i>K.Venkatesh Sharma</i>	106 - 114
20.	ICT Impact in Modern Education ➤ <i>Vijaya Kumar A V</i> ➤ <i>Dr. Yogesh Kumar Sharma</i>	115
21.	The impact of employee agility on the marketing team performance of pharmaceutical firms, India: A qualitative study ➤ <i>Venkateswarlu Nalluri</i>	116

Expert System for Patchouli Species

^[1]Dr. Sangeeta Ahuja

^[1]Scientist (S.S.)IASRI (CAR), New Delhi-12, INDIA

^[1]reach2san@yahoo.com

Abstract:-- Patchouli (*Pogostemon cablin*) is normally propagated vegetative through stem cuttings. Number of factors such as climate, type of cuttings, rooting media, etc. governs the growth and survival of the saplings. Striking effects of different cutting lengths and cutting diameters on growth and survival were observed under Mist Chamber and Agronet shade conditions. The present study was conducted to come out with recommendations regarding appropriate ranges of cutting lengths and cutting diameters for optimum growth and survival of Patchouli in nursery stage. Through the efficient statistical computer algorithm RCDA by varying the different diameters and lengths, results are computed, tested and verified with the maximum survival and growth. The RCDA algorithm helped in processing of datasets into performance groups to better understand the effects of different diameters, lengths of cuttings on survival and growth of patchouli plant.

Index Terms: Precision Agriculture, Optimality, Irrigation, CV, RSquare, Efficiency etc.

1. INTRODUCTION

Patchouli (*Pogostemon cablin* (Blanco) Benth. syn *P. patchouli* Pellet var. *suavis* Hook.f.) belonging to the family Lamiaceae is an erect, well-branched, pubescent small aromatic bushy herb attaining a height of about 0.5-1.2 m remaining in the field for about 3-4 years giving 3 or even more harvests of leaves annually. Its fragrant leaves containing very sweet smelling oil is of immense commercial importance. Patchouli is native to Philippine Islands and grown in a number of South East Asian Countries as commercial crop. Attributed with a number of cosmetic and medicinal properties, the plant is also used as insect repellent and as main ingredient in modern Aromatherapy. In view of the versatile commercial potential of Patchouli in Indian northeast region, there is need to optimize its production by extending the areas under cultivation as well as to increase the productivity by extensive research efforts. Out of the several ways to increase the productivity, standardization of site-specific nursery techniques is also considered most important. Keeping the fact in view, experimental trials on optimization of cutting size (in respect of length and diameter) of Patchouli were laid out to study the effect on its growth and survival in nursery stage.

With a view to promote the large-scale cultivation of Patchouli, attempt has been made by various workers, to develop agropractices and agroforestry models under site specific conditions [2,3]. Cultivation trails had been undertaken by various workers under varying condition [4,5]. Possibility of growing this plant as an intercrop with some species viz., coconut, papaya, oilplam, rubber, *Pinus* sp etc. has also been explored [6]. According to [9] normally stem cuttings are used as propagating material.

Three noded cuttings had maximum rootability than two node cuttings in all types of cuttings. In the present study, appropriate ranges of cutting lengths and cutting diameters for optimum growth and survival of Patchouli in nursery stage have been suggested.

II MATERIALS AND METHODS

Modules (Computer Programs) have been developed for the expert system. The technology is the Visual C# with .NET have been used. This platform and technology[10-12] is suitable for software development. It utilizes various key features of object oriented technologies such as its ability to programme in an event driven operating system with great ease, write code for events automatically, optimize code capability for native platform, etc. The basic reason behind selection of this technology was its superior abilities for code reusability, inheritability, encapsulation, portability and modular development. The concept of various scripting languages have been used and this expert system is very easy to use and beneficial for everyone who is directly or indirectly related to this field.

The material of the patchouli species has been taken from the real experiment data under mist chamber condition and under Agronet shade condition.

Standard methods for vegetative propagation were adopted under mist chamber condition and under Agronet shade condition. Experiment was laid out in randomized block design (RBD). Each treatment was replicated four times and planted in root trainers under Mist Chamber and Agronet shade conditions (75:25). The mist was run for 10 seconds after every 30 minutes. The root trainers bearing the cuttings were taken out after 20 days from the Mist Chamber to shade condition and

data were recorded on two parameters i.e. survival percentage and height increment. All the computations have been done with the help of Expert System. The advanced computer algorithms with statistical techniques with innovative methodologies have been utilized through Expert System. The best decision is also suggested by the expert system in order to increase the survival percentage of patchouli by keeping all the parameters into consideration.

III EXPERIMENTAL ANALYSIS

The real data of the experiment have been used and through the expert system the result have been analyzed and interpreted. The home page of the expert system is as shown in fig. 1.



Fig. 1 Expert System for Patchouli Species

Rigorous experimentation through the algorithms embedded by varying the diameter, length and height with different sets of treatments with various conditions and situations and after implementation of statistical significant testing(Johnson andWichern,1979) and verified with the all quality measures with the survival (%) has been computed as shown in Tables.

Representations

Cutting diameters - D1 - 2mm, D2 – 4mm, D3 – 6mm
Cutting lengths-L1 – 5cm, L2 – 7.5 cm, L3 – 10cm, L4 – 12.5 cm

The two conditions : Agronet Shade Conditions (T1), Mist Chamber Conditions (T2), Survival-WL (%) Survival With Leaves, Survival-WoL (%) Survival Without Leaves

Condition	Different Diameters	No. of plants survived	Survival %
Agronet T1	D1	54	75.000

Shade (T1)	T1	D2	48	66.667
	T1	D3	54	75.000
Mist Chamber (T2)	T2	D1	66	91.667
	T2	D2	60	83.333
	T2	D3	54	75.000

Table 1 : Effect of different diameters of leafy cuttings on Survival

Condition	Different Diameters	No. of Plants Survived	Survival %	
Agronet Shade (T1)	T1	D1	56	77.778
	T1	D2	53	73.611
	T1	D3	66	91.667
Mist Chamber (T2)	T2	D1	56	77.778
	T2	D2	60	83.333
	T2	D3	53	73.611

Table 2: Effect of different diameters of leafless cuttings on Survival

Result through Expert System

Performance Group 1

Treatment Cluster	Treatment	Survival-WL (%)
T2	D1	91.667
T2	D2	83.333

Performance Group 2

Treatment Cluster	Treatment	Survival-WL (%)
T1	D1	75
T1	D3	75
T1	D3	75

Performance Group 2

Treatment Cluster	Treatment	Survival-WL (%)
T1	D2	66.667

Table Result 1: Effect of different diameters of leafy cuttings on Survival

Performance Group 1

Treatment Cluster	Treatment	Survival WoL (%)
T1	D3	91.667

Performance Group 2

Treatment Cluster	Treatment	Survival WoL (%)
T1	D1	77.778
T2	D1	77.778
T2	D2	83.333

Performance Group 3

Treatment Cluster	Treatment	Survival WoL (%)
T1	D1	73.611
T2	D1	73.611

Table Result 2: Effect of different diameters of leafless cuttings on Survival

Conditions		Different Lengths	No. Of Plants Survived	Survival %
Agronet Shade (T1)	T1	L1	61	84.722
	T1	L2	66	91.667
	T1	L3	55	76.389
	T1	L4	58	80.556

Mist Chamber (T2)	T2	L1	72	100.000
	T2	L2	72	100.000
	T2	L3	67	93.056
	T2	L4	61	84.722

Table 3: Effect of different lengths of leafy cuttings on Survival

Condition		Different Lengths	No. of plants Survived	Survival %
Agronet Shade (T1)	T1	L1	44	61.111
	T1	L2	60	83.333
	T1	L3	48	66.667
	T1	L4	48	66.667
Mist Chamber (T2)	T2	L1	54	75.000
	T2	L2	53	73.611
	T2	L3	60	83.333
	T2	L4	66	91.667

Table 4: Effect of different lengths of leafless cuttings on Survival

Results through RCDA Algorithm

Performance Group 1

Treatment Cluster	Treatment	Survival-WL (%)
T1	L2	91.667
T2	L1	100
T2	L2	100
T2	L3	93.056

Performance Group 2

Treatment Cluster	Treatment	Survival-WL (%)
T1	L1	84.722

T2	L4	84.722
----	----	--------

Performance Group 3

Treatment Cluster	Treatment	Survival-WL (%)
T1	L3	76.389
T1	L4	80.556

Table 3 Result: Effect of different lengths of leafy cuttings on Survival

Performance Group 1

Treatment Cluster	Treatment	Survival-WoL (%)
T1	L2	83.333
T2	L3	83.333
T2	L4	91.667

Performance Group 2

Treatment Cluster	Treatment	Survival-WoL (%)
T2	L1	75
T2	L2	73.611

Performance Group 3

Treatment Cluster	Treatment	Survival-WoL (%)
T1	L1	61.111
T1	L3	66.667
T1	L4	66.667

Table 4 Result: Effect of different lengths of leafless cuttings on Survival

Interpretation

The data on survival percentage and height increment of Patchouli cuttings of different diameter and length under

Mist Chamber conditions and Agronet shade conditions have been taken in the above data set.

Effect of different cutting diameters on survival percent (Table 1 and 2), recorded maximum survival in leafy cuttings of 2 mm diameter (100%) followed by 4 mm diameter (91.66) under Mist Chamber conditions whereas leafless cuttings of 4 mm diameter shown survival of 83.33 per cent as compared to other cuttings of different diameters. Under Agronet shade conditions survival of leafy cuttings of 2 mm and 4 mm diameter (75% each) were obtained whereas leafless cuttings shown maximum survival of 91.66 per cent in 6 mm diameter. Effect of different cutting diameters on height increment shown in Table 3 and 4. Under Mist Chamber conditions, leafy cuttings of 2 mm diameter shown the increment of 13.3 cm in height followed by increment of 6.36 cm and 5.67 cm from leafy cuttings of 6 mm and 4 mm diameter respectively. Leafless cuttings of 4 mm diameter shown increment of 3.04 cm whereas 2 mm and 6 mm leafless cuttings shown increment of - 0.75 cm and - 1.47 cm respectively. Under Agronet shade conditions only leafy cuttings of 2 mm diameter shown positive increment of 2.62 cm followed by 4 mm and 6 mm diameter cuttings shown - 0.02 cm and - 0.92 cm respectively. Whereas, leafless cuttings of 6 mm diameter put 0.28 cm increment but others showed negative increment.

CONCLUSION

The growing interest in fragrance has led to patchouli’s widespread cultivation throughout tropical Asia. The advantage in growing this plant for the Fragrance industry is that the potential is enormous and almost unlimited, the returns are satisfactory, and more interestingly, it can be grown as a second crop, in partial shade, under Coconut, or Areca Nut, with very little additional costs. Expert System gives the maximum survival percent by keeping all the other parameters to the optimum.

REFERENCES

1. Jiawei Han and Micheline Kamber ,” Data Mining : Concepts and Techniques” Second Edition, Morgan Kaufmann Publishers, San Diego, USA, 2006.
2. Dhuria, S.S. and Tiwari, S.K., “Vegetative propagation of Patchouli (Pogostemon cablin) in mist condition”, Vaniki Sandesh, 17(1) : 8-10,1993.
3. Goennadi, D.H. and Sundharama, I.M., “Shoot initiation by humic acids of selected tropical crops grown in tissue culture”, Plant Cell Reports, 15 : 1-2,1995.

4. Anon, "The Wealth of India- Raw Materials" VolVIII (Ph-Re) 177-183 pp, 1989.
5. Rusli, S. and Wahid, P., "Prospect of the essential oils development in Indonesia", *Industrial Crops Research Journal*, 2(2) : 24-29,1990.
6. Sarawak, "Minor Crops, Annual Report for 1973 &1975", Department of Agriculture, Research Branch, 252 pp,1975.
7. Vishwanathan, Radhakrishnan, Reghunath, Sosamma-Cherian and Cherian, S., "Patchouli (*Pogostemon cablin*) as an intercrop in young coconut (*Cocos nucifera*) garden", *Ind. J. Agric. Sci.*, 62(9): 616-617 pp,1992.
8. Ram, M, Ram, D., Singh, S., Naqui, A.A. and Kumar, S., "Studies on intercropping of patchouli with papaya (*Carica papaya*)", *J. of Med. & Arom.Pl. Sci.*, 21(2) : 358-360,1999.
9. Anup Kumar, Gauniyal, A.K. and Virmani, "O.P., "Cultivation of *Pogostemon patchouli* for its oil". *Cromap*, 8(2); 79-83 pp, 1986.
10. Richard A. Johnson and Dean W. Wichern, "Applied Multivariate Statistical Analysis", Prentice Hall, Upper Saddle River, New Jersey, 1979.
11. Ahuja, S, et al., SPFE 1.0 Software, 2005.
12. SAS Software., 2015.

A Model for Estimation of Capacity and Critical Gap at Unsignalized Intersections in Hyderabad city

^[1]M.Satya Deepthi, ^[2]A. Ramesh

^[1]Post Graduate student, ^[2]Professor

^{[1][2]}Department of Civil Engineering, VNR Vignana Jyothi Institute of Engineering and Technology, Hyderabad.

^[1]satyadeepthi21@gmail.com, ^[2]ramesh_a@vnrvjiet.in

Abstract:-- Traffic congestion on urban road network is a result of increase in vehicular traffic as it is characterized by slow speed, longer trip lengths, and longer delays. Unsignalized intersections are provided for to low volume traffic flow and its performance is used to evaluate urban road networks .Delay is considered as the important parameter and evaluation of unsignalised intersections is achieved through Gap acceptance behavior. Gap acceptance behavior is an important parameter for determination of capacity at unsignalized intersection.

This article explicitly presents the overview of estimation of capacity of unsignalised intersection using Indo HCM 2017 for better identification of traffic characteristics. Estimation of critical gap, occupation time and delay are some of the major factors considered for the analysis. Data is collected through video graphic techniques at 2 locations in Hyderabad city. Traffic Parameters like volume, approaching vehicle type, accepted and rejected gaps were extracted. The study has also examined the variables associated with occupancy factor, vehicle type and socio demographic features. It is observed that the capacity of pragathi nagar T intersection is 845vehicles /hour and critical gap is 4.29 seconds and the capacity of bahadurpally (4 legged) Intersection is 647 vehicles / hour and critical gap is 4.02 seconds.

Index Terms Critical gap, stratified sampling technique, conventional methods, and occupancy factor..

1. INTRODUCTION

Traffic congestion is a condition on road networks occurs as use increases, and is characterized by slower speeds, longer trip times, and increased vehicular queuing. U.S.A, alone bears a congestion cost of \$ 305 billion every year. In India just in 4 metropolitan cities the congestion cost is \$ 22 billion every year. India is a developing country and cities have has rapid urbanization and modernization as result there is an immense growth in road traffic following heterogeneous traffic causing delay and congestion to road users . This leads to longer trip lengths, slower speeds of vehicles, increased vehicle queuing and vehicle operation cost. (pande, 2012) Generally in semi urban and urban scenarios unsignalised intersections are primary locations where a conflict occur. Diesel and petrol consumption in city is nearly 2.4 Mega liters/day and 1.7 Mega liters/day respectively. The average time spend by any driver in traffic jam is 102 hours /year. Approximately there are 1.3 million deaths and 20-50 million fatalities takes place in a year globally. Unsignalised intersection are implemented to regulate low volume traffic flow. Based on relative importance of two roads, they are generally designated as major and minor roads.

Capacity of an intersection affects the total capacity of road network due to traffic movements like merging, diverging and conflicting. An intersection is considered as node in a traffic network of urban roads. (prasad, 2014).In mixed traffic conditions roads carry different modes of vehicles like Heavy commercial vehicles HCV, low commercial vehicles LCV, cars, 2 wheelers, 3 wheelers, animal driven carts and cycles leading to complex behavior of interaction between the vehicles. There are several techniques for estimation of capacity of unsignalised intersections. conflict model or modified tanners model which is based on critical gap and follow up times of vehicles from minor road traffic has mathematical relation of interaction and impact between flows at intersection Vehicular interactions are complex at unsignalised intersections, a driver must find a safe moment for moving into intersection area. Drivers intending to enter an unsignalised intersections have a series of gaps between vehicles in a stream, where they cross or merge.

Conflicts in traffic are created when two or more roads cross and they results in delay and congestion. The capacity at an unsignalised intersection is important for evaluation of road network capacity (Mourya, 2016).Gap acceptance is an essential skill for safe driving and determines the delay and capacity at an unsignalised intersection. Gap acceptance behavior explains the road

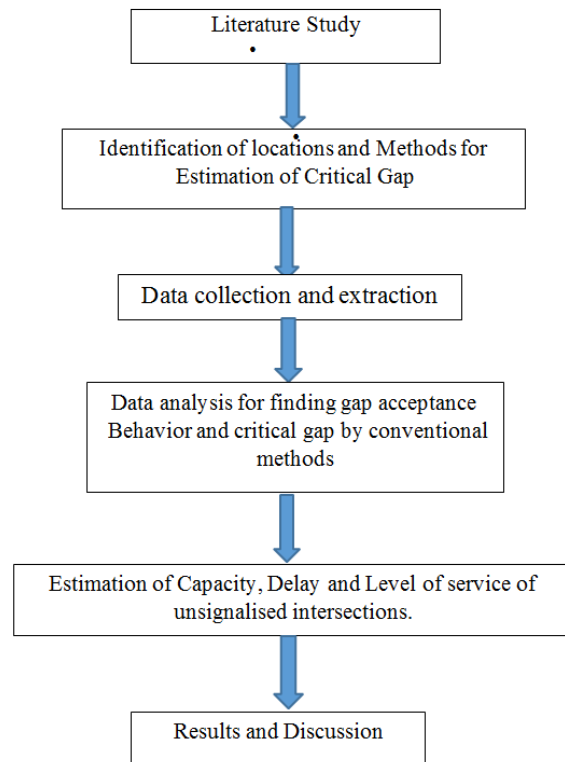
user behavior in traffic stream and develops training and technology to lower risk of crashes (Guler, 2017). Critical gap as explained in Indo HCM is as the shortest time interval on the major approach that allows the minor stream vehicles go into the intersection. Therefore, the driver's critical gap is the lowest gap that would be acceptable. (Harsh.J, 2015) A specific vehicle would reject any gaps smaller than the critical gap and would accept gaps larger than or equal to the critical gap. Critical gap is an important aspect of driver's behavior which is considered in the design and analysis of intersections. Transportation Research Board (2000) suggested that driver's critical gap can be calculated based on the observations of the greatest rejected and lowest accepted gap for a given intersection. (Astalatha.R, 2011) Critical gap is an important parameter for calculation of capacity which cannot be measured directly on field .Rejected and accepted gaps of single vehicle in a minor stream can be analyzed and some statistical methods are used for estimation of critical gaps by conventional methods like Raff's ,Maximum Likelihood Method ,Probability Of Equilibrium Method ,Ashworth , Greensheild , Logit ,Harder ,Wu ,Acceptance Curve Methods etc. (Wu, 2012).Estimation of delay, capacity ,Gap acceptance behavior are extensively studied at unsignalized intersections. The effect of Delay on critical gap is calculated by considering the average delays of vehicle to that of critical gaps in second (Tian, 2015).The distribution of Accepted and rejected gaps are divided into different ranges according to movements on major and minor roads. (Sahraei, 2016).

2. OBJECTIVE:

The objective of Present study is to determine

- To determine capacity of intersection using Gap acceptance capacity model and Indo HCM 2017
- To determine gap acceptance behavior, critical gap of priority junction using conventional methods.

3.METHODOLOGY



4. DATA COLLECTION:

Traffic data is collected through video graphic technique at the selected site. In the present study traffic data was collected for 9 hours for a week i.e. from 19.11.2018 to 25.11.2018 from traffic police department and at each intersection peak hour traffic is determined. At all locations the peak hour was observed to be 18.00-19.00P.M.on Friday. .

- Vehicle Classification
- Turning movements
- Direction of travel

Study location: Intersection was selected in such a way that they have fair geometry and least interference by pedestrians and parked vehicles.

Major traffic problems occurring at unsignalised intersections in Hyderabad city were identified

1. Pragathi Nagar –T intersection
2. Bahadurapally Intersection.(4 legged Intersection)



Figure 1: study locations

4.2 Site selection criteria: Intersections consisting major and minor road on an urban road in Hyderabad city were selected. At these intersections following are major factors considered

1. There are few pedestrian and cyclists
2. Roads are two lane divided
3. There is no road side parking adjacent to the lane
4. Intersections are located in educational, recreational and residential areas



Figure 2 : Pragathi Nagar



Figure 3 : Bahadurpally

4.3:Road Inventory Data: Road geometric data like carriage way width, parking facilities, type of

intersection, bus bay, median width, footpaths and street lights are taken from selected junctions.

Road geometric data		
Facility	Location 1 Pragathi Nagar	Location 2 : Bahadurpally
Carriage way Width	17	15.5
Type of intersection	T – Intersection	4 legged intersection
Bus Bay	No	Yes
Median Width	1 Meter	0.5 Meter
Foot Path	No	No
Street Light	Yes	Yes

Table 1: Road geometric Data At study locations.

4.4 Volume count study: Traffic Volume Survey is an essential part of Town Planning, in a road network. It includes counting the number of vehicles passing through the selected intersection. The study of Classified Traffic Volume Count is to understand factors that form the basis of:

Establishing the use of the road network by vehicles of different categories, traffic distribution, and PCU. Need of median shifting or road widening. The peak hour volume of locations 1 and 2 i.e. pragathi nagar and bahadurpally are given in the above figures. It is noted that the peak hour volumes are 4106 PCU and 4243 PCU respectively. Peak Hour flow was calculated by video data collected from Police department, Hyderabad. The accepted and rejected gaps from the video are extracted by stratified sampling technique for analysis and determination of capacity and Critical gaps.

S.no	Leg	Movement	P.H.V	
			1	2
1	3	Bachupally-Gandimaisamma	1298	1322
2	5	Gandimaisamma-Bachupally	889	986
3	1	Bachupally-Pragathinagar	323	496
4	4	Pragathi nagar – bachupally	405	429

5	2	Pragathinagar-gandimaisamma	514	606
6	6	Gandimaisamma-pragathinagar	469	514

Table 2: Traffic volume count of pragathi nagar T intersection

S.no	Leg	Movement	P.H.V 1	P.H.V 2
1	3	Gandimaisamma –Bahadurpally	294	460
2	1	Gandimaisamma –Pragathinagar	170	184
3	2	Gandimaisamma-suraram	192	213
4	5	Suraram –gandimaisamma	421	462
5	6	Suraram-Pragathinagar	490	509
6	4	Suraram-Bahadurpally	86	95
7	9	Pragathinagar-Gandimaisamma	301	326
8	8	Pragathinagar –Bahadurpally	190	230
9	7	Suraram-Bahadurpally	570	609
10	10	Bahadurpally –Gandimaisamma	256	323
11	12	Bahadurpally-Suraram	402	498
12	11	Bahadurpally-Pragathinagar	320	334

Table 3 : Traffic volume study at Bahadurpally Intersection

5.1 Critical Gap Estimation by Indo HCM Method:

Indo HCM 2017 Define critical gap as “The minimum major stream headway during which minor street vehicle can make a maneuver”, uses occupancy factor method for calculation of critical gap and it considers drivers behavior. Data containing Geometry of road and classified volume count of peak hour traffic is taken. The following are the steps to calculate critical gap and capacity of an unsignalised intersection by Indo HCM method.

1. Input Data (Geometry of road and traffic volume)

2. Convert the volume of traffic into PCU
3. Calculate conflict traffic flow
4. Determine Critical Gap
5. Capacity of Turning Moments

The critical gap for any movement can be obtained by the equation

$$T_{c,x} = t_{c,base} + f_{LV} * \ln(P_{LV}) \dots\dots\dots 1$$

Where

PLV = Proportion of Heavy Vehicles

FLV = Adjustment factor for proportion of Large vehicles in conflicting Traffic Stream

T_{c, base} =base critical gap for various movements

Capacity of each turning movement is given by the equation

$$a * V_{c,x} * e^{-v_{c,x}(t_{c,x}-b)} / 3600$$

$$C_x = \frac{a * V_{c,x} * e^{-v_{c,x}(t_{c,x}-b)} / 3600}{1 - e^{-v_{c,x} t_{c,x} / 3600}} \dots\dots\dots 2$$

The Base critical gap for four lane divided and the adjustment factor for heavy vehicles are taken from Indo HCM.

Adjustment Factor	Base critical Gap	Leg	Critical Gap Formula	tc (sec)
0.46	2.7	Bachupally To Pragathi Nagar (1)	tc=2.7+0.46*ln(0.17)	1.9
0.58	3.8	Pragathi Nagar To Gandimaisamma (7)	tc=6.8+0.58*ln(9.46)	4.29
0.88	6.8	Gandimaisamma To Bachupally (5)	tc=3.8+0.88*ln(1.76)	8.1

Table 4: critical gap for location 1 –Pragathi Nagar

Movement	Base Critical Gap	Adjustment Factor for light and heavy vehicle F _{LV}	Proportion of Heavy veh in conflicting stream	Critical gap
Gandimaisamma –Pragathinagar (1)	2.7	0.457	17.98	4.02
Suraram-Bahadurpally (4)	2.7	0.457	12.19	3.84

Suraram-Bahadurpally (7)	3.8	0.885	15.06	6.2
Bahadurpally-Gandiamaisamma (10)	3.8	0.885	18.02	6.35
Pragathinagar-Bahadurpally (8)	6.8	0.583	19.05	8.51
Bahadurpally-Pragathinagar (11)	6.8	0.583	20.87	8.56

5.2 Capacity and LOS estimation using Indo HCM 2017:

Highway capacity is defined by the Highway Capacity Manual as the maximum hourly rate at which persons or vehicles can be reasonably expected to traverse a point or a uniform segment of a lane or roadway during a given time period under prevailing roadway, traffic and control conditions. Level of service (LOS) is a qualitative measure used to relate the quality of motor vehicle traffic service. LOS is used to analyze roadways and intersections by categorizing traffic flow and assigning quality levels of traffic based on performance measure like vehicle speed, density, congestion, etc. The following tables explain the capacity and level of service at each leg of both intersections.

Table 5 : Critical gap for location 2 – Bahadurpally

Movement	Tc,x	Follow up Time	Conflictin g flow	a(Adjustment factor)	b(adjustment factor)	Capacity cx	v/c	LOS
Movement 1	1.9	1.14	514	0.8	1.3	769.68	0.66781	D
movement 7	4.29	2.574	622	1	2.16	825	0.753939	D
movement 5	8.1	4.86	986	0.9	1.971	1200	0.821667	E

Table 6: Capacity and LOS of intersection 1 Pragathi nagar

Movement	critical Gap	Follow up time	conflictin g Flow	Adjustment Factor' a'	Adjustment Factor 'b'	Capacity	volume	v/c	LOS
1	4.02	2.412	498	0.8	1.3	645.02	345	0.535	D
4	3.84	2.304	230	0.8	1.3	359.23	298	0.830	E
7	6.2	3.72	1263	1	2.16	571	173	0.303	B
10	6.35	3.81	1139	1	2.16	604.36	128	0.212	B
8	8.51	5.106	1388	0.9	5.04	425.5	217	0.510	C
11	8.56	5.136	1873	0.9	5.04	740.6	599	0.809	E

Table 7 : Capacity and LOS of intersection 2 bahadpally

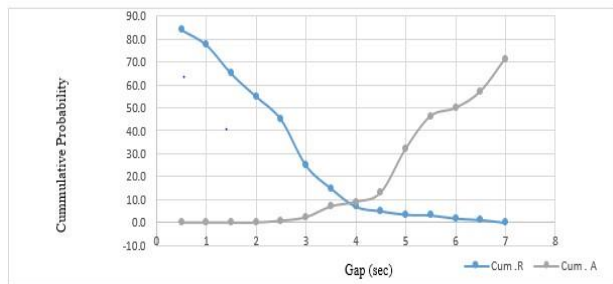


Figure 4 : critical gap of bahadurpally intersection (4 legged)

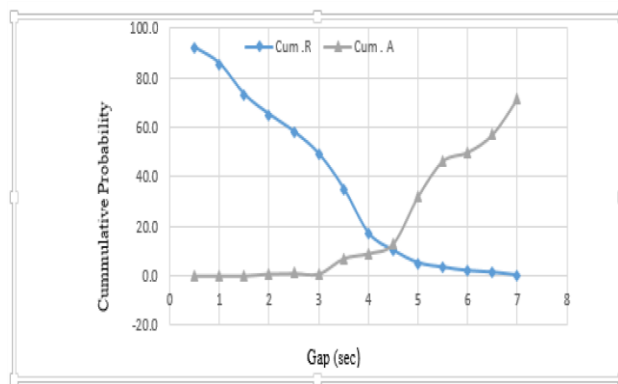


Figure 5 : critical gap of pragathi nagar intersection (T intersection)

6. RESULTS AND DISCUSSION:

Geometry	T int ersection (Pragathi Nagar)		
Movement	Major Left (1)	Major Right(7)	Minor Left(5)
Adjustment For Base Critical Gap	2.7	3.8	6.8
Critical Gap	1.9	4.29	8.1s
Heavy Vehicle Adjustment Factor	0.46	0.58	0.88
Adjustment Factor 'a'	0.8	1	0.9
Adjustment Factor 'b'	1.3	2.16	6.8
Capacity	770	825	1200
V/C	0.67	0.75	0.82
LOS	D	D	E

Table 6 : Results Of location 1 Pragathi Nagar intersection

The paper provides detailed notes on determination of critical gap using Indo HCM method and Raff’s Method .The stepwise analysis of collection of data, extraction of traffic volume, accepted and rejected gaps calculation and plotting the critical graph, Capacity estimation and determination of LOS explains the procedure of Indo HCM method .Both Indo HCM method and Raff’s method were analyzed to investigate the potential factors of the methods and compared. The following are some of the observations made during the investigation process.

- The peak hour traffic of the 3 legged pragathi nagar intersection is 4102 PCU and 4 legged intersection is 4323 PCU under mixed traffic conditions.The capacity and LOS of intersection 1 calculated from Indo HCM method is 845 veh/hr with v/c ratio as 0.753 and LOS D
- The capacity and LOS of intersection 2 calculated from indo HCM method is 647veh/hr and V/C ratio as 0.535 and LOS D .The critical gap of intersection 1 and intersection 2 were observed as 4.29 and 4.02 sec respectively for vehicles travelling from minor road to major road right turns.
- Raff’s method explains the critical gap of intersection 1 and intersection 2 as 4.35 and 3.90 respectively for vehicles travelling from minor road to major road right turns.It is observed that both Indo HCM 2017 and Raff’s method provides similar results and Indo HCM method is accurate method compared to Raffe’s

Geometry	4 legged Intersection (Bahadurpally Intersection)					
	Major Right (1)	Major Right (4)	Minor Right(7)	Minor Right(10)	Major Through (8)	Major Through (11)
Adjustment For Base Critical Gap	2.7	2.7	3.8	3.8	6.8	6.8
Critical Gap	4.02	3.84	6.2	6.38	8.51	8.56
Heavy Vehicle Adjustment Factor	0.457	0.457	0.885	0.885	0.583	0.583
Adjustment Factor 'a'	0.8	0.8	1	1	0.9	0.9
Adjustment Factor 'b'	1.3	1.3	2.16	2.16	5.04	5.04
Capacity	345	298	173	128	217	599
V/C	0.535	0.83	0.303	0.212	0.51	0.809
LOS	D	E	B	B	C	E

Table 7 : Results of location 2 bahadurpally Intersection

7.REFERENCES

1. Brilon. (1999). Useful estimation procedures for critical gaps. Transportaation Research Board (TRB) ,National Research council, Washington .
2. Guler, S. (2017). Methodology for estimating capacity and vehicle delays at un signalised multimodal intersections.
3. J., H. (2015). A Review of Critical Gap Estimation Approaches at Uncontrolled Intersection in case of Heterogeneous Traffic Conditions.
4. Mourya, A. K. (2016). Estimation of critical gap for through movement at four legged uncontrolled intersection. ELSEVIER, 203-212.
5. pande, P. M. (2012). Evaluation of Delay and LOS for Signalised intersection. 372-377.
6. R., A. (2011). Critical Gap through clearing Behaviour of drivers at Unsignalised intersection. springer, 1427-1434.
7. Sahraei, M. A. (2016). Determination of Gap Acceptance at Priority Junctions. Elsevier.
8. Tian, Z. Z. (2015). A further investigation on critical gap and follow up time. Interanational symposium on Highway Capacity (pp. 397-408). USA: Transportation Reasearch Circular.
9. Wu, N. (2012). Estimating Distribution Functions of Critical Gaps at unsignalised intersections based on Equilibrium of probabilities. 1-25.

Design and Verification of Serial Peripheral Interface Protocol using QuestaSim

^[1] P. Naga Gayathri, ^[2] Sri. K. Naga Koushil Reddy

^[1] M.Tech (VLSI & ES), PG Scholar, ^[2] Assistant Professor, MS_{LONDON}

^{[1][2]} Department of Electronics and Communication Engineering, G. Pulla Reddy Engineering College (Autonomous), Kurnool, A.P.

^[1] pgayathri115@gmail.com, ^[2] koushilreddy4999@gmail.com

Abstract:-- The Serial Peripheral Interface bus or SPI bus is a synchronous serial data that operates in full duplex mode. Devices communicate in master/slave mode where master device initiates the data frame. Slave select lines are allowed to select the slave devices. The main objective of this project is to design SPI verilog and verify the code and functionality using systemverilog. SPI can be simulated using Questa Sim 10.0b tool and symmetrical structure can be synthesized using XILINX ISE 14.7. Sometimes SPI called a four-wire serial bus. SPI is often referred to as Synchronous Serial Interface. SPI are used to provide board level interfaces between devices such as Analog to Digital Converters, Digital to Analog Converters, microcontrollers

Index Terms : SPI, SystemVerilog, QuestaSim, XILINX ISE.

1. INTRODUCTION

System-on-Chip (SoC) is a linkage of distinct Intellectual Property (IP) blocks which are connected using composite protocols. IP cores are the Register Transfer Level codes that attain secure desiderate process. Most of the digital designs based on Hardware Description Languages in place of schematic representation. These codes are well certified codes that must be accessible for any SoC expansion. Mostly buses are used in CPUs for communicate purpose between the CPU, memory and peripheral devices. ARM processors use distinct protocols to build on the core to achieve the goals. These distinct protocol interfaces are SPI, I2C, and UART. All these protocols are verified with the help of hardware verification language i.e. SystemVerilog. Exponentially developing the elaboration of chips for SoCs for that the validation is highly required. Primarily the part of evolution time is worn out on validation. Here the validation is carried out based on the assertion technique and the code coverage technique. The conceal result and the 100% coverage details of produced test cases are provided using systemverilog

SPI is a synchronous protocol that allows serial communication between a master device and a slave device. Generally, we prefer Serial communication over Parallel communication because it has advantage like high speed, noise integrity. We use different protocols like Ethernet, USB and SATA for long distance communications and I2C, SPI for short distance communications. Ethernet, USB, SATA are used for outside the box communications. SPI is meant for

communication between Integrated Circuits for low or medium data transfer speed with onboard peripherals. SPI protocol is divided into a master and slave device for transmitting the data. The chip selects or slave select and serial clock have to be generated by the master when the data exchange has been processed.

II. SPI MODULE

The operation of the SPI protocol necessarily is based on the contents of an eight bit serial shift register present in both the master device and slave device. SPI interface grants to transmit and receive the data concurrently on two lines namely MOSI and MISO. SPI uses four signals: master out slave in (MOSI), master in slave out (MISO), serial clock (SCK), slave select (SS).

SS: Slave select wire is used to initiate communication between master and slave

SCK: Wire for the clock signal

MOSI: Wire for the master to send data to the slave. The MOSI wire is designed as output in a master device and as an input a slave device

MISO: Wire for the slave to send data to the slave. The MISO wire is designed as input in a master device and as an output in a slave device

In SPI, the master can determine the clock polarity and phase. Clock polarity and clock phase are the supreme specifications that describe a clock configuration to be worn by the SPI bus. The clock polarity bit establishes the polarity of clock signal at the time of idle condition. The ideal condition is describes as the period when the

chip select is HIGH and transformation to LOW at the initial phase of the communication. The clock phase bit establishes the phase of the clock signal. Based on the clock phase bit the leading or trailing edge is used to representative and/or shift the data. The master definitely preferred the CPOL and CPHA as per the necessity of the slave. Based on the clock polarity and clock phase bit choice, the four modes are possible. Below table 1 manifest the SPI modes.

Table 1: CPOL and CPHA Modes

SPI Mode	CPOL	CPHA	Clock polarity in Idle State	Clock Phase used to sample and/or shift the data
0	0	0	Low	Data sampled on positive edge and shifted out on negative edge
1	0	1	Low	Data sampled on negative edge and shifted out on positive edge
2	1	1	High	Data sampled on negative edge and shifted out on positive edge
3	1	0	High	Data sampled on positive edge and shifted out on negative edge

A. Block Diagram

SPI is established on the stipulation of master and slave interfaces. But here uses single master-single slave. Below figure 1 represents the general block diagram of SPI protocol model. Initially design the master and slave model based on the specifications. Master-Slave communication will be done with respective to miso and mosi signals

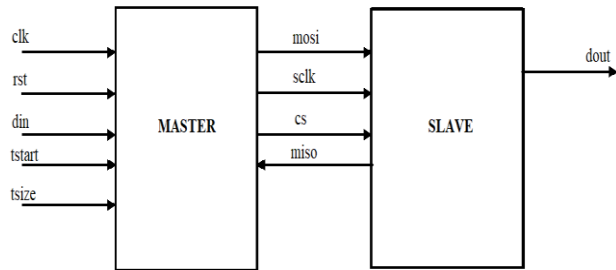


Fig 1: SPI Block Diagram

In SPI system, the eight bit shift register plays a major part. SPI performs the full duplex transmission. When a SPI communication takes place a bit of data gets shifted serially from master to slave and slave to master based on the control register signals. Therefore, by the time SPI transmission completes i.e. after eight clock cycles, the data present in the master and slave will have been shifted.

B. FSM Design Flow

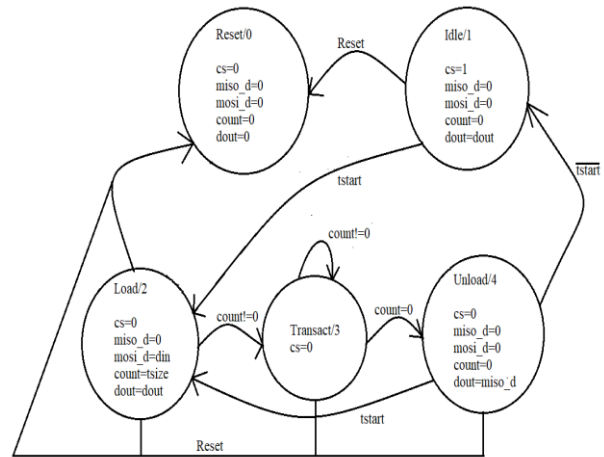


Fig 2: SPI FSM Design Flow

Above figure 2 represents the FSM design flow for the SPI design. The inputs to the FSM are tstart, reset and count. The outputs of the state machine are the chip select line, mosi register and output data i.e. dout.

Initially the machine is in reset state i.e. S0. State S1 is the idle state, where the module will spend most of its time. State S2 is the load state, where the module will starts a transaction after one clock cycle on the state transaction. State S3 is the transact state, where actual shifting operation will occur. State S4 is the unload state, where store the contents of the miso shift register into the output data register i.e. dout

Assertions have two types' namely immediate and concurrent assertions. An immediate assertion checks the condition at present time. A concurrent assertion that checks for the sequence of events spread over the multiple clock cycles. It executes in parallel with design blocks. SystemVerilog assertions constructed from properties and sequences. Sequences contain of Boolean expressions expand with temporal operator (##), this operator performs integration. It works by regularly pursue to check a sequence or property

The validation of SPI has been compassed by using the assertion properties and sequences come under the concurrent assertions. Based on the clock pulse, the concurrent assertions are used. The below figure shows the assertion report and here get the 100% assertion coverages and this coverage get only when the signals would get asserted. The figure 5 represents assertion report and it shows the 100% assertion graph for the SPI module

VI. COVERAGE ANALYSIS

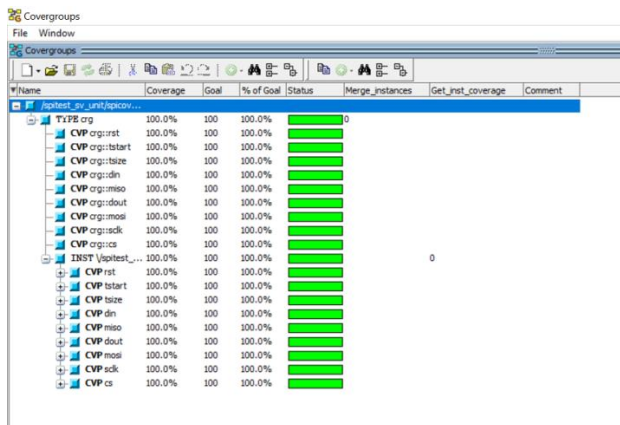


Fig 6: Coverage Report

Above figure 6 shows the coverage analysis report that it verifies the functionality of design parameters and for that achieves the 100% coverage Coverage is a metric to check the improvement of functional verification activity. It has to check the functionality of the DUT to meet the exact specifications or not. Coverage is used to measure, tested and untested the portion of the design Coverage done in two ways namely code coverage and the functional coverage. Code coverage suggests that to determine the coverage of the code. Functional coverage establishes the performance of design based on its description Coverage is characterized using the construct of covergroup. Covergroup is a user-defined that covers the spec of a coverage model. It is worn to identify the variables/transitions to be sampled that are happens at the

positive edge of the clock. A coverpoint is a variable that covers the functionality of design parameters. These coverpoint comes under covergroup. Under covergroup all these coverpoint are written.

Below table 2 shows the overall coverage and assertion percentage for the desired model.

Coverage Summary by Structure:		Coverage Summary by Type:			
Design Scope	Coverage (%)	Weighted Average:			100.00%
spiton	100.00%	Coverage Type	Bins	Hits	Misses
dut	100.00%	Covergroup	12	12	0
spitest_sv_unit	100.00%	Assertion Attempted	13	13	0
spicoverage	100.00%	Assertion Failures	13	0	-
		Assertion Successes	13	13	0

Table 2: Overall Assertion and Coverage

VII. SYNTHESIS

The design is synthesized in the Xilinx ISE tool. For this, the Artix 7 package is used and in which the selected device is xc7a100t-3csg324. For this the synthesis report has been get. From the below table, observe the comparison of time period and delay for the existing and proposed methods.

Table 3: Timing Summary Report

Timing Summary		
	Existing Method	Proposed Method
Timing	Value	Value
Minimum Period	7.491ns	2.046ns
Minimum Input Arrival Time Before Clock	6.981ns	1.363ns
Maximum Output Required Time After Clock	7.913ns	2.581ns
Maximum Delay Path	7.491ns	1.061ns

Above table 3 represents the timing summary for the AHB-Lite model. In the result observe the comparison in the time period it is reduced by 72.68%

CONCLUSION

In this paper, the SPI single master-single slave protocol was designed. The design and the validation of SPI protocol is evaluated in MODELSIM and QUESTASIM tools. By using MODELSIM the simulation of design was done and using QUESTASIM the validation analysis was done. Further for the verification purpose done with the coverage and assertion technique so that for the desired design achieved the 100% assertion and

coverage. To synthesize purpose XILINX ISE 14.7 tool is used. When the synthesis was completed then observes the timing analysis for the design with respective to the desired specifications.

REFERENCES

- [1] Prakriti Porwal, "Study and Implementation of SPI using VHDL and its synthesis using Xilinx", International Journal of Innovative Research in Science, Engineering and Technology Volume 5, Issue 6, June 2016.
- [2] Mr. Akshay K. Shah; "High Speed SPI Slave Implementation in FPGA using Verilog HDL", International Journal of Advanced Research in Computer Engineering & Technology (IJARCET) Volume 4, Issue 12, December 2015.
- [3] Min-Chun Tuan, Shih-Lun Chen, Yu-Kuen Lai, Ho-Yin Lee "A 3 wire SPI protocol Chip Design with ASIC and FPGA Verification", Proceedings of the 3rd World Congress on Electrical Engineering and computer systems and science, June 2017.
- [4] G. Sai Ram, G. Ravi Chandra, K. Mohan Rao, B. Hemanth Nag, "Design and Implementation of SPI with Built-In-Self-Test Capability over SPARTAN 2", International Journal of Advanced Research in Computer and Communication Engineering Vol. 4, Issue 4, April 2015
- [5] S. Choudhury, G.K.Singh, R.M.Mehra "Design and Verification Serial Peripheral Interface Protocol for Low Power Applications", International Journal of Innovative Research in Science, Engineering and Technology Vol. 3, Issue 10, October 2014
- [6] S. Saha, M. A. Rahman, A. Thakur, "Design and Implementation of a BIST Embedded Inter-Integrated Circuit Bus Protocol over FPGA," in Proc. 2013 International Conference on Electrical Information and Communication Technology (EICT), pp. 1-5, Feb.2014.
- [7] Das, R, Singh. G.K., Mehra. R.M., "Two-Phase Clocking Scheme for Low-Power and High-Speed VLSI", International Journal of Advances in Engineering Science and Technology, Volume 2, Number 2, 2013
- [8] K. Aditya, M. Siva Kumar, Fazal Noor basha, T. Praveen Blessing ton, "Design and Functional Verification of a SPI Master Slave Core Using System Verilog", International Journal of Soft Computing and Engineering (IJSCE) Volume-2 Issue-2, May 2012.
- [9] Ananthula Srinivas, M. Kiran Kumar , Jugal Kishore Bhandari "Design and Verification of Serial Peripheral Interface", International Journal of Engineering Development and Research ISSN: 2321-9939
- [10] A.K. Oudjida, M.L. Berrandjia, A. Liacha, R. Tiar, K. Tahraoui& Y.N. Alhoumay "Design and Test of General-Purpose SPI Master/Slave IPs on OPB Bus," 2010 IEEE.2002. International Journal of Scientific Research in Science, Engineering and Technology.
- [11] H Ananthula Srinivas, M.K.Kumar and Jugal Kishore Bhandari," Design and Verification of Serial Peripheral Interface", International Journal of Engineering Development and Research, ISSN: 2321-9939.
- [12] Pachler W; Pressel K.; Grosinger J; Beer G; Bosch W; Holweg G; Zilch, C; Meindl M.A novel 3D packaging concept for RF powered sensor grains, Electronic Components and Technology Conference (ECTC), 2014 IEEE 64th , PP: 1183 – 1188, 2014
- [13] Amos, D.;Lesea, A.;& Richter, R. (2011). FPGA-Based Prototyping Methodology Manual. Mountain View, California: Synopsys, Inc.
- [14] Abdul Ikram, T.MuniKumar,"Customizable Uart To Spi Ip Core" Vol.1, Issue.2, 2013, ISSN: 2321-7758
- [15] F. Leens, "An Introduction to I2C and SPI Protocols," IEEE Instrumentation & Measurement Magazine, pp. 8-13, February 2009.

Design and Verification of Advanced High-Performance Bus Lite Protocol using QuestaSim

^[1] B. Chinna Munaiah, ^[2] Dr. S.M. Shamsheer Daula

^[1] M.Tech (VLSI & ES), PG Scholar, ^[2] MIEEE, Associate Professor

^{[1][2]} Department of Electronics and Communication Engineering, G. Pulla Reddy Engineering College (Autonomous), Kurnool, A.P.

^[1] chinnamunaiah.badiginchala@gmail.com, ^[2] shamsheerdaula@gmail.com

Abstract: In the SoC quantity, validation is most vital part in chip manufacturing and in the testing. Verification contributes with definite execution and functionality of DUT (Design under Test) and check that the exact designations meet or not. In this paper, the AHB-LITE Protocol is validated according to the model listing. Assertion Based Verification (ABV) is most commonly used validation technique to build up the validation standard and minimizing the debugging time of complicated design and also ease the validate process. Coverages are used to check the exact functionality specifications meet or not. Initially the architecture of AHB Lite model is designed using single master-multiple slaves in verilog language and simulates the design using MODELSIM tool and the protocol is validated with the assertions and coverages technique i.e. done in QUESTASIM tool. The model is integrated and appliance in XILINX ISE tool. In this synthesize will be done for the respective design based on the stipulation. So that observed the timing analysis for the respective design.

Index Terms : AHB-LITE, SystemVerilog, QuestaSim, XILINX ISE.

1. INTRODUCTION

System-on-chip (SoC) is a linkage of distinct Intellectual Property (IP) blocks which are connected using composite protocols. IP cores the Registers Transfer Level codes that attain secure desiderate process. Most of the digital designs based on Hardware Description Language in place of schematic representation. These codes are well certified codes that must accessible for any SoC expansion. Advanced Microprocessor Bus Architecture (AMBA) is extensively used in SoC design, which is established for on-chip bus purpose. AMBA is evolved by ARM in 1996. The AMBA blueprint typically used for the high-profile embedded micro controllers. AMBA's vital judicial is to feed technology independence and to motivate modular system design. It is used in multiple peripherals, embedded processors and signal processors. AMBA is mostly used on an orbit of SoC/ASIC parts as well as in processors worn in contemporary portable mobile devices like smartphones. Mostly buses are used in CPUs for communicate purpose between CPU, memory and peripheral devices, ARM uses distinct protocols to build on the core to achieve the goals. These distinct protocols interfaces are explained in the AMBA stipulation namely ASB, APB, AHB, AXI and ATB. All these protocols are verified with the help of Hardware Verification Language (HVL) in systemverilog. Progressively develops the elaboration of chips for SoCs for that the validation is highly required. Primarily the part of evolution time is worn out on

validation. Here the validation is carried out based on the assertion technique and coverage technique. The conceal result and the 100% coverage details of produced test cases are provided using systemverilog.

II. AHB-LITE MODULE

The updated specification of AHB is the AHB-Lite, which is the subset of AHB comes under AMBA 3 version. AHB Lite manages the functional block in SoC design. It develops the communication between the master and each slave. The AHB Lite provides the higher bandwidth and also higher performance synthesizable designs. For each AHB Lite bus protocol model the communication happens between the peripheral devices. In this paper, design the module with single master-multiple slaves and each slave is activated based on the particular address generated. The stipulations of the AHB Lite are

1. Hold up high clock frequency, high bandwidth and high performance
2. Operates bus for write and read transfers
3. Hold up burst and pipelined operations
4. No use of arbitration
5. Hold up single master and more than one slave

A. Block Diagram

AHB-Lite block representation is shown in the figure 1. This model is developed based on the specifications of master and slave interfaces. In this design, the single

master module, multiple slave modules, decoder module and the multiplexer is used. Particular module is works based on their respective designations. When the design is done for that communication will develops between the master and slave based on read and write operations. For that also checks burst transfer operation with respective to the address generated by the address. Decoder module is used for the selection purpose i.e. used to select the particular slave from the different slaves. That salve would get selected with respective to the particular address that is generated by the master.

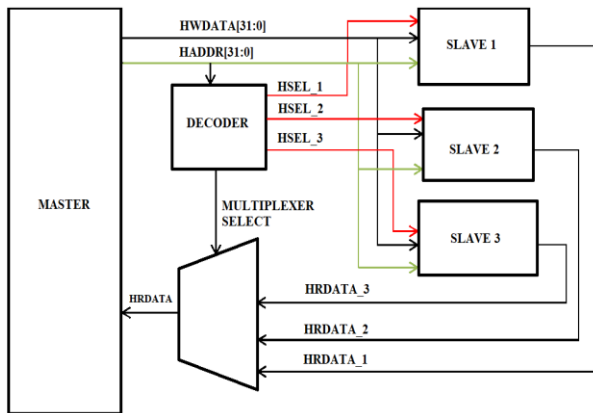


Fig 1: AHB-Lite Block Representation

B. Master Interface

AHB-Lite master interface diagram is shown in the figure 2. Master provides the control signals and addresses information to initiate the write and read activities and also performs the burst transfer operation depends on the size and the transfer responses. Through master develops the high performance synthesizing design with the necessity of master generated address.

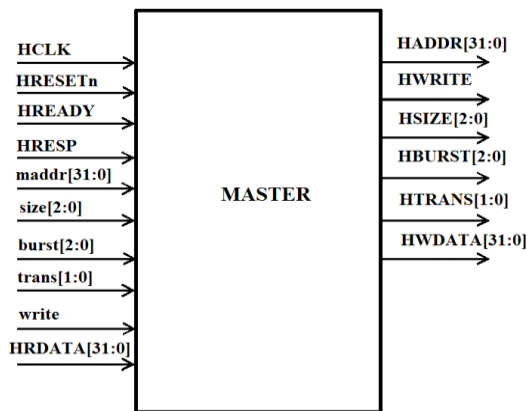


Fig 2: AHB-Lite Master Interface Diagram

Generally in the master module do the transfer operations. When observe the below table 1 it shows the

operation flow of various transfer types they are idle, busy, non-sequential and sequential types.

In each type, they have their own operation based on the type it performs. When it is in idle state i.e. “00” case then no operation will takes place. When it is in busy state i.e. “01” case then the waiting state condition will occur. In the waiting state the particular signal will be waited until it gets to do the next operation. When it is in non-sequential state i.e. “10” case then the address will transferred in a non-sequential manner i.e. the continuous manner will not happens here and the transfer is not related to the previous transfer address. When it is in sequential state i.e. “11” case then the address will transferred in a sequential flow and the address is related to the previous address.

Table 1: Transfer types

Cycle Type	Description	HTRANS[1:0]
Idle	No Activity	00
Busy	Inserting waiting states	01
Non-Sequential	Transfer Address not related to previous transfer	10
Sequential	Transfer Address related to previous transfer	11

C. Slave Interface

AHB-Lite slave interface diagram is shown in the figure 3. A slave will acknowledge to the transfers proposed by the master. Slave module is activated based on the decoder module. In the slave module uses the HSELx signal when the HSELx is active High then it says that slave is activated otherwise it is in inactive state so no slave will get activated. When the salve is activated then it performs the transfer operation related to the master module and gives the read data as output for the slave module.

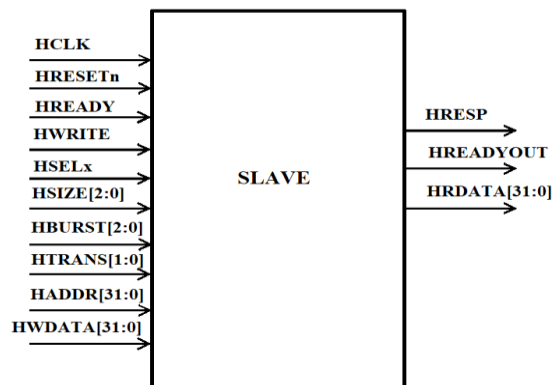


Fig 3: AHB-Lite Slave Interface Diagram

D. Decoder Interface

AHB-Lite decoder interface diagram is shown in the figure 4. Decoder component decodes the address of all transfer and give a preferred signal to the particular slave i.e. to be sophisticated in the transfer.

A slave to multiplexer is needed to multiplex the data and response signals from the master to the slave. A centralized multiplexer is needed in all implementations that uses two or extra slaves. From the master module the output of address is passed to the decoder and in the decoder write the logic for address selection based on the address selection the particular address data will be send to the particular slave only then that the particular slave would get activated among from different slaves.

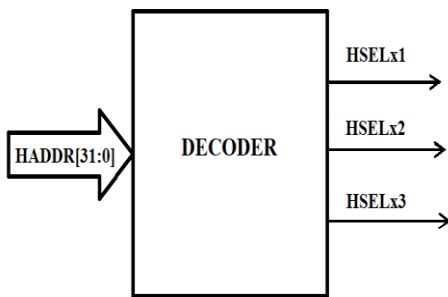


Fig 4: AHB-Lite Decoder Interface Diagram

III. VERIFICATION ENVIRONMENT FLOW

Verilog comes under hardware description language. For the complex designs in verilog the verification is not possible because it is difficult to find the debugs and the exact timing requirements are also not occur. So to overcome all these we deal with systemverilog comes under hardware verification language. SystemVerilog is a combination of both hardware description and hardware verification language. For the complex designs it is efficient one and easy to find the debugs and also verify the design using different test cases. Figure 5 represents the verification environment flow and this flow is followed by any design for the verification purpose.

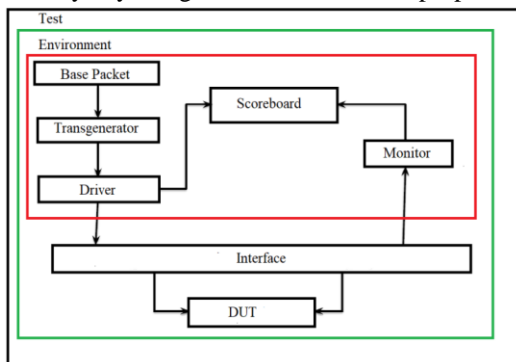


Fig 5: Verification Environment flow

Verification plan is center of attention for describing absolutely what use to be proved and drives the coverage specification. It gives a time to the modern and evaluates the plan for functional validation before the verification engineer has gone into design to appliance it.

To validate the entire design for that use different test cases for the respective module. Those different test cases write under the testbench module. In DUT, the entire RTL code is programmed based on the specifications. In environment, it uses the OOPS concept to develop the blocks. So instead of “module” here use the “class” through this communication is done easily between the classes. To communicate with the DUT and environment use the “interface” block. Through interfaces the communication will happens. By using the “virtual” keyword the connection will develops between the DUT and the environment. With the help of top module the entire design goes to simulate and run it

IV. SIMULATION

AHB-Lite module is designed based on the specifications and perform the burst operation with the help of transfer response signals. The desired model is implemented using verilog programming language and the simulation is done by ModelSim. To run the simulation uses different test cases based on multiple transfer operations. All those test cases will be verified with respective to the AHB Lite slave. For this the output waveform is observed in the figure 6.

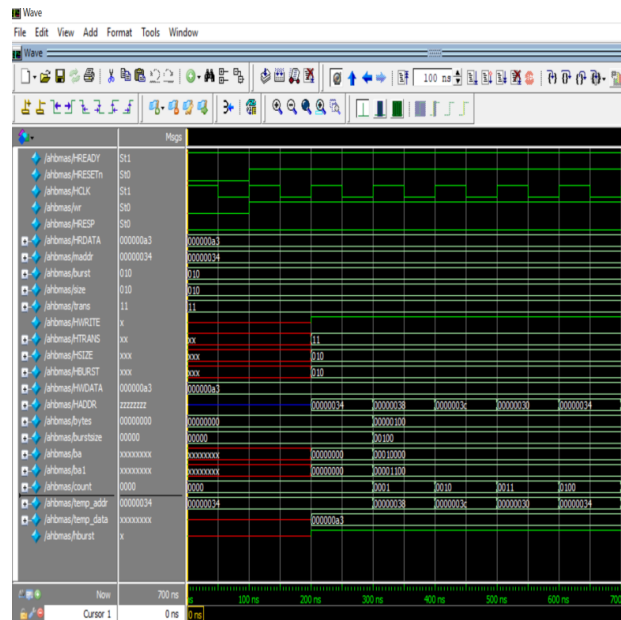


Fig 6: Wave form for AHB Lite Master Burst Operation of Size 4

To perform the discrete transactions like Trans, write, burst operations all will be carried out in the design. If the size is given as “010” and the burst is given as “010” then the four continuous operation will happens with respective to the generated address.

To know the details of wrapping here count variable would consider. When initiate the address based on the initial address the address will be generated and wrapping would occur. Meanwhile count values are incremented. Here the write operation happens like that only the burst operation happens but different here is the value of count is examine for the burst size. Here checks the count value and burst length both are not equal then the count will get enhanced and the address will produced based on the size and the operation will carried out. The burst length and count value will equal then the burst operation will terminated and count value reset to zero. During the operation of burst the HREADY signal made HIGH for each operation but the HREADY signal is LOW the burst won't do the operation. So initially HREADY signal is HIGH then only comparison of count and burst length occurs.

From the figure 7 observe the output waveform for the particular slave selection line from different slaves. Different addresses were generated in the master based on the particular address the particular slave is going to be activated. For the selection purpose uses the decoder operation. From the design of decoder the particular slave should be selected with respective to the specific address.

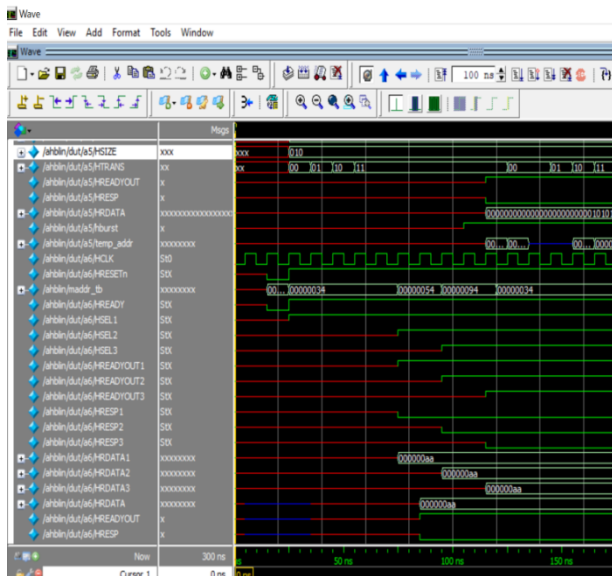


Fig 7: Wave form for Particular Slave selected based on particular address

From master module HADDR signal is generated i.e. it is the output for master and this signal is send to the decoder. The main operation of decoder is used to covert the n-inputs to the 2n outputs. HRESETn and HADDR signals were used as inputs and HSELx1, HSELx2 and so on are the output signals. Based on particular address signal generation only one slave should be activated and in the slave the respective operation be performed.

V. ASSERTION BASED VERIFICATION

Below figure 8 represents the assertion report

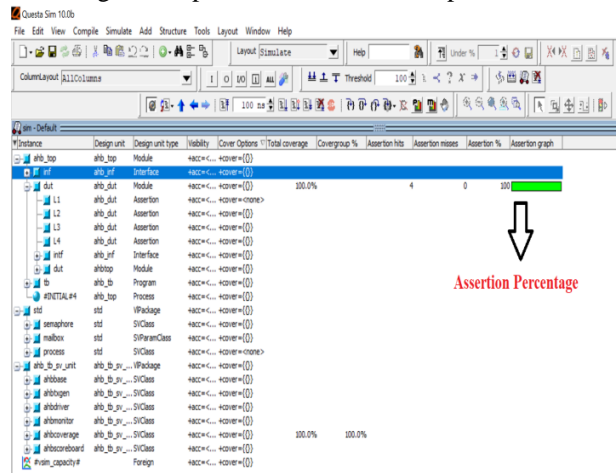


Fig 8: Assertion Report

Assertion aid a comment that is true. From validation aspect, an assertion describes the conventional behavior. Assertions can efficiently use to detect and debug the functional errors. SystemVerilog assertions constructed from properties and sequences. Properties are a hypernym of sequences; any sequence may be worn as if it were a property. Sequences contain of Boolean expressions expand with temporal operator (##), this operator performs integration. It works by regularly pursue to check a sequence or property.

The validation of AHB-Lite has been compassed by using the assertion properties and sequences. Based on the clock pulse, the concurrent assertions are used. For different signal pins, respective property and sequence would write based on those sequences the assertion gets verified and it compassed through the report. The below figure shows the assertion report and here get the 100% assertion coverages and this coverage get only when the signals would get asserted. The figure 8 represents the assertion report and it shows the 100% assertion graph for the AHB-Lite module.

VI. COVERAGE ANALYSIS

Coverage is a metric to assess the progress of functional verification activity. Coverage is used to measure, tested and untested the portion of the design. It has to check the functionality of the DUT to meet exact specifications or not.

Coverage is characterized using construct of covergroup. Covergroup is a user-defined that covers the specifications of coverage model. It is worn to identify the variables/transitions to be sampled that are happens at the positive edge of the clock. A coverpoint is a variable that covers functionality of the design parameters. These coverpoint comes under the covergroup. Under the covergroup all these coverpoints are written.

Coverage done in two ways namely code coverage and the functional coverage. Code coverage suggests that to estimate the coverage of the code. Functional coverage establishes the performance of design based on its description.

Below figure 9 shows the coverage analysis report that it verifies the functionality of design parameters and for that achieved the 100% coverage.

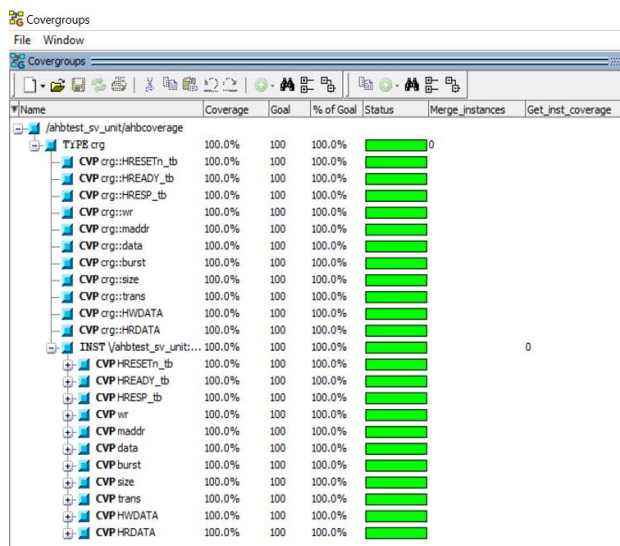


Fig 9: Coverage Report

VII. SYNTHESIS

The design is synthesized in the Xilinx ISE tool. For this, the Vertex 5 package is used and in which the selected device is XC5VLX50T-2ff1136. For this the synthesis report has been get. From Below tables 2 and 3 observe the utilization summary analysis and also from the timing summary observe the time period comparison, input

arrival time before clock and output required time after clock for the existing and proposed methods.

A. Utilization Report

Below table 2 represents the utilization summary for the AHB-Lite model. From the table observe that how much utilization takes place for the registers, LUTs, IOBs and LUT-FF pairs for the desired design.

Table 2: Utilization Summary

Device Utilization Summary						
	Existing Method			Proposed Method		
Logic Utilization	Used	Available	Utilization	Used	Available	Utilization
Slice Registers	65	28800	0%	155	28800	0%
Slice LUTs	511	28800	1%	405	28800	1%
Fully used LUT-FF pair	62	514	12%	145	415	34%
Bonded IOBs	158	480	32%	150	480	31%
BUFG/BUFCT RLS	3	32	9%	1	32	3%

B. Timing Report

Below table 3 represents the timing summary for the AHB-Lite model. From the result observe the comparison in the timing period it is reduced by 46.68%

Table 3: Timing Summary

Timing Summary		
	Existing Method	Proposed Method
Timing	Value	Value
Minimum Period	6.173ns	3.291ns
Minimum Input Arrival Time Before Clock	8.341ns	4.956ns
Maximum Output Required Time After Clock	8.965ns	2.864ns

CONCLUSION

In this paper, the AHB-Lite single master-multiple slaves' bus protocol was designed. By using MODELSIM the simulation of design was done and using QUESTASIM the validation analysis was completed. Further for the verification purpose done with the coverage and assertion technique so that for the

respective design achieved the 100% coverage and assertion. To synthesize purpose XILINX ISE 14.7 tool is used. When the synthesis was completed then observed the utilization summary and the timing analysis for the desired design with respective to the desired specifications.

REFERENCES

- [1] P. Poorani; B.M.E. Vijayashree "Implementation of AHB bus protocol for system on chip security", IEEE Xplore, 2nd International conference on Electronics & Communication Systems (ICECS), June 2015
- [2] Pragati Agarwal, "AMBA 3 AHB LITE PROTOCOL Verification through an Efficient and Reusable Environment with an Optimum Assertion and Functional and Code Coverage in UVM", Journal of Innovative Research in Computer and Communication Engineering Vol. 4, Issue 1, January 2016.
- [3] Prince Gurha, R. R. Khandelwal, "SystemVerilog Assertion Based Verification of AMBA-AHB", Conference on Micro Electronics and Telecommunication Engineering, 2016
- [4] M.B.R. Srinivas and Sarada Musala, "Verification of AHB_LITE protocol for waited transfer responses using re-usable verification methodology." 2016 IEEE
- [5] Salita Sombatsiri; Kazuhiro Kobashi; Keishi Sakanushi, "An AMBA hierarchical shared bus architecture design space exploration method considering pipeline, burst and split transaction", IEEE Xplore International Conference on Electrical/Electronics, Computer, Telecommunication and Information Technology, 2013
- [6] P.C. Hsiu, C.K. Hsieh, D.N. Lee, and T.W. Kuo, "Multilayer bus optimization for real-time embedded systems," IEEE Trans. Compute. Vol. 61, no. 11, pp. 1638–1650, Nov. 2012
- [7] Rishabh Singh Kurmi, Miss.Shruti Bhargava, Mahendra Vucha, Sandeep "Implementation of an AMBA Advanced High Performance Bus protocol IP block", Journal of Electronics Communication and Computer Engineering, Volume 1, Issue 1 2011.
- [8] S. Hwang, D. Kang, H. Park and K. Jhang, "Implementation of a self-motivated arbitration scheme for the multilayer AHB bus matrix", IEEE Trans. VLSI System volume 18 no.5, pp.818-830, May 2010
- [9] Dr. S.M. Shamsheer Daula, "VLSI Design of a novel high speed parallel self-timed adder (pasta)", International Journal of Eminent Engineering Technologies (IJOEET), volume 4 Issue 5, October 2016
- [10] Yashdeep Godhal, Krishnendu Chatterjee, Thomas A. Henzinger, "Synthesis of AMBA AHB from Formal Specification: A Case Study", in International Journal on Software Tools for Technology Transfer, July 2011
- [11] Anurag Shrivastav, G.S. Tomar and Ashutosh Kumar Singh, "Performance Comparison of AMBA Bus-Based System-On-Chip Communication Protocol", Conference on Communication Systems and Network Technologies, IEEE Xplore: 2011
- [12] C. Dhanunjaya Varma, PG Scholar, G. Ramesh, "Probability Driven Multi Bit Flip Flop Design Optimization with Clock Gating", Journal of Advance Research in Dynamic and Control Systems, Vol. 10, 05-Special Issue, 2018
- [13] Pravin S. Shete Shruti Oza; "Study of High Performance AMBA AHB Reconfigurable Arbiter for On-Chip Bus Architecture", International Journal of Electrical, Electronics and Data Communication, March 2014
- [14] Bogala Gayathri, PG Scholar, Dr. S.M. Shamsheer Daula, Associate Professor, Department of ECE, G.Pulla Reddy Engineering College Kurnool, "Implementation of Efficient Architecture for Montgomery Modular Multiplication Using FPGA", Journal of Advance Research in Dynamical & Control Systems, Vol. 10, 05-Special Issue, 2018.
- [15] Akshay Mann, Ashwani Kumar, "Assertion Based Verification of AMBA-AHB Using Synopsys VCS®" Journal of Scientific & Engineering Research, Volume 4, Issue 11, November-2013.
- [16] Harshil Gajjar, Nirav Patel, "Write Transfer of AMBA-AHB Lite Master Communication Protocol", International Journal for Scientific Research & Development Vol. 2, Issue 01, 2014.
- [17] .M. Naresh, P. Ravi Kumar Reddy, D. Sri Harsha, K.H. Murali, "Multiple Slave-Single Master Communication over Amba-AHB Bus using VHDL", IJECT Vol. 3, Issue 2, April - June 2012
- [18] M. Caldari, M. Conti, M. Coppola, P. Crippa, S. Orcioni, L. Pieralisi, C. Turchetti, "System-Level Power Analysis Methodology Applied to AMBA AHB Bus", Proceedings of the Design, Automation and Test in Europe Conference and Exhibition, March 2003 IEEE
- [19] Shaila S Math, Veerabhadrayya Math, "Design and Analysis of Xilinx Verified AMBA Bridge for SoC Systems", Proc. of Int. Conf. on Control, Communication and Power Engineering 2013
- [20] P. Hari Shankar, Mr. Chusen Duari, Mr. Ajay Sharma, "Design and Synthesis of Efficient FSM for Master and Slave Interface in AMBA AHB", Journal of Engineering Development and Research, Volume 2, Issue 3, 2014

Performance Evaluation of Pox Controller for Software Defined Networks

^[1] Elfreda Albert, ^[2] Adarsh V Srinivasan, ^[3] Mr. N. Saritakumar, ^[4] Dr. S. Subha Rani
^[1] M.E Communication Systems, ^[2] Bachelor of Engineering, ^[3] Assistant Professor, ^[4] Head of Department
^{[1][2][3][4]} Department of Electronics and Communication Engineering, PSG College of Technology, Coimbatore, India
^[1] elfredaalbert@yahoo.com, ^[2] adarshsrinivasan@gmail.com, ^[3] skumarpsg@gmail.com

Abstract:-- In traditional network the coupling of data plane and control plane makes the data forwarding, processing and managing of the network hard and complex. Here each switch takes its own decision, makes the network logically decentralized. To overcome the limitations in traditional network the Engineers developed a new model network known as Software Defined Network (SDN). This network the control plane is decoupled from the data plane making it less complex. It moreover has a logically centralized approach unlike the existing network. This separation enables the network control to be directly programmable and the architecture to be abstracted for applications and network services. SDN platform provides advantages like programmability, task virtualization and easy management of the network. However, it faces new challenges towards scalability and performances. It is a must to understand and analyze the performances of SDN for implementation and deployment in live network environments. SDN working with POX is studied. This paper analyses the working of POX controller and evaluates the performance metrics of POX controller for SDN environment. The emulation is done using the Emulation software.

Index Terms : Traditional Network; SDN; Mininet; Emulator; Firewall; OpenFlow Protocol

1. INTRODUCTION

Today due to increasing network traffic and the users are rising exponentially. The network providers find it difficult to cope with it this phase of explosive expansion. The Traditional Architecture Network (TAN) has only two planes the application plane and the control plane as in Figure 1. The TAN is defined by the physical topology consisting of switches, routers and servers all cabled together. This indicates that once they are set, it is difficult to make changes in them. It is expensive and complex. This existing network model is not compatible for varying workload demand that is mostly the case in Datacenter's and Cloud Environment.

The traditional network has logical distributed control and device specific management. This network has low dynamic configurability because it has device specific management. In this network, the routing table is built up by the control plane based on the learning and awareness. The protocol support for each device varies with depending upon each of the vendor's each release. Thus, making the traditional network less compatible to multi-vendor devices.

Troubleshooting in Traditional networks is difficult as the cause and the area of the error in specific is hard to be determined in the old network. All network devices have a control plane that provides information which is used to

build a forwarding table. They consist of a data plane that consults the forwarding table. The forwarding table is used by the network device in decision making process, where to send the frames or packets entering the device. Both of the planes co-exist directly in a networking device. As the network expands in TAN increases the devices used, cost, complexity and time for the network too increases. Mostly the functionality of an appliance is implemented in dedicated hardware i.e. an Application Specific Integrated Circuit (ASIC) is often used for this purpose. Also, when a single device is needed to be added or removed in the traditional network, the network administrator will have to manually configure multiple devices like switches, routers, firewalls etc. on a device-by-device basis.

One of the major issue with the traditional networks that it is more prone to attacks from various sources, as the control and data are in the same plane. So enhanced security given is such that the intruders access to the controller to be blocked or terminated. Also, the authentications given to the packets are heavy and not always compatible for all kinds or types of devices working in a multi-user environment.

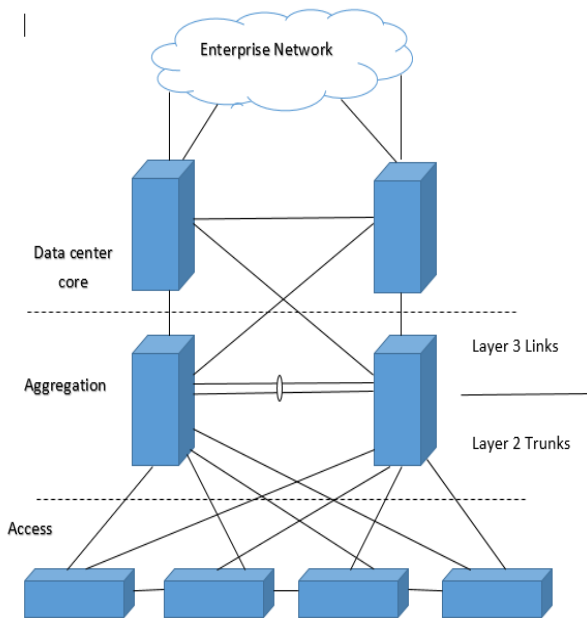


Fig 1 : Traditional Network structure

The CAP (Consistency, Availability and Partition Tolerance) theorem is a major issue faced in traditional network. So, moving on to Software Defined Network (SDN) where the control plane is decoupled from the data plane and also, it permits dynamic configuration in the network [1]. Hence, it is much preferred.

II. BACKGROUND

SDN

As mentioned in Fig 2, the Software Defined Network (SDN) has three main planes [14].

They are:

- a. Application plane
- b. Control Plane
- c. Data plane

This network is flexible and agile. This makes it user-friendly for the users to design, build and manage the network based on the needs. The deployment time taken by the Software Defined Network (SDN) is minimal. Also, the controllers can be easily programmed based on needs of the network. The Software Defined Network (SDN) has a logically centralized control plane which is programmable. The SDN has three types of controllers. They are:

- a. SDN controller,
- b. Southbound API's (Application Programming Interface),
- c. Northbound API's

The SDN controller acts as the brain of the network in coordinating the flows within inter-domain and intra-domain networks [4]. The Southbound API's (Application Program Interface) relies on information to the switches and routers in the network. They form the connecting bridge between control and forwarding elements. The Northbound API's regulate the communications with the applications and the deployed services. They are crucial to promote application portability and interoperability among different control platforms. There are many controllers currently used in Software Defined Network. They are POX, NOX, ONOS(Open Networking Operating System), Floodlight, Trema and Ryu [10][13].

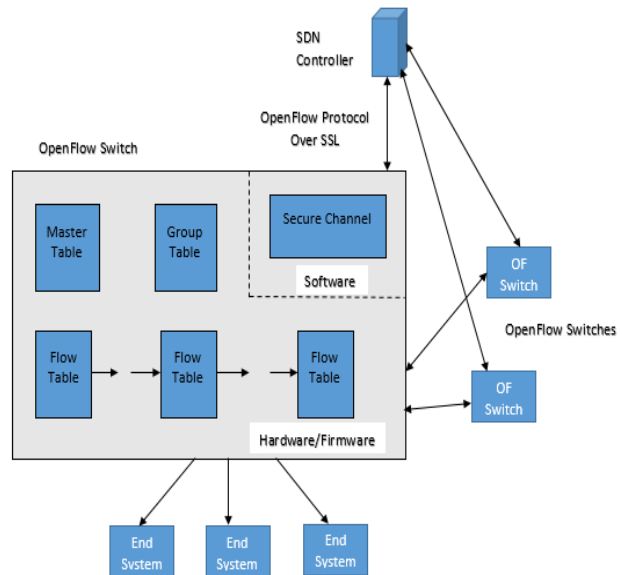


Fig 2 : Software Defined Network structure

The application plane is the layer that allows the applications to interact and manipulate the behavior of network devices through the control plane. Mostly the network information is provided to an application via the Northbound API of the controller. The SDN applications are traffic engineering, mobility and wireless, measurement and monitoring, security and dependability and data center networking [11].

The data plane consists of the switches, routers, and all the data forwarding devices. The forwarding devices contain the flow tables. They are reconfigured and reprogrammed based on the needs of the network. The data traffic is much reduced due to the systematic check in the data packet headers. They are analyzed by an application so-called the Virtual Network Function

(VNF) analyzer. The packets headers are analyzed and then are routed to their destination based on the “Best Path to be Travelled”. Most of the OpenFlow switches used in SDN supports OpenFlow (OF) protocol [8]. The major security threats in SDN are Unauthorized Access, Data Leakage, Data Modification, Malicious /Compromised Applications, Denial of Service and Configuration Issues [6]. Also, by abstracting the network from the hardware, policies no longer are to be executed in the hardware, instead, they use of a centralized software application functioning as the control plane makes network virtualization possible in SDN.

OpenFlow Protocol

OpenFlow protocol is one amongst the initially used protocol in Software Defined Networking standards [3]. The recently used version is 1.3.0. The OpenFlow network policies and its applications are implemented as the OF applications, such that any application that works in SDN should support OF protocol. The application plane interacts with the northbound API via the control plane.

The OF controller interacts with the data plane is via the Southbound API. The controllers are distinct from the switches. This separation of the control from the forwarding allows for more sophisticated traffic management than is feasible for users by the Access Control Lists (ACLs) and routing protocols. Also, OpenFlow allows switches from different vendors mostly of each one with their own proprietary interfaces and scripting languages to be manage remotely using a single, open protocol. To work in an OF environment, any device needs should be communicated to the SDN Controller which mostly supports the OpenFlow protocol. Through this interface, the SDN Controller pushes down any changes to the switch/router related to the flow-table allowing network administrators with partitioning of traffic, controlling the flows for optimal performance, and start testing new configurations and applications.

The OF protocol is mainly supported by OF switches in the data plane. It runs over the “Secure Socket Layer” (SSL) in switches. The OpenFlow protocols defines three types of tables in the logical switch architecture as in figure 3. They are:

- Flow tables
- Group tables
- Meter tables

The flow tables are dynamically configured on the arrival of the packets. They match the incoming packets in the flow to the flow rules specified in the table and specified the action for the packet is defined in the flow-table. When they receive a data packet, depending upon the specified action in the packet, the work needed to be done is determined. There is also a possibility for the creation of multiple flow tables in a pipeline fashion. It also directs the flow to the Group tables which triggers the various actions in the flow. The Meter table can also trigger actions which leads to performance variations in the flows.

Mininet

It’s a network emulator [2] [7]. In this software, the creation of Virtual hosts, switches, controllers and links are possible. It runs in standard LINUX platform. The switches used here support OpenFlow protocol which is highly flexible for custom routings and Software Defined Network. Mininet is actively developed, supported and is released under a permissive BSD Open Source license. It’s simple, open-sourced and less expensive, so mostly preferred for developing OpenFlow applications. It also, permits multiple developers to access the same topology. It has its own Command Line Interface (CLI) for debugging and running network wide tests.

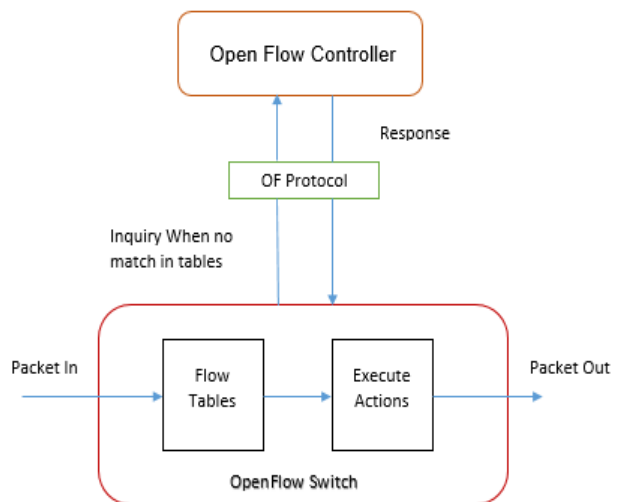


Fig 3 : Open Flow working structure

It supports arbitrary custom topologies and basic parametric topologies. Also provides a straight-forward approach and extensible Python API for the network creation and experimentation. The MiniNet network runs the real code in the network application, Linux kernel and the network stack.

POX Controller

POX is the upgraded Python based version of NOX controller [12]. It is an open source controller. It has a high level for query-able topology and support for virtualization. It was initially used as an OpenFlow(OF) controller but now it is used as a switch too. It provides reusable components, path selection, topology discovery, load balancing etc. It is the default controller used when a controller is evoked in Mininet software. It supports Graphic User Interface (GUI) and visualization tools.

Its architecture is simple compared to other controllers as in figure 4. The communication between the controller and the switches is using OF protocol. The OF switches behave just like forwarding devices. They perform only on the instruction from the controller. When the switch is ON, at the next instant it will immediately connect with the controller. Each switch has its own flow table. Initially they are empty.

At the arrival of a packet, the switch sends a Packet-in message to the controller. Then the controller inserts flow entry in the flow table of the switch regarding how to handle the packet. The flow entry has 3 parts: rule, action and counters. So as each packet passes a flow entry is installed in the switch such that it may be able to handle the packet without the intervention of the controller. If the flow entries do not match with the one in the controller, it sends a response to discard the packet.

The benefits of using POX is that it needs less memory space to operate unlike other controllers but has low throughput performance when compared with other controllers.

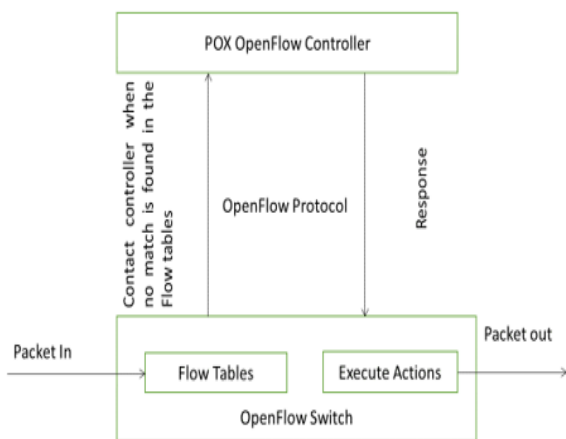


Fig 4 : POX Controller architecture

D-ITG

D-ITG (Distributed Internet Traffic Generator) is a platform that can generate traffic which adheres to the patterns where the inter departure time of the packets and the packet size can be defined [9]. It supports a lot of probability distribution like Pareto, Cauchy, Poisson, Normal and Gamma. It also supports a wide number of protocols like: TCP, UDP, ICMP, Telnet and VoIP. The users can obtain the details of the flow of packet like the One-Way-Delay(OWD), Round-Trip-Time (RTT), packet loss, Jitter and the throughput measurement. It also permits the users to set the Type of Service(TOS) and the Time to Live(TTL) of the packet

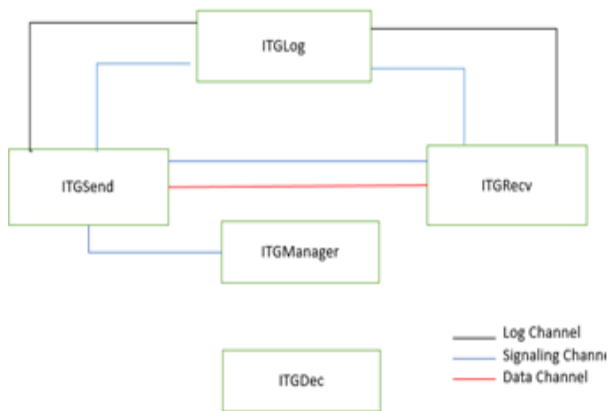


Fig 5 : D-ITG Software Architecture

The D-ITG has a Distributed multi-component architecture. The figure 5 displays the software architecture of D-ITG. As it is in the architecture a separate signaling channel between the sender and receiver for communication and it is ruled by a special protocol Traffic Specification Protocol(TSP). D-ITG mainly comprises of ITGSend, ITGRecv and ITGLog. The ITGSend is the only source of traffic generation. It can operate in various modes like single flow mode, multiple flow mode and daemon mode. In single flow mode just generates a one flow.

A single thread is responsible for this flow generation and management. In multiple flow mode sets of flows are generated. It has many threads to manage flow. One among them implements the TSP while the other generates traffic flows. To collect the statistics of the flow, connect to the log host for it. ITGRecv works by listening to the TSP connections. When a connection requesting thread arrives, it generates a thread that is responsible for its communication with the sender. Each flow is received as a separate thread. ITGLog indicates a

log server running on a different host than the sender and the receiver. It is capable to receiving and storing multiple information from multiple sender's and receivers. Mostly the log information is usually sent using reliable TCP channel or rarely in unreliable UDP channel.

III. NETWORK TOPOLOGY

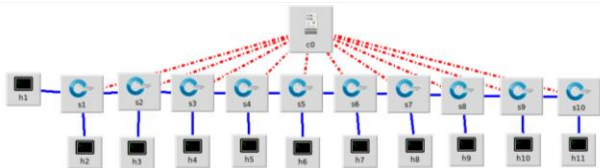


Fig 6 : The Topology of the Simulated Network

A linear topology was implemented with 10 switches and 11 hosts and all the further analysis and simulations were done using the above-mentioned topology.

IV. IMPLEMENTATION

This work mainly focusses on the performance of POX controller using Mininet software. As POX is the default controller used when a controller is evoked in for any purpose in Mininet. All the switches used here operate with OF protocol. This protocol helps it easily and effectively communicate with the controller regarding the flow. Performance evaluation of POX controller is checked. Certain parameters are deemed for testing purpose [5][15].

They are:

1. Bandwidth Utilized
2. CPU load allocation
3. Packet Loss
4. Scalability

The topology used is mostly linear topology with the size of hosts or switches increasing exponentially i.e. 5,10,15...80. or a tree topology with depth=1 and fanout=2. For test purpose the fanout is increased from 2 to 80 i.e. the number of hosts connected to the switch connected to the controller is increased exponentially.

Bandwidth Utilized

For performance analysis the bandwidth usage is also an important factor. To test the Bandwidth utilization, initially a linear topology with 80 hosts and switches can be seen in figure 6 is used. Then a bandwidth of 10Mbps is allocated and the utilized bandwidth by the switches using iPerf is recorded. Then gradually the allocated

bandwidth is increased by ten to 20Mbps and then at an exponential phase till 50 Mbps.

The simulation is run and the test results are tabulated in the Table 1 for reference.

Table 1 : Bandwidth utilized by the Network

Switch Count	Utilized BW (For allocated 10 Mbs)	Utilized BW (For allocated 20 Mbs)	Utilized BW (For allocated 30 Mbs)	Utilized BW (For allocated 40 Mbs)	Utilized BW (For allocated 50 Mbs)
1	9.388	19	27.8	35.6	40.3
10	9.366	18.3	27.9	24.3	45.6
20	9.285	18.5	27	17.3	44.6
30	9.26	18.3	26.8	31.3	37.7
40	8.946	18.1	24.5	32.4	37.4
50	8.84	17.2	22.1	28.2	40.3
60	8.796	14	24.9	27.3	38.6
70	8.28	16.9	24	24.9	36.3
80	8.11	14.5	23.1	22.6	35.1

Then the values in Table 1 is plotted as a graph as in figure 7. From the figure it can be analyzed that for 10Mbps the bandwidth utilized is minimum and constant. For 20Mbps the effective utilization is till 50 switches and for 30Mbps it is till 45 switches. At 40Mbps unlike others effective utilization of bandwidth is at 40 to 50 switches and at 50Mbps effective bandwidth utilization is at 10 to 20 switches. This brings to the conclusion that effective bandwidth utilization happens at 20 to 50 switches. After that wastage of bandwidth is detected.

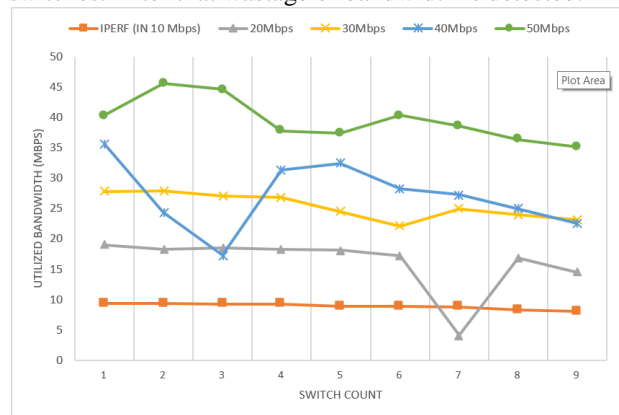


Fig 7 : Plot of Bandwidth Utilization Vs Switch count

CPU Load Allocation

This checks the efficiency of how the POX controller works depending on the amount of load given. So, for this test a Tree topology is considered as in figure

6 with depth = 1 and fanout = 2. Initially 10% of the CPU is allocated and 10×10^9 bits is sent from the controller to the Hosts. The number of bits received per second value is taken. Gradually the CPU load is increased by 10 to 20%.

From the figure 9, initially as the load is 10% the rate of bits received is less i.e. speed is less. But at 75-80% allotment better performance is achieved i.e. when maximum CPU space is allocated to CFS (Completely Fair Scheduler), maximum packets are received.

Table 2 : Packets received based on the CPU Load

CPU (% allocated)	Received Bits per Sec
10	5.90E+08
20	1.23E+09
30	1.83E+09
40	2.38E+09
50	3.50E+09
60	3.09E+09
70	4.91E+09
80	6.20E+09
90	3.50E+09
100	4.29E+09

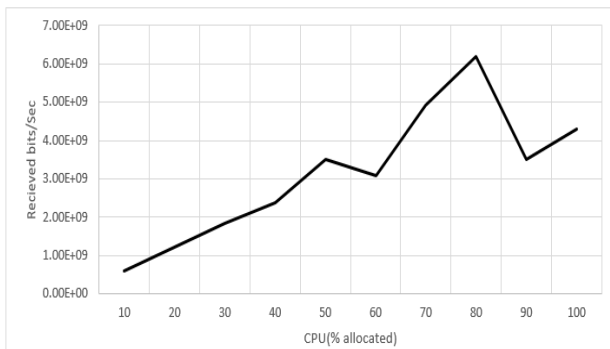


Fig 8 : Space Allocated to CPU Load Vs Received bits/sec

Packet Loss

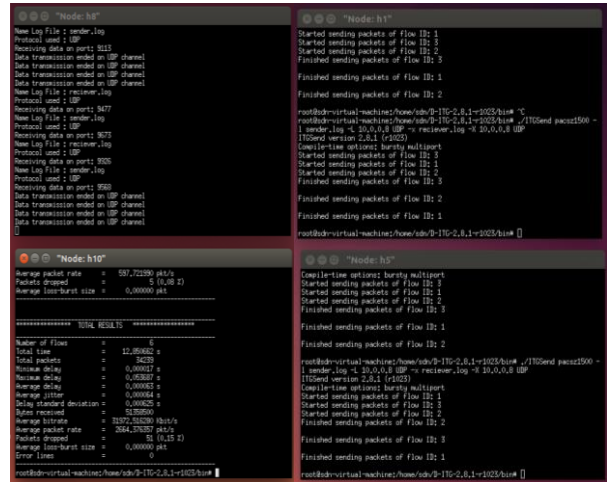


Fig 9 : D-ITG used in Linear topology

The final test is to check the Packet loss. It is an important factor when it comes efficiency of packet delivered. It also determines the networks reliability. For this a traffic generator known as D-ITG (Distributed Internet Traffic

Generator) is used. For this test a linear topology is taken into consideration with 10 hosts and switches. Here hosts h6 and h8 are the senders. Host h1 is considered as the receiver and h10 is made remote log host as in Fig 9. flows with varying the packet size from 64 to 1450 bytes are sent.

Table 3 : Packet loss based on Packet size

Packet size (Bytes)	Loss (No. of packets)
64	0
128	0
192	116
256	60
384	28
512	58
768	57
924	107
1024	81
1200	47
1450	85

From the Fig 10, at 200 and 900 bytes there is a sharp rise in the packets lost. At about 450 to 800 the packet loss is stable. After 1200 the loss is rising exponentially. Initially there is no packet loss, but from 192 there is a small loss which gradually increases

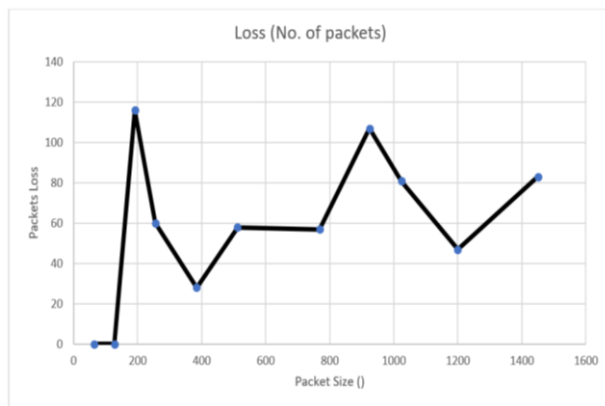


Fig 10 : Plot of Packet Size Vs Packet Loss

V. ADVANTAGES

There are certain advantages of using a Software Defined Network (SDN). The programmability of a Network is very essential to any organization where the operational costs are reduced by many folds. The existing conventional network can be expanded which in turn increases the scalability and provides the users with a lot of re-usability options.

The SDN provides a Centralized view of the entire network, making it easier to centralize enterprise management and provisioning. The SDN also provides centralized security as it can be controlled virtually.

The ability to shape and control data traffic is another advantage of using a SDN. Being able to achieve this, the Quality of Service (QoS) is increased and this system also provides flawless user experience. So content delivery is Guaranteed.

VI. CONCLUSION

This work specifically uses POX controller and evaluated its performance factors as Bandwidth utilization, CPU load and Packet Loss using iPerf and D-ITG. It was analyzed that effective bandwidth utilization happens with 20 to 50 switches in the network. When 75-80% of the CPU load is given to Completely Fair Scheduler, it performs better. The packet loss drastically increases after 1200 bytes, which makes this controller less reliable after. Mainly the SDN is a boon for data centers where large amount of data, user's and devices are handled. So, reliability, scalability, are some important parameters needed for SDN to be deployed. The latest hardware for Software Defined Network, the OpenFlow switch Zodiac FX can be deployed with POX controller.

VII. REFERENCES

- [1] Diego Kreutz, Fernando M. V. Ramos, Paulo Verissimo, Christian Esteve Rothenberg, Siamak Azodolmolky, and Steve Uhlig, "Software Defined Networking : A Comprehensive Survey," 2014, in Proceedings of the second workshop on Hot topics in software defined networks
- [2] Faris Ket, Shavan Askar," Emulation of Software Defined Networks Using MiniNet in Different Simulation Environments", 2015, 6th International Conference on intelligent Systems, Modelling and Simulation, pp 9-2,2016
- [3] Fei Hu, Qii Hao and Ke Bao, "A Survey on Software Defined Network and OpenFlow: From Concept to Implementation" in IEEE Communication surveys & Tutorials,vol.16,No.4,Fourth Quarter 2014
- [4] Fetia Bannour, Sami Souihi and Abdelhamid Mellouk, "Distributed SDN Control: Survey, Taxonomy and Challenges," 2017, in Proceedings of the IEEE Communications Surveys & Tutorials •
- [5] Madhukrishna Priyadarshini, Padmalochan Bera and Rohan Bhampal, "Performance Analysis of Software Defined Network Controller Architecture- A Simulation Based survey" presented in IEEE WiSPNET 2017 conference
- [6] S. Sezer, S. Scott-Hayward, P. Chouhan, B. Fraser, D. Lake, J. Finnegan,N. Viljoen, M. Miller, and N. Rao, "Are we ready for sdn? Implementation challenges for software-defined networks," CommunicationsMagazine, IEEE, vol. 51, no. 7, pp. 36–43, 2013.
- [7] Rogerio Leao Santos de Oliveria, Christiane Maire Schweitzer, Ailton Akira Shinoda, Ligia Rodrigues Prete," Using mininet emulation and prototyping Software Defined networks", 2014, IEEE Colombian Conference on Communication and Computing(COLCOM), pp 4-6,2014
- [8] The Openflow Switch, openflowswitch.org.
- [9] S.Avallone, S.Guadagno, D.Emma and A.Pescape," D-ITG Distributed Internet Traffic Generator," 2014, Proceedings of the First international conference on Quantitative Evaluation of Systems (QEST'04).
- [10] Saleh Asadollahi, Bhargavi Goswami and Mohammed Sameer," Ryu Controller's Scalability Experiment on Software Defined Networks", 2016, 7th International Conference on intelligent Systems, Modelling and Simulation, pp 9-2,2017
- [11] Semaliansky R.L, "SDN for Network Security", 2014 IEEE International Conference.

- [12] N. Gude, T. Kopenon, J. Pettit, B. Pfaff, M. Casado, N. McKeown, and S. Shenker. "Nox: towards an operating system for networks". ACM SIGCOMM Computer Communication Review, 38(3):105-110, 2008
- [13] Sukhveer Kaur, Japinder Singh and Navtej Singh Ghumman," Network Programmability Using POX controller", 2015, proceedings of First International Conference on Communication, Computing and Systems (ICCCS-2014)
- [14] W. Han, H. Hu, and G.-J. Ahn, "LPM: Layered policy management for software-defined networks," Data and Applications Security and Privacy XXVIII. Berlin, Germany: Springer-Verlag, 2014
- [15] Zuhran Khan, Muhammad Awais and Adan Iqbal," Performance Evaluation of OpenDayLight SDN Controller", 2014, 5th International Conference on intelligent Systems, Modelling and Simulation, pp 5-2,2015

An Experimental Investigation on Mechanical Properties of Mixed Synthetic Fiber Reinforced Concrete

^[1]G.Gopala Krishna, ^[2] A.S. SwethaSri, ^[3] P. Ravi Kishore

^[1] P.G. Student, Department of Civil Engineering, Aditya Engineering College (A), Surampalem

^{[2][3]} Assistant Professor, Department of Civil Engineering, Aditya Engineering College (A), Surampalem

Abstract:-- There is a tremendous demand for concrete which is highly workable and durable. As a result plain cement concrete is brittle in nature and weak in tensile strength there is no minimum resistance to cracking. In order to overcome deficiencies in concrete to increase performance of concrete fibers were added.

This project aims to study the synthetic fibers consisting of three different fiber combinations i.e. Polypropylene, HDPE, Recorn 3s. The objective of this study is investigating the mechanical properties of concrete containing fibers. The properties that were studied includes workability of fresh concrete mix also. The addition of synthetic fibers in concrete is by 0%, 0.25%, 0.5%, 0.75%, and 1% by volume of cement. These fibers are used in concrete to increase strength of the reinforced concrete.

In present work, attempt is made to see effects of fibers on compressive strength, split tensile strength and flexural strength of 3 days, 7 days and 28 days is compared with the strengths of nominal mix concrete of grade M40 with percentage variation along with orientation in plain concrete.

Index Terms : Concrete, Fibre, Recorn 3s, Polypropylene, HDPE, Compressive Strength Test, Split Tensile Strength, Flexural Strength Tests

1. INTRODUCTION

Concrete is used as building material, but fragile concrete has a disadvantage of relatively low tensile strength, low resistance to cracking and propagation, and weak tension. Under some assumptions, deformed reinforcing bars or pre-stressed tendons are provided in concrete to improve margins (RCC). It can usually be reinforced with a stronger material.

Tension defects in plastic cement concrete and hardened concrete can be overcome by using existing reinforcing steel reinforcements and by including a sufficient amount of specific fibers. So we are using fibers as secondary reinforcements.

Fiber reinforced concrete (FRC) is a concrete containing fibrous material that increases the structural integrity of concrete. It contains a uniform distribution and randomly oriented short discrete fibers. Fiber is a reinforcing material. A fiber is a small piece of stiffener with certain characteristics. Fiber is a building material to increase flexural and tensile strength and is considered a binder that can combine Portland cement and cement matrix. Fibers include steel fibers, glass fibers, synthetic fibers and natural fibers. The characteristics of fiber-reinforced concrete also depend on the various concrete, fiber materials, geometry, distribution, direction and density. Fiber is a small stiffener with specific properties. It can

be round or flat. Fiber is often described as a convenient parameter called "aspect ratio". The aspect ratio of fibers is the ratio of length to diameter. Typical aspect ratios range from 30 to 150.

DIFFERENT TYPES OF FIBRES :

SFRC - Steel Fiber Reinforced Concrete

GFRC - Glass Fiber Reinforced Concrete

SNFRC - Synthetic Fiber Reinforced Concrete

NFRC - Natural Fiber Reinforced Concrete

Why should we use Synthetic Fibers?

Fibers benefit the concrete in both the plastic and hardened state includes:-

Plastic precipitate crack reduction

Plastic shrinkage crack reduction

Low permeability

Increased impact and abrasion resistance

Providing shatter resistance.

Synthetic fiber work on hardened concrete: Synthetic fiber specially designed for concrete prevents the crushing force by tightly binding the concrete. When synthetic fiber is used, the water cement ratio becomes uniform bleeding because it gives abrasion resistance. Synthetic fiber reduces plastic cracking of concrete. This improves the impact resistance of concrete. The relatively low coefficient of synthetic fibers provides shock absorption properties. Synthetic fibers help the

concrete develop optimum long-term shelf life with reduced plastic settling and shrinkage crack formation, reduced permeability and increased resistance to abrasion. Shatter and impact force. Synthetic fibers are compatible with all mixtures of silica fume and cement chemicals.

II. LITERATURE REVIEW:

Konapure and Kalyankar (2015). In this study aims to investigate the normal mixing of HFRC such as basalt fiber reinforced concrete (BFRC) and polypropylene fiber (PP). Adding 0.5% fiber slightly increases the compressive strength and bending strength of the concrete. Flexural strength is improved for 0.5% fibers and decreased for 1% fibers. This may be due to the fibrillated nature of basalt and polypropylene fibers affecting the homogeneity of the concrete.

Harish and Anandh (2015). An overview of this paper on M20 grade concrete using various combinations of hybrid fibers, namely coconut fibers and recron fibers. Overall test results showing maximum compressive strength and tensile strength are achieved when the fiber content is 1% for coconut fibers and 1% for recron fibers.

Leshma (2015). In this document author studied, steel and synthetic fibers (polypropylene) are used to highlight the HFRC of the outer beam. M40 grade concrete was used. The compressive strength of the HFRC reached a maximum at 0.38% ST & 0.12% PP volume fraction and was 7.5% higher than SFRC.

Sudarshan, Manjulavani, V Bhikshma (2015). In this study, we wanted to investigate HDPE (High Density Polyethylene Fiber Reinforced Concrete) for M30 grade concrete. The percentage of HDPE considered in this experiment is 0-6%. A series of test blends were conducted for the investigation to achieve the desired target strength of the various proportions of HDPE concrete. Mechanical properties are evaluated for all percentages.

High-density polyethylene concrete has shown a slight improvement in all properties compared to conventional concrete. HDPE fibers are mainly derived from cement bags and require 50 bags of one layer of HDPE fiber-reinforced concrete, Sexual waste is gone. The volume of the fibers is 3.0%.

III. MATERIAL USED:

- 1)Cement: OPC 53 Grade Deccan cement was used for this experiment..
- 2)Fine Aggregate: used in this investigation was clean river sand and the tests was carried out in sand according to IS. 2386:1968. Fine adjustment sizes less than 4.75 mm are considered fine aggregates.
- 3)Coarse Aggregate: A dry angular coarse aggregate of 20 mm maximum size and 10 mm minimum size was used for experimental work.
- 4)Water: Water is an important ingredient in concrete because it is actively involved in chemical reactions with cement. This is due to the strength imparted to the cement gel and the workability of the concrete.
- 5)Recorn 3s: Recron-3 is a discrete discontinuous staple fiber that can be used for concrete to suppress and inhibit cracks. Recorn 3s is the incorporation of discontinuous and discrete staple fibers into the concrete matrix that provides a multipoint secondary reinforcement, distributed at random, resulting in three-dimensional crack control and a crack-arrest mechanism.

Table 1: Recorn 3s properties

Recorn 3s Fiber	Cut length	6mm
	Diameter	0.04mm
	Tensile strength	4000-6000 kg/cm ²
	Aspect ratio	150
	Specific gravity	1.34-1.40 cc/g
	Melting point	> 250 ^o C
	Elongation	>100%



Fig1: Recron 3s

6) Polypropylene:

Polypropylene is a tough and rigid, crystalline thermoplastic produced from propene (or propylene) monomer. It is a linear hydrocarbon resin. The chemical formula of polypropylene is (C3H6)n. PP is among the cheapest plastics available today.

Table 2: Properties of polypropylene fibers

Diameter (D) mm	Length (l) mm	Aspect Ratio (l/D)	Tensile Strength Mpa	Specific gravity
0.0445	6.20	139.33	308	1.33



Fig.2: Polypropylene

7) HDPE: High density polyethylene is a polyethylene thermoplastic made from petroleum. When used for pipes, it is sometimes referred to as "alkathene" or "polythene".

Table 3: HDPE properties

HDPE Fiber	Density	970 Kg/m ³
	Diameter	0.40mm
	Tensile strength	50-71 Ksi
	Elasticity Modulus	725 Ksi
	Water absorption	Nil
	Aspect ratio (30mm)	75



Fig3: HDPE

IV. TABLES, RESULTS & GRAPHS

Table 1: Compressive Strength Test

S. no	Fiber percent age	3 days Compressive strength (N/mm ²)	7 days Compressive strength (N/mm ²)	28 days Compressive strength (N/mm ²)
1	0 %	18.46	32.56	49.53
2	0.25%	19.63	33.27	51.03
3	0.5%	20.78	33.75	51.93
4	0.75%	21.98	36.86	53.64
5	1%	19.18	32.19	50.46

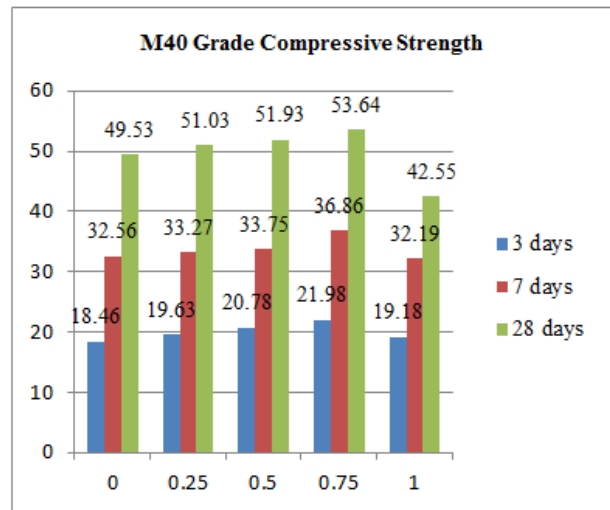


Fig .4: Graph of Compressive Strength Test

Table 2: Split Tensile Strength Test

S.no	Fiber percent age	3 days Split Tensile Strength (N/mm ²)	7 days Split Tensile Strength (N/mm ²)	28 day Split Tensile Strength (N/mm ²)
1	0	1.43	2.5	3.19
2	0.25	1.56	2.59	3.70
3	0.5	1.87	2.91	3.83
4	0.75	2.04	3.28	4.27
5	1	1.59	2.60	3.62

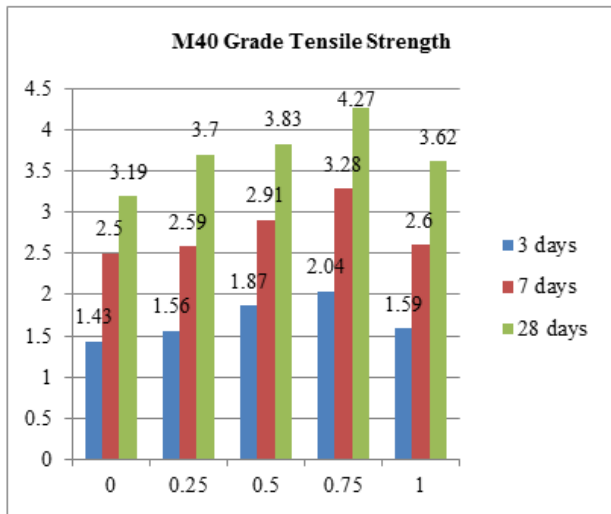


Fig 5: Graph of Split Tensile Strength Test

Table 3: Flexural Strength Test

S.no	Fibers Percentage	3 days Flexural tensile strength (N/mm ²)	7 days Flexural tensile strength (N/mm ²)	28 days Flexural tensile strength (N/mm ²)
1	0%	2.07	3.19	4.81
2	0.25%	2.86	4.31	5.34
3	0.5%	3.43	4.89	6.33
4	0.75%	3.04	4.46	5.87
5	1%	2.27	3.93	5.28

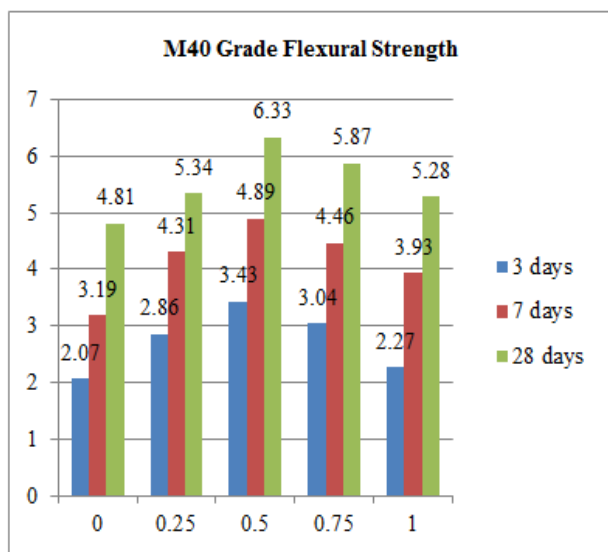


Fig 6: Graph of Flexural Strength Test

V. CONCLUSION:

1. An observational study on cubes, cylinders, beams for Compressive Strength, Split tensile Strength and flexural Strength respectively by mixing of Polypropylene, HDPE and Recorn 3s fibers.
2. Based on the investigation the following conclusions are drawn they are:
3. From the results, it was found that the fibers of optimum strength were 0.75% in compressive strength and split tensile strength. 0.5% in the flexural strength test.
4. The use of 0.75% of fibers is the optimal combination to achieve the desired need.
5. The use of fibers improves durability by reducing maintenance cracks by reducing micro cracks and permeability. The use of Recron3s fibers has been shown to reduce segregation.
6. Compressive strength shows an increase of 7.66% compared to ordinary concrete.
7. The split tensile strength of fibers was increased at 0.75%.
8. Split tensile strength shows an increase of 25.29% compared to conventional concrete.
9. The flexural strength of fibers were increased at 0.5%.
10. Flexural strength increased by 24.01% compared to conventional concrete.
11. It has been found that cracking during split tensile testing is slower than conventional concrete. This shows that synthetic fibers are better in avoiding propagation of cracks.
12. Research on Pozzolanic materials and fibers is still limited. But it promises a great range for future research. The following aspects are considered for the following study and survey.
13. While testing the specimens, the plain cement concrete specimens have shown a typical crack propagation pattern which led into splitting of beam in two piece geometry. But due to addition of fibers to the concrete cracks eliminates the cracks that lead to ductile behavior of the fibrous concrete.

VI. SCOPE OF STUDY:

Usage of fibers is satisfying the flexural values and addition of Polypropylene, HDPE, and Recorn 3s with respect to cement is giving high early strength properties. Fibers is proven performance in various experiments and comes in various lengths to suit applications. By usage of

fibers in practical experiments gives enhanced durability to whole structure and increases the bonding strength completely. By using these materials in practically results from flexural are completely satisfied. In construction of tanks and pavements gives best results in construction industry. Further the chemical reactions and elevated temperatures are studied like very low permeability to chloride and water intrusion to structures.

REFERENCES

1. Konapure and Kalyankar, "Effect of Basalt and Polypropylene Fibers on Hybrid Fiber Reinforced Concrete", International Journal Current engineering and technology. Vol.04, Issue No.4, E-ISSN: 2277-4106, P-ISSN 2347-5161, 2015.
2. Harish Kumar and Anandh., "Bond behavior of coconut fiber and recron 3s fiber in concrete", IJRET: Journal of Engineering Technology, Vol.04, Issue No.04, eISSN: 2319-1163, pISSN: 2321-7308, 2015.
3. Leshma.K.R. "Experimental Investigation on Hybrid Fibre Reinforced Concrete Exterior Beam Subjected to Monotonic Loading", International Journal of Science and Engineering Research , Vol 3, Issue No.04 , pp.3221 -5687, 2015.
4. Anand S, Leeladhar Pammar., "Experimental Study on Hybrid Fiber Reinforced Concrete Structures", International Association for Science and Technology Innovation (ISO 3297: 2007 Certification Organization) Vol. 5, Special Issue 9, May 2016 By copyright Lee MyungBak: 10.15680 / IJIRSET.2016.0505510 59.
5. Ramesh. Bhaskar1, rudhvirajnaidu3., "A Review on Various Fiber Reinforced Self - Compacting Concrete" International Journal of Applied Mathematics, Vol.19 No.117 2018, 2771-2783.
6. AkimChoudappaYallappa,MarabathinaMaheswaraRao,VinodNagpue,"Experimentl Study of Recron 3s Fiber Reinforced Concrete", International Journal of Engineering and Development Emerging Trends, Issue 5, Vol. 6 (October-November 2015) ISSN 2249-6149.
7. Rudraswamy MP, BR Patagundi, KB Prakash, "Ductility Behavior of Hybrid Fiber Reinforced Concrete Using Different Aspect Ratio Fiber," Journal of Civil Engineering and Technology (IJCIET) Vol.9.
8. Thisnkat Narsimha Rao, M Mahesh, ChSatya Sri, "Recon Fiber Reinforced Concrete Pavements", 2016 IJEDR | 4, Issue 4 | ISSN: 2321-9939.
9. Sudarshan, Manjulavani, V Bhikshma, "Strength Properties of High Density Concrete".IJRET: International Journal of Engineering and Technology Studies eISSN: 2319-1163 | pISSN: 2321-7308

Experimental Study of Geopolymer Concrete by Addition of Nano-Silica and Steel Fiber

^[1] Nitesh Kumar Yadav, ^[2] A. Satish Kumar, ^[3] P. Ravi Kishore

^[1] P.G. Student, Department of Civil Engineering, Aditya Engineering College (A), Surampalem

^{[2][3]} Assistant Professor, Department of Civil Engineering, Aditya Engineering College (A), Surampalem

Abstract:-- Geopolymer concrete an innovative material that is characterized by long chains or networks of inorganic molecules is a potential alternative to conventional Portland cement concrete for use in transportation infrastructure construction. It relies on minimally processed natural materials or industrial by products to significantly reduce its carbon footprint, while also being very resistant to many of the durability issues that can plague conventional concrete.

However, the development of this material is still in its infancy, and a number of advancements are still needed. This briefly describes geopolymer concrete materials and explores some of their strengths, weaknesses, and potential applications. In this paper we discuss the strength and behaviour of geopolymer concrete.

In the present study, a geopolymer concrete of M35 grade is considered and addition of nano-silica at 1%, 2% and 3% respectively and steel fiber at 0.5%, 1% and 1.5% respectively to percentage of cement for testing the compression and split tensile strength at 7th and 28th days and the durability of the fiber added concrete is checked by Electro-Chemical Corrosion Test.

Index Terms : Geopolymer concrete, sodium hydroxide (NaOH) , sodium silicate (Na₂SiO₃) , Hooked end Steel fiber reinforced concrete, accelerated corrosion.

1. INTRODUCTION

Geopolymers are a group of materials that are manufactured from an alumino silicate mixture and an alkaline solution. They have a wide variety of uses and advantages over OPC. Alternative binders to OPC including geopolymers belong to the Alkali Activated Materials (AAM) group. A major advantage of using geopolymers and AAM over OPC is an increase in durability. Cements analyzed from Egyptian and Roman structures are shown to have crystalline zeolitic phases in addition to the OPC like hydrates. These crystalline phases are one of the reasons why researchers believe that ancient cement was so much more durable to modern cement. This durability comes from the three dimensional polymeric chain and ring structure of the alumino silicates. Unlike cement, water is not used in the reaction of the alumino silicates; instead water is evaporated out during the curing process. Applications for geopolymer cements stem from their high heat tolerance, affordability and reduced environmental impact.

1.1 Research significance

The aim of the project work is to use the Geopolymer concrete with Nano-silica and Hooked End Steel Fiber.

The objective of the study is to add the Nano- silica with Geopolymer solution , Al₂O₃ and Steel Fiber to the concrete and to study the strength properties of concrete with the variation in Nano-silica content. i.e., to study the

strength properties of concrete (M35 Grade) of 0%, 1%, 2% and 3% at 7 and 28 days. To the optimum obtained, steel fibers are added at 0%, 0.5%, 1%, 1.5% to the study the strength properties at 7 and 28 days. The strength properties being studied are as follows:

1. Compressive strength.
2. Split Tensile Strength.
3. Corrosion resistance Test.

1.2 Scope of work

This study is limited to investigate the compressive strength , split Tensile Strength and corrosion resistance of the Nano-silica and steel fiber concrete cubes. Variation in Nano-silica content. i.e., to study the strength properties of concrete (M35 Grade) of 0%, 1%, 2% and 3% at 7 and 28 days. Later on getting strength , addition of steel fiber of 0%, 0.5%, 1%, 1.5% at 7 and 28 days are used.

2. TEST MATERIALS

2.1 Materials

The materials used in this present work are steel fiber, Ordinary Portland cement (53 grade), coarse aggregates and fine aggregates and Geopolymer solution.

2.2 Cement

Cement is a binder, a substance that hardens and sets and can bind other materials together. It is used in construction and it can be characterized as being either non hydraulic or hydraulic, depending upon the ability of the cement to be used in the presence of water.

2.3 Aggregates

Crushed granite was used as coarse aggregate passing through 20 mm having specific gravity of 2.62 and water absorption is 0.45. The fine aggregate has specific gravity 2.44 and water absorption 1.

2.4 Steel fiber

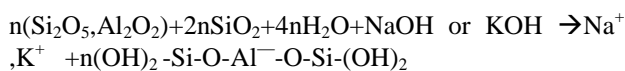
Steel wire fibers are dispersed randomly in the cement concrete can lessen or even supplant traditional rebar and welded reinforcement which expands the rigidity or tensile strength. It can be connected in modern industrial floors, street roads, strip foundation, street surfacing, bridge spans and different developments with standard basic requests. Steel fibers of 4mm width and 50mm length are utilized.



Figure 1: Hooked end steel fiber

2.5 Geopolymer solution

Geopolymer concrete is prepared by addition of Activating solution (NaOH + Na₂SiO₃) and (Al₂O₃)₂ subsequently Polymerizes into molecular change and become the binders. The polymerization process involves a substantially fast chemical reaction under alkaline conditions results in a three-dimensional polymeric chain and ring structures with the materials must often considers for using transportation infrastructure typically having an Si:Al between 2 and 3.5.



The temperature during curing is very important, and depending upon the source materials and activating solution, heat often must be applied to facilitate polymerization, although some systems have been developed that are designed to be curing at 100°C temperature.

3. EXPERIMENTAL TESTING PROCEDURE

3.1 Accelerated corrosion process

The electro chemical procedure of Corrosion test for steel is finished with various responses happening at the anodic and cathodic destinations. A supply of oxygen and water is required to keep up the response. In new cement concrete the pores solution pH is around 12.5. In these conditions a steady oxide "passive" layer is formed

on the surface of the steel which gives assurance from corrosion. In the event that the cement concrete carbonates to the depth of the steel as well as chlorides are available at above threshold limit the insurance can be traded off.

All specimens were put in the tank containing salt solution and associated with the positive end of the power supply at titanium poles utilizing copper core cable. The negative connection of the circuit was given utilizing a bit of exposed steel electrode partly submerged in the arranged solution. Figures demonstrate the accelerated corrosion test setup. A consistent 16A current was gone through the NaCl solution and samples for 45 days. In this arrangement plan steel fibers went about as an expending anode to keep up the present course through the concrete samples.

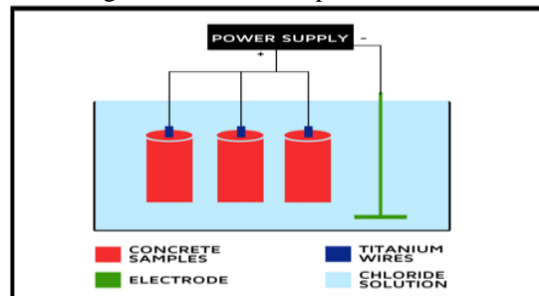


Figure 2: Schematic diagram of the accelerated corrosion test used

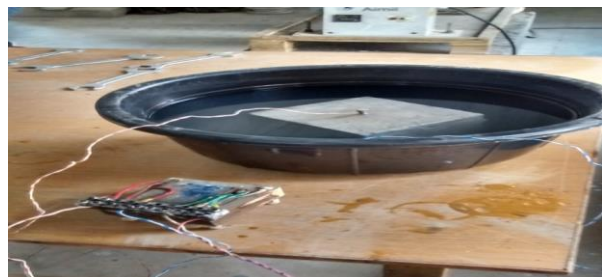


Figure 3: Accelerated Corrosion apparatus

3.2 Compressive strength

Compressive strength of cement is a standout the most critical and valuable properties of cement. In structural applications concrete is utilized principally to oppose compressive stress. In those situations strength in tension or in shear is of essential significance, the compressive strength is utilized as a measure for these properties. Along these lines, the concrete making properties of different ingredients of mix are typically measured in the terms of compressive quality.



Figure 4: Compression testing machine

3.3 Split Tensile Strength

For Split Tensile strength test, a cylindrical barrel sample of measurement 150 mm diameter across and 300 mm length were cast. The casted samples were demoulded following after 24 hours of casting and were cured in curing tank wherein they were permitted to cure for 7 and 28 days. These examples were tested under (CTM) compression testing machine. In every classification three Cylinder barrels samples were tested and their mean average value is taken. Split Tensile quality was computed as takes after as split elasticity:

Split Tensile quality (MPa) = $2P/\pi DL$, Where, P = , D = distance across of chamber, L = length of chamber

4. RESULTS AND DISCUSSIONS

The present experimental study is carried out to find out the workability, compressive strength, Split Tensile Strength and corrosion resistance of 150mm*150mm*150mm cubes for different ratios of Nano-silica and steel fiber to the cement. The cubes are tested for compressive strength and Split Tensile Strength at 7 days, 28 days. The compressive strength and Split Tensile Strength values are taken as the average of the three test results. The results of compressive strength and Split Tensile Strength of specimens are presented in the tabular forms. Also the graphical representation of compressive strength and Split Tensile Strength of concrete cubes of various mixes is also presented. The cubes are immersed in NaCl solution and current is passed 48 hour duration and the compressive strength and Split Tensile Strength is reported in tabular form and the graphical representations for various ratios are presented.

4.1 Compressive strength of percentage of Nano-silica

Chart 2: Variation of Compressive Strength gives the higher strength for percentage of Nano-silica for 7 and 28 days

4.2 Compressive Strength gives the higher strength for percentage of Nano-silica and steel fiber for 7, 28 days

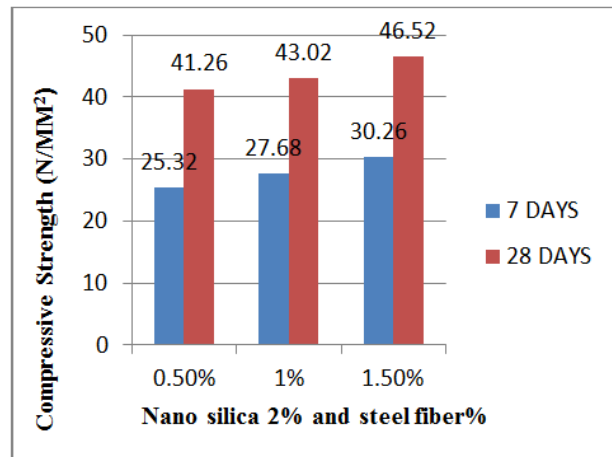


Chart 3 Variation of Compressive Strength gives the higher strength for percentage of Nano-silica and steel fiber for 7, 28 days

4.3 Split Tensile Strength result for 7 and 28 days

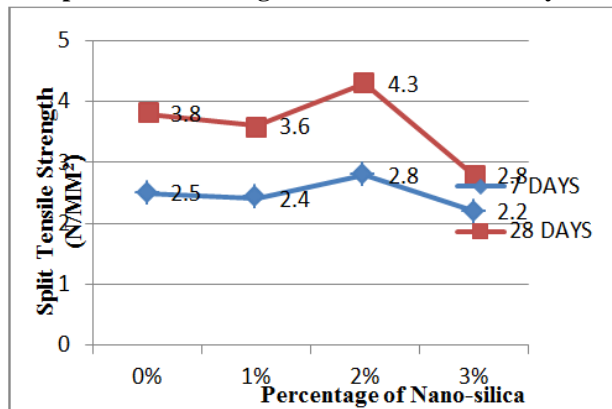


Chart 4: Variation of Split tensile Strength gives the higher strength for the different percentage of Nano-silica for 7 and 28 days of the specimens.

4.4 Split Tensile Strength result for 7 and 28 days

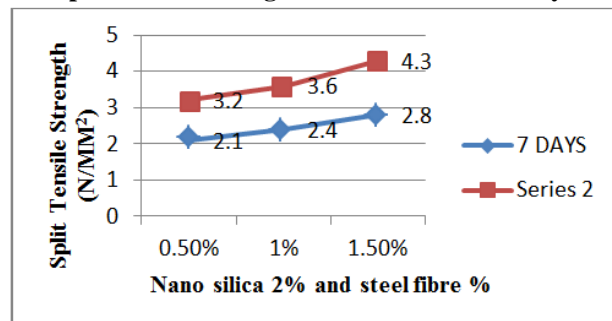


Chart 5: Variation of Split tensile Strength gives the higher strength for the different percentage of Nano-silica for 7 and 28 days

4.5 Compressive strength for steel fiber and accelerated corrosion

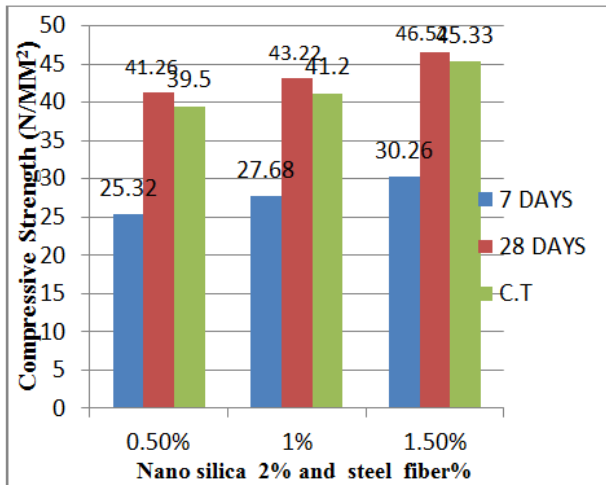


Chart 6: Variation of compressive Strength gives the higher strength for the different percentage of Nano-silica and accelerated corrosion for 7 , 28 days

5. CONCLUSIONS

1. The current experimental procedure Utilized for accelerate corrosion in steel fiber reinforced concrete which can be considered as a good technique to implement corrosion in concrete specimens in a small period of time.
2. Steel fibers appear to present less damage than the normal steel bar used normally in corrosion tests.
3. It is observed that the workability of steel fiber reinforced concrete gets reduced as the percentage of steel fibers increases.
4. From compression behavior of corrosion steel fiber concrete it was observed that the performance of specimens was not much influenced by corrosion attack. This has very less influence on the compressive strength of the specimens.
5. From Split Tensile behavior of corrosion steel fiber concrete it was observed that the performance of specimens was not much influenced by corrosion attack. This has very less influence on the Split Tensile strength of the specimens.
6. Steel fiber reinforced concrete has very slight decrease in compressive strength and Split tensile Strength after conducting accelerated corrosion test at 1.5% dosage of steel fiber due to discontinuity of fibers. Hence it is preferable to use 1.5% dosage of steel fibers to decrease corrosion effect
7. Geopolymer concrete exhibited higher compressive strength when compared to ordinary Portland concrete.

8. In medium grade Geopolymer concrete NaOH plays a vital role in attaining strength, in view of trials and cost parameter 12M is recommended as optimum molarity for NaOH.

9. The reaction of Nano Silica is extremely slow during ambient temperatures, subsequently heat curing is recommended for Nano Silica based Geopolymer concrete in order to achieve higher strength at early age.

10. Geopolymer concrete has gained strength in contradiction to loss of weight in case of ordinary Portland concrete, post exposure to aggressive environment.

11. Geopolymer concrete exhibited superior performance in terms of mechanical properties and durability in aggressive environment when compared to ordinary Portland concrete.

12. Compressive strength of Geopolymer concrete is comparatively higher than ordinary concrete for the same grade of concrete. It is also observed that the 7 days compressive strength is almost equals to two third of 28 days strength which supports the application of this concrete.

13. When compared with flexural strength for M35 grade normal concrete estimated as per IS456 : 2000, the flexural strength of GPC is 3.31 N/mm² which is marginally less than the estimated value.

14. The temperature resistance of Geopolymer concrete is very much higher and behaves good enough under 3 hours of oven curing at 200oC.

SCOPE FOR FURTHER STUDY

1. The mix done for grade M35 in this study can be extended for other grades.
2. Different alternatives to sand and coarse aggregates can be used like the materials discussed above.
3. The percentage of Sodium Hydroxide and Sodim Silicate can be varied and can be used with different alternatives of ingredients of concrete.
4. Finally it can be said that there is alot of scope for the study of sustainable concrete.

6. REFERENCE

1. Prakash R.Vora, Urmil V.Dave, “Parametric studies on compressive strength of geopolymer concrete”, science direct,2013,procedia engineering 51,pp.210-219.
2. Kolli Ramujee,M.Potharaju, development of low calcium fly ash based geopolymer concrete,IJET,2014,Vol.6, pp.1-4.

3. L. Krishnan, S.Karthikeyan, S.Nathiya, geopolymer concrete an eco- friendly construction material, IJRET, 2014, Vol.3, special issue.11, pp.164-167.
4. P.Vignesh, K.Vivek, an experimental investigation on strength parameters of fly ash based geopolymer concrete with GGBS, IRJET, 2015, Vol.2, issue.2, pp.135-142.
5. Neetu Singh, Sameer Vyas, R.P.Pathak, effect of aggressive chemical environment on durability of green geopolymer concrete, IJEIT, 2013, Vol.3, issue.4, pp.277-284.
6. Bapugouda patil, Veerendra kumar. M, Dr.H .Narendra, durability studies on sustainable geopolymer concrete, IRJET, 2015, Vol.2,
7. Milind V.Mohod⁸“Performance of steel fiber reinforced concrete”,International Journal of Engineering and ScienceISSN: 2278-4721, Vol. 1, Issue 12 (December 2012), PP 01-04.
8. Nikhil A.Gadge⁹“Mix design of fiber reinforced concrete (frc) usingslag& steel fiber”, ISSN: 2249-6645 International Journal of Modern Engineering Research (IJMER) Vol. 3, Issue. 6, Nov - Dec. 2013 pp-3863-3871.
9. Ranjitsinh K. Patil¹⁰ “Comparative study of effect of basalt, glass and steelfiber on compressive and flexural strength ofconcrete”,eISSN: 2319-1163 International Journal of Research in Engineering and Technology.
10. Tejas R Patil¹¹ “Comparative study of steel fiber reinforced over control concrete”, ISSN 2250-3153 International Journal of Scientific and Research Publications, Volume 2, Issue 5, May 2012.
11. Vikrant S. Vairagade¹²“Introduction to steel fiber reinforced concrete on engineering performance of concrete”, ISSN 2277-8616 International Journal of Scientific & Technology Research Volume 1, Issue 4, May 2012.12. Concrete technology by M.S. Shetty , S.Chand publishing company IS 10262:2009 Guidelines for mix design of concrete.

Comparative Study of the Strength Properties of the Concrete with Partial Replacement of the Coarse Aggregate with Pumice and Over Burnt Bricks

^[1] S.Anka Rao, ^[2] A. Satish Kumar, ^[3] P. Ravi Kishore

^[1] P.G. Student, Department of Civil Engineering, Aditya Engineering College (A), Surampalem

^{[2][3]} Assistant Professor, Department of Civil Engineering, Aditya Engineering College (A), Surampalem

Abstract: -- Concrete is the universally accepted material for its adverse properties with high usage of the concrete for all type of the works in the world, it leads to depletion of natural resources like river sand, and granite. Which are the components of the concrete as fine aggregate and coarse aggregate in this project M30 grade concrete is taken in which 10%,20%&30% of coarse aggregate is replaced with over burnt bricks and 10%,20%and 30% of coarse aggregate replaced with pumice by volume. And the compressive, flexural and split tensile strength properties at 7,28& 56 days and the unit weights of the concrete compared. In order to safe guard the natural resources, alternate material like over burnt bricks, pumice considered in the present project.

1. INTRODUCTION

Light weight concrete

Structural lightweight concrete has an internal density (unit weight) of 1440 ~ 1840kg / m³ compared to normal weight concrete with density of 2240 ~ 2500kg / m³. For structural use, the concrete strength must be at least 17.0 MPa. The concrete mixture is made of lightweight coarse aggregate. In some cases, some or all of the micro aggregates may be lightweight products. Lightweight aggregate used in structural lightweight concrete is a lightweight shale, clay or slate pumice material usually fired from a rotary furnace to develop a porous structure. Other products such as air-cooled blast furnace slag and hematite are also used. There is a different class of unstructured lightweight concrete made from other aggregate materials and with higher air voids in cement paste matrices (eg cellular concrete). These are typically used for insulation properties. The main use of structural lightweight concrete is to reduce the dead load of concrete structures, and structural designers can reduce the size of pillars, foundations and other load bearing elements. Structural lightweight concrete mixtures can be designed to achieve similar strength to normal weight concrete. The same is true for other mechanical and endurance performance requirements. Structural lightweight concrete provides more efficient strength-to-weight ratio of structural elements. The mild cost of most lightweight concrete is offset by a reduction in the size of the structural members, reinforcement of the steel and reduction in the volume of concrete, thus reducing overall costs.

Over burnt bricks

Bricks are the most important part of development work and are used by humans for a long time. Its history dates back to the earliest times of human civilization. Many world-renowned archaeological excavations provide a wealth of information on brick usage in many parts of the world. A few years ago, bricks were made in warm places and hardened with simply sunlight. The sun-dried mud-brick hand was made and used in pre-porcelain neolithic times. The oldest brick use case was first discovered in southern Turkey. The Sumerian palace in Kish, Mesopotamia, is another excellent example of the use of ancient bricks.

The brick burned in the 5th century BC was used as part of the city of Babylon. The ancient Egyptians also used sun-dried clay bricks in world-famous sites. During the Roman Empire, the use of bricks spread throughout Europe spreading to Italy and the Byzantine area. 11th In the development work, the use of blocks spread from this land. After the great fire in London in 1666, the city was rebuilt with most of the block structures. Bricks in the United States have been used in Virginia since 1611, and Sundried bricks have been made and used centuries in Central America, especially in Mexico. Brick walls that are only visible in the mid-18th century are again popular. A beautiful example of brick was found in India in the 20th century.

Pumice stone

Pumice stone is a textural material formed from rapidly cooling viscous molten rock by trapping gas bubbles which results in a foamy whipped glass. The word pumice is derived from Latin word pumeu, that

meaning foam. It is even formed in deep undergrounds and when the magma erupts from a vent by forming the gases which leaves a frothy structure. The transformed magma is the amorphous rock or pumice. Pumice is found in various textures such as pyroclastic flows, accumulated drifts, and piles at the river banks by the action of wind. The pure pumice is obtained in a floating mass or near the shore as it saturates by sinking and near the water bodies by the action of wind. Pumice is an amorphous plentiful rock that is found all over the country where not all pumice is ideal for refining and use in industry. In ancient days many innovative techniques are adopted in concrete mixtures with pumice by Greeks and Romans. The majority of the ancient structures were built with the pumice stone. It is not a localized product by its varying characteristics. The market demand of pumice is high because of its Mohr scale hardness, purity level, whiteness and the ability of the company that mines and refines. There is an increasing demand of pumice stone particularly for water filtration, chemical spill containment, manufacturing of cement, horticulture and in pet industry.

Materials used

- 1) Cement: OPC 53 Grade Deccan cement was used for this survey. We assessed the quantity required for this work and purchased the entire quantity and stored it in the casting shop. The following tests were performed according to the IS code.
- 2) Fine aggregate: used in this investigation was clean river sand and the following test was carried out in sand according to IS: 2386-1968. Fine adjustment sizes less than 4.75 mm are considered fine aggregates.
- 3) Coarse aggregate: Dried angular coarse aggregate of 20 mm maximum sized and 10 mm minimum size locally available was used for experimental work.
- 4) Water: Water is an important ingredient in concrete because it is actively involved in chemical reactions with cement. This is due to the strength imparted to the cement gel and the workability of the concrete,
- 5) Over burnt bricks: Because many bricks are chosen for fire, many bricks are rejected or discarded due to incompatibility is an uneven form of brick created by the high temperature control of the kiln. These bricks can also be a real source of coarse aggregate.
- 6) Pumice stone: Pumice stone is a textural material formed from rapidly cooling viscous molten rock by trapping gas bubbles which results in a foamy whipped glass. The word pumice is derived from Latin word pumeu, that meaning foam.



Fig1: Over Burnt Bricks



Fig 2: pumice stone

Table 1: Composition of good brick earth

INGREDIENTS	PERCENTAGE
Silica	50-60%
Alumina	20-30%
Lime	10-15%
Magnesia	<1%
Other Ingredients	1%

Table 2: chemical composition of pumice

Oxide composition	Oxide composition
SiO ₂	71.91
Al ₂ O ₃	12.66
Fe ₂ O ₃	1.13
CaO	1.46
Mgo	0.32
Na ₂ O	3.45
K ₂ O	4.30
Calcification Ions	4.53
Specific Gravity	0.81

Mix design: in this study we are using the M30 grade mix design

V. TABLES, RESULTS & GRAPHS

Table 3: Compressive Strength Test Values for over burnt bricks:

S.No.	Over burnt bricks partially replaced (%)	Average compressive strength (N/mm ²)		
		7Days	28Days	56Days
1	0%	25.41	32.31	40.16
2	10%	39.40	49.60	46.61
3	20%	36.58	38.10	38.03
4	30%	37.19	36.43	36.32

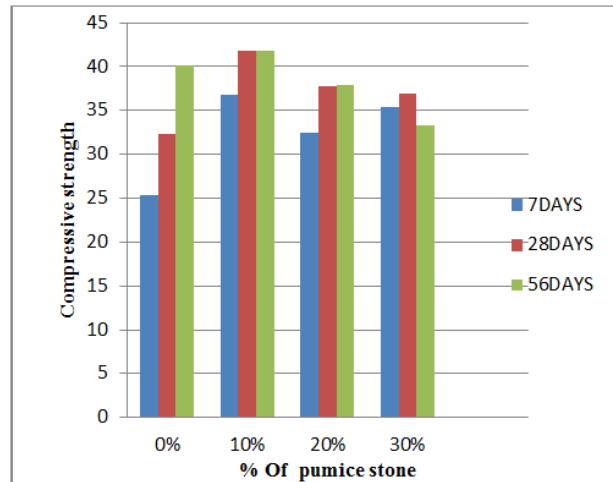


Fig 4: Variation of Compressive Strength gives the higher strength for the replacement 10% for 7, 28 and 56 days by pumice stone

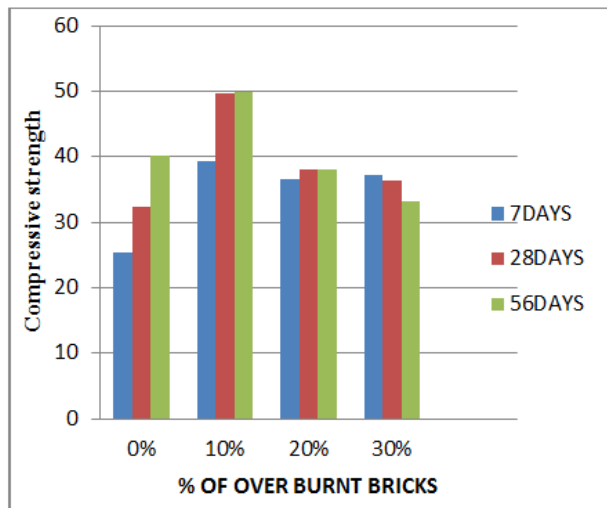


Fig 3: Variation of Compressive Strength gives the higher strength for the replacement 10% for 7, 28 and 56 days by over burnt bricks

Table 4: Compressive Strength Test Values for pumice stone:

S.No.	Pumice stone partially replaced (%)	Average compressive strength (N/mm ²)		
		7Days	28Days	56Days
1	0%	25.41	32.31	40.16
2	10%	36.79	41.85	41.78
3	20%	32.47	37.83	37.87
4	30%	35.35	36.97	33.28

Table 5: Split Tensile Strength Test Values for over burnt bricks:

S.No.	Over burnt bricks partially replaced (%)	Average split tensile strength (N/mm ²)		
		7Days	28Days	56Days
1	0%	2.15	3.68	3.76
2	10%	2.20	3.69	3.85
3	20%	1.94	3.36	3.56
4	30%	1.66	2.81	3.31

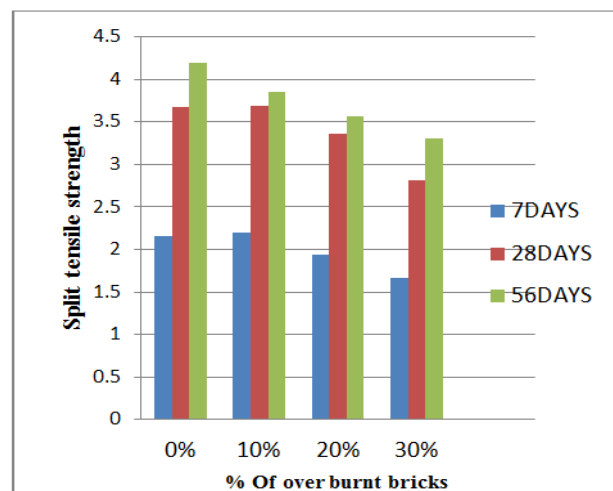


Fig 5: Variation of Split tensile Strength gives the higher strength for the replacement 10% for 7, 28, 56 days by over burnt bricks

Table 6: Split Tensile Strength Test Values for pumice stone:

S.No.	pumice stone partially replaced (%)	Average split tensile strength (N/mm ²)		
		7Days	28Days	56Days
1	0%	2.15	3.68	3.76
2	10%	2.25	3.80	3.92
3	20%	1.98	3.46	3.92
4	30%	1.69	2.89	3.44

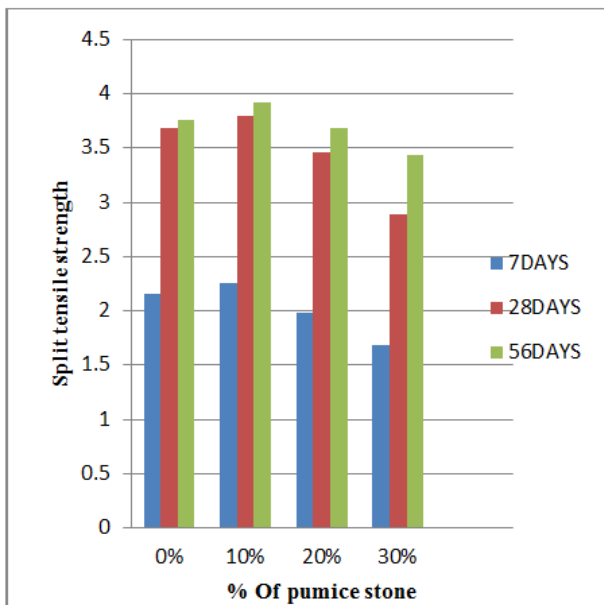


Fig 6: Variation of Split tensile Strength gives the higher strength for the replacement 10% for 7, 28, 56 days by pumice stone

Table 7: flexural Strength Test Values for over burnt bricks:

S.No.	Over burnt bricks partially replaced (%)	Average flexural strength (N/mm ²)		
		7Days	28Days	56Days
1	0%	3.10	3.88	3.94
2	10%	3.17	4.39	4.43
3	20%	2.95	4.25	4.29
4	30%	2.86	4.18	4.22

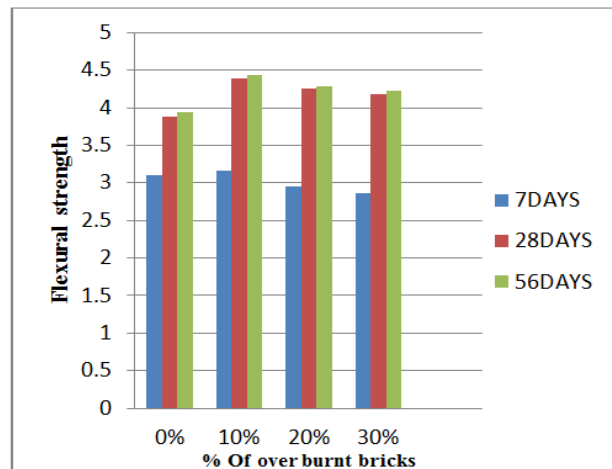


Fig 7 : Variation of Flexural Strength gives the higher strength for the replacement 10% for 7, 28, 56 days by over burnt bricks

Table 8: flexural Strength Test Values for pumice stone:

S.No.	Pumice stone partially replaced (%)	Average flexural strength (N/mm ²)		
		7Days	28Days	56Days
1	0%	3.10	3.88	3.94
2	10%	3.14	4.30	4.32
3	20%	3.01	3.88	3.96
4	30%	2.95	3.87	3.88

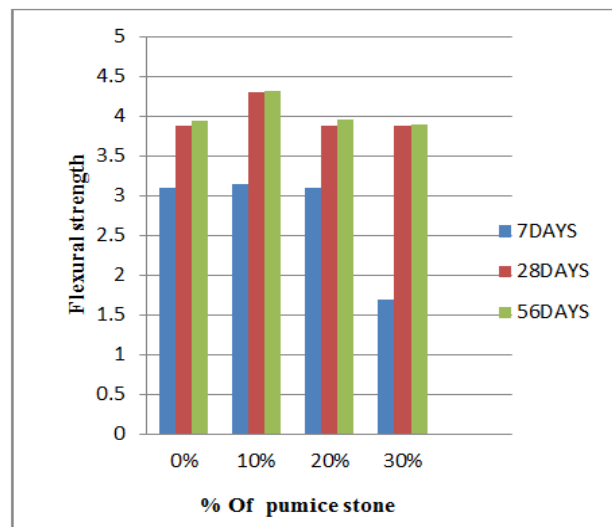


Fig 8: Variation of Flexural Strength gives the higher strength for the replacement 10% for 7, 28, 56 days by pumice stone

Comparison of over burnt brick and pumice concrete

The comparison of the both over burnt brick and pumice concrete, the 10% results are getting more. The over burnt brick concrete get more result when compared to pumice stone concrete. Like compressive strength, flexural strength and split tensile strength.

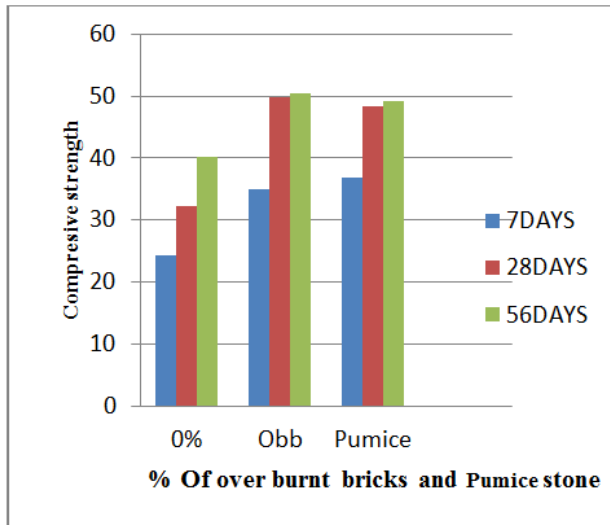


Fig 9: Comparison of compressive Strength of over burnt bricks and pumice concrete for the replacement 10% for 7, 28, 56 days

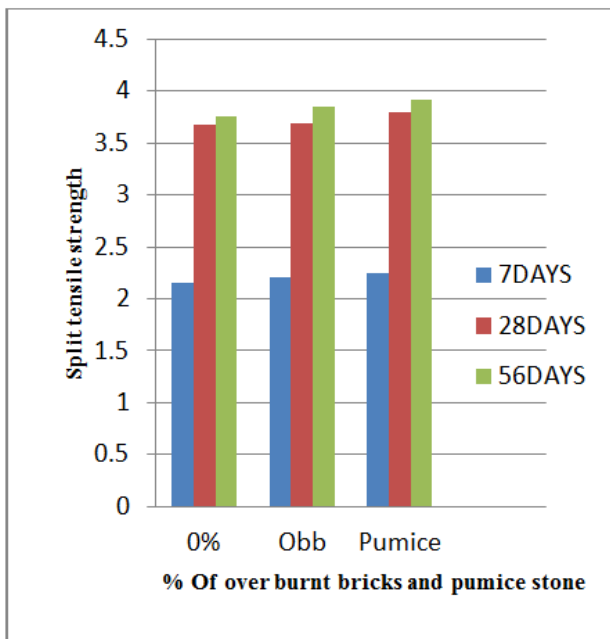


Fig 10: Comparison of split tensile Strength of over burnt bricks and pumice concrete for the replacement 10% for 7, 28, 56 days

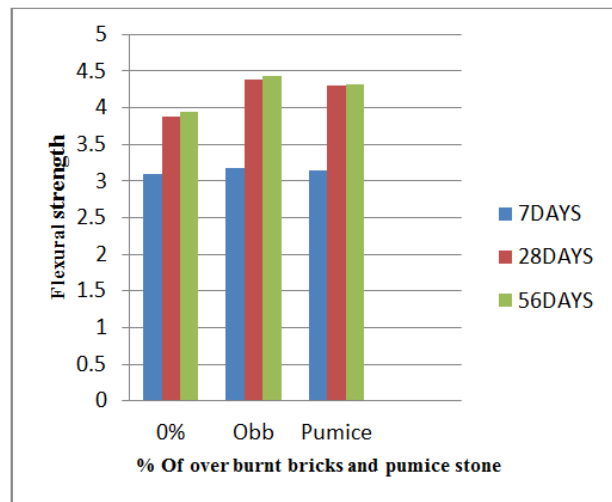


Fig 11: Comparison of flexural Strength of over burnt bricks and pumice concrete for the replacement 10% for 7, 28, 56 days

CONCLUSION

- 1) Use of over burnt bricks and pumice stone as coarse aggregate in concrete results in the increased strength properties, which may be because of the internal self curing of the over burnt bricks and pumice, which are soaked in water before mixing in concrete.
- 2) Over burnt brick aggregate is giving higher strength of 10% when compared with the pumice concrete.
- 3) Over burnt brick aggregate is giving increased percentage of compressive strength, flexural strength and split tensile strength of 10%, 20% and 30% respectively, when compared with the strength properties of the pumice concrete.
- 4) The unit weight of concrete is greatly reduced in over burnt brick concrete and pumice concrete with a percentage of 17.44%, 24.62%.
- 5) Using reduction in this self weight of the structure, there will be a lot of reduction dimensions of the structural members, as well as the material.

REFERENCES

1. G.S. Patil, Mr. P.B. Autade. Effect of partial replacement of coarse aggregate by jhama class brick in concrete, IJERGS: International Journal of Engineering Research and General Science. ISSN: 2091- 2730. Volume3, Issue 4, Part-2, July-August,2015.
2. Salman Siddique, Mohd. ShadabSiddiqui, ShariqMasoodKhan. Assessing the Scope of Utilizing Waste from Brick Production for Building Material. IJATES: International

- Journal of Advanced Technology in Engineering and Science. ISSN:2348-7550. Volume 03, Special Issue 01, May20015.
3. N.S. Apebo, M.B. Iorwus, J.C. Agunwamba, Comparative “Analysis of the Compressive Strength of concrete with Gravel and Crushed over Burnt Bricks as Coarse Aggregates. NJT: Nigreian Journal of Technology, ISSN 1115-8443, Volume 32, no. 1, March 2013,pp.7-12.
 4. IS: 383-1970. Specification for coarse and Fine Aggregates from natural sources forconcrete.
 5. IS: 10262-2009. Guidelines for concrete mix designproportioning.
 6. IS: 456-2000. Specification for plain and reinforcedConcrete.
 7. Ahmad S.I., Roy s., (2012), —Creep behavior and its prediction for normal strength concrete made from crushed clay brick as coarse aggregate. Journal of Material in Civil Engineering, Vol.-24, pp.308-314.
 8. “Effects of Different Mineral Admixtures on the Properties of Fresh Concrete”.SadaqatUllahKhan, Muhammad FadhilNuruddin, TehminaAyub, and NasirShafiq“*The Scientific WorldJournal*”2014.
 9. B.Vamsi Krishna et al., “A Study on the mechanical properties of light weight concrete by replacing coarse aggregate with (pumice) and cement with (fly ash)” *IJERT*, ISSN: 2278-0181,[Vol.4, Issue 8, August-2015 Pg.No (331-336)].
 10. Lakshmi Kumar Minapu et al., “Experimental Study on Light Weight Aggregate Concrete with Pumice Stone, Silica Fume and Fly Ash as a Partial Replacement of Coarse Aggregate.”*IJRSET*, ISSN: 2319-8753,[Vol. 3, Issue 12, December 2014].
 11. Geoffrey, et al., “Properties of Pumice Lightweight Aggregate”*IISTE*, ISSN 2222-1719 (Paper) ISSN 2222-2863 (Online) [Vol 2, No.10,2012].
 12. N. ShivalingaRao, Y.RadhaRatnaKumari, V. Bhaskar Desai, B.L.P. Swami “Fibre Reinforced Light Weight Aggregate (Natural Pumice Stone) Concrete” *International Journal of Scientific & Engineering Research*, ISSN 2229-5518Volume 4, Issue 5,May-2013]

Influence of Sisal Fibers on the Properties of Rammed Earth

^[1] P. Vinay Kumar, ^[2] M.Eswar Kumar Yadav

^[1] P.G. Student, Department of Civil Engineering, Aditya Engineering College (A), Surampalem

^[2] Assistant Professor, Department of Civil Engineering, Aditya Engineering College (A), Surampalem

Abstract:-- The use of rammed earth has been increasing widely during recent years in many countries as an alternative material for building houses due to its valuable characteristics such as affordability, environment friendly, comfort, strength and durability. This thesis presents the result of an experimental study to evaluate the compressive strength and bond strength properties of untreated, treated bamboo splints and steel reinforced cement stabilized rammed earth blocks. To overcome the deficiencies of blocks, sisal fibers are added to improve the performance of CSRE blocks. Fibers are secondary reinforced materials and acts as crack arresters which improves the strength of cement stabilized rammed earth blocks.

In this experimental study, red soil is mixed by adding four different percentages (5%, 10%, 15%, and 20%) of OPC and sisal fiber with 0.2%, 0.4%, 0.6%, 0.8%, and 1.0% by weight of soil respectively. The bamboo splints were treated by soaking them in chemical solution of boric acid, Copper -Sulphate and Potassium Di-chromate (1.5:3:4). The resin-based adhesive with coarse sand will be applied to the top of bamboo splints. After 28 days of curing period the cubes were tested for compressive strength, pull-out test is done for a series of CSRE blocks in which Bamboo splints and steel bars are embedded to find out its bond strength.

Keywords: Rammed Earth, Cement Stabilised Rammed Earth (CSRE), Sisal Fiber, Compressive Strength, Bond Strength.

1. INTRODUCTION

a) Rammed Earth: As demand for housing construction increases with affordable materials, it is best for us to choose the rammed earth, and the earth is an ancient form of monolithic earth wall construction. The use of mudguards for the application of load bearing and no-load bearing can be seen all over the world.

The properties of the rammed earth can be enhanced by physical, chemical and mechanical stabilization. Physical stabilization is achieved by the proper mix ratio material of gravel, sand and clay. Mechanical stabilization is achieved by dynamic compression using a manual hammer (or) pneumatic hammer. Chemical stabilization can be achieved by mixing chemicals such as cement and lime to improve soil properties.

Rammed earth construction can be classified into two groups: stabilized rammed earth and unstabilized rammed earth. In an unstabilized rammed earth, the soil consists of a mixture of sand, gravel, silt and clay. On the other hand, stabilized soil can be obtained by adding cement, lime, etc. to the soil. The mixture is wetted with the optimum moisture content before sanding between the molding operations. China's Great Wall of China, built about 3000 years ago, has a wide area based on Japanese Horyuji temples and rammed earth, just like the wall of the earth built about a year ago.

b) Sisal Fiber: Sisal fiber is one of the most widely used natural fibers and grows very easily. This plant starts with teeth and gradually grows, making roses with

sword-shaped leaves. Each leaf contains several long, straight fibers. While peeling, the leaves are suitable to leave behind rough fibers and to remove pulp and plant material. The fibers can be spun for the production of yarns and fabrics or can be pulped to make paper products. The sisal fiber is completely biodegradable and the green complex is made of soy protein resin modified with gelatin. Commercial use of sisal in composites has increased due to strength, low density and environmental friendliness and cost effectiveness.



Fig 1. Sisal Plant.



Fig.2 Sisal Fiber.

2. OBJECTIVE

- To identify various materials that can be used in construction as a replacement of concrete materials.
- To make the construction works eco-friendly.
- To enhance the strength of CSRE blocks by adding the Sisal fiber.
- To motivate engineers and contractors regarding the usage of natural fibers.

3. MATERIAL CHARACTERISTICS

a) Red Soil: Red soil is the most important part of the Indian land that we can look around like in TamilNadu, Karnataka, Andhra Pradesh and some parts of Madhya Pradesh, Chhattisgarh and Odisha. It is a combination of rock material and ignition part of rock and mountain. Red soils are formed by changes in the atmosphere and the properties of crystalline and metamorphic land. Soil colour is red because iron content is very high. They are found in areas with low precipitation and this colour turns red to reach the heat. There is no nitrogen, phosphorus, or organic material in Indian red soil, but the soil is rich in iron. Some of the major crops grown in our local red soil are peanuts, potatoes, millet, sorghum, palm trees, wheat, and tobacco.

Here, we first collected the soil from our environment (Peddapuram-Andhra Pradesh) and collected the soil at a depth of 0.5-1.5 m. The soil size was determined according to Indian standard 2720-1995 and the soil was exposed. After standing for 24 hours in the atmosphere, the soil was sieved and passed through an IS 4.5 sieve, then the soil was oven dried at 105 ° and subjected to a basic soil test.

Table.1: Properties of Soil Used.

Sl.No.	Property	Quantity
1	OMC (%)	19.3
2	Liquid Limit	35
3	Plastic Limit	18.21
4	Plasticity Index	16.79

b) Cement: Cement is an adhesive material used to make all types of concrete. Of the various types of cement on the market, the 53 grade ordinary Portland cement is identified as ISC 2631-1976 and the final compressive strength of 28 N / mm² as tested by the DECCAN Company in accordance with ISC 4031-1988. Used for project work. Details of the various tests for cement are as follows.

Table.2: Properties of Cement.

Sl.No.	Test Name	Results
1	Specific Gravity	3.15
2	Normal Consistency	33%
3	Initial Setting Time	55 min.
4	Final Setting Time	210 min.

c) Sisal Fiber: Sisal is a fiber obtained from the leaves of the Agave Sisalana plant. It is from Mexico and is currently being maintained and cultivated in Assam and Indonesia, East Africa, Brazil, Haiti and India.

Healthy sisal plants produce about 200-250 leaves consisting of about 1200 fiber bundles per leaf containing about 4% fiber, 0.75% cuticle, 8% dry matter and 87.25% water. Thus, normal leaves will produce about 3% w / w fiber. The sisal leaf is composed of three fibers:-

1. Mechanical, 2. Ribbon and 3. Xylem.

Mechanical fibers are mostly extracted from the edges of the leaves. They have a roughly thick horseshoe shape and almost divide during the extraction process. They are commercially most useful of Sai Fine fibers.

Ribbon fibers occur in the middle of the leaf in relation to conductive tissue. The associated conductive tissue structure of the ribbon fibers provides significant mechanical strength. They are long and can be easily

divided longitudinally during machining compared to mechanical fibers.

Xylen fibers are inaccurate in shape and are located on opposite sides of the ribbon fibers through the connections of blood vessels. It is mainly composed of thin-walled cells, which can be easily broken or sometimes lost during the extraction process.

Sisal fiber consists of 65.8% cellulose, 12% hemicellulose, 9.9% lignin, and 0.3% wax and water soluble compound. In many applications, fiber composites require mechanical properties, such as flexibility, good tensile strength, and low wear characteristics. As in previous studies, fibers have been shown to increase the toughness of polymers rather than to increase strength and elastic modulus. Siphon fiber composites have a maximum toughness of about 1250 MNm⁻² and a strength of 580 than other fibers. MNm⁻².

d) Bamboo: Bamboo is a huge pasture and trees are generally incredible. They belong to Bambu-soideae. Bamboo is very long and mature bamboo is about 30 meters. Bamboo has more benefits and grows fully within a few months. Bamboo is richer in tropical and subtropical regions. Bamboo is found in western Bengal, Sikkim, Manipur, Meghalaya, Nagaland, Tripura, Uttar Pradesh, Arunakul Pradesh and more. There are different types of bamboo depending on the area. They are: 1. Bambusa balcooa. 2. Bambusa pallida. 3. Bambusaburmanica. 4. Melocanna baccifera.

In this project we have taken the bambusa balcooa, these bamboos grow in the tropical forest. The bamboo is called as Mullam in this region, we have gathered them from our nearby location (Kakinada-Andhra Pradesh) where they import the bamboo from the tropical forest. The bamboo was harvested at an age greater than 2years, and the bamboo was seasoned for 2months respectively.

The bamboo will then chopped down into the pieces of 1meter length and of equal diameter respectively, with the help of carpenter. Now the bamboo pieces were made into splits of 8mm, 10mm, 12mm diameter and thickness of length 1meter.



Fig 3. Bamboo Splints of 1m Length.

e) Chemicals and Treatment of Bamboo splints: Chemicals are the substances which are pure, in this

project we have used boric acid copper sulphate, potassium dichromate as the part of the chemical treatment. Bamboo when exposed to atmosphere it has a chance of attack by insects in-order to prevent the bamboo from insect attacks chemical treatment was done to the bamboo splints. Here the chemicals like Boric acid, copper sulphate and Potassium di-chromate were taken as per IS 1902:2006 with a ratio of 1.5:3:4, now the chemicals per 10 litres of water were taken (150gm: 300gm: 400gm) and mixed separately first and then they were added to the water and mixed thoroughly with a help of a spoon till the colour changes to thick.



Fig 4. Chemical Solution.



Fig 5. Bamboo Splints in Chemical Solution

f) Epoxy Resin Treatment: Epoxy is one of the basic components of the epoxy resin or the cured end product and is the colloquial name of the epoxide functional group. Epoxy resins, also known as polyepoxides, are a family of reactive prepolymers and polymers that contain epoxide groups. A wide range of epoxy resins are produced industrially. Here we have considered the SIKADUR-32 epoxy resin binder, and we have purchased this product from a local retailer.



Fig 6. Sikadur 32 Gel.

Firstly we have taken the SIKADUR 32 gel where the mixture is applied to both the treated and untreated bamboo splints, and with this we have applied the sand which is passed from IS-2.0 and retained on IS-10 MM Sieve, which help as bonding agent for bamboo and soil, now the splints were allowed to dry for 24hours.

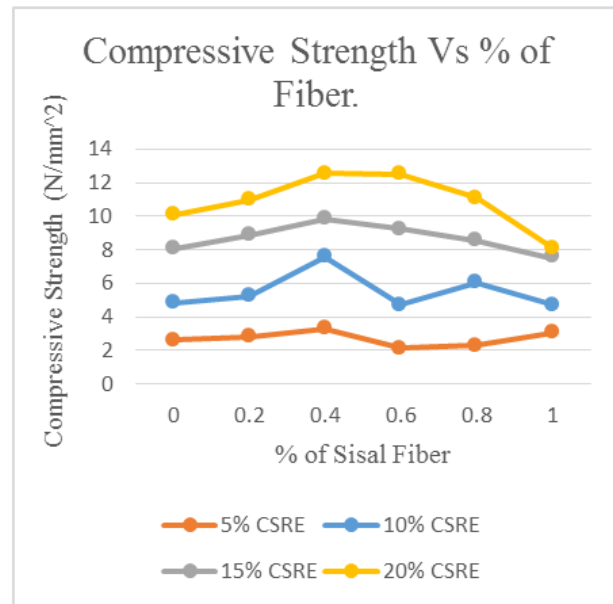
g) Steel: Steel is an alloy of iron, carbon and other elements. High tensile strength and low cost are the main components used in buildings, infrastructure, tools, ships, cars, machinery, electrical products and weapons. Iron is the base metal of steel. Two types of crystals can be taken depending on the temperature. Iron and steel are widely used in road construction, household appliances, railways, and construction.

In our project we are using three different sizes of steel such as 8mm, 10mm, and 12mm diameter respectively of VIZAG TMT.

4. EXPERIMENTAL PROGRAMME

In this experimental study, red soil is mixed by adding four different percentages (5%, 10%, 15%, and 20%) of OPC and sisal fiber with 0.2%, 0.4%, 0.6%, 0.8%, and 1.0% by weight of soil respectively. The bamboo splints were treated by soaking them in chemical solution of boric acid, Copper -Sulphate and Potassium Di-chromate (1.5:3:4).The resin-based adhesive with coarse sand will be applied to the top of bamboo splints. After 28days of curing period the cubes were tested for compressive strength, pull-out test is done for a series of CSRE blocks in which. Bamboo splints and steel bars are embedded to find out its bond strength.

5. TEST RESULT & GRAPH



Graph 1. Compressive strength vs percentage of fiber graph

TABLE 5.1: CUMMULATIVE COMPRESSIVE STRENGTH OF SISAL FIBERED CUBES.

Sl.No.	Percentage of Fiber	Percentage of Cement	Compressive Strength (N/mm ²)
1	0	5%	2.616
		10%	4.831
		15%	8.086
		20%	10.065
2	0.20%	5%	2.808
		10%	5.213
		15%	8.873
		20%	10.99
3	0.40%	5%	3.263
		10%	7.586
		15%	9.83
		20%	12.546
4	0.60%	5%	2.122

		10%	4.754
		15%	9.239
		20%	12.46
5	0.80%	5%	2.308
		10%	6.004
		15%	8.523
		20%	11.094
6	1%	5%	3.054
		10%	4.737
		15%	7.516
		20%	8.113

9	12BTN	150	42.6	7600	1.35
10	8BUTP	150	28.4	5800	1.54
11	10BUTP	150	35.7	7600	1.62
12	12BUTP	150	42.6	9800	1.74
13	8BUTN	150	28.4	9600	2.56
14	10BUTN	150	35.7	9600	2.04
15	12BUTN	150	42.6	10400	1.84

TABLE 5.2: DETAILS OF MODE OF FAILURE OF TEST SPECIMEN.

Sl.No.	Series	Length (mm)	Average Perimeter (mm)	Average Ultimate Bond Stress (Mpa)	Bond Strength
1	S8	150	28.4	7600	2.02
2	S10	150	35.7	5400	1.152
3	S12	150	42.6	4200	0.74
4	8BTP	150	28.4	11800	3.14
5	10BTP	150	35.7	10600	2.26
6	12BTP	150	42.6	12400	2.20
7	8BTN	150	28.4	6000	1.60
8	10BTN	150	35.7	6400	1.36

6. CONCLUSION

In this Project the Compressive Strength of CSRE blocks are obtained from compressive strength test and Bond strength characteristics of untreated, treated bamboo splints and steel rebar's embedded in Cement Stabilized Rammed Earth (CSRE) blocks were obtained from pullout test. After going through all the project work done we have made some of the conclusions. They are:

- The Compressive strength is more for 20% CSRE blocks compared to other percentages (5%, 10% and 15%) of CSRE Blocks.
- In addition of Sisal fiber to CSRE blocks the compressive strength increases from 0% of sisal fiber to 0.4% of sisal fiber and it gradually decreases afterwards.
- The compressive strength is more for 0.4% sisal fibered CSRE blocks.
- Compared to all the compressive strength values we have observed that the compressive strength is more for 0.4% sisal fibered 20% CSRE blocks which is 12.546 N/mm².
- So we can conclude that the 0.4% is the required optimum fiber content and 20% is the required optimum cement content for casting the pullout test blocks.
- Finally in the Pullout test we have obtained the greater Strength and deflection of the Reinforced CSRE Blocks.
- The study can add value in areas such as green and sustainable housing and waste utilization.

7. FUTURE SCOPE OF STUDY

In Regard of project “INFLUENCE OF SISAL FIBER ON THE PROPERTIES OF RAMMED EARTH” following things can be taken for future study.

- We can use different natural fibers like banana fiber, Jute fiber etc., in the place of sisal fiber and can test for compression and bond strength.
- A study on the effect of corrosion on the bond strength of Reinforced Rammed earth blocks.
- Study on Bond strength of Bamboo reinforced Rammed earth with different stabilizers.

REFERENCE

- [1] Abrishami, H. H., and D. Mitchell. 1996. “Analysis of Bond Stress Distributions in Pull-out Specimens.” *Journal of Structural Engineering* 122 (3): 255–261. Berge, B. 2009.
- [2] Ghavami, K. 2005. “Bamboo As Reinforcement in Structural Concrete Elements.” *Cement and Concrete Composites* 27 (6): 637–649.
- [3] Ghavami k, Hombeeck RV, Application of bamboo as a construction material: Part 1-Mechanical properties and water repellent treatment of bamboo, Part II-Bamboo reinforced concrete beams. In: Proc of Latin American Symp ON Rational Organization of Building Applied to Low Cost Housing. CIB, Sao Paulo, Brazil, 1981. P. 49-66.
- [4] Ghavami K. Application of Bamboo as a low-cost construction material. In: Proc of Int Bamboo Workshop, choin, India, 1988. P, 270-9.
- [5] Janssen JA. Bamboo in building structures, PhD thesis, Endio-ven University of Technology, Holland, 1981.
- [6] Morel JCM, Meshah A, Oggerto M, Walker P. Building Houses with Local Materials: Means to drastically reduce the environmental impact of construction, *Building and Environment* 2001:36:119-26
- [7] Janssen JA. The importance of bamboo as a building material. Bamboos current research. In: Proc of the Int Bamboo Workshop, Kerala Forest Research Institute—India & IDRC—Canada, 1988 .p.235-41.
- [8] Dunkelberg K et al. Bamboo as a building material. Bamboo-IL31, Institute for light weight Structures, University of Stuttgart, 1985. P. 1-431.
- [9] Walker, P.J., and S.Dobson. 2001. “Pullout Test on Deformed and Plain Rebars in cement-stabilized Rammed Earth” *Journal of Materials in civil engineering* 13(4):291-297.
- [10] Yankelevsky, D.Z.1985 “Bond Action between Concrete and a Deformed Bar- A New Model...” *Journal of American Concrete Institute* 82(2): 154-161

Performance Analysis of Spectrum Sensing Techniques

^[1] Anitha Bujunuru, ^[2] Prof.Srinivasulu Tadisetty

^[1]ECE Department, Guru Nanak Institutions Technical Campus, Hyderabad, India.

^[2] ECE Department ,Dean, Kakatiya University, Warangal, India

Abstract:-- Upgrading usages of wireless communication applications have many constraints on the utilization of accessible wireless spectrum. Cognitive radio (CR) technology is an emanate and auspicious solution to the issue of insufficient licensed spectrum. The spectrum sensing is the majority demanding issues in cognitive radio applications to find out the accessible spectrum bands and which can be utilized by secondary user without providing any unfavorable intervention to the primary user. Several conventional spectrum sensing procedures are presented to perceive the primary user signals.

This paper reviews the performance of three significant spectrum sensing methods such as Energy detection(ED), matched filtering detection (MFD) and Cyclostationary detection (CD) techniques. All the methods are interpreted based on the parameters of probability of detection (Pd), probability of false alarm (Pf) and signal to noise ratio(SNR) using MATLAB under AWGN channel.

Keywords: Cognitive radio, Spectrum sensing, probability of detection, probability of false alarm.

1. INTRODUCTION

As demand for housing construction increases with The radio spectrum available is limited and wide increase in usage of wireless communication rises to the issue of spectrum scarcity. Most of the pre allocated radio spectrum is underutilized by the primary user which creates holes are also called spectrum holes. Spectrum holes are the unutilized chunk of spectrum by the licensed user at the given specific time. Therefore most of the pre allocated radio spectrum is underutilized due to the uninspired approach of spectrum management schemes (fixed spectrum assignment schemes) and can be solved using cognitive radio [1]. CR is a smart dynamic spectrum management system that adjusts the environment conditions [1], [2].Cognitive Radio is defined as “Cognitive Radio could be a radio for wireless communication that automatically detects the available channels depends on the interaction with the environment to communicate more effectively to prevent interfacing to authorized users.”

CRN nodes can be classified as primary (licensed) users (PUs) and secondary (cognitive or unlicensed) users (SUs). PU has absolute liberty to access the particular licensed spectrum band, whereas SU detects unutilized chunks of spectrum momentarily through its PU and opportunistically utilize them. CRN enables unlicensed users for exploiting the spatially and/or temporally under-utilized spectrum by communicating over the licensed bands. CRNs is an overlay network with dynamic spectrum access where SU should have spectrum sensing capability for sensing whether there is

presence of PU before transmission, thereby provide spectrum efficiency and improves network performance.

II. COGNITIVE RADIO MODULES

The important tasks of cognitive radio are: Spectrum sensing, spectrum sharing, spectrum management and spectrum mobility are shown in Fig 1. Spectrum sensing is a procedure of identifying the unused spectrum portions by secondary user. Spectrum management is the procedure of assigning available portion of spectrum to the user. Spectrum Mobility is a task of exchanging of frequency of operation of cognitive users. Spectrum sharing is a method of sharing the available primary user spectrum with the secondary user [3]. Depending on the sensing results; SUs can get status of the channels to access.

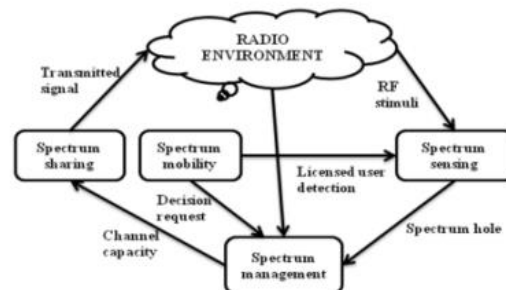


Fig.1 Cognitive cycle modules

Spectrum sensing is a procedure of identifying the unused spectrum portions by continuous monitoring of primary user and make use of the free spectrum by

unlicensed users. The process of making use of the spectrum whenever the user required is known as dynamic spectrum access (DSA) which improves the spectrum efficiency. The dynamic spectrum access of wireless spectrum by the secondary users is shown in Fig 2.

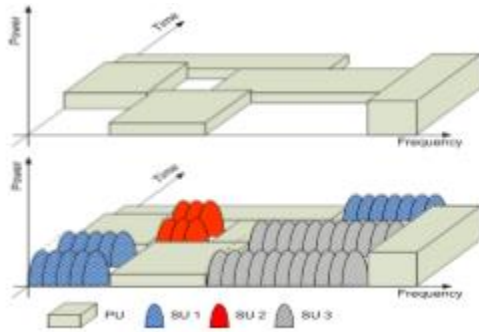


Fig.2 Dynamic spectrum access of wireless spectrum

III. SPECTRUM SENSING

The main intention of spectrum sensing is to know the appearance of primary user so that SU can use the channel without providing intervention to the primary user. Spectrum sensing means sense spectrum holes of primary user continuously using the channel parameters transmit power, noise and interference levels.

SU acquire the signal from the primary user and then apply different sensing methods to find out the residence of primary user by comparing the obtained signal with the threshold. If the received signal is less than threshold, then SU takes the decision that PU is available otherwise PU is not utilizing the channel. The flow of spectrum sensing is stated in Fig 3.

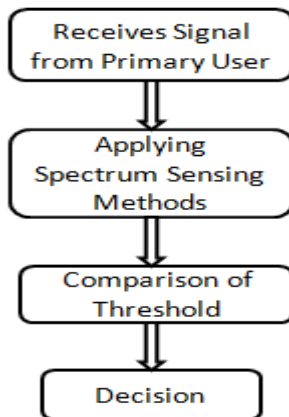


Fig.3 Flow of spectrum sensing

Spectrum sensing is mainly categorized into three groups, non cooperative sensing, co- operative sensing and interference based sensing [2]. The other name for non cooperative sensing is transmitter detection Non cooperative sensing methods are Energy detection(ED), Matched filtering detection (MFD) and Cyclostationary feature detection (CSFD).

A. Energy Detection Spectrum Sensing

The most common and simple sensing method is ED Spectrum Sensing. It is a non-coherent detection process that can sense the appearance of primary user based on the energy of the sensed primary signal [2]. The SU can calculate the average energy (E) of PU signal and compare with the threshold value (λ). If calculated energy $E \geq \lambda$ SU takes the decision that PU is available (H1) otherwise SU make a decision that PU is absent (H0). Fig4 shows the Basic model of energy detector [6]. PU received signal energy can be calculated by using equation (1)

$$E = \frac{1}{T} \int_{-\infty}^{\infty} s^2(t) dt \tag{1}$$

PU detection is done with hypothesis test given in equation (2)

This technique does not necessitate any of the prior knowledge

$$\left. \begin{aligned} y(t) &= n(t), & H0 \\ y(t) &= h * s(t) + n(t), & H1 \end{aligned} \right\} \tag{2}$$

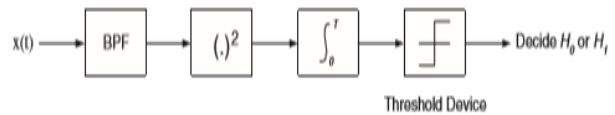


Fig.4 Block diagram of Energy Detector

The Energy detector output is the collected signal energy is calculated by

$$E = \sum_{n=0}^N y(n)^2 \tag{3}$$

Where number of sample are n and y(n) is the signal collected by the SU. Decision of the energy detector is obtained by calculated energy (E) of the energy detector and the threshold value (λ) [4], i.e.

If $E \geq \lambda$ PU signal is available

If $E \leq \lambda$ PU signal is not available

The performance measures of probability of detection (Pd) and probability of false alarm (Pf) are calculated by utilizing on the below equations.

$$P_d = Q\left(\frac{\lambda - N(\delta_n^2 + \delta_s^2)}{\sqrt{2N(\delta_n^2 + \delta_s^2)^2}}\right) \tag{4}$$

$$P_f = Q\left(\frac{\lambda - N\delta_n^2}{\sqrt{2N}\delta_n^4}\right) \quad (5)$$

Where $Q(\cdot)$ represents the Q-function, δ_n^2 is the variance of noise and δ_s^2 is the variance of the PU signal. Sensing threshold depends on noise power and is calculated by

$$\lambda = (Q^{-1}(P_f)\sqrt{2N} + N)\delta_n^2 \quad (6)$$

Two calculations of probability of detection (Pd) and probability of false alarm (Pf) are also represented by using SNR (γ) and are given in following equations.

$$P_d = Q\left(\frac{\bar{\lambda} - N(1+\gamma)}{\sqrt{2N(1+\gamma)^2}}\right) \quad (7)$$

(8)

Where $\bar{\lambda}$ is the average threshold and is given by $\bar{\lambda} = \frac{\lambda}{\delta_n^2}$

Advantage

- (i) This technique does not necessitate any of the previous information of PU
- (ii) Implementation is also easier.

Drawback

- It cannot perform well at low SNR conditions.
- Selection of threshold is difficult.
- It cannot discriminate PU signal and noise.

B. Cyclostationary Feature Detection

CSFD is the procedure of checking PU signals by using the periodicity of the collected primary signal [3]. Cyclostationarity is a habitual property of carriers like sinusoidal, pulse trains are used in some signals for synchronization purposes.

A signal is known as Cyclostationary, if its autocorrelation function is a periodic with same period of signal. These recurrences can be recognized by an appropriate Cyclostationary model. CSFD is realized by examine the cyclic autocorrelation function (CAF) of received signal that can be utilized to distinguish the primary signal from noise [7],[8],[9]. The model of Cyclostationary feature detection is shown in Fig. 5.

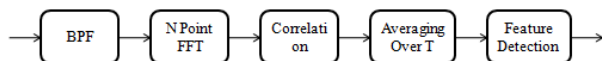


Fig. 5 Model of Cyclostationary feature detection

Probability of detection and probability of false alarm can be calculated by using following expressions

$$P_{fa} = e^{-\frac{\lambda^2}{2\sigma_v^2}} \quad (9)$$

$$P_d = Q\left(\frac{\sqrt{2\gamma}}{\sigma_n}, \frac{\lambda}{\sigma_v}\right) \quad (10)$$

Where σ_n^2 is the noise power, σ_v^2 is the standardized Gaussian complementary cumulative distribution function and I_0 is zero order Bessel function.

Advantage

- (i) This detection is good at noise unreliability
- (ii) Performance preferable than energy detection with low SNR.

Drawback

- (i) It needs the prior knowledge about received primary signal characteristics [10].
- (ii) Needs more sensing time.

C. Matched Filter Detection

MFD is the method of finding the appearance of PU signal by calculating SNR at the output using coherent pilot sensor. Primary user transmitter sends the pilot along with the data. In Matched filter detection SU must require the priori data of PU signal. It is the optimal technique when the SU is having the some particulars of PU [5],[7],[9]. Matched filter detector operation is shown in Fig6.

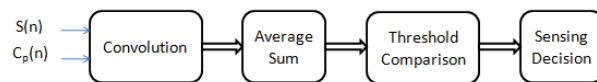


Fig.6 Model of Matched filter detector

The matched filter operation is convolution of $S(n)$ and $C_p(n)$ and is given below

$$y(n) = \sum_N s(n) * C_p(n) \quad (11)$$

Where $S(n)$ is the PU signal, $C_p(n)$ is the pilot signal and $y(n)$ is the convolved output signal.

The calculated value of $y(n)$ is gets match with threshold to determine the availability of spectrum.

If $y(n) \geq \lambda$ PU signal is present

If $y(n) < \lambda$ PU signal is absent

Probability of detection (Pd) and probability of false alarm (Pf) are calculated from the following formulas.

$$P_d = Q\left(\frac{\lambda - E}{\sqrt{E}\delta_n^2}\right) \quad (12)$$

$$P_f = Q\left(\frac{\lambda}{\sqrt{E}\delta_n^2}\right) \quad (13)$$

Where $Q(\cdot)$ represents the Q-function, σ_n^2 is the variance of the noise. Sensing threshold depends on noise power and is calculated by

$$\lambda = (Q^{-1}(P_f)\sqrt{E}\delta_n^2) \quad (14)$$

Advantage

MFD maximizes the SNR and faster technique compared to other methods.

Drawback

- (i) Matched filter performance is very poor if the knowledge about the PU is not correct [10].
- (ii) Its computational complexity is high compare to other techniques.
- (iii) The most important limitation is that CR requires a faithful receiver for all primary users.

IV. RESULTS AND DISCUSSIONS

This section compares spectrum sensing techniques based on different parameters. Performance detection is analyzed using Receiver Operating Characteristics curves of three different scenario Energy detection, Matched filter and Cyclostationary detection. Comparison of different techniques has shown in Table.1 and point out that the matched filter is the best among the three techniques.

Table.1: Comparison of different techniques

Parameter	Energy Detection	Cyclostationary	Match Filter
Implementation	Easy to implement	Complex	Complex
Prior knowledge	Don't require any prior information	Require partial information	Require full information
Time and cost	Requires less time and cost	Requires moderately high time and cost	Requires more time and cost among three

Simulation result of SNR verses total probability of error is shown in Fig.7 and probability of error is decreases with increase in SNR. Simulation outcomes of spectrum sensing techniques of probabilities of Pd against Pf have shown in Fig.8. , and Probabilities of missed detection against Pf has shown in Fig 9. From the simulation results, Matched filter is the best method of sensing among three.

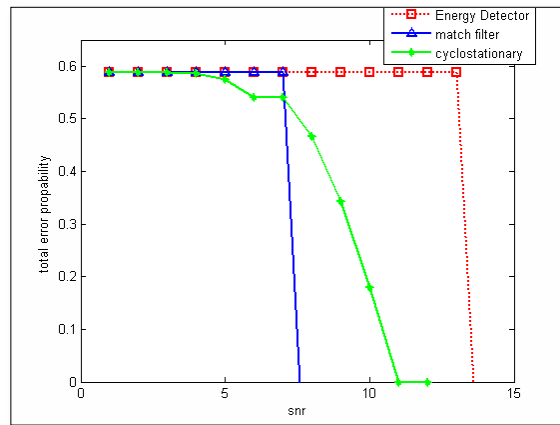


Fig.7 Simulation results of total error probability with SNR

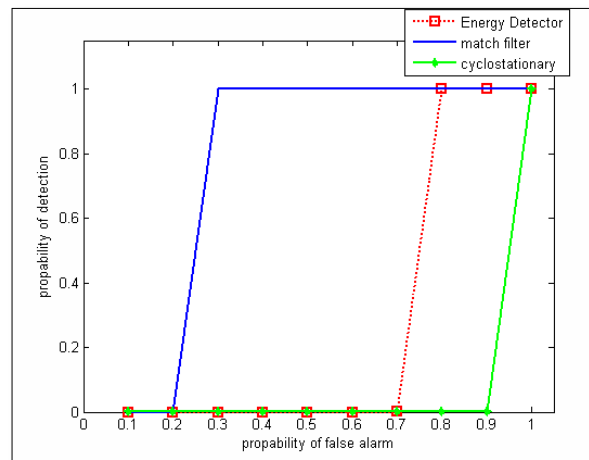


Fig.8 Receiver Operating Characteristics curves of sensing techniques

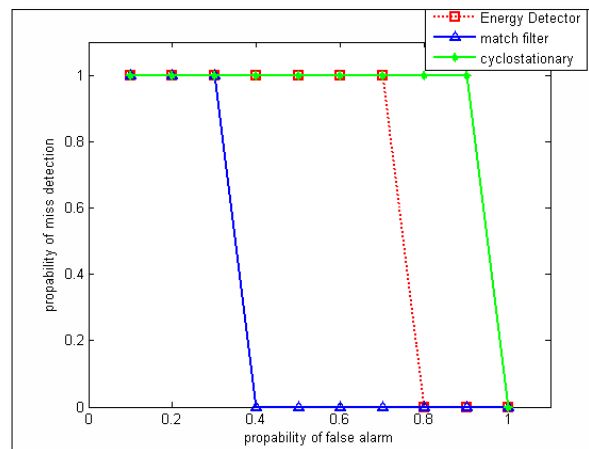


Fig.9 Simulation results of sensing techniques Pm Vs Pf

V. CONCLUSION

In this paper, we have compared the accuracy and the performance in three techniques energy detection, matched filter and Cyclostationary by using various parameters. The total error probability with snr variation is analyzed and among three techniques matched filter will give better performance. Total error probability is decreased with increasing snr and remains constants after certain value. The performance metrics of probability of missed detection is analyzed with probability of false alarm (Pfa) and is decreased with increasing the Pfa. Performance and accuracy of the technique is increased with the availability of prior knowledge, it also increases the complexity, time and cost. Therefore cooperative spectrum sensing techniques are used to implement with minimum prior knowledge, minimum time, low cost and less complexity.

REFERENCES

1. Mohsen Riahi Manesh, Md. Shakib Apu, Naima Kaabouch, and Wen-Chen Hu, "Performance evaluation of spectrum sensing techniques for cognitive radio systems"2016 IEEE 7th Annual Ubiquitous Computing, Electronics & Mobile Communication Conference (UEMCON)
2. Manish Gupta, Gaurav Verma and Rahul Kumar Dubey, "Cooperative Spectrum Sensing for Cognitive Radio Based on Adaptive Threshold",2nd International conference on Computational Intelligence &Communication Technology.
3. Ayaz Ahmad, Sadiq Ahmad, Mubashir Husain Rehmani and Naveed Ul Hassan, "A Survey on Radio Resource Allocation in Cognitive Radio Sensor Networks", 2015 IEEE.
4. Raza Umar, , and Asrar UH Sheikh, "A comparative study of spectrum awareness techniques for cognitive radio oriented wireless networks", Physical Communication, Elsevier , pp. 148-170, 2013.
5. Sana Ziafat, Waleed Ejaz, and HabibUllah Jamal, "Spectrum sensing techniques for cognitive radio networks: Performance analysis", 2011 IEEE MTT-S International Microwave Workshop Series on Intelligent Radio for Future Personal Terminals
6. Goutam Ghosh, Prasun Das and Subhajit Chatterjee, "Simulation And Analysis Of Cognitive Radio System Using MATLAB", International Journal of Next-Generation Networks (IJNGN) Vol.6, No.2, June 2014.
7. Luis Miguel Gato Díaz, Luis Miguel Gato Díaz, Jorge Torres, "Performance Comparison Of Spectrum Sensing Techniques For Cognitive Radio Networks", VII Simposio de Telecomunicaciones, March 2016.
8. Bommidi Sridhar, Dr T.Srinivasulu , "A Novel High Resolution Spectrum Sensing Algorithm for Cognitive Radio Applications", IOSR Journal of Electronics and Communication Engineering (IOSR-JECE)e-ISSN: 2278-2834,p-ISSN: 2278-8735.Volume 8, Issue 4 (Nov. -Dec.2013), PP 30-38.
9. Fanan, A. M., N. G. Riley, M. Mehdawi, M. Ammar, and M. Zolfaghari, "Survey: A Comparison of Spectrum Sensing Techniques in Cognitive Radio", Int'l Conference Image Processing, Computers and Industrial Engineering (ICICIE), pp.15-16, 2014.
10. Weifang Wang, "Spectrum Sensing for Cognitive Radio", 3rd International Symposium on Intelligent Information Technology Application Workshops,pp. 410-412, 2009.

Accelerated PVT analysis of UCM architecture using Cadence ADE-XL

^[1] Rajkumar Sarma, ^[2] Cherry Bhargava, ^[3] Shruti Jain

^{[1][2]} School of Electronics & Electrical Engineering, Lovely Professional University, Phagwara, Punjab, India.

^[3] Department of Electronics and Communication Engineering, Jaypee University of Information Technology, Waknaghat, Himachal Pradesh, India

Abstract:-- A Process-Voltage-Temperature (PVT) Variation check is run on the novel Universal Compressor based Multiplier (UCM) architecture, which promises for fast multiplication in ultra-low supply voltages (less than 0.9 V) for higher order operation. The analysis further shows that for 5x5 bit & 9x9 bit operation with supply voltage as low as 0.6 V, the delay has reduced by 0.73% & 5.05% (mean values) respectively than Wallace tree multiplier architecture. The analysis is carried out in Cadence Spectre tool using ADE-XL at CMOS 90 nm technology.

Keywords: Multiplier, Compressor design, ADE-XL, Low power, High speed, Cadence Virtuoso, PVT analysis, Delay optimization.

1. INTRODUCTION

A multiplier is a key element in a digital system. For the applications such as digital signal processing, digital image processing, Multiply and Accumulate architecture etc. uses multiplier rigorously. Though a multiplication is performed using repetitive addition method, where a multiplicand is added with itself for as many as number of times the multiplier, in digital system the multiplication process is slightly different. A basic design of a multiplier is as shown in the Fig. 1.

As shown in the Fig. 1, the multiplicand's & the multiplier's individual terms are ANDed to produce the partial products & positioned as per their weights. For example, as shown in Fig. 1, 'A2B0', 'A1B1' & 'A0B2' are aligned in a single column because the weight is two for all of the mentioned partial products. i.e. the summation of the bit location is any of 2+0, 1+1, 0+2, which are in all cases is equal to 2. Hence, for the addition of partial products, its alignment is vital. At the next step, the partial product with same weights are added using fulladder (in the case of 3 partial products), halfadder (in the case of 2 partial products) or any compressor circuit (for adding 'n' number of partial products simultaneously).

In this research paper the novel UCM architecture as proposed in [1] is further validated with the PVT analysis in Cadence spectre tool using ADE-XL in 90 nm CMOS technology. The UCM architecture uses a novel compressor-based multiplier algorithm which reduces the delay substantially.

The following sections are discussed as follows: in section 2, various different notable architectures related to multiplier are discussed in detail, in section 3, a quick

review on the novel UCM architecture has been explained, in section 4, a detailed PVT analysis of the UCM architecture is discussed & in section 5, conclusion, future scopes & application of the UCM architecture is discussed.

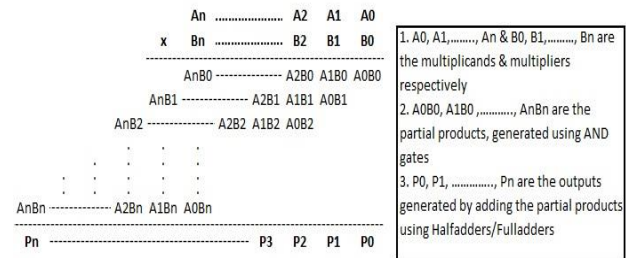


Fig. 1, Basic multiplication operation

II. VARIOUS MULTIPLIER ARCHITECTURES

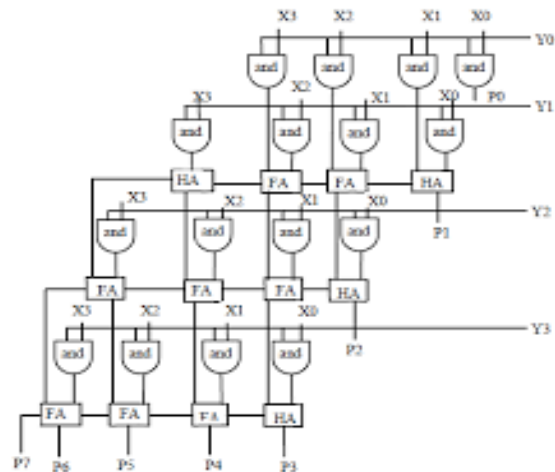


Fig. 2, Array multiplier architecture

In any application, the processing elements basically consists of the multiplication of different inputs or raw data. So, there is a huge demand of multiplier in such kind of processing elements. Various high speed & power efficient multipliers are explained in the literature. Array multiplier (as shown in Fig. 2) is a basic multiplier which produces the partial products using an array of AND gates & then the ANDed products are added using summer/adder. But the main disadvantage of array multiplier is that it can add a maximum of three product terms at a time (in case of full adder) & therefore, this architecture becomes bulkier with higher PDP when the total number addition levels are more.

Wallace tree multiplier based on Wallace tree algorithm can solve the issue of bulkier structure of Array multiplier. By replacing the adder/summer part with Wallace tree algorithm, the multiplier can be made much more efficient. Here a multiplier is designed which generates the product of two numbers using purely combinational logic, i.e., in one gating step. Using straight forward diode-transistor logic, it appears presently possible to obtain products in under 1 micro sec, and quotients in 3 micro sec. A rapid square-root process is also outlined [18]. The Fig. 3 shows the same.

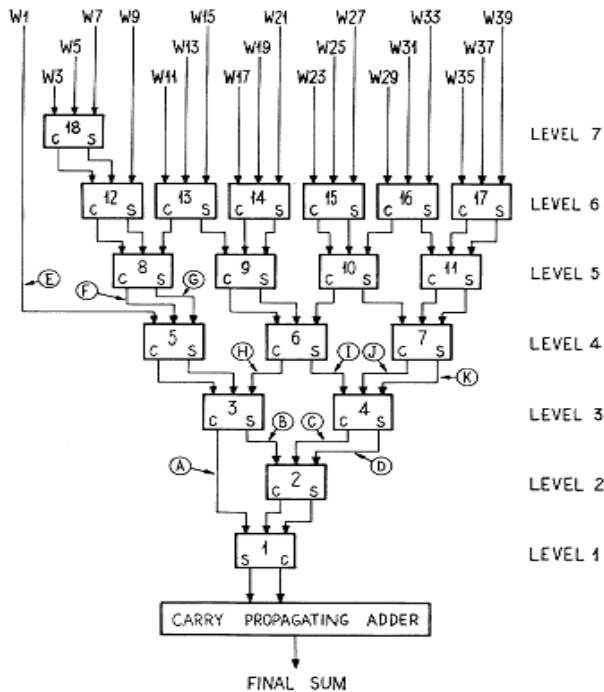


Fig. 3, Wallace tree multiplier (addition of partial product)

However, the problem with Wallace tree multiplier is that the addition of partial product is done in a single direction due to which the number of adder increases.

This problem was sorted by a rectangular styled Wallace tree multiplier [3] in which the partial products are categorized into two groups and they are added in the opposite direction. The downward addition is done for the first group of the partial products & similarly upward addition is done for the second group of the partial products. On the other hand, in [12] a phase mode parallel multiplier [12] is proposed where it has a Wallace-tree structure which consists of trees of carry save adders for partial products addition. This structure has a regular layout & therefore, it is suitable for pipeline processing.

The conventional Wallace tree multiplier is basically consisting of carry save adder (CSA), which adds three variables at a time. Therefore, to enhance the speed of operation further, instead of CSA, compressor circuits can be used. In a similar approach, in [20], the speed of the multiplier is improved by using different compressors instead of the CSA. 3:2 compressor, 4:2 compressor, 5:2 compressors & 7:2 compressors are used rigorously to improve the speed of the existing Wallace tree multiplier. In the same study, it is summarized that the higher order compressors (4:2, 5:2 or 7:2) performs better than 3:2 compressor. Therefore, the delay of the multiplier can be reduced by using higher order compressors.

As adder is a core unit in multiplier (and divider) circuit, the optimization on delay in multiplier can be further achieved by optimizing the adder circuit. Same kind of study is also seen in the literature, which optimized the adder circuit. In a novel approach, a Carry-Select-Adder (CSA) Optimization Technique [9] is proposed where a carry-select-adder (CSA) partitioning algorithm is used for Booth-encoded Wallace tree algorithm. By taking into various data arrival times, a branch-and-bound algorithm is proposed and a generalized technique to partition an n-bit carry-select adder into a number of adder blocks is proposed such that the overall delay of the design can be minimized. In a different approach, an algorithm [17] for implementing an efficient modulo $(2n + 1)$ multipliers had been proposed. By manipulating the Booth tables and by applying a simple correction term, the proposed multiplier is the most efficient among all the known modulo $(2n + 1)$ multipliers and is almost as efficient as those for ordinary integer multiplication. A comparative study in [16] is done for implementing multiplier using complementary MOS (CMOS), complementary pass-transistor (CPL) & double-pass transistor (DPL) logic style. A single precision reversible floating-point multiplier is proposed in [11]. A 24-bit multiplier is proposed in this work by decomposing the whole 24 bit in three portions of 8 bit each.

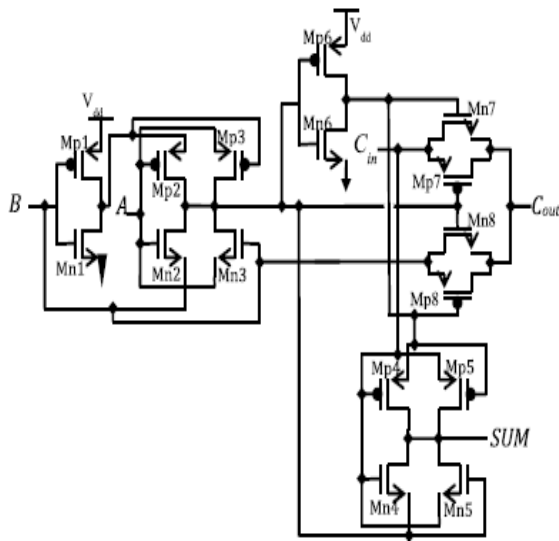


Fig. 4, Full adder design in [21] which consumes very less power.

The internal to the multiplier is adder. Therefore, an optimized adder can further enhance the performability of a multiplier. An adder or summer circuit adds two or three variables. Adder is very common in logic circuits as it is used not only for summation but also to calculate the location addresses, increment/decrement operations, table indices etc. The common adders not only operate on binary number system but also for weighted & non-weighted codes. In the literature there are plenty number of full adders which are proposed to be efficient than others. A novel low power MOSIS 90 nm technology-based hybrid full adder is proposed in [6]. The low power design is compared with conventional full adder consisting of 28 transistors. In a different approach, a hybrid 1-bit full adder is proposed which uses CMOS as well as TG logic styles [21]. The design is implemented in 90nm CMOS technology as well as 180nm CMOS technology. At 1.8V supply voltage, the proposed full adder, offers very little power and moderately low delay. The proposed adder in [21] is shown in Fig. 4.

III. UCM ARCHITECTURE

The basic UCM architecture consists of three stages. The stage 1 & stage 3 remains the same for UCM architecture (as that of Wallace tree), because whether it is partial product generation or addition of intermediate sum or carry using fast adder, these can be chosen according to the requirement of the designer. Hence, it is more important to replace the stage 2 i.e. addition of partial product which creates sum & carry separately.

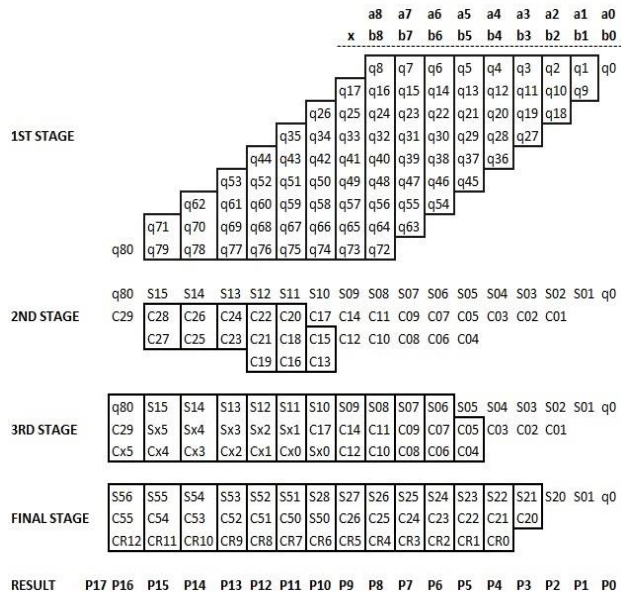


Fig. 5, UCM architecture for 9 x 9 bit multiplication

A. Addition of partial products

While adding partial products, the partial products are aligned in such a way that the summation of bit location of multiplicand & multiplier are equal. The summation of bit location can be called as 'weight' of a particular partial product. For example, in the Fig. 5, 'q35', 'q43', 'q51', 'q59', 'q67' & 'q75' are aligned in a single column because of the reason that the weight is eleven for all of the mentioned partial products, i.e. $q35 = a8b3$, $q43 = a7b4$, $q51 = a6b5$ etc. So, the summation of the bit location is either of $8+3$ or $7+4$ or $6+5$, which is in all cases are equal to 11. Hence, for the addition of partial products, its alignment is very important. Once the partial products are aligned the next step is to add all the partial product falling in that particular column. For adding a particular column firstly, the total number of stages & levels need to be identified. Each stage consists of an AND-XOR gate pair & the total number of stages in one level is counted from top to bottom. The total number of stages in the first level is 'i-1', where 'i' is the total number of partial products to be added in a particular column. On the other hand, the horizontal count of AND-XOR pair is the total number of levels required for the design. In a different angle, we can say that the total number of levels required in a design is the total number of AND-XOR pair required in the bottom most stages. Basically, it is the count of AND-XOR pair from right to left. In each level, the total number of stages required will be decremented by one until it satisfies the formula:

$$\begin{aligned}
 2^n - 1 &\geq i \\
 \Rightarrow 2^n &\geq i + 1 \\
 \Rightarrow n(\log_{10} 2) &\geq \log_{10}(i + 1) \\
 \therefore n &\geq \frac{\log_{10}(i + 1)}{\log_{10} 2} \\
 \text{or } n &\geq \log_2(i + 1)
 \end{aligned}$$

where 'i' is the total number of the partial product to be added & 'n' is the total number of levels required. 'i' & 'n' are integers starting from 1, 2, 3,, ∞. For example, for adding 3 partial products in a column, the total number of levels will be: $2n - 1 \geq 3$, so $n = 2$. Similarly, if suppose $i = 8$, i.e. $2n - 1 \geq 8$, so $n = 4$ & so on. The basic block diagram for K stages & L levels is shown in Fig. 6. In Fig 6, A0, A1, A2 up to AK are the partial products; the term Y0 is the sum & Y1, Y2, Y3,....., YL are the carries. Therefore, in simple words, the algorithm shown in the Fig. 6 is a N-bit compressor circuit which generates sum of a particular column & single/multiple carries.

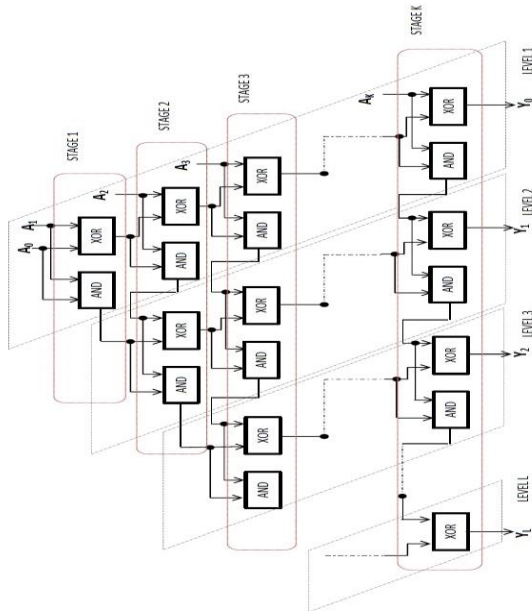


Fig. 6, AND-XOR gate arrangement with K stages & L levels having A0, A1, A2,....., AK partial products (with equal weights) for a particular column

B. Special cases

- i. In the last level, instead of AND-XOR pair, only XOR gate is to be used.
- ii. If $i = 2$, only one level is to be used to get the sum as well as carry. In this case, the output from the AND is the carry.

iii. For $i = 1$, the input itself is the output (sum) & there is no carry output.

It is very important to note that the output through the level 1 is the sum of the partial products present in a particular column & the outputs of rest of the levels i.e. level 2 to level L are the corresponding carry bits. After getting the sum as well as carry bit of all columns, the next step is to add up the sum bits with the carry bit of the previous columns. For this any of the efficient algorithms such as Dadda algorithm, Wallace tree algorithm or even ripple carry adder can be used as the number of rows has reduced substantially. A detailed design is shown in Fig. 5.

IV. PVT ANALYSIS

VLSI is an art of chip design, where specification is transformed to functional hardware. Cadence provides tools for front end as well as back end designs, where, after rigorous design steps, GDS-II file are finally sent for fabrication. But due to process complexity (i.e. pressure, supply voltage, temperature etc.) the YIELD of the fabricated designs is found to be very low. Major reason for yield loss is fabrication parameter variation among wafer to wafer. To improve the yield of design; the IC should be able to sustain extreme variation. Therefore, validation of the design cycle through PVT and 3-sigma variation becomes essential before fabrication.

The work published in [1], provides a comparison of delays for 5x5 bit as well as for 9x9 bit operation for 0.6V, 0.7V, 0.8V & 0.9V. The same has been shown in the Fig. 7 & Fig. 8.

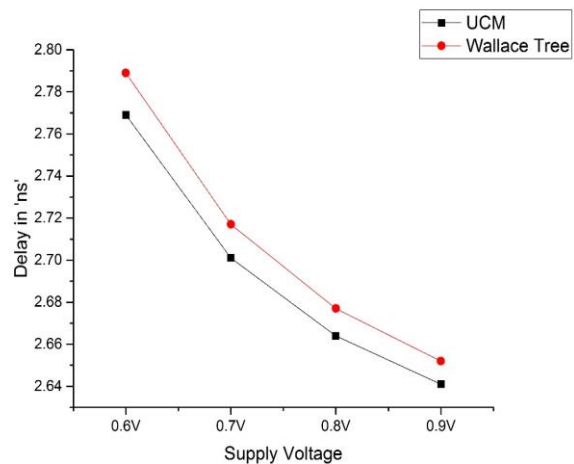


Fig. 7, Graphical comparison of 5x5 bit UCM & 5x5 bit Wallace tree multiplier at voltages below 1V

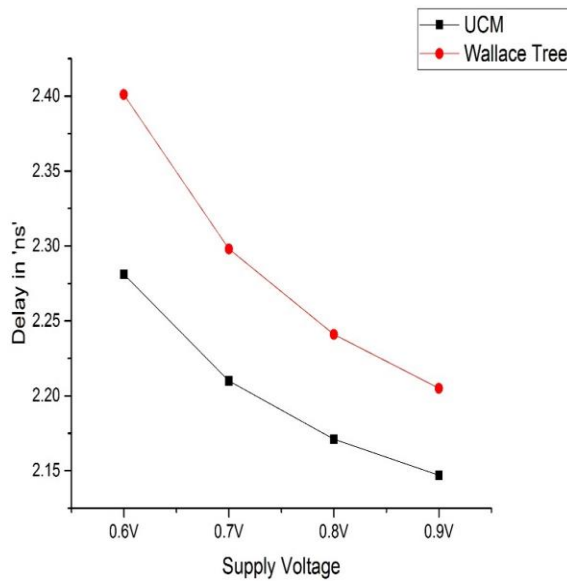


Fig. 8, Graphical comparison of 9x9 bit UCM & 9x9 bit Wallace tree multiplier at voltages below 1V

The comparison shows that the UCM [1] architecture performs better than Wallace tree architecture at ultra-low supply voltages (less than 0.9V). Moreover, the UCM architecture performs even better for higher order bit multiplication. For example, the difference in delay of UCM & Wallace tree architecture for 9x9 bit operation is more than 5x5 bit operation (120 ps & 20 ps respectively). Therefore, the author [1] summarized that UCM architecture performs better than Wallace tree for higher order bit multiplication at ultra-low supply voltages (less than 0.9V).

To validate the performance of the UCM [1] architecture further, a PVT analysis is carried out at different corners (Fast-Fast, Fast-Slow, Normal-Normal, Slow-Fast & Slow-Slow) & at three different extreme temperatures (-40o, 0o & +50o Celsius). Table I & II shows the delay comparison of UCM & Wallace tree 5x5 bit & 9x9 bit architecture respectively at 0.6 V & 0.9 V supply voltage in different corners along with variation in temperature (-40o,0o & +50o Celsius)

Table I, Delay comparison of UCM & Wallace tree 5x5 bit architecture at 0.6 V & 0.9 V supply voltage in different corners along with variation in temperature (-40o,0o & +50o Celsius)

	UCM (in ns @ 600mV)	Wallace tree (in ns @ 600mV)	UCM (in ns @ 900mV)	Wallace tree (in ns @ 900mV)
Nominal (27)	2.281	2.401	2.147	2.205
FF_0 (-40)	2.171	2.239	1.138	1.195
FF_1 (0)	2.192	2.27	1.153	1.222
FF_2 (+50)	2.218	2.31	1.247	1.257
FS_0 (-40)	2.258	2.353	2.126	2.171
FS_1 (0)	2.291	2.402	2.145	2.198
FS_2 (+50)	2.334	2.463	2.169	2.233
NN_0 (-40)	2.228	2.322	1.235	1.252
NN_1 (0)	2.259	2.369	2.134	2.187
NN_2 (+50)	2.3	2.43	2.157	2.221
SF_0 (-40)	2.239	2.351	2.123	1.259
SF_1 (0)	2.274	2.406	1.421	1.289
SF_2 (+50)	2.32	2.479	2.168	1.439
SS_0 (-40)	2.339	2.484	2.162	2.227

Nominal (27)	2.769	2.789	2.641	2.652
FF_0 (-40)	2.665	2.677	2.59	2.597
FF_1 (0)	2.684	2.698	2.601	2.61
FF_2 (+50)	2.709	2.725	2.616	2.626
FS_0 (-40)	2.75	2.766	2.623	2.632
FS_1 (0)	2.782	2.801	2.64	2.651
FS_2 (+50)	2.822	2.845	2.663	2.676
NN_0 (-40)	2.72	2.735	2.613	2.622
NN_1 (0)	2.749	2.767	2.629	2.64
NN_2 (+50)	2.786	2.809	2.651	2.663
SF_0 (-40)	2.728	2.746	2.617	2.627
SF_1 (0)	2.76	2.782	2.635	2.647
SF_2 (+50)	2.802	2.829	2.658	2.673
SS_0 (-40)	2.826	2.849	2.656	2.668
SS_1 (0)	2.875	2.902	2.682	2.697
SS_2 (+50)	2.937	2.97	2.716	2.734

Table II, Delay comparison of UCM & Wallace tree 9x9 bit architecture at 0.6 V & 0.9 V supply voltage in different corners along with variation in temperature (-40o,0o & +50o Celsius)

	UCM (in ns @ 600mV)	Wallace tree (in ns @ 600mV)	UCM (in ns @ 900mV)	Wallace tree (in ns @ 900mV)
Nominal (27)	2.281	2.401	2.147	2.205
FF_0 (-40)	2.171	2.239	1.138	1.195
FF_1 (0)	2.192	2.27	1.153	1.222
FF_2 (+50)	2.218	2.31	1.247	1.257
FS_0 (-40)	2.258	2.353	2.126	2.171
FS_1 (0)	2.291	2.402	2.145	2.198
FS_2 (+50)	2.334	2.463	2.169	2.233
NN_0 (-40)	2.228	2.322	1.235	1.252
NN_1 (0)	2.259	2.369	2.134	2.187
NN_2 (+50)	2.3	2.43	2.157	2.221
SF_0 (-40)	2.239	2.351	2.123	1.259
SF_1 (0)	2.274	2.406	1.421	1.289
SF_2 (+50)	2.32	2.479	2.168	1.439
SS_0 (-40)	2.339	2.484	2.162	2.227

SS_1 (0)	2.391	2.561	2.19	2.268
SS_2 (+50)	2.456	2.659	2.227	2.323

Moreover, a graphical comparison of delay of UCM & Wallace tree 5x5 bit & 9x9 bit architectures at 0.6 V & 0.9 V supply voltage in different corners along with variation in temperature (-40o,0o & +50o Celsius) are shown in Fig. 9 & Fig. 10. The graphs in Fig. 9 & Fig. 10 clearly shows that there is a significant improvement in delay of UCM architecture in comparison to the Wallace tree architecture for 5x5 bit as well as 9x9 bit multiplication. Most important part is that, for 5x5 bit multiplication, at different corners & at extreme temperatures, the UCM architecture proves to be the better performer than Wallace tree architecture at ultra-low supply voltages.

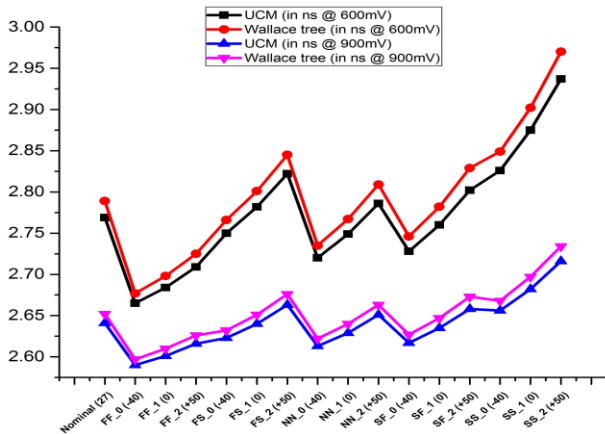


Fig. 9, Graphical comparison of delay of UCM & Wallace tree 5x5 bit architecture at 0.6 V & 0.9 V supply voltage in different corners along with variation in temperature (-40o,0o & +50o Celsius)

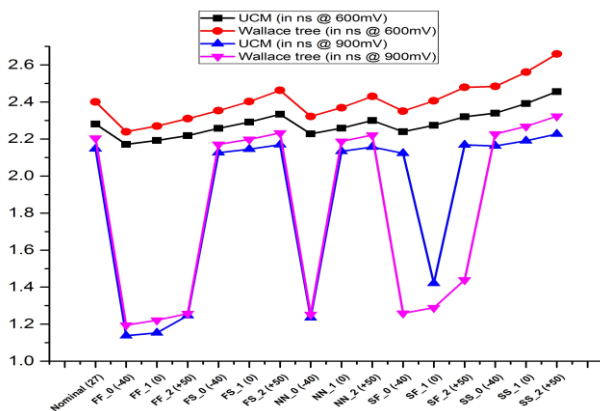


Fig. 10, Graphical comparison of delay of UCM & Wallace tree 9x9 bit architecture at 0.6 V & 0.9 V supply voltage in different corners along with variation in temperature (-40o,0o & +50o Celsius)

On the other hand, for 9x9 bit multiplication, the delay of UCM has a much more significant drop in comparison to the Wallace tree at 600 mV (at different corners & at extreme temperatures). Whereas, the delay of the UCM architecture is seems to be slightly higher than Wallace tree at slow-fast (SF) corner in -40o, 0o & +50o Celsius for 9x9 bit multiplication at 900 mV. The reason for the same might be the use different process at SF corner. Moreover, as shown in the Table I, the minimum & maximum delay for 5x5 bit multiplication using UCM architecture at 600 mV are 2.665 ns & 2.937 ns respectively. Whereas the same for Wallace tree are 2.677 ns & 2.97 ns respectively. Similarly, the minimum & maximum delay for 5x5 bit multiplication using UCM architecture at 900 mV are 2.59 ns & 2.716 ns respectively. Whereas the same for Wallace tree are 2.597 ns & 2.734 ns respectively. Same thing if we observe for 9x9 bit multiplication using UCM architecture at 600 mV, the minimum & maximum delays are 2.171 ns & 2.456 ns respectively whereas for Wallace tree the values are 2.239 ns & 2.659 ns. On the other hand, for 9x9 bit multiplication using UCM architecture at 900 mV, the minimum & maximum delays are 1.138 ns & 2.227 ns respectively whereas for Wallace tree the values are 1.195 ns & 2.323 ns.

V. CONCLUSION

The UCM architecture has a wide range of acceptability in the field of digital system design. UCM architecture not only performs the best in a nominal Process, Voltage & Temperature but also in a wide range of variation in extreme temperature, process & ultra-low supply voltages. Especially, in the case of the higher order multiplication (9x9 bit) operation with supply voltage as low as 0.6 V, the delay has reduced by 5.05% (mean value) than Wallace tree multiplier architecture. Therefore, UCM multiplier will have a wide range of acceptability in the circuits where speed is the top most priority.

REFERENCES

1. R. Sarma, C. Bhargava, S. Dhariwal, and S. Jain, "UCM: A novel approach for delay optimization," International Journal of performability Engineering, vol. 15, no. 4, pp. 1190-1198, 2019.
2. D. Guevorkian, A. Launiainen, V. Lappalainen, P. Liuha, and K. Punkka, "A Method for Designing High-Radix Multiplier-Based Processing Units for Multimedia Applications," IEEE Transactions on Circuits and Systems for Video Technology, vol. 15, no. 5, pp. 716-725, 2005.

3. N. Itoh, Y. Naemura, H. Makino, Y. Nakase, T. Yoshihara, and Y. Horiba, "A 600-MHz 54 54-bit Multiplier with Rectangular-Styled Wallace Tree," *IEEE Journal of Solid-State Circuits*, vol. 36, no. 2, pp. 249-257, 2001.
4. K. B. Jaiswal, N. Kumar, P. Seshadri, and L. G, "Low Power Wallace Tree Multiplier Using Modified Full Adder," in *Proceedings of the 3rd International Conference on Signal Processing, Communication and Networking (ICSCN)*, 2015.
5. I. Kataeva, H. Engseth, and A. Kidiyarova-Shevchenko, "Scalable Matrix Multiplication With Hybrid CMOS-RSFQ Digital Signal Processor," *IEEE Transactions on Applied Superconductivity*, vol. 17, no. 2, pp. 486-489, 2007.
6. S. Khan, S. Kakde, and Y. Suryawanshi, "VLSI Implementation of Reduced Complexity Wallace Multiplier Using Energy Efficient CMOS Full Adder," in *Proceedings of the IEEE International Conference on Computational Intelligence and Computing Research*, 2013.
7. R. D. Kshirsagar, E. V. Aishwarya, A. S. Vishwanath, and P. Jayakrishnan, "Implementation of Pipelined Booth Encoded Wallace Tree Multiplier Architecture," in *Proceedings of the International Conference on Communication and Green Computing Conservation of Energy (ICGCE)*, Chennai, 2013.
8. T. Y. Kuo and J. S. Wang, "A Low-Voltage Latch-Adder Based Tree Multiplier," in *Proceedings of the IEEE International Symposium on Circuits and Systems*, Seattle, WA, 2008.
9. M. Liao, C. Su, C. Chang, and A. C. Wu, "A Carry-Select-Adder Optimization Technique for High-Performance Booth-Encoded Wallace-Tree Multipliers," *IEEE International Symposium on Circuits and Systems, ISCAS 2002*, 2002.
10. X. V. Luu, T. T. Hoang, T. T. Bui, and A. V. Dinh-Duc, "A High-speed Unsigned 32-bit Multiplier Based on Booth encoder and Wallace-tree Modifications," in *Proceedings of the International Conference on Advanced Technologies for Communications (ATC'14)*, 2014.
11. M. Nachtigal, H. Thapliyal, and N. Ranganathan, "Design of a Reversible Single Precision Floating Point Multiplier Based on Operand Decomposition," in *Proceedings of the 10th IEEE conference on Nanotechnology*, Kintex, Korea, 2010.
12. T. Onomi, K. Yanagisawa, M. Seki, and K. Nakajima, "Phase-Mode Pipelined Parallel Multiplier," *IEEE Transactions on Applied Superconductivity*, vol. 11, no. 1, pp. 541-544, 2001.
13. C. Paradhasaradhi, M. Prashanthi, and N. Vivek, "Modified Wallace Tree Multiplier using Efficient Square-Root Carry Select Adder," in *Proceedings of the International Conference on Green Computing Communication and Electrical Engineering (ICGCCEE)*, Coimbatore, 2014.
14. M. J. Rao and S. Dubey, "A High Speed and Area Efficient Booth Recoded Wallace Tree Multiplier for fast Arithmetic Circuits," in *Proceedings of the Asia Pacific Conference on Postgraduate Research in Microelectronics & Electronics (PRIMEASIA)*, BITS Pilani, Hyderabad, 2012.
15. B. M. Reddy, H. N. Sheshagiri, B. R. Vijaykumar, and S. S., "Implementation of Low Power 8-Bit Multiplier using Gate Diffusion Input Logic," in *Proceedings of the 17th IEEE International Conference on Computational Science and Engineering*, 2014.
16. A. K. Singh, B. P. De, and S. Maity, "Design and Comparison of Multipliers Using Different Logic Styles," *International Journal of Soft Computing and Engineering (IJSCE)*, vol. 2, no. 2, pp. 374-379, 2012.
17. L. Sousa, "Algorithm for modulo $(2n+1)$ multiplication," *Electronics Letters*, pp. 752-754, 01 May 2003.
18. C. S. Wallace, "A Suggestion for a Fast Multiplier," *IEEE Transactions on Electronic Computers*, pp. 14-17, 1964.
19. Q. Yi and H. Jing, "An Improved Design Method for Multi-bits Reused Booth Multiplier," in *Proceedings of the 4th International Conference on Computer Science & Education*, 2009.
20. K. Gopi Krishna, B. Santhosh, and V. Sridhar, "Design of Wallace Tree Multiplier using Compressors," *International Journal of Engineering Sciences & Research Technology*, vol. 2, no. 9, pp. 2249-2254, 2013.
21. P. Bhattacharyya, B. Kundu, S. Ghosh, V. Kumar, and A. Dandapat, "Performance Analysis of a Low-Power High-Speed Hybrid 1-bit Full Adder Circuit," *IEEE Transactions on Very Large Scale Integration (VLSI) Systems*, , pp. 1-8, 2014.

Text Detection and Recognition for Calorie-conscious Life style

^[1]Mr Aran Nash, ^[2]Ms Swathika R, ^[3]Ms N Radha

^[1]Student, ^{[2][3]}Assistant Professor

^{[1][2][3]}Department of Information Technology, SSN College of Engineering, Kalavakkam – 603110, Chennai

Abstract:-- Humans may not like tracking our food and the calories that every food item offers, as it can be more difficult than it sounds. We would need to do a lot of research and always keep a track of what we are eating every day. But, it can be one of the best things we can do to maintain a healthy weight and improve overall health. The amount of calorie we may intend to have depends on number of factors including our age, gender, daily schedule, weight and etc. Hence, in this paper we develop a system that recognizes the text on the restaurant bills and calculate corresponding calorie count thereby enlightening the user on the calories consumed. To detect text from the images, we use the help of a widespread technology – Optical Character Recognition (OCR). It is the mechanical or electronic conversion of images of handwritten or printed text into machine encoded text whether or not from a scanned document or photograph of a document. The user can be aware of the calorie consumed using the application developed. The objective of this system is to help users to keep track of calories on their smart phones, also helping their dietician prepare a calorie-based chart thereby improving their lifestyle.

Keywords: Text detection, OCR, Text recognition, Caloriechart, Smart phones

1. INTRODUCTION

In our day to day lifestyle, keeping a journal or tracking our meals on our smart phone, make better choices. You become responsible to yourself, and you will track your progress finer. There is no more fooling yourself concerning what proportion you are or are not consuming once you write it down. Journaling and working your food decisions results in creating higher choices. We need some calories daily to support the normal functioning of the body. The amount of calorie we may take depends on many factors including our age, gender, daily schedule and weight along with many other factors. So, we would like to monitor these calories. Our work aims to utilize the Optical character recognition technique to detect the text on the restaurant bill accurately.

Text detection is the method of detecting the text exists in the image, followed by enclosing it with a rectangular bounding box. This can be achieved through image based techniques or frequency based techniques. In image based techniques, an image is divided into multiple segments. Each segment is a connected component of similar characteristics pixels. The statistical features of connected components are utilized to group them and form the text. Machine learning approaches are used to classify the components into text and non-text. In frequency based approaches, discrete Fourier transform (DFT) or discrete wavelet transform (DWT) are used to extract the high frequency coefficients. Here the assumption

is that the text present in an image has high frequency components and selecting only the high frequency coefficients filters the text from the non-text regions in an image. Text is the most excellent way of communicating information. It can be enclosed into documents, images and videos. The high performance mobile devices capable of acquisition and processing of images anytime, anywhere provides a way to recognize text in various environments. there have been numerous text related applications for both images and video, which includes page segmentation [1], [2], address block location [3], license plate location [4], [5], and contentbased image/video indexing [6], [7].

Text detection and recognition in images with complex backgrounds, variations of text layout and fonts, and the existence of uneven illumination, low quality, degraded data and multilingual environments present a much greater challenge than well-formatted documents. So advanced computer vision and pattern recognition techniques are required to solve these problems. The performance of text detection and recognition in color imagery are examined and various technical challenges are discussed [8].

The aim of this paper is to develop a system that recognizes the text on the restaurant bills using optical character recognition techniques and to calculate corresponding calorie count thereby enlightening him/her on the calories consumed. We aim to provide this software on android platform which will ease the task of detecting text and computing calories.

The rest of this paper is organized as follows. Section II gives survey about the various text detection and recognition techniques from image. It also provides information about the OCR system. The proposed system is presented in Section III. Section IV reports about how the experiment is done and how the results are obtained. It also describes the challenges faced by the system and finally the conclusion and future enhancements are drawn in Section V.

II. REVIEW OF EXISTING WORK

Text comes in two categories: Graphic text and Scene text. The graphic text is machine printed text which is found in captions, subtitles and annotations in video and digital images on the web and in email [9]. The scene text refers to text on objects, includes text on signs, packages and clothing in natural scenes, and handwritten material [10]. Our proposed application uses graphic text i.e. printed text from restaurant bills.

The process of extracting text from mixed-type documents is a pre-processing and necessary step for several document related applications. A new method is proposed to automatically detect and extract text in mixed-type color documents based on a combination of an adaptive color reduction (ACR) technique and a page layout analysis (PLA) approach [11].

While the recent methods relies on visual cues only, a novel fine-grained object classification using recognized text in natural images is proposed. This approach combines textual as well as visual cues. Another new thing is the textual cue extraction. Unlike the state-of-the-art text detection methods, this method relies more on the background instead of text regions. Once text regions are found, they are further processed by two process to perform text recognition, i.e., OCR engine and a state-of-the-art character recognition algorithm [12]. A novel Text-Attentional Convolutional Neural Network (Text-CNN) system is developed for scene text detection. This method focuses on extracting deep text feature from an image component. Also it is able to discriminate ambiguous text from complicated background [13].

Edge based methods perform more efficiently in case of natural scene images having sharp edges. A method is presented in which candidate edge recombination and edge classification are used to stroke width transform are added. In candidate edge recombination, over segmentation and region merging is done. The edge of the image is segmented into small segment that separates the edge of text from the background. Then the merging of neighboring edge segment have been done the on the basis of similarity of color and stroke width. With this

each character is explicated by a candidate boundary. The candidate boundaries are combined into text chains in the boundary classification process. The character based and chain based features are used in chain classification [14].

A real-time system which extracts text from natural scene images can prove to be very useful [15], [16]. These systems can be used to automatically read and understand addresses and landmarks from images, banners and posters on roads, and sign boards without much difficulty. Although number of state-of-the-art approaches [17], [18], [19] have been proposed to detect and recognize text in scene imagery, there exists some research challenges like low detection rates and recognition rates [20]. By contrast, OCR achieves recognition rates higher than 99 percentage for scanned documents [21]. OCR is an electronic tool that converts scanned documents into text searchable form. A typical OCR system consists of the following basic components: Input scanned Image, Pre-processing, Feature Extraction, Classification, and Post-processing [22].

OCR [23] is a technology that converts different types of documents, such as scanned paper documents, PDF files or images captured by a digital camera into editable and searchable data. Possibly the most well-known use case for OCR is converting printed paper documents into machinereadable text documents. In OCR processing, the scanned-in image or bitmap is analyzed for light and dark areas in order to identify each alphabetic character or numeric digit. When a character is recognized, it is converted into an ASCII code.

This technology has proven immensely useful in digitizing historic newspapers and texts that have now been converted into fully searchable formats and had made accessing those earlier texts easier and faster.

III. PROPOSED WORK

This application captures an image of a restaurant bill using the mobile phone camera. This image is then processed to find the text related to food items. The text should be detected irrespective of certain parameters like font type, font size and should be detected in low contrast images also. Figure 1 shows the system diagram which consists of four modules. The first step is to scan the printed restaurant bills and extract the text from it. Next we refer the extracted text with food database and the text extracted is forwarded for calculating the corresponding calorie-count. The user is then enlightened of the calories consumed.

The system proposed in this paper is built using the OCR

algorithm. Instead of creating a new OCR implementation, the open-source OCR engine called Tesseract [24] was used here. The engine is being developed and used by Google since 2006. However, several OCR engines use similar techniques to “read” the text in an image. The Tesseract supports various operating systems (Linux, Windows, and Mac OS) and several languages. It has been used for both handwritten as well as printed character recognition. The workflow and architecture can be found in [25]. Tesseract uses a two-pass approach to character recognition. The second pass is known as adaptive recognition and uses the letter shapes recognised with high confidence on the first pass to recognise better the remaining letters on the second pass. This is advantageous for unusual fonts or low-quality scans where the font is blurred or faded.

A. Preprocessing

OCR software often "pre-processes" images to improve the chances of successful recognition. The first step of the processing will consist of different pre-processing tasks, such as converting a color image into grayscale image, remove positive and negative spots, smoothing edges and binarisation. The task of binarisation is performed as a simple way of separating the text or any other desired component of the image from the background.

B. Text Extraction

Once the images are captured, we now have this file that we can easily view from any computer system. The software that extracts text from image should always be equipped with three factors. First, it should be able to retain text and data formatting during the conversion step. Second aspect of the text extraction from image would be the extract data for content aggregation. Third and last, the text extraction from image should be able to preserve in full the text quality from the printed document.

C. Text Recognition

The OCR algorithm uses feature extraction or matrix matching technique to produce a ranked list of candidate characters. Matrix matching is the process of comparing an image to a stored glyph on a pixel-by-pixel basis. This technique works best with typewritten text. It does not work well when new fonts are encountered. Feature extraction segments glyphs into "features" like lines, closed loops, line direction, and line intersections. This reduces the dimensionality of the representation and hence makes the recognition process computationally efficient. These features are matched with an abstract

vector-like representation of a character, which might reduce to one or more glyph prototypes. Nearest neighbour classifiers such as the k-nearest neighbours algorithm are used to compare image features with stored glyph features and choose the nearest match.

D. Calorie count generation

The text recognized is checked for availability in the database .If the text is available in the database, its corresponding calories is fetched, and displayed to the user. If the text is not available in the database, no calories are returned. Once all text in the image is checked, and their corresponding calorie count has been returned, their overall calorie count is generated. Finally the user is enlightened with the overall calorie count.

Here the preprocessing, text extraction and text recognition is done by the help of Google vision API. The Vision API can detect and extract text from any images. There are two annotation features that support optical character recognition. TEXT_DETECTION detects and extracts text from any image. DOCUMENT_TEXT_DETECTION also extracts text from an image, but the response is optimized for dense text and documents. The JSON includes page, block, paragraph, word, and break information.

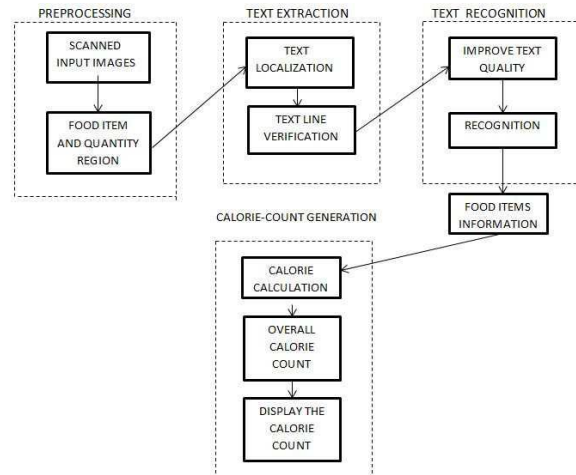


Fig. 1. System design

IV. IMPLEMENTATION AND RESULTS

The proposed system is developed using Android studio and Firebase to detect text on the restaurant bills and show corresponding calories. Figure 2 shows the Application user interface. Also we have used Google vision API to perform the optical character recognition. We need restaurant bills for recognizing the food items on the bill. For the purpose of evaluation, the bills from various restaurants have been collected and scanned

using our application. One of such collected restaurant bill is shown in figure 3a. The bills are generally in the form of printed text. The color of the text in the bills will generally be in blue or black.

The first step is to create a database in Firebase console and to feed the different food items and their calories. The calories of various food items have been taken from Nutritionix [26] the world’s largest verified nutrition database.

Over 100+ health apps make 5M+ queries to nutritionix every month. We have also referenced MyFitnessPal [27] for calories.

The next step is to register the app with Firebase. The dependencies required for the system include both the Google Vision API as well as the Firebase. On opening the application, there is an icon, which when clicked takes the picture of the bill. The scanned text from the image is mapped with the Firebase and the corresponding calories of the food items are displayed in the same intent. Figure 3b shows the result of the sample restaurant bill.

On conducting the experiment on various restaurant bills we get accurate calorie count of the food consumed. The accuracy depends on the quality of the bill, the environment and the quality of the camera. The images of the restaurant bills that we collected for our experiment and the outcome of the experiment is shown in figure 4.

The proposed system faces certain difficulties while implementing the experiment. Some of the most important challenges faced by the system are:

- Difficulties in the quality of the camera: Since our objective is to capture and detect text in the restaurant bill, the phone’s camera must be in a condition such that it focuses the bill, and the text in it, thereby helping the Google vision.
- Difficulties faced in the environment: Since the data on the restaurant bill is used to detect the calories, there rises a compulsion in setting the lights of the room an optimal one. Adequate lighting is required for the experiment to be done.
- Difficulties in the Quality of the bill: Since data on the text is used to show the corresponding calories, the quality of the bill comes into play. Handwritten bills are seldom recognized by the API. Bad quality bills do not cooperate with extracting text.

Figure 5 and 6 shows the bills of different quality of the camera.

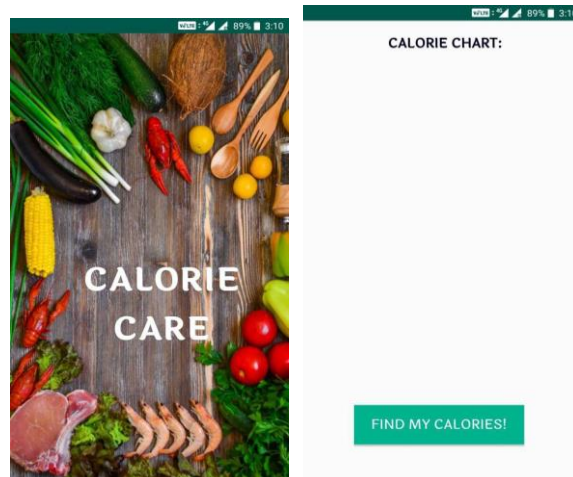
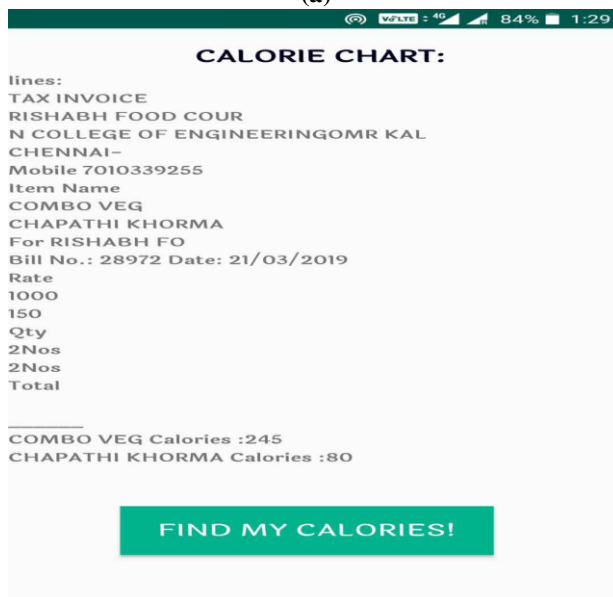


Fig. 2. Application UI



(a)



(b)

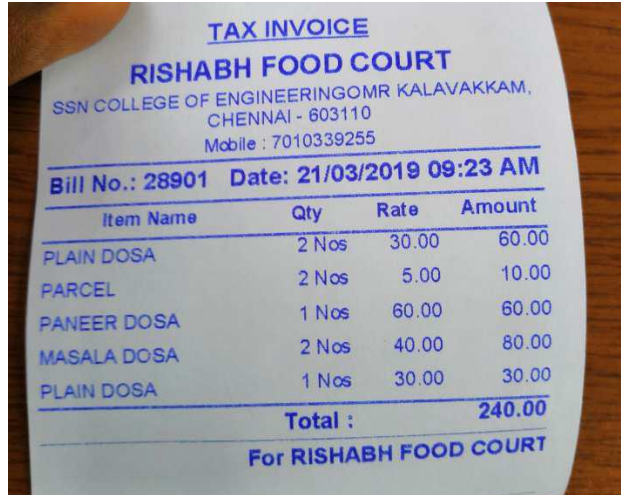
Fig. 3. a) Restaurant bill b) Result



Fig. 4. Bills and Consumed Calories

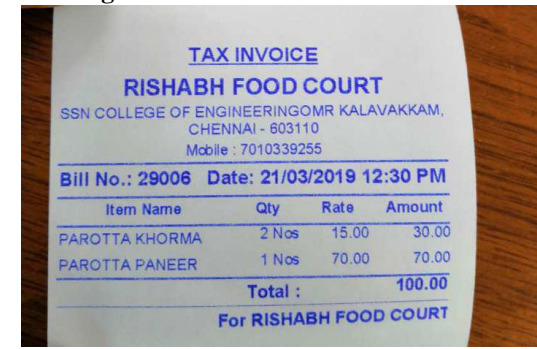


(a)



(b)

Fig. 6. a) Faulty bill b) Ideal bill



(a)



(b)

Fig. 5. a) High clarity camera b) Low clarity camera

V. CONCLUSION AND FUTUREWORK

The recent advancements in technology have always been beneficial to the mankind. This system takes a initiative in attainment of a goal that would help the people to live in healthy life style independently. In this paper, OCR is used to develop a system that recognizes the text on the restaurant bills .We have also calculated corresponding calorie count, thereby enlightening him/her on the calories consumed. Although we faced many challenges during our experiment, we can say with a reasonable level of confidence that above results helped to attain our proposed solution. Our future work is to include handwritten bills to detect and recognize the text on them and calculate the corresponding calories of the

food consumed. We would also like to extend the functionality of detecting text on bills from videos.

REFERENCES

- [1] K. Jain, Y. Zhong Page segmentation using texture analysis *Pattern Recognition*, 29 (5), 1996, pp. 743-770
- [2] Y.Y. Tang, S.W. Lee, C.Y. Suen Automatic document processing: a survey *Pattern Recognition*, 29 (12), 1996, pp. 1931-1952
- [3] B. Yu, A.K. Jain, M. Mohiuddin, Address block location on complex mail pieces, *Proceedings of International Conference on Document Analysis and Recognition*, Vancouver, BC Canada, 1997, pp. 897-901.
- [4] Y. Cui, Q. Huang, Character extraction of license plates from video, *Proceedings of IEEE Conference on Computer Vision and Pattern Recognition*, San Juan, Puerto Rico, 1997, pp. 502-507.
- [5] D.S. Kim, S.I. Chien, Automatic car license plate extraction using modified generalized symmetry transform and image warping, *Proceedings of International Symposium on Industrial Electronics*, Vol. 3, 2001, pp. 2022-2027.
- [6] H.J. Zhang, Y. Gong, S.W. Smoliar, S.Y. Tan, Automatic parsing of news video, *Proceedings of IEEE Conference on Multimedia Computing and Systems*, Boston, 1994, pp. 45-54.
- [7] J.C. Shim, C. Dorai, R. Bolle, Automatic text extraction from video for content-based annotation and retrieval, *Proceedings of International Conference on Pattern Recognition*, Vol. 1, Brisbane, Qld, Australia, 1998, pp. 618-620.
- [8] Ye Q, Doermann D. Text detection and recognition in imagery: A survey. *IEEE transactions on pattern analysis and machine intelligence*. 2015 ,37(7):1480-500.
- [9] D. Karatzas, S. Robles Mestre, J. Mas, F. Nourbakhsh, "ICDAR robust reading competition: Challenge 1: Reading text in born-digital images", *Proc. IEEE Int. Conf. Doc. Anal. Recognit.*, 2011, pp. 1491-1496.
- [10] P. Shivakumara, A. Dutta, U. Pal, C. L. Tan, "A new method for handwritten scene text detection in video", *Proc. IEEE Int. Conf. Front. Handwritten Recognit.*, 2010, pp. 387-392.
- [11] C. Strouthopoulos, N. Papamarkos, A.E. Atsalakis Text extraction in complex color document *Pattern Recognition*, 35 (8), 2002, pp. 1743- 1758
- [12] Karaoglu S, Tao R, van Gemert JC, Gevers T. Context: Text detection for fine-grained object classification. *IEEE transactions on image processing*, 2017, 26(8), pp. 3965-80.
- [13] He T, Huang W, Qiao Y, Yao J. Text-attentional convolutional neural network for scene text detection. *IEEE transactions on image processing*, 2016, pp. 2529-41.
- [14] Chong Yu, Yonghong Song, Quan Meng, Yuanlin Zhang, Yang Liu, "Text detection and recognition in natural scene with edge analysis", *Computer Vision IET9*, 2015, no. 4, pp. 603-613.
- [15] Anand Mishra, Karteek Alahari, C.V. Jawahar, "An MRF model for Binarization of Natural Scene Texts", *International Conference on Document Analysis and Recognition (ICDAR)*, 2011.
- [16] Udit Roy, *Text Recognition and Retrieval in Natural Scene Images*, Hyderabad:CVIT, International Institute of Information Technology, 2015.
- [17] L. Neumann, J. Matas, "Scene text localization and recognition with oriented stroke detection", *Proc. IEEE Int. Conf. Comput. Vis.*, 2013, pp. 97-104.
- [18] J. L. Feild, "Improving text recognition in images of natural scenes", 2014.
- [19] J. J. Weinman, Z. Butler, D. Knoll, J. Feild, "Toward integrated scene text reading", *IEEE Trans. Pattern Anal. Mach. Intell.*, vol. 3, no. 2, pp. 375-387, Feb. 2014.
- [20] X. C. Yin, X. Yin, K. Huang, H. Hao, "Robust text detection in natural scene images", *IEEE Trans. Pattern Anal. Mach. Intell.*, vol. 36, no. 5, pp. 970-983, May 2014.
- [21] J. J. Weinman, E. Learned-Miller, A. Hanson, "Scene text recognition using similarity and a lexicon with sparse belief propagation", *IEEE Trans. Pattern Anal. Mach. Intell.*, vol. 31, no. 10, pp. 1733-1746, 2009.
- [22] Deshpande S, Shriram R. Real time text detection and recognition on hand held objects to assist blind people. In 2016 International Conference on Automatic Control and Dynamic Optimization Techniques (ICACDOT), 2016, pp. 1020-1024, IEEE.
- [23] How does OCR document scanning work?. Explain that stuff, 2012. <http://www.explainthatstuff.com/how-ocr-works.html>
- [24] R. Smith, "An Overview of the Tesseract OCR Engine," *Ninth International Conference on Document Analysis and Recognition (ICDAR 2007)*, vol. 2, pp. 629-633, 2007.
- [25] Tesseract-OCR, <https://code.google.com/p/tesseract-ocr/>
- [26] Nutritionix - Largest Verified Nutrition Database <https://www.nutritionix.com/>
- [27] MyFitnessPal - Calorie Chart, Nutrition Facts in Food <https://www.myfitnesspal.com>

Investigation of temperature dependent DC conductivity and frequency dependent dielectric property of polysiloxane - TiO₂ nanocomposites

^[1]Md Nasir Ali, ^[2]Dr S Chakradhar Goud

^[1]Research Scholar, Department of Mechanical Engineering, Shri Jagdishprasad Jhabarmal Tibrewala University, Jhunjhunu, Rajasthan, India

^[2]Professor & Principal Springfields Engineering College Hyderabad, Telangana, India

Abstract:-- The polysiloxane - TiO₂ nanocomposites were prepared by solvent casting method in triethanolamine and tetrahydrofuran solvents. The prepared nanocomposites were characterized by X-ray's diffraction, Fourier transform infrared spectroscopy for structural study and surface morphology was carried by scanning electron microscopy. The XRD spectra indicate that the pure polysiloxane is amorphous in nature and TiO₂ nanoparticles have anatase (tetragonal crystal system) structure which remains same even after dispersion in polysiloxane. FTIR spectra shows the characteristics peaks of Si - CH₂, Si - CH₃ and Ti - O - Ti confirms the formation of nanocomposites. The surface morphology shows that the nanoparticles are completely embedded in the polysiloxane. Further, the DC conductivity shows that the conductivity increases with increase in temperature due to tunnelling phenomena. Among all nanocomposites, 0.3 wt % shows the high DC conductivity of 6×10^{-5} S/cm. The dielectric spectroscopy study reveals that the 0.3 wt % shows low dielectric constant and dielectric loss as a result it shows high conductivity of 1.35×10^{-4} S/cm. The quality factor confirms that there is small damping loss for 0.3 wt % of nanocomposites which is favourable for the high conductivity.

Keywords: Polysiloxane, Titanium dioxide, Nanocomposites, Dielectric

1. INTRODUCTION

The nanoparticles doped polysiloxane (PS) nanocomposite has unique properties such as absorption of heavy metal ions from aqueous and organic solvents, corrosion resistance, chemical inertness, anti-grafting and low permeability of gases made a potential candidate in many different technological applications [1]. It is well known that the polysiloxane have low surface energy, high dielectric and high temperature resistance up to 760 °C made suitable for insulation, electronic coating, automobile gaskets, sealing and lubricating greases. However, there is a great challenge in maintaining the transparency which is depends on the concentration of filler, solvent used, preparation methods and curing temperature [2].

The inorganic oxides dope in polysiloxane matrix may change the surface energy due to the presence of oxygen vacancies which are predominant at the higher temperature. It is reported that the electrical conductivity of the titanium dioxide (TiO₂) depends on the nonstoichiometry oxygen and which varies from 10^{-14} to 10^{-5} S/cm. It is expected that the addition of inorganic oxide nanoparticles may fill the interfacial cracks and improve significantly its mechanical properties [3, 4]. Pei Huang et al., reported that the packing resin of light emitting diode significantly effects its efficiency due to mismatch of refractive index (RI). The RI of

nanocomposites can be enhanced by doping high RI nanoparticles and it is found that the addition of TiO₂ in polysiloxane increase its RI from 1.42 to 1.6. During chemical processing, the polysiloxane nanocomposite losses its transparency due to the agglomeration causes significant reduce in refractive index (RI) and this problem can be overcome by doping inorganic nanoparticles in matrix. Therefore, author made an attempt to investigate the temperature dependent electrical conductivity and dielectric properties of TiO₂ nanoparticles doped polysiloxane nanocomposites [5, 6]. The nanocomposites of polysiloxane have been prepared by high intense ultra sonication in tetrahydrofuran (THF) media. Further, the prepared nanocomposites were characterized by Fourier transmission infrared spectroscopy (FTIR), X-ray's diffraction (XRD) method and scanning electron microscopy (SEM) for structural and surface morphology analysis. The temperature dependent DC conductivity was carried out by two probe method and dielectric properties were studied by using Hioki LCR Q source meter.

2. MATERIALS AND METHOD

2.1 Materials

All chemicals used for the preparation of nanocomposites are analytical grade. The polysiloxane (99.99 % pure), titanium dioxide (TiO₂), triethanolamine (TOEA) and

tetrahydrofuran (THF) was purchased from Sigma Aldrich, India.

2.2 Synthesis of polysiloxane - TiO₂ nanocomposites

The nanocomposites films were prepared by solution casting method. 5 gm of polysiloxane was dissolved in 150 ml of tetrahydrofuran (THF) and stirred for 72 hrs to obtain a clear solution. Then 0.1, 0.3 and 0.6 wt % of TiO₂ and 0.25 ml of triethanolamine (TOEA) were mixed with the above solution with high intense ultra sonication until dissolution takes place. The homogeneous mixture then poured in to a round Teflon mould and dried in room temperature to remove the solvent and later heated with 50 °C to form dried thin film of nanocomposites. In similar procedure, pure polysiloxane thin film was prepared as following in preparation of nanocomposites [7 – 9].

3. CHARACTERIZATION

The X-ray's diffraction study was carried out by using Philips X-ray diffractometer for the range of 10° to 80° at the rate of 2° per second with CuK α radiation of wave length $\lambda = 1.5406 \text{ \AA}$. The functional group of the polysiloxane and its nanocomposites were studied by using PerkinElmer1600 spectrophotometer in KBr medium. The nanocomposite was mixed with KBr crystals in the ratio of 1:5 and grounded the mixture to obtained homogeneous compound. The surface morphology of the nanocomposites was characterized by Scanning electron microscopy model of Philips XL 30 ESEM spectroscopy. The nanocomposites films were fixed onto the carbon coated copper grid and introduce into the microscopic sample holder for the image scanning.

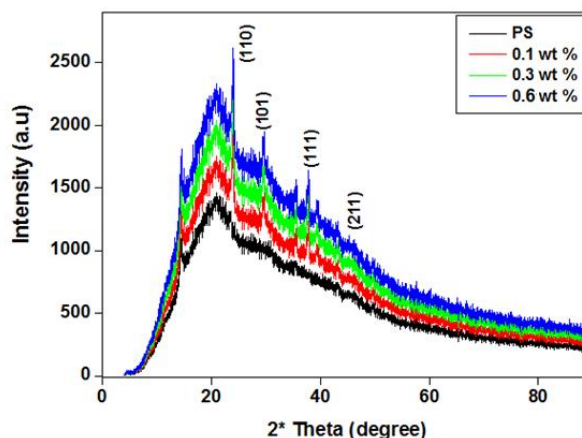
Further, the temperature dependent DC conductivity was studied using indigenous two probe Kelvin set up from room temperature to 220 °C using Keithly source meter by applying silver paste both the side for better connectivity. The impedance spectroscopy of the nanocomposites was carried out by Hoki LCR-Q meter from the frequency range of 50 Hz to 5 MHz.

4. RESULTS AND DISCUSSION

4.1 X-ray's diffraction study

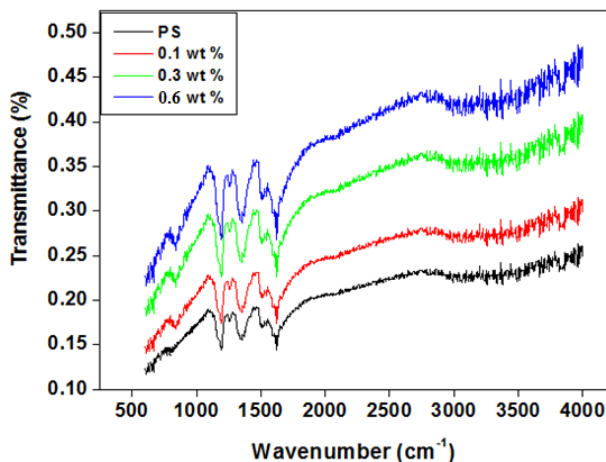
Figure 1 shows the X-ray's diffraction pattern of pure polysiloxane and polysiloxane - TiO₂ nanocomposites for different weight percentages (0.1, 0.3 and 0.6 wt %). It is observed that the pure polysiloxane (PS) is showing a broad peak around 23° which indicate that the polysiloxane is having amorphous in nature. The broad peaks appeared at 23° is due to the diffraction occurs at the interplanar spacing of the polymer. The polysiloxane - TiO₂ nanocomposites for different weight percentages shows the characteristics peaks of TiO₂ in polysiloxane

at 26.30°, 33.22°, 42.12° and 51.23° are corresponding to the plan of (110), (101), (111) and (211) respectively, which is matched with reported data [10, 11]. The crystallite size of the polysiloxane - TiO₂ nanocomposite is calculated by using Debye Scherrer equation and it is found that the crystallite size is around 13nm. It is also important to note that the TiO₂ structure is not distracted even after incorporating in polysiloxane.



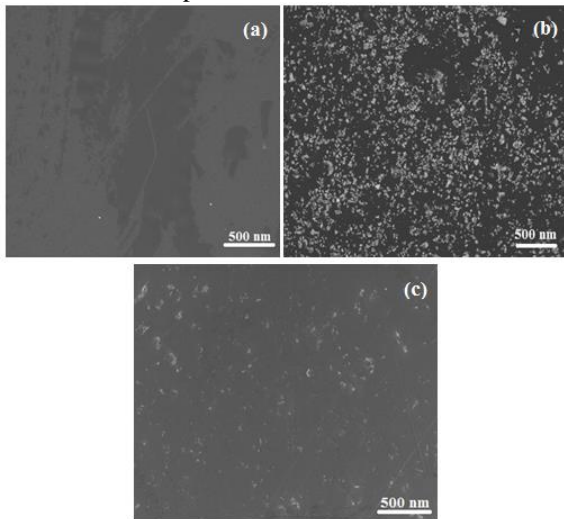
4.2 Fourier transforms infrared spectroscopy

Figure 2 shows the FTIR spectra of pure polysiloxane and polysiloxane - TiO₂ nanocomposites for different weight percentages. The important characteristic peaks appeared for pure polysiloxane is around 1106 cm⁻¹ is corresponding to Si - CH₂ wagging deformation along with the plan of vertical axis, 1453 cm⁻¹ is due to the Si - CH₃ systematic stretching wagging deformation, 1503 cm⁻¹ for C - H stretching because of presence of CH₂, 1613 cm⁻¹ is due to the Si - OH stretching band. However, the polysiloxane - TiO₂ nanocomposites shows all the characteristic peaks along with the peak at 708 cm⁻¹ is corresponding Ti - O - Ti vibration band in plan [12 - 15].



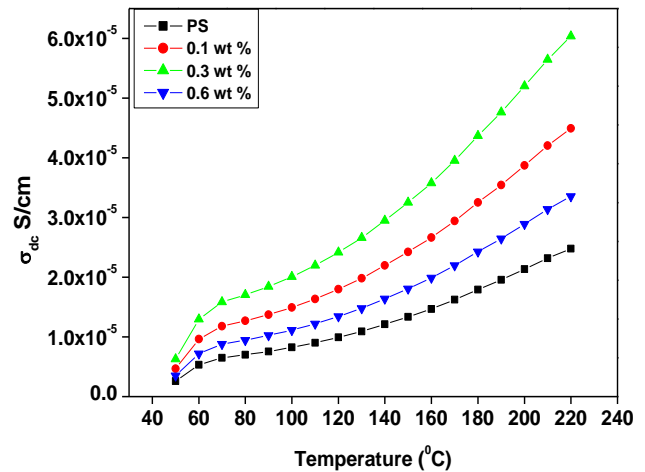
4.3 Scanning electron microscopy

Figure 3 (a - c) shows the SEM image of pure polysiloxane, TiO₂ and polysiloxane - TiO₂ nanocomposites. From the image of pure polysiloxane (a), it is observed the polysiloxane film is having very smooth surface without any crack or agglomeration at the polymer films interface. It is also interesting to note that the solvent aging effect does not appears on its surface and therefore its surface is very smooth. Figure (b) shows that the TiO₂ nanoparticles are form an indusial nanoparticle without any agglomeration and having average particles size of about 13 nm. When these titanium nanoparticles doped in polysiloxane matrix in tetrahydrofuran solvent, the nanoparticles embedded in to the matrix without any formation of crack as shown in figure (c). The nanocomposite films are dried at 50 °C for an hour in presence of helium gas the solvent aging effect almost negligible as a results surface of the nanocomposites appeared very smooth with embedded of TiO₂ in nanocomposites.



5. DC CONDUCTIVITY

Figure 4 shows the DC conductivity of polysiloxane and polysiloxane - TiO₂ nanocomposites with different weight percentages as a function of temperature from 40 °C to 220 °C. It is observed that the conductivity of the polysiloxane and its nanocomposites increases with increase in temperature as well as weight percentages of TiO₂ in polysiloxane up to 3 wt %. The gradual increase in conductivity is due to the tunnelling of charge carriers from one conducting site to another. Among all the nanocomposites, 0.3 wt % of polysiloxane - TiO₂ nanocomposite show high conductivity of 6×10^{-5} S/cm in compare to other nanocomposites. It is also important to note that the after 0.3 wt % conductivity decrease due to the blocking of charge carriers at the interface of the polymer nanocomposites [16, 17].



6. DIELECTRIC STUDY

Figure 5 shows the real part of permittivity of polysiloxane and polysiloxane - TiO₂ nanocomposites with different weight percentages as a function of applied frequency from 50 Hz to 5 MHz. It is observed that the real permittivity value decreases with increase in applied frequency up to 10³ Hz after that it's almost remains constant which is may be due to the dipole polarization where the polarization occurs due to the Si - O and Ti - O - Ti along with symmetry axis. The titanium dioxide nanoparticles have many hydroxyl ions due to the hydrophilic nature of nanoparticles and high surface area to the volume ratio causes high surface energy [18 - 21]. Among all the nanocomposites, 0.3 wt % of polysiloxane - TiO₂ nanocomposite shows lowest real permittivity of 1240 F/m which is due to the two reason i.e., homogeneous distribution of TiO₂ nanoparticles in polysiloxane matrix and negligible solvent aging effect causes smooth surface. However, after 0.3 wt % of TiO₂ in polysiloxane matrix dramatically increase the real permittivity value due to the blocking of charge carriers at the interface.

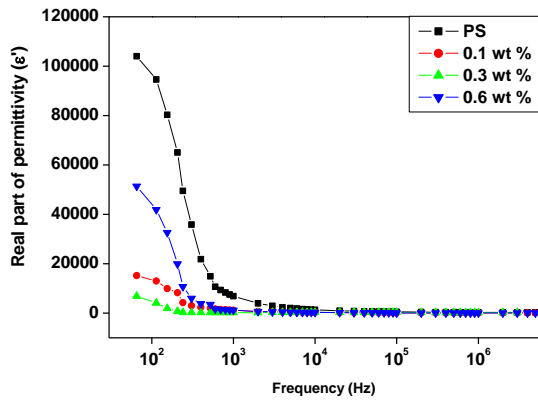


Figure 6 shows the imaginary part of permittivity of polysiloxane and polysiloxane - TiO₂ nanocomposites with different weight percentages as a function of applied frequency from 50 Hz to 5 MHz. The similar behaviour is observed like real part of permittivity for polysiloxane and polysiloxane - TiO₂ nanocomposites except smaller in magnitude of imaginary permittivity. Among all the nanocomposites, 0.3 wt % of shows the lowest value of imaginary permittivity value of 687 F/m due to the polarization effect and distribution of TiO₂ nanoparticles in polysiloxane [22].

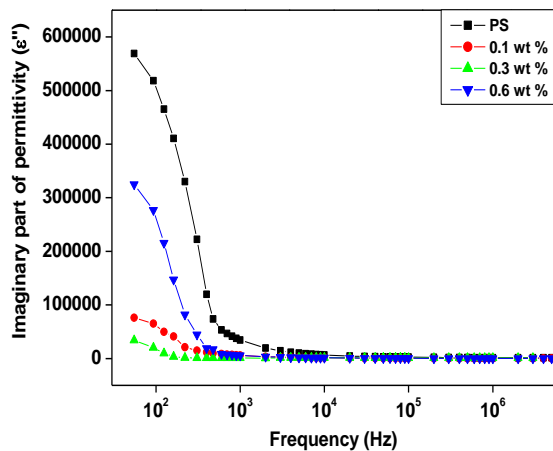


Figure 7 shows the variation of quality factor (Q) as a function of applied frequency for different weight percentages of polysiloxane and its nanocomposites. The damping loss in the nanocomposite is due to the different types of energy loss such as vibrational energy, translation energy and kinetic energy at the higher frequency range. It is observed that the damping loss of polysiloxane and polysiloxane - TiO₂ nanocomposites of all compositions have the value less than 0.5 indicates that the vibrational energy and translation energy loss is almost zero due to the embedded TiO₂ in polysiloxane [23]. For all the nanocomposites, the hump are formed at

the mid frequency range between 10⁴ to 10⁵ Hz due to steady state of electron flow at the equilibrium. Among all the nanocomposites, 0.3 wt % of polysiloxane - TiO₂ nanocomposites shows lowest value of 0.002 because of the fact that there is no free space in between the nanoparticles and polymer matrix results no oscillation at all [24].

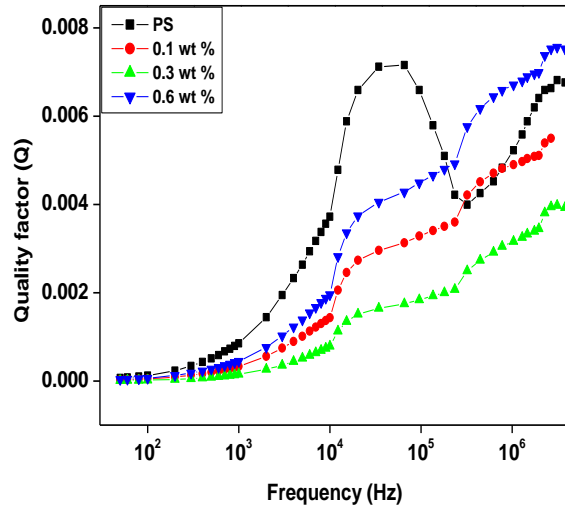


Figure 8 shows the real part of electric modulus of polysiloxane and polysiloxane - TiO₂ nanocomposites with different weight percentages as a function of applied frequency from 50 Hz to 5 MHz. It is observed that the real electric modulus value initially at the lower frequency almost constant for all compositions, however after 10⁴ Hz the electric modulus increases because it is independent of dipole formation at the higher frequency range. It is also indicates that the lower frequency associated with magnetic field perpendicular to the electrical field [25]. However, it is found that with increase in frequency range the magnetic field slowly decrease as a results electric modulus increases gradually. Among all the nanocomposites, 0.3 wt % shows higher electric modulus of 0.0392 which is followed by other compositions and pure polysiloxane. The another reason could be for higher electric modulus due to formation of permanent dipole of Si - OH and Ti - O - Ti along with symmetry axis due to the hydrophilic nature of TiO₂ and high surface energy [26].

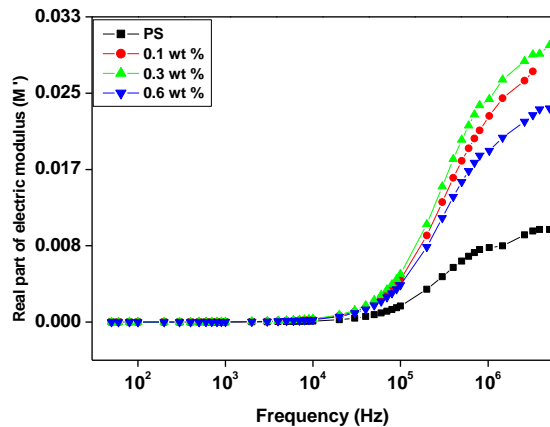


Figure 9 shows the imaginary part of electric modulus of polysiloxane and polysiloxane - TiO₂ nanocomposites with different weight percentages as a function of applied frequency from 50 Hz to 5 MHz. The similar behaviour is observed like real part of electric modulus for polysiloxane and polysiloxane - TiO₂ nanocomposites except higher in magnitude of imaginary electric modulus. Among all the nanocomposites, 0.3 wt % of shows the highest value of imaginary electric modulus of 0.0492 due to the formation of permanent dipole polarization and distribution of TiO₂ nanoparticles in polysiloxane [27 - 30].

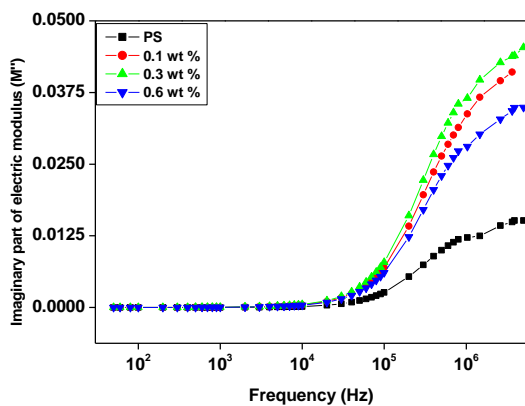


Figure 10 shows the variation of tangent loss as a function of applied frequency for different weight percentages of TiO₂ in polysiloxane. It is observed that the tangent loss value decreases with increase in frequency up to 10⁴ Hz after that it's almost constant for all compositions. Among all the nanocomposites, 0.3 wt % of shows the lowest tangent loss value of 0.2 due to the non-debye's type of relaxation process where the charge carriers are relaxed at the higher energy state for longer time. Hence, 0.3 wt % of polysiloxane - TiO₂ nanocomposite can be used as low *k* - dielectric materials

electrochromic and electrochemical device, capacitor, varistor etc [31].

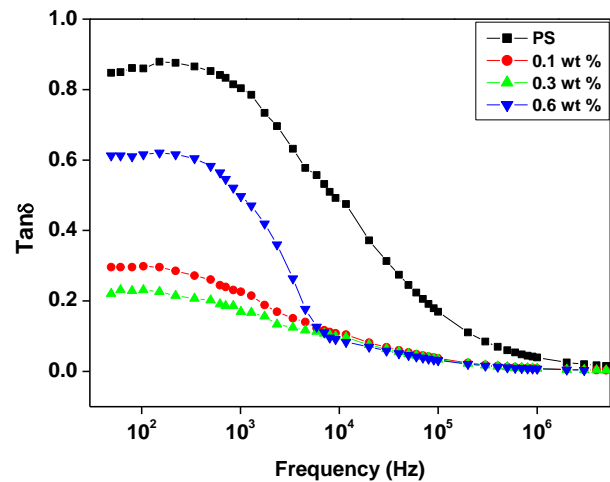
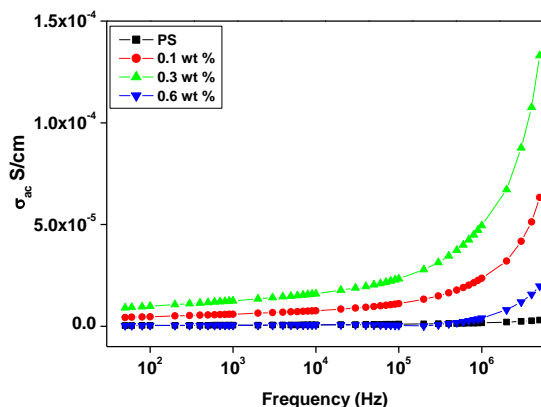


Figure 11 shows the variation of σ_{ac} conductivity for different weight percentages of TiO₂ in polysiloxane as a function of frequency. It is observed that the conductivity of pure polysiloxane and its nanocomposites increases with increase in frequency. The conductivity of the nanocomposites depends on the several factors such as size and shape of the nanoparticles, distribution factor, orientation of nanoparticles in polymer matrix, surface morphology, grain boundary which define the bulk resistance of the samples. Therefore, it is very carefully illustrated the solvent casting process without any aging effects results smooth surface morphology that influence the conductivity [32]. Among all the nanocomposites, 0.3 wt % shows the high conductivity of 1.35×10^{-4} S/cm due to the low dielectric constant and tangent loss due to the favourable surface morphology without any agglomeration or cracking on the surface and also null solvent aging effect [33]. Therefore, these nanocomposites can be potential candidates for the self cleaning coating materials in superhydrophobic glass, capacitors, varistor etc.



7. CONCLUSION

The polysiloxane – TiO₂ nanocomposites have been prepared by solvent casting method in triethanolamine and tetrahydrofuran solvents. The structural study was carried out by X-ray's diffraction and Fourier transmission infrared spectroscopy. The XRD pattern shows that the anatase structure of TiO₂ in polysiloxane and it is found that the crystallite size is around 13nm. The FTIR spectra confirms the important characteristics peaks for pure polysiloxane is around 1106 cm⁻¹ is corresponding to Si - CH₂ wagging deformation along with the plan of vertical axis, 1453 cm⁻¹ is due to the Si - CH₃ systematic stretching wagging deformation and the metal oxide peaks at 708 cm⁻¹ which indicates the formation of nanocomposites. The SEM image of TiO₂ shows rod like structure embedded in polysiloxane with smooth surface morphology without any crack or agglomeration. The temperature dependent conductivity shows that the conductivity increases with increase in temperature as well as TiO₂ weight percentage up to 0.3 % in polysiloxane. Among all nanocomposites, 0.3 wt % shows the high DC conductivity of 6 x 10⁻⁵ S/cm due to the tunnelling phenomena. The dielectric spectroscopy study reveals that the 0.3 wt % shows low dielectric constant and dielectric loss as a result it shows high conductivity of 1.35 x 10⁻⁴ S/cm. The quality factor confirms that there is small damping loss for 0.3 wt % of nanocomposites which is favourable for the high conductivity. Therefore, these nanocomposites can be potential candidates for many high dielectrics engineering applications.

8. REFERENCES

[1] Vu BTN, Mark JE, Schaefer DW. Interfacial modification for controlling silica-polysiloxane interactions and bonding in some elastomeric composites. *Compos Interfaces*. 2003;10:451-73.

- [2] Li B, Zhang J. Polysiloxane/multiwalled carbon nanotubes nanocomposites and their applications as ultrastable, healable and superhydrophobic coatings. *Carbon*. 2015; 93: 648-658
- [3] Fadeev AY, Kazakevich YV. Covalently attached monolayers of oligo(dimethylsiloxane)s on silica: a siloxane chemistry approach for surface modification. *Langmuir*. 2002;18:2665-72
- [4] Klonos P, Sulym IY, Borysenko MV, Gun'ko VM, Kriptou S, Kyritsis A, Pissis P. Interfacial interactions and complex segmental dynamics in systems based on silica-polydimethylsiloxane core-shell nanoparticles: dielectric and thermal study. *Polymer*. 2015;58:9-21.
- [5] Okamoto M, Suzuki S, Suzuki E. Polysiloxane depolymerisation with dimethyl carbonate using alkali metal halide catalysts. *Appl Catal*. 2004; 261:239-45.
- [6] Protsak IS, Kuzema PO, Tertykh VA, Bolbukh YM, Kozakevych RB. Thermogravimetric analysis of silicas chemically modified with products of deoligomerization of polydimethylsiloxane. *J Term Anal Calorim*. 2015; 121:547-57.
- [7] Mironuk IF, Kurta SA, Gergel TV, Voronin EP, Cheladin VL, Kyrta OC. The chemisorbtion of oligomeric polymethylsiloxane on the surface of fumed silica. *Phys Chem Solid State (in Ukr)*. 2009;10:157-65.
- [8] Guo J, Saha P, Liang J, Saha M, Grady BP. Multi-walled carbon nanotubes coated by multi-layer silica for improving thermal conductivity of polymer composites. *J Term Anal Calorim*. 2013;113(2):467-74.
- [9] Roy A.S, Gupta S, Seethamraju S, Madras G, Ramamurthy P.C, Impedance spectroscopy of novel hybrid composite films of polyvinylbutyral(PVB)/functionalized mesoporous silica, *Composites Part B* 2014; 58:134-139.
- [10] Roy A.S, Gupta S, Sindhu S, Parveen A, Ramamurthy P.C, Dielectric properties of novel PVA/ZnO hybrid nanocomposite films, *Compos. Part B Eng*. 2013; 47: 314-319.
- [11] Fragiadakis D, Pissis P. Glass transition and segmental dynamics in poly(dimethylsiloxane)/silica nanocomposites studied by various techniques. *J Non-Cryst Solids*. 2007; 353:4344-52.
- [12] Klonos P, Kyritsis A, Pissis P. Interfacial dynamics of polydimethylsiloxane adsorbed on fumed metal oxide particles of a wide range of specific surface area. *Polymer*. 2015;77:10-3.
- [13] Lewicki J. P, Liggat J J, Richard A. P. Mogon P, Rhoney I. Investigating the ageing behavior of

- polysiloxane nanocomposites by degradative thermal analysis. *Polymer Degradation and Stability*. 2008; 93: 158-168
- [14] Chengjie L, Meng X, Xiaowen Z, Lin Y, In Situ Synthesis of Monomer Casting Nylon-6/Graphene-Polysiloxane Nanocomposites: Intercalation Structure, Synergistic Reinforcing, and Friction-Reducing Effect. *ACS Appl. Mater. Interfaces*, 2017; 9: 33176-33190
- [15] Paquien, J.-N., J. Galy, and J.-F. Gérard. Rheological studies of fumed silica-polydimethylsiloxane suspensions. *Colloids Surf. A*, 2005; 260: 165-172
- [16] Davis A, Yeong Y. H, A. Steele, Bayer I. S, Loth E, "Superhydrophobic nanocomposite surface topography and ice adhesion," *ACS Applied Materials & Interfaces*, 2014; 6: 9272-9279.
- [17] Yeh J, Huang H, Chen C, Su W, Yu Y. Siloxane-modified epoxy resin-clay nanocomposite coatings with advanced anticorrosive properties prepared by a solution dispersion approach," *Surface and Coatings Technology*. 2006; 200: 2753-2763
- [18] Roy. AS. Antistatic and dielectric properties of one-dimensional Al²⁺:Nd₂O₃ nanowire doped polyaniline nanocomposites for electronic application. *Sensors and Actuators A* 2018; 280: 1-7
- [19] Xie Y, Geng C, Liu X, Xu S, Xing W, Zhang X, Zhang Z H, Zhang Y, Bi W. Synthesis of highly stable quantum-dot silicone nanocomposites via in situ zinc-terminated polysiloxane passivation. *Nanoscale*, 2017; 9:16836-16842
- [20] Li C, Xiang M, Zhao X, Ye L. In Situ Synthesis of Monomer Casting Nylon-6/Graphene-Polysiloxane Nanocomposites: Intercalation Structure, Synergistic Reinforcing, and Friction-Reducing Effect. *ACS Appl Mater Interfaces*. 2017; 27: 33176-33190.
- [21] Chiu Y C, Huang C C, Tsai H C. Synthesis, characterization, and thermo mechanical properties of siloxane-modified epoxy-based nano composite. *J. Appl. Polym. Sci.* 2014; 131: 40984
- [22] Ma T, Yang R, Zheng Z, Song Y. Rheology of fumed silica/polydimethylsiloxane suspensions. *Journal of Rheology* 2017; 61: 205
- [23] Mobuchon, C., P. J. Carreau, and M.-C. Heuzey. Structural analysis of non-aqueous layered silicate suspensions subjected to shear flow," *J. Rheol.* 2009; 53: 1025-1048
- [24] Cassagnau, P., "Melt rheology of organoclay and fumed silica nanocomposites," *Polymer* 2008; 49: 2183-2196
- [25] Camenzind, A., T. Schweizer, and M. Sztucki, "Structure & strength of silica-PDMS nanocomposites," *Polymer* 2010; 51: 1796-1804
- [26] Yue, Y., C. Zhang, and H. Zhang, "Rheological behaviors of fumed silica filled polydimethylsiloxane suspensions," *Composites, Part A* 2013; 53: 152-159
- [27] Smith, J. S., O. Borodin, and G. D. Smith, "A molecular dynamics simulation and quantum chemistry study of poly(dimethylsiloxane)-silica nanoparticle interactions," *J. Polym. Sci., Part B* 2007; 45: 1599-1615
- [28] Kirst, K. U., F. Kremer, and V. M. Litvinov, Broad-band dielectric spectroscopy on the molecular dynamics of bulk and adsorbed poly(dimethylsiloxane). *Macromolecules* 1993; 26: 975-980
- [29] Roy AS, Gupta S, Seethamraju S, Ramamurthy PC, Madras G. Fabrication of Poly(Vinylidene Chloride-Co-Vinyl Chloride)/TiO₂ Nanocomposite Films and Their Dielectric Properties. *Science of Advanced Materials*. 2014; 6: 946-953
- [30] Bruzard S, Levesque G. Polysiloxane-g-TiNbO₅ Nanocomposites: Synthesis via in Situ Intercalative Polymerization and Preliminary Characterization. *Chem. Mater.*, 2002; 14: 2421-2426
- [31] Ansari JN, Khasim S, Parveen A, Hartomy O AA, Khattari Z, Badi N, Roy AS. Synthesis, characterization, dielectric and rectification properties of PANI/Nd₂O₃:Al₂O₃ nanocomposites. *Polymers for Advanced Technologies*. 2016; 27: 1064-1071
- [32] Polmanteer, K.E.; Hunter, M.J. Holms, D.R.; Bumm, C.W.; Smith, D.I. Polymer composition versus low-temperature characterization of polysiloxane elastomers. *J. Appl. Polym. Sci.* 1959; 1: 3-10
- [33] Harshe, R.; Balan, C.; Riedel, R. Amorphous Si(Al)OC ceramics from polysiloxanes: Bulk ceramic processing, crystallization behavior and applications. *J. Eur. Ceram. Soc.* 2004; 24: 3471-3482.

Multi – Level Wavelet and Curvelet based Video Watermarking for Copyright Protection

^[1]M. Selvaganapathy, ^[2]Dr. R. Kayalvizhi

^[1]Ph.D Scholar, ^[2]Professor

^{[1][2]}Annamalai University, Chidambaram, Tamil Nadu, India

Abstract:-- Nowadays, security plays a vital role in every field of applications. The main aim of this research work is to increase the authentication and security by means of multi-level Video Watermarking using Discrete Wavelet Transform (DWT). The nature of watermarking used in this work is Invisible Watermarking. In invisible watermarking, the input data such as image, video and audio can be embedded into the original video. This invisible video watermarking has to be attained in multi-level by using DWT. DWT algorithm has to be written using MATLAB coding. In order to have more secure data, a secret key is used during an embedded process. The original image can be extracted only if the correct secret key is matched at the output side. DWT is used to convert the spatial domain data into a spectral domain data. This algorithm may be used in variety of applications like copyright protection, defence applications, broadcasting applications, Meta – data applications, etc. Similar to Discrete Wavelet Transform (DWT), Discrete Curvelet Transform also used to increase the authenticity of the input image with better quality. Curvelet transform is used for embedding the images into the video. In this research as a secondary, the procedure of watermarking is repeated with the Curvelet transform. The outcome of this research is to make secure digital data transmission that helps in variety of applications like broadcast monitoring, ownership assertion, medical applications and mostly used in defence department.

Keywords: Multi – level video watermarking, DWT, SVD, MATLAB, Color Image Processing, DCLT

1. INTRODUCTION

With a tremendous change over the field of electronics, science and technology, the internet signifies a fundamental role. While entering into the era of advanced communication, the digital communication plays a vital role. The digital communication not only relies on the digital signals but also the digital images as the sources of communication. Digital Image Processing uses a computer algorithm on the digital images. For a digital image processing, the security and authentication are the important most criteria. So, this research paper investigates about the multi – level video watermarking using Discrete Wavelet Transform (DWT) and Singular Value Decomposition (SVD) which improves the authenticity of the input images. The Digital Watermarking is a digital concept where the image is hid into the image for the security purpose. There are two types of watermarking namely. They are Visible Watermarking and Invisible Watermarking. The visible watermarking is a type of digital watermarking where the embedded image is visible even after the embedding process is over. For an example, some registered channel adds a watermark in a form of copyright logo that can be displayed during the broadcasting process. This visible watermarking can be used for enhanced copyright protection and for indicating ownership originals. Likewise, the invisible watermarking is a type of watermarking that aims to provide secure data transmission through a data hiding concept. There are

two digital video watermarking technique used to guard the video from digital handling and offers the copyright substantiation. Digital video watermarking techniques are spatial domain and spectral domain. Spatial Domain technique is not strong for many image processing attacks. Spectral Domain method ensures the robustness of watermark. Spectral domain is subdivided into DFT (Discrete Fourier Transform), DCT (Discrete Cosine Transform) and DWT (Discrete Wavelet Transform). The Discrete wavelet transform is more frequently use because of its excellent multi-resolution and spatial localization characteristics. In this paper, the video watermarking with multiple levels DWT and SVD is being proposed. The copyright owners needs to face the one of the major issues are Intellectual and copyright protection. Internet access and all the digital media access such as audios, videos, images and digital documents gives great threat to copyright owners as their work gets manipulated, forged and redistributed expediently through illegal means. This paper presents the digital watermarking techniques applied on the videos. This digital video watermarking is used to protect the video from various attacks & noises also protect the video from digital manipulation. Mainly it is used to provide the copyright authentication. Spatial domain watermarking and spectral domain watermarking are two video watermarking methodologies to embed the watermark bits on the video or image. Spatial domain method is not robust against various signal processing methods and noises. But spectral domain method ensures high robustness against various processes. In this paper a

video watermarking technique based on curvelet transform is proposed. The proposed curvelet transform based watermarking is providing high level security to the digital data. And this algorithm follows the strong embedding and extracting algorithm. Hence it is difficult for the attackers to seize the original information. This type of watermark also provides the better watermark parameters such as Noise Correlation (NC), Peak Signal to Noise Ratio (PSNR).

II. CURRENT AND FUTURE SYSTEM (DWT)

A. CURRENT SYSTEM

The existing system uses the embed watermark in high frequency sub – band initially and uses a portion of low frequency sub – band for embedding (which depends on the significance of the sub – band). The watermark embedding process uses different embedding formula. The algorithm was incorporated with some of the features of visual masking of human vision system. In this research, the Discrete Wavelet Transform is applied to each of the frames. For 2D frames, the DWT is applied by means of applying 1D filter in two dimensions. The filter is initially divided into four non – overlapping sub bands like LL1, LH⁻¹, HL1, HH1. Where, L stands for the Low frequency sub – region and H stands for High frequency sub – region. The second level of transformation is applied to the lower most frequency sub – region to get non – overlapping LL2, LH⁻², HL2, HH2 sub – regions.

B. FUTURE SYSTEM (PROPOSED SYSTEM)

The following modifications are allowed in the proposed system:

- a.The watermark video is selected with proper coefficient.
- b.Watermark image is extracted and separated with R, G and B panels.
- c.With the watermark coefficient, the watermark is extracted.

C. OBJECTIVES

The objective of the research are:

- a.To convert the spatial domain data into the frequency domain data having low and high frequency components.
- b.To extract the embedded watermark with good resolution.
- c.Robust against various attack and noises.

D. MOTIVATION:

- a.Algorithm is founded to be highly robust for various attacks.
- b.Extracted watermark should be equal to the proportion of original watermark.

- c.Improved security for various processing operations such as averaging, histogram equalization, etc.

E. RESEARCH DESCRIPTION

This research proposes a digital watermarking over a high authenticity which made us to take video watermarking to the multi – level. This chapter proposes the flow graph of the research. The proposed video watermarking algorithm emphasizes on:

- (i)Improved security with a secret key.
- (ii)Multi – Level Watermarking.
- (iii)Enhanced quality of watermark video.
- (iv)Lower Mean Square Error.
- (v)Unsize video size of a host video.

The input video has continuous video frames. From that, the video shots can be captured which consists of single or a multiple video frames. The block diagram for the proposed research is explained with the following blocks

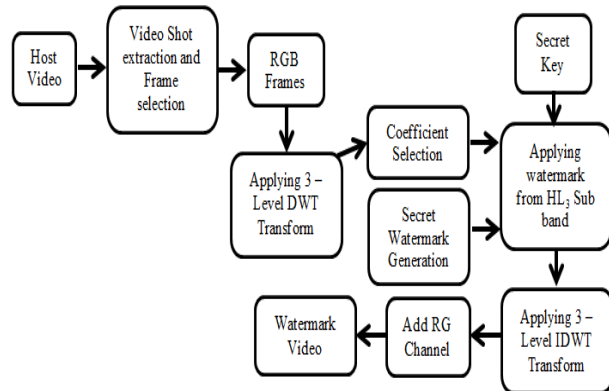


Fig. 1 – Block Diagram for the proposed multi – level video embedding

This research proposes a digital watermarking over a high authenticity which made us to take video watermarking to the multi – level. This chapter proposes the flow graph of the research. The proposed video watermarking algorithm emphasizes on:

- (i) Improved security with a secret key.
- (ii) Multi – Level Watermarking.
- (iii) Enhanced quality of watermark video.
- (iv) Lower Mean Square Error.
- (v) Unsize video size of a host video.
- (vi) The input video has continuous video frames. From that, the video shots can be captured which consists of single or a multiple video frames. The block diagram for the proposed research is explained with the following blocks.

The above fig. 1 represents the diagram for the multi – level video watermarking embedding process. The watermarking embedding is a process of hiding the watermark video into the original video for the purpose

of authenticity. Here, the 3 – level video watermarking embedding process is being proposed.

In the extraction process, the host video is retrieved from the watermarked video. The extraction process have the following steps;

- a. Read the video and separate it into multiple video frames.
- b. Read the watermarked image with desirable size.
- c. R, G and B panels are separated.
- d. Apply multi – level DWT on B – panel of the watermarked image. (The no. of levels considered here was 3).
- e. Enter the secret key to extract the image from the video.
- f. If the secret key is correct, then the watermarked image is extracted from the video.
- g. If not, the pop – up message will be displayed with the message as that “the entered key is incorrect”.

The figure 2 represents the block diagram of multi – level video watermarking video extraction process.



Fig. 3 – Watermarked images using DWT

F. RESULTS AND DISCUSSION

The proposed algorithm is implemented using MATLAB as the basic tool on the video database consists of the image database with multiple web images, standard video database and also on the video captured from the laboratory under non – standard conditions as specified in table 1.

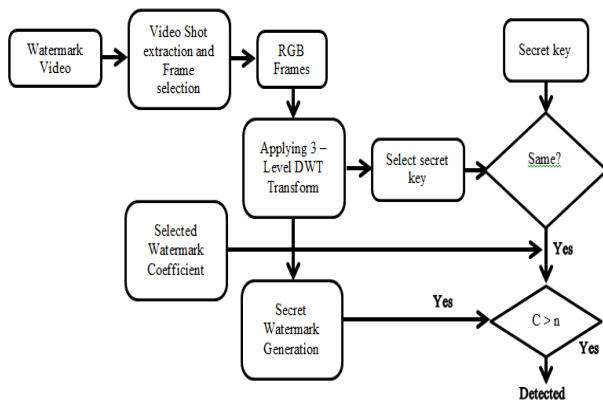


Fig. 2 – Block Diagram for the proposed multi – level video extraction

S. No	Video Name	Specifications			Source
		Frame Size	Duration (in Sec.)	No. of Frames	
1	viptraffic.avi	120 x 160	8	120	Standard Database
2	rhinos.avi	240 x 320	6	114	Standard Database
3	Shaky_car.avi	240 x 320	4	132	Standard Database
4	Scenevideoclip.avi	160 x 120	7	92	Standard Database
5	Video_1.avi	240 x 320	44	448	Downloaded
6	Video_2.avi	288 x 360	43	1077	Downloaded

7	Video_3.avi	480 x 640	5	67	Downloaded
8	Video_4.avi	640 x 480	18	543	Captured in Lab
9	Video_5.avi	480 x 640	14	140	Captured in Lab
10	Video_6.avi	480 x 640	15	155	Captured in Lab

Table 1 – Types of Video Database

The computations are carried out on the system with the following configuration: Intel ® Core™ i7 – 4770 processor having maximum clock frequency of 3.4 GHz and 32 GB RAM.

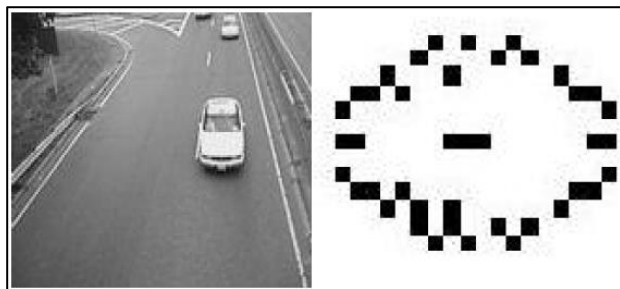
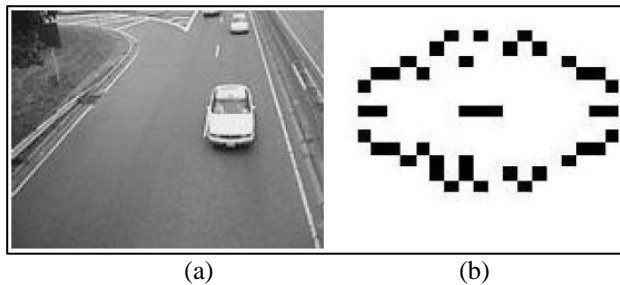


Fig. 4 – For ‘viptraffic.avi’ (a) Original frame #20 (b) Original watermark testpat1 (c) Watermarked video Frame (d) Extracted watermark from (c)


The video algorithm is tested with large no. of videos but in this paper only selective videos are indicated. The figures are shown only for one video (i.e.) viptraffic.avi which is a standard video available in the MATLAB directory. The watermark image used in this example is taken again from the directory of MATLAB (i.e.) testpat1 of dimension 256 x 256. The results with no attacks are discussed in fig. 4. The robust video watermarking algorithm is proposed by embedding watermark on each frames of the video. This algorithm realizes blind video watermarking embedding and extraction which are found to be highly robust for various common attacks. The Normalized Correlation



Coefficient (NCC) and Structural Similarity (SSIM) index are calculated towards the reconstructed image.

Video	Parameters	No attacks	Average Filter	Median Filter	Gaussian Filter	Salt and Pepper Noise	Histogram equalization
viptraffic.avi	PSNR (dB)	Inf.	22.101	19.749	13.778	12.93	15.970
	NCC	1	0.993	0.987	0.956	0.947	0.969
	SSIM	1	0.994	0.989	0.957	0.948	0.969
rhinos.avi	PSNR (dB)	Inf.	26.637	25.921	17.743	17.165	12.570
	NCC	1	0.997	0.997	0.9776	0.975	0.9301
	SSIM	1	0.998	0.998	0.9842	0.983	0.9258

Shaky_car.avi	PSNR (dB)	Inf.	21.714	19.094	18.883	18.020	11.4421
	NCC	1	0.993	0.985	0.986	0.982	0.896
	SSIM	1	0.993	0.986	0.987	0.986	0.929
Scenevideoclip.avi	PSNR (dB)	Inf.	25.914	24.817	17.864	16.876	7.934
	NCC	1	0.997	0.996	0.983	0.979	0.838
	SSIM	1	0.998	0.997	0.992	0.989	0.934
Video_1.avi	PSNR (dB)	Inf.	27.842	28.759	19.946	19.183	13.685
	NCC	1	0.998	0.998	0.989	0.987	0.942
	SSIM	1	0.999	0.999	0.993	0.992	0.942
Video_2.avi	PSNR (dB)	Inf.	25.428	22.071	16.076	15.351	17.964
	NCC	1	0.997	0.993	0.975	0.975	0.983
	SSIM	1	0.998	0.995	0.981	0.977	0.987
Video_3.avi	PSNR (dB)	Inf.	27.908	25.682	18.071	17.120	13.320
	NCC	1	0.998	0.997	0.984	0.997	0.953
	SSIM	1	0.998	0.998	0.988	0.986	0.967
Video_4.avi	PSNR (dB)	Inf.	32.350	32.453	19.919	19.633	8.893
	NCC	1	0.999	0.999	0.989	0.989	0.870
	SSIM	1	0.999	0.999	0.992	0.992	0.899

Table 2 – Watermark Result after various Attacks

Video Name	viptraffic.avi
Parameter	Extracted Watermark
No Attack	

Average Filter	
Median Filter	



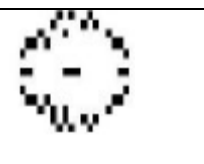
Gaussian Filter	
Salt and Pepper	
Histogram Equalization	

Fig. 5 – Extracted watermark of frame #20 after various attacks on viptraffic.avi

G. SIMULATION RESULT

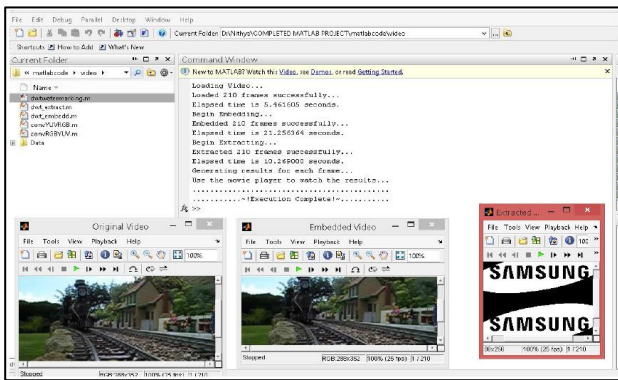


Fig. 6 – Simulation Result: An output console indicating original video, embedded video and the watermark image

III. CURRENT AND FUTURE SYSTEM (DCLT)

A. CURRENT SYSTEM

Curvelet transform has been proposed to overcome the limitations of wavelet transform. Curvelet transforms are Non-adaptive technique for multiscale object representation. This transform differs from directional wavelet transform in that the degree of localization in orientation varies with scale. Higher resolution is achieved in curvelet transform than the wavelet transform. And also efficient numerical algorithms exist for computing the discrete data of curvelet transform.

B. FUTUTRE SYSTEM

The proposed system is presented with single level transform. Which means the watermarking is performed by using single level curvelet transform. Because the possibility of multilevel transform in curvelet domain is

less. Hence in future, the multilevel curvelet transform will be performed.

C. OBJECTIVE

- a. To increase the authenticity a video watermarking technique using curvelet transform is performed.
- b. To achieve high robustness against various noise attacks such as Gaussian noise, Salt and pepper noise.
- c. To make digital data into highly secure against various processing such as cropping, noise addition, etc.

D. RESEARCH DESCRIPTION

Curvelet Transform Algorithm

Curvelet transform has been proposed to overcome the limitations of wavelet transform. Curvelet transforms are Non-adaptive technique for multiscale object representation. This transform differs from directional wavelet transform in that the degree of localization in orientation varies with scale. Higher resolution is achieved in curvelet transform than the wavelet transform. And also efficient numerical algorithms exist for computing the discrete data of curvelet transform.

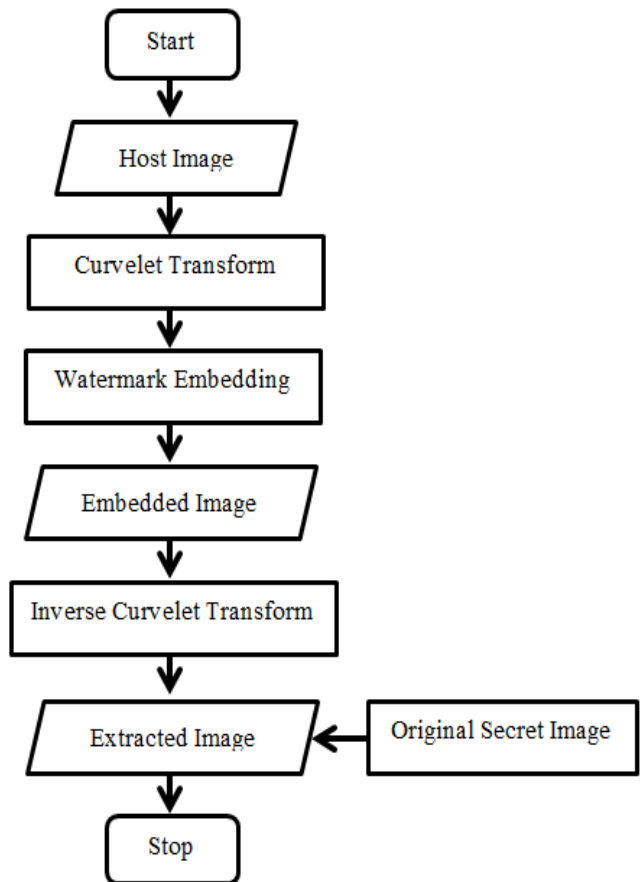


Fig.7 Flow Diagram of The Proposed Scheme

Embedding Algorithm using DCLT

- Step1: Read the host video and divide the video into frames.
- Step2: Split each of the frame into Red, Green and Blue components.
- Step3: Convert the RGB components of each of the frames into Grey components.
- Step4: Apply random number generator to select random set of frames for watermark embedding.
- Step5: Apply Curvelet Transformation using db wavelets to each of the randomly selected frames in order to obtain four frequency sub bands
- Step6: Take the watermark image which is to be embedded in the host video frames and split it into red, blue and green components.
- Step7: Convert the RGB components of the watermark image into grey component.
- Step8: The watermark bits are then embedded into significant coefficients of the host video frames.
- Step9: Apply Reverse Curvelet Transformation to obtain the watermarked frames.
- Step10: Reconstruct the watermarked video by combining frames.

Extraction Algorithm using DCLT

- Step1: Read the watermarked video and split it into frames
- Step2: Convert the red, blue and green components into grey component.
- Step3: Apply wavelet transformation using db wavelets upto three level decomposition to obtain sub-bands.
- Step4: Evaluate the difference between the watermarked frame and the decomposed frequency sub band of the host frame to get the watermark.

E. RESULT AND ANALYSIS

In the project work, the experiments are carried using Matlab coding. We have prepared a GUI layout with a list of menus. Clicking on each menu will perform an independent function. The inputs used are a coloured video of .avi type and a coloured watermark image that will be embedded inside the video frames. All the frames are of same size. The watermark image used is of the same size of rows and columns as the video frames. The proposed technique uses a random number generator that generates a set of numbers that will be used as a secret key at the time of watermark extraction. Those numbers will be used as the references for selecting the random frames that will be further used for watermark embedding.

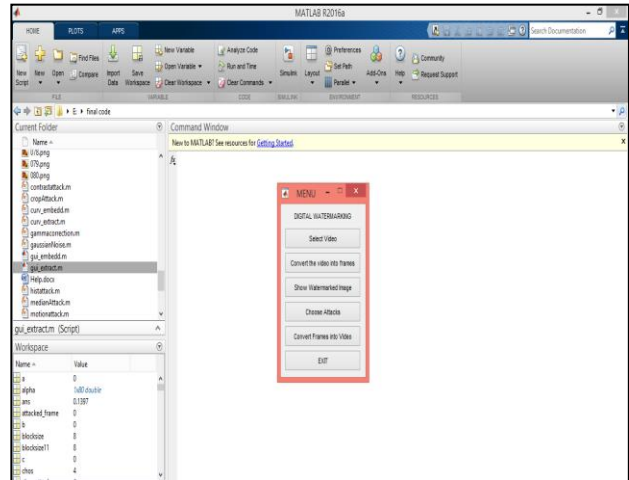


Fig 8. Graphical user Interface

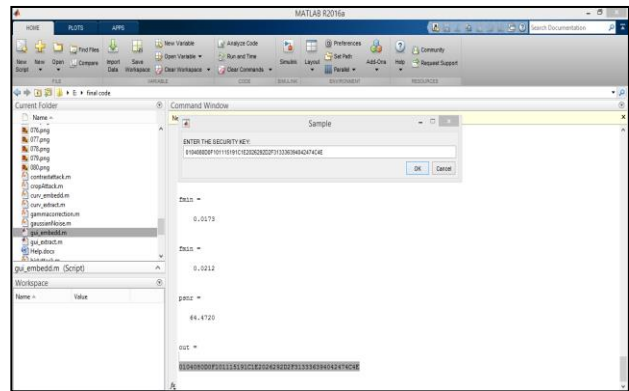


Fig 9. Secret Key Generation

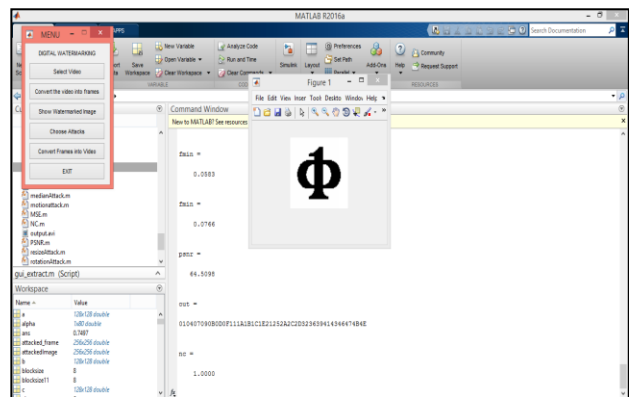


Fig 10. Watermark Image without attack

Performance Metrics

The quality of the watermark can be analyzed by calculating the Mean Square Error (MSE), Peak Signal to Noise Ratio (PSNR), Normalized Cross Correlation (NC).


```
psnr =  
  
    64.4989  
  
out =  
  
010407090B0D0F111A1B1C1E21252A2C2D323639414346474B4E  
  
nc =  
  
    0.6534
```

REFERENCES

[1] Md. Asikuzzaman, Md. Jahangir Alam, Mark R. Pickering, "A blind and robust video watermarking scheme in the DT CWT and SVD domain", Picture Coding Symposium (PCS) 2015, pp. 277-281, 2015.

[2] X. Ye, X. Chen, M. Deng, S. Hui and Y. Wang, "A Multiple-Level DCT Based Robust DWT-SVD Watermark Method," 2014 Tenth International Conference on Computational Intelligence and Security, Kunming, 2014, pp. 479-483.

[3] X. Chang, W. Wang, J. Zhao and L. Zhang, "A survey of digital video watermarking," 2011 Seventh International Conference on Natural Computation, Shanghai, 2011, pp. 61-65.

[4] H. Y. Huang, C. H. Yang and W. H. Hsu, "A Video Watermarking Technique Based on Pseudo-3-D DCT and Quantization Index Modulation," in IEEE Transactions on Information Forensics and Security, vol. 5, no. 4, pp. 625-637, Dec. 2010.

[5] S. Kadu, C. Naveen, V. R. Satpute and A. G. Keskar, "Discrete wavelet transform based video watermarking technique," 2016 International Conference on Microelectronics, Computing and Communications (MicroCom), Durgapur, 2016, pp. 1-6.

[6] Srinivasa Rao, T & Rajasekhara Rao, K. (2016). Integrity based video watermarking using Gaussian based DWT embedding and extraction process. 11. 3235-3240.

[7] M Rizvana and M. Selvaganapathy, "A Video Watermarking Technique using SVD and DWT", International Journal for Research in Applied Science & Engineering Technology (IJRASET), Volume 5 Issue X, October 2017, pp. 2217 – 2226.

[8] R. Surya Prakasa Rao & Dr. P. Rajesh Kumar "PSO based Lossless and Robust Image Watermarking using Integer Wavelet Transform" Publisher: Global Journals Inc. (USA) Volume 17 Issue 1 Version 1.0 Year 2017 Online ISSN: 0975-4172 & Print ISSN: 09754350.

[9] Masato Ogura, Yosuke Sugiura and Tetsuya Shimamura "SVD Based Audio Watermarking Using Angle-Quantization" International Conference on

Electrical, Computer and Communication Engineering (ECCE), February 16-18, 2016, Cox's Bazar, Bangladesh.

[10] Sneha Kadu, Ch.Naveen,V.R.Satpute and A.G.Kesar "Discrete Wavelet Transform Based Video Watermarking Technique" 2016 IEEE.

[11] G.Ramkumar and M.Manikandan, "Uncompressed Digital Video Watermarking Using Stationary Wavelet Transform," 2014 IEEE International Conference on Advanced Communication Control and Computing Technologies (ICACCCT), pp.1252-1258, May 2014.

[12] PragyaAgarwal, and AnkurChoudhary , "Protecting Video Data Through Watermarking: A Comprehensive Study," 2014 5th International Conference- Confluence The Next Generation Information Technology Summit(Confluence),pp.657662,Sept 2014.

[13] Y. RaghavenderRao, Dr.E.Nagabhooshanam, Nikhil Prathapani, "Robust video watermarking Algorithm Based on SVD transform", 2014 International Conference on Information Communication and Embedded System ICICES2014, pp.1-5, Feb 2014.

[14] Mr Mohan A Chimanna and Prof.S.R.Khot , "Robustness of video watermarking against various attacks using wavelet Transform Techniques and Principle Component Analysis", 2013 International Conference on Information Communication and Embedded System(ICICES),pp.613,Feb 2013.

[15] BhavnaGoel and CharuAgarwal, "An Optimized Un-compressed Video Watermarking Scheme based on SVD and DWT " 2013 Sixth International Conference on Contemporary Computing (IC3), pp. 307-312, Aug 2013.

An Intelligent Model for Residual life Prediction of Thyristor

^[1]Cherry Bhargava, ^[2]Jagdeep Singh, ^[3]Pardeep Kumar Sharma

^[1]SEEE, Lovely Professional University, Phagwara, Punjab 144411, India.

^[2]IIIEE, Lund University, Lund, Sweden.

^[3]LSPS, Lovely Professional University, Phagwara, Punjab 144411, India.

Abstract:-- Modern age is the age of integration, where millions of electronic components are integrated and installed on a single chip, to minimize the size of device and automatically increases the speed. But, as a greater number of components are placed on a single device, reliability becomes a concern issue, as failure of one component can degrade the complete device. From dimmer to high voltage power transmission, thyristors are widely used. The failure of thyristor can be proven dangerous for mankind, so the reliability prediction of thyristor is highly desirable. This paper is based on the accelerated life testing based experimental technique for reliability assessment. An intelligent model is designed using artificial intelligence techniques i.e. ANN, Fuzzy and ANFIS and comparative analysis is conducted to estimate the most accurate technique. Fuzzy based Graphical User Interface (GUI) is framed which informs the user about the live status of thyristor under various environmental conditions. The intelligent techniques are validated using experimental technique. An error analysis is conducted to predict the most accurate and reliable system for residual life prediction of thyristor. Out of all prediction techniques, ANFIS has the highest accuracy i.e. 95.3%, whereas ANN and Fuzzy inference system has accuracy range 86.1% and 89.2% respectively.

Keywords: Multi – Artificial Intelligence, Accelerated life testing, Graphical user interface, Reliability Prediction, Thyristor.

1. INTRODUCTION

The world is facing the fastest growing problem of electronic and electrical waste. It has hazardous material which is dangerous of human being. It is expected that by year 2020, the waste of electrical and electronics equipment (WEEE) will grow up-to 12 million tones. The reliability prediction is the key parameter for successful operation of the device or equipment. When a manufacturer releases a product in market, a datasheet is provided along with the component, which states the life of the component. If the component fails within warranty period, manufacturer has to bear the replacement cost or repairing charges. Moreover, failure before time, degrades the market reputation of the manufacturer. So, the reliability estimation is the crucial issue for the manufacturers. On the other side, the failure of the component may cause the financial as well as professional loss to the consumer. This failure rate drifts for the duration of the life of the item with time. Life is an important aspect while choosing the electronic hardware. Residual life estimation and life prediction are two distinct terms. If the remaining useful life (RUL) is calculated, it can save the user from complete shutdown or system failure [1]. The predicted life can direct the user for re-use of the component, that in-turns decreases the waste of electrical and electronics equipment (WEEE) problem to a great extent[2].

Many researchers are working on the untimely failure and fault analysis of electrical and electronic components and equipment. Various experimental, statistical as well as standard methods are deployed for failure prediction. For live health monitoring of the components, artificial intelligence techniques are used, which has capability to predict the end of life status of the component at various operating conditions and input parameters[3]. So, failure and fault prediction of the component becomes an important parameter for lucrative performance.

Thyristor

The Thyristor is semiconductor device. It is four layered device which acts as a switch. Thyristor word is composed of two words (the thyatron and the transistor). A thyristor works on the similar principle as a transistor. It is constructed of three electrodes: the gate, the anode and the cathode. The gate work as the controlling. It is mostly used in ac circuits. P type material and N type material used in thyristor[4]. SCR (Silicon-controlled rectifier) is like a thyristor. It behaves like a rectifying diode. Four layers of thyristors.

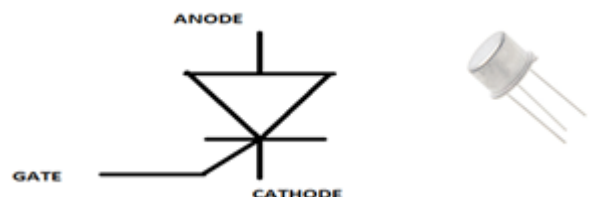


Figure 1. Symbol of thyristor 2N-2324

II. METHODS AND MATERIALS

Compact size and high speed are the prime need of the users. So, millions of components are integrated on a small size chip, which is known as integrated chip. The performance of the equipment depends on the reliability of the components inserted inside. A failure of single component can accelerate the failure of whole device. Thyristor is used in majority of power electronic devices and high-speed electronic devices, so its reliability prediction is a challenging issue[5]. There are various methods for reliability assessment of thyristor, which is summarized in below mentioned flow chart. Although standard methods are there, to predict the residual life of the component i.e. military handbook, but such method is not accurate as it does-not covers all aspects. For realistic estimation of residual life, experimental approach is adopted. An expert model is designed using artificial intelligence technique which guides the user to estimate the remaining useful life of the thyristor at different temperature and operational time[6].

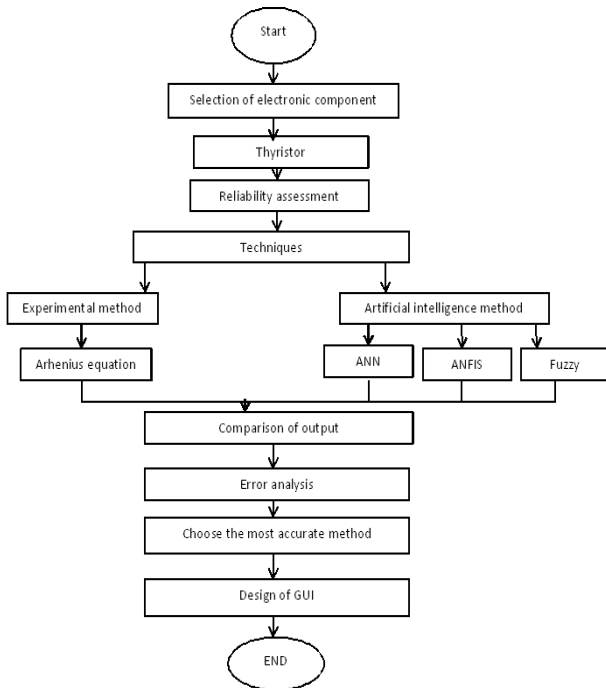


Figure 2. Flowchart for life estimation techniques

A. Failure estimation using experimental method (ALT)

Accelerated life testing is an experimental technique for failure prediction of components. This type of test is highly recommended by big production units because, it has an advantage of time saving. It is based on the fact of increase the stress level and decrease the test duration. The actual parameters of the components are specified in

datasheet. The accelerated life testing suggests the experiment at the maximum stress level. The specified components are placed on the testing machine, for the maximum range of stressors[7].



Figure 3. Experiment setup of thyristor testing

The specified working parameters of Thyristor 2N-2324, have been analyzed. The specification of 2N-2324 are:

Table 1. Specification of 2N-2324

Parameter	Value
Voltage (Forward)	100V
Voltage (Gate)	6V
Current (On-state)	1.6A
Gate Threshold Current	200uA

The process of accelerated life testing consists of following steps [8]:

- a) Regular check the component using digital multimeter and inspect for physical damage.
- b) Place the 20 thyristors on the hot plate. Cover the thyristors using sand, so that all the components get uniform heat.
- c) Set the temperature of the hotplate and note the readings from initial to maximum temperature.
- d) The experiment is specified for a fix duration of time. There is variation in time corresponding to temperature. At higher temperature, time duration is lesser.
- e) Measure the value and check the functioning of all components after specified time duration.
- f) Collect the functional data of components and calculate the residual life of thyristor using:

$$Residual\ Life = \frac{Acceleration\ Factors}{Test\ duration\ (hours) \times Number\ of\ devices} \tag{1}$$

Where, failure rate is specified by acceleration factor, which is calculated as:

$$Acceleration\ Factors = e^{\frac{E_a(T_1 - T_2)}{K(T_1 \times T_2)}} \tag{2}$$

T1 is the temperature during test and T2 is maximum temperature, as mentioned in datasheet. Boltzmann’s constant ‘K’ and Activation energy is specified as Ea.

Using accelerated life testing (ALT), remaining useful lifetime of thyristor is calculated at various set of temperature and time, as shown in following table.

Table 2. Estimated life using experimental technique

Run	Temperature (C)	Time (hours)	Estimated Life (hours)
1	110	20	29601.2
2	115	17	21701.4
3	120	16	18881.1
4	125	14	18007.6
5	130	13	16782.2
6	135	10	15632.4
7	140	09	13214.5
8	145	07	11014.8
9	150	05	9265.1
10	155	03	7372.9
Mean estimated life			16147.3

The mean life estimated using accelerated life testing is 16147.3 hours.

III. LIFE PREDICTION OF USING EXPERT ARTIFICIAL INTELLIGENCE MODELLING

After assessment of thyristor life using experimental approach, an intelligent model is designed which predicts the end of life status of thyristor using artificial intelligence techniques. Artificial neural network, fuzzy logic and adaptive neuro fuzzy inference system techniques are deployed for life time estimation.

A. Artificial neural network model for life estimation of thyristor

Artificial neural network is a type of artificial intelligence technique which is similar to brain neuron. For natural neural processing, ANN is the computational unit. Several processes are trained and tested in parallel manner[9]. For thyristor life estimation, the number of input layers are two i.e. temperature and time, whereas the output layer is one which is residual life estimation.

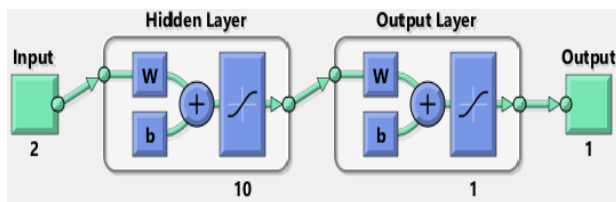


Figure 4. ANN model for residual life of thyristor

The best result is obtained by the method of training and testing at different epochs[10].

B. Fuzzy inference model for life estimation of thyristor

It is acceptable but definite output in response to unfinished, dual meaning, distorted, or not accurate input. It is a method of reasoning that like human reasoning[11]. Fuzzy logic has a lot of real time applications. The system selects the inputs and then through the process of fuzzification the inputs are converted into language quantities (L- low, M – medium, H – high)[12]. Therefore, defuzzification a fuzzy quantity represented by a membership function is converted in to a precise or crisp quantity[13].

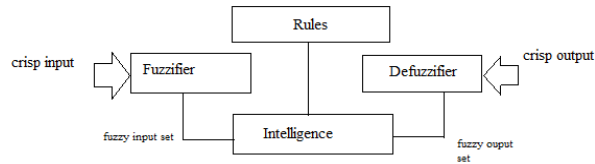


Figure 5. Flow chart of fuzzy inference system

The flow process of fuzzy inference system is depicted as in figure 6. For residual life assessment of thyristor, Mamdani type inference is used.

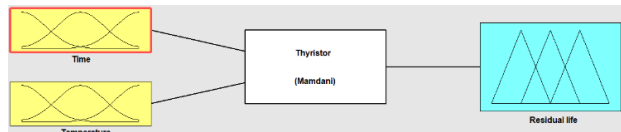


Figure 6. Fuzzy inference model for residual life of thyristor

The gaussian membership is used for input parameters i.e. temperature and time as well as output parameter i.e. residual life.

Adaptive Neuro-fuzzy Inference System (ANFIS)

ANFIS is a hybrid type of prediction technique which comprises of both ANN as well as fuzzy tool[14]. It has advantage of both the techniques, as ANN has this self-learning mechanism but it doesn't know how the hidden process is following to reach the particular target and the disadvantage is that the output is not that user understandable, precise and accurate[15]. It can't handle ambiguity. On the other hand, the advantage with fuzzy logic is that it can handle uncertain data and also, linguistic variable to have better understanding but no self-learning is there. Hence, to omit each other advantages, these two techniques have been combined to formed third technique that is ANFIS (Adaptive neuro-fuzzy Inference system). Here the rules needed by fuzzy get self-updated through the self-learning mechanism possessed by ANN[16]. So, lesser number of errors is shown by the predicted data of ANFIS.

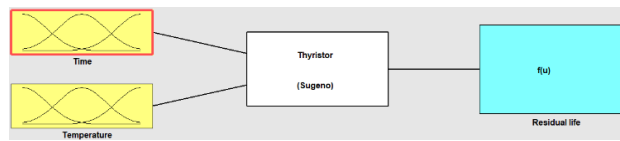


Figure 7. ANFIS model for residual life of thyristor

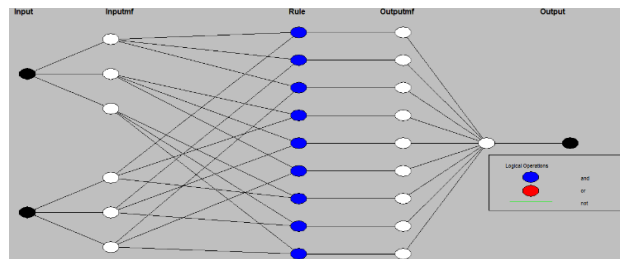


Figure 8. ANFIS structure

IV. Design of decision support system

The graphical user interface has been created using different life estimation techniques. This is based on fuzzy logic and results have been interpreted to choose the most accurate method[17].

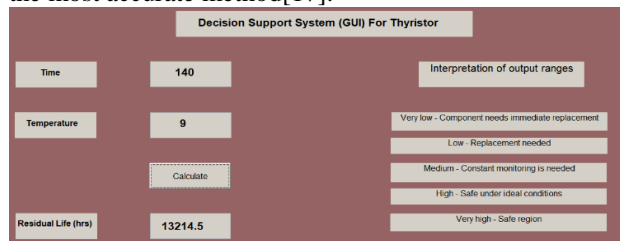


Figure 9. Decision support system for thyristor

Using decision support system using graphical user interface (GUI), the consumer can directly interact with the system and calculate the remaining useful lifetime of thyristor. It also displays the warning, if the estimated life is less than threshold value for immediate replacement.

A. Comparative analysis of prediction techniques

Different techniques have been used for calculating the useful life of thyristor in this paper. The comparison has been summarised in table 3. This shows that ANFIS has the least error and estimated lifetime using ANFIS is the most accurate one. The graphical user interface has been created as a decision support system which calculates the life, based on different techniques[18].

Table 3. Comparison of different artificial intelligence techniques

Parameter	Residual lifetime using artificial intelligence techniques		
	ANFIS	ANN	Fuzzy
Estimated lifetime(hours)	15372.28	13934.12	14566.56
Average error %	4.7	13.9	10.8
Accuracy %	95.3	86.1	89.2

Estimated lifetime(hours)	15372.28	13934.12	14566.56
Average error %	4.7	13.9	10.8
Accuracy %	95.3	86.1	89.2

The residual life of thyristor is calculated using experimental approach i.e. accelerated life testing and it shows an average life of 16147.3 hours. The residual life predicted by ANN, fuzzy and ANFIS are compared with experimental lifetime and error analysis is conducted, which shows that ANFIS has the least error i.e.4.7%.

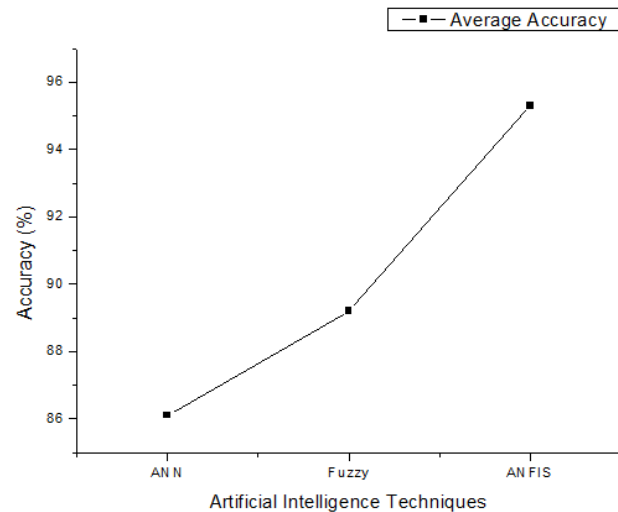


Figure 10: Accuracy comparison of prediction techniques

The figure 10 depicts the graphical comparison of all the intelligent prediction models with respect to the residual life calculated using experimental technique.

CONCLUSION

The electronic component such as thyristor are used widely. But this component has limited time period for useful operation. For successful operation of thyristor, it is necessary to predict its health condition for various set of input parameters. Accelerated life testing is used as an experimental approach for calculating the useful time. The residual life is calculated by assessing the acceleration factors at stressed values. An expert system is designed using various artificial intelligence techniques, which predicts the end of life status of thyristor well before, it actually occurs. The predicted models are validated using experimental technique and comparison is made in between all the intelligent techniques in terms of error and accuracy. After analysing all the techniques and their output, ANFIS is proven as the most accurate technique, which has 95.3% accuracy, as compare to ANN which has 86.1% and fuzzy inference system has 89.2% accuracy.

REFERENCES

1. K. Aggarwal, Reliability engineering. Springer Science & Business Media, 2012, pp. 32-45.
2. C. Bailey, H. Lu, S. Stoyanov, C. Yin, T. Tilford and S. Ridout, "Predictive reliability and prognostics for electronic components: Current capabilities and future challenges," in 31st IEEE International Spring Seminar on Electronics Technology, ISSE'08, 2008, pp. 67-72.
3. Cherry Bhargava, Vijay kumar Banga and Y. Singh, "Reliability Prediction of Thyristor using Artificial Intelligence Techniques." Indian Journal of Science and Technology, 9(18). pp.
4. C. Bhargava and V. K. Banga, "Failure Rate Prediction of Thyristor with Variable Duty Cycle and Change in Junction Temperature." pp.
5. F. Barnes, Component Reliability. Springer, 1971, pp. 7-10.
6. S. Al-Zubaidi, J. A. Ghani and C. H. C. Haron, "Prediction of tool life in end milling of Ti-6Al-4V alloy using artificial neural network and multiple regression models." Sains Malaysiana, 42(12). pp. 1735-1741.
7. R. Jano and D. Pitica, "Accelerated ageing tests of aluminum electrolytic capacitors for evaluating lifetime prediction models." Acta Technica Napocensis, 53(2). pp. 36.
8. X. Huang, P. M. Denprasert, L. Zhou, A. N. Vest, S. Kohan and G. E. Loeb, "Accelerated life-test methods and results for implantable electronic devices with adhesive encapsulation." Biomed Microdevices, 19(3). pp. 46.
9. Z. Effendi, R. Ramli, J. A. Ghani and M. Rahman, "A Back Propagation Neural Networks for Grading *Jatropha curcas* Fruits Maturity." American Journal of Applied Sciences, 7(3). pp. 390.
10. Z. Tian, "An artificial neural network method for remaining useful life prediction of equipment subject to condition monitoring." Journal of Intelligent Manufacturing, 23(2). pp. 227-237.
11. C. Chen, B. Zhang, G. Vachtsevanos and M. Orchard, "Machine condition prediction based on adaptive neuro-fuzzy and high-order particle filtering." IEEE Transactions on Industrial Electronics, 58(9). pp. 4353-4364.
12. A. Hossain, A. Rahman, A. Mohiuddin and Y. Aminanda, "Fuzzy logic system for tractive performance prediction of an intelligent air-cushion track vehicle." International Journal of Aerospace and Mechanical Engineering, 6(1). pp. 1-7.
13. K.-C. Lee, S.-J. Ho and S.-Y. Ho, "Accurate estimation of surface roughness from texture features of the surface image using an adaptive neuro-fuzzy inference system." Precision engineering, 29(1). pp. 95-100.
14. K. Sathiyasekar, K. Thyagarajah and A. Krishnan, "Neuro fuzzy based predict the insulation quality of high voltage rotating machine." Expert Systems with Applications, 38(1). pp. 1066-1072.
15. T. Özel and Y. Karpat, "Predictive modeling of surface roughness and tool wear in hard turning using regression and neural networks." International Journal of Machine Tools and Manufacture, 45(4). pp. 467-479.
16. J. Antony, R. Bardhan Anand, M. Kumar and M. Tiwari, "Multiple response optimization using Taguchi methodology and neuro-fuzzy based model." Journal of Manufacturing Technology Management, 17(7). pp. 908-925.
17. J. E. Aronson, T.-P. Liang and E. Turban, Decision support systems and intelligent systems. Pearson Prentice-Hall, 2005, pp. 111-118.
18. S. Begum, M. U. Ahmed, P. Funk, N. Xiong and B. Von Schéele, "A case-based decision support system for individual stress diagnosis using fuzzy similarity matching." Computational Intelligence, 25(3). pp. 180-195.

Experimental Study on Performance and Emission Characteristics of Country Borage Methyl Ester - Diesel Blend In a Compression Ignition Engine

^[1] Anbarasan B, ^[2] Venkatesh J, ^[3] Jamunarani M

^[1] Assistant Professor, Department of Mechanical Engineering, PSNA College of Engineering and Technology, Dindigul, Tamil Nadu, India.

Abstract: -- An experimental study was conducted to evaluate the use of Country borage oil, nonedible straight vegetable oil was blended with petroleum diesel in various proportions to evaluate the performance and emission characteristics of a single cylinder direct injection constant speed diesel engine. In the past few years, the investigation on the biofuels has been of considerable interest by virtue of their unique physical and chemical properties. The present work involves the usages of country borage oil diesel blend and to study its effect on performance, combustion and emission characteristics in a diesel engine. Diesel and country borage oil fuel blends were used to conduct short-term engine performance and emission tests at varying loads in terms of 25% load increments from no load to full loads. Tests were carried out for engine operation and engine performance parameters such as Brake thermal efficiencies of CBM20 blend were slightly higher 3% than that of std. diesel. Significant reduction in HC emissions by 22% and 33% respectively were recorded for cbm 20 blend and cbm40 blend. A significant reduction in smoke emissions by 20% and 40% respectively were recorded for cbm 20 blend and cbm40 blend. A slight increase of 5% and 8% NOx emissions were recorded for cbm20 and cbm40 respectively.

Keywords: Multi – Biodiesel, Performance, Emission, Engine.

1. INTRODUCTION

Depleting petroleum reserves and increasing the cost of the petroleum products demands an intensive search for new alternative fuels petroleum reserves. Which will make renewable energy sources more attractive. Biofuels are proved to be very good substitutes for the existing petrol fuels. Plant oils are renewable and have low sulfur in nature.

As biofuels are more expensive than fossil fuels, the widespread use of biofuel was restrained from its use in C.I. Engines. In recent years, systematic efforts were undertaken by many researchers to determine the suitability of vegetable oil and its derivatives as fuel or additives to the diesel.

Reducing greenhouse gases in the transport sector is one of the most important, initiate to promote biofuels. In a recent study by jatropa, soap nut, mahua oil, country borage oil different biofuels were compared in terms of both the economics (cost of avoided CO₂) and the potential for CO₂ emission reduction compared with a conventional fuel using crude oil

Engine manufacturers worldwide have achieved in developing diesel engines with high thermal efficiency and specific power output, within the frame of imposed regulations. Significant achievements for the development of cleaner diesel engines have been made, by following various engine-related techniques, such as the use of common-rail systems, fuel injection control

strategies, exhaust gas recirculation, exhaust gas after-treatment, etc.

Furthermore, especially for the reduction of pollutant emissions, researchers have focused their interest on the domain of fuel-related techniques, such as the use of alternative fuels often in fumigated form or gaseous fuels of renewable nature that are friendly to the environment or oxygenated fuels that show the ability to reduce particulate emissions usually with an increase of the emitted nitrogen oxides.

Another aspect of the problem concerns the use not only of diesel fuel but also the use of alternative fuels of renewable nature. Favorable fuels of the last category are bio-fuels made from agricultural products. Furthermore, concerning the environmental aspect, rational and efficient end-use technologies are identified as key options for the achievement of the targets of greenhouse gas emissions reduction.

1.1 COUNTRY BORAGE OIL

This oil is extracted from country borage leaves. It is available in our country. Its properties are approximately the same to diesel properties. Performance emission characteristics are to be tested using this oil is non-edible oil. This oil has been considered as an alternative fuel for the compression. And it has low viscosity oil compare than other bio diesel, moisture content also less in this oil.

The blends of varying proportions of country borage oil and diesel will be prepared, analyzed and compared with the performance of diesel fuel and studied using a single cylinder C.I. engine.

Misra and Murthy (2011) have investigated diesel and soapnut oil (10%, 20%, 30%, and 40%) fuel blends were used to conduct an engine performance and emission tests at varying loads in terms of 25% load increments from no load to full loads. Tests were carried out for engine operation and engine performance parameters such as fuel consumption, brake thermal efficiency, and exhaust emissions (smoke, CO, UBHC, NOx, and O2) were recorded.

Among the blends, SNO 10 has shown a better performance with respect to BTE and BSEC. All blends have shown higher HC emissions after about 75% load. Lower CO emissions at full load. NOx emission for all blends was lower and 40 blends achieved a 35% reduction in NOx emission. SNO 10% has an overall better performance with regards to both engine performance and emission characteristics

Combustion characteristics were analyzed in a compression ignition engine fuelled with diesel-ethanol blends with and without a cetane number improver, the same brake mean effective pressure, engine speed, the maximum cylinder pressure the ignition delay, the premixed combustion duration, and the fraction of heat release in premixed combustion phase will increase, while the diffusive combustion duration, the fraction of diffusive combustion phase, and the total combustion duration decrease with increase in the ethanol fraction in the blends.

The center of the heat release curve moves close to the top dead center, and the maximum rate of heat release and the maximum rate of pressure rise increase with an increase in the ethanol fraction in the blends. The addition of a cetane number improver is beneficial to the decrease in the ignition delay, the cylinder peak pressure, the maximum rate of pressure rise, and the combustion noise when operating on diesel-ethanol blends.

SukumarPuhan and Vedaraman (2005) have studied the vegetable oils can be used in diesel engines, high viscosities, low volatilities, and poor cold flow properties have led to the investigation of various derivatives. Biodiesel is a fatty acid alkyl ester, which can be derived from any vegetable oil by transesterification. Biodiesel is a renewable, biodegradable and non-toxic fuel. This biodiesel was tested in a single cylinder, four strokes, direct injection, at a constant speed, compression ignition diesel engine to evaluate the performance and emissions. In this present study, mahua oil was transesterified using 6:1 mol ratio of methanol to oil to obtain methyl ester of low viscosity (5.2 cSt) and good conversion (92%). The ester was washed with phosphoric acid to remove traces of alkali and

substantially with distilled water. Lower calorific value around 12% compared to diesel. The specific gravity does not vary much compare to diesel. The kinetic viscosity is slightly higher than that of the diesel however within the biodiesel standard limits (5.2 cSt). Cetane number is slightly high (10%). which is favorable for combustion. Flash and fire points are high which is advantages for fuel transportation.

The performance of a diesel engine with biodiesel does not vary much. The specific fuel consumption is higher (20%) than that of diesel and thermal efficiency is lower (13%) than that of diesel. Exhaust pollutant emission is reduced compared to diesel Carbon monoxide, hydrocarbon, smoke number, oxides of nitrogen were reduced by 30%, 35%, 11%, 4%, respectively, compared to diesel

Leenus Jesu Martin and Edwin Geo (2012) In this investigation the viscosity of cottonseed oil, which has been considered as an alternative fuel for the compression Ignition (C.I) engine. And cottonseed oil was decreased by blending with diesel. The blends of varying proportions of cottonseed oil and diesel were prepared, analyzed and compared with the performance of diesel fuel and studied using a single cylinder C.I. engine. Significant improvement in engine performance was observed compared to neat cottonseed oil as a fuel.

2. EXPERIMENTAL LAYOUT

The schematic diagram of the experimental set-up used to carry out the present investigation is shown in Fig.2.1. The specification of the engine used for the study is given in Table 2.2. A single cylinder four-stroke air-cooled diesel engine developing 4.4 kW at 1500 rpm was used for the research work.

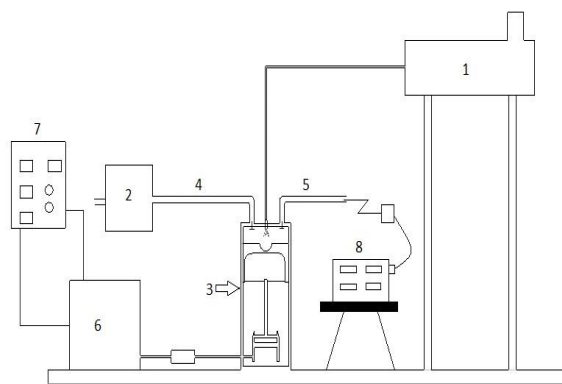


Figure 2.1 Schematic diagram of the experimental setup

1. Fuel tank
2. Surge tank
3. Engine
4. Inlet 5. Exhaust
6. Eddy current dynamometer
7. Load cell
8. Exhaust gas analyzer

Model	Kirloskar TAF-1
Type	Single cylinder, four strokes, direct injection
Piston Type	Bowl-in-piston
Capacity	660cc
Bore x stroke	87.5mm x 110mm
Compression Ratio	17.5:1
Speed	1500 rpm (constant)
Rated Power	4.4 kW at 1500 rpm
Dynamometer	Electrical type
Cooling system	Air cooling
Injection Timing	23°C Btdc
Injection Pressure	200 bar
Ignition	Compression Ignition

Table 2.2 Properties of country borage oil

Properties	Indian borage oil
Density (kg/m ³)	910
Viscosity (at 40°C) (cs)	5.2
Flashpoint (°C)	95
Fire point (°C)	110

Free fatty acid (%)	1.8
Moisture content (%)	10.8
pH value (at 25 °C)	6.5

Table 2.3 Comparisons of fuel properties

Properties	Diesel	Country borage oil	Jatropha oil	Neem oil
Density (kg/m ³)	840	910	918	912
Viscosity (at 40°C)	4.9	5.2	7.9	7.2
Flash point (°C)	61	95	186	134
Fire point (°C)	64	110	210	160
Free fatty acid (%)	0.2	1.8	5.31	0.5
Moisture Content (%)	Nil	10.8	15	14

3. RESULTS AND DISCUSSION:

3.1 PERFORMANCE ANALYSIS

The variation of cylinder pressure with a crank angle for methyl ester of country borage oil and its diesel blends. The cylinder peak pressure decreases as the proportion of methyl ester in the blends increases but, CBM20% slightly increases compare than diesel, for all methyl ester blends peak cylinder pressure is lower than for diesel. At all engine loads, combustion starts earlier for methyl ester blends than for diesel

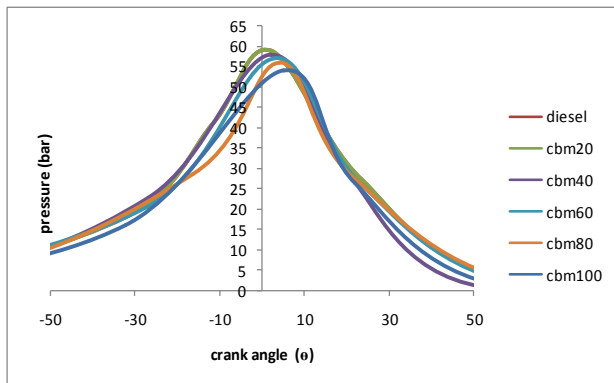


Fig.3.1.1 Variation of pressure with the crank angle at full load

3.1.2 RATE OF HEAT RELEASE

Fig. 3.1.2 shows the comparison of the heat release rate of the methyl ester of country borage oil and its diesel blends. The premixed heat release is lower for the cbm blends compared to that of diesel, possibly because of the lower heating value of the methyl ester blend. As the percentage of cbm in the blend increases, the maximum heat release rate decreases and the crank angle at which it takes place advances. It is observed that the ignition delays of cbm and its diesel blends are lower than that of diesel and are decreasing with an increase in the % cbm in the blend. As a result of the high in-cylinder temperature existing during fuel injection, biodiesel may undergo thermal cracking as a result of this, lighter compounds are produced, which might have ignited earlier, resulting in a shorter ignition delay

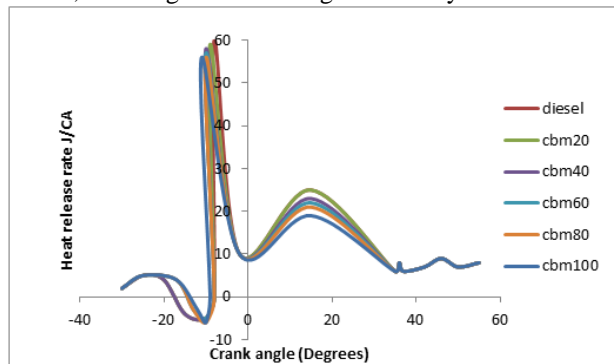


Fig. 3.1.2 Comparison of heat release rate with Crank angle for methyl ester blends and diesel at full load.

3.2 PERFORMANCE ANALYSIS

3.2.1 Brake thermal efficiency

The trends of the brake thermal efficiency of the methyl ester of country borage oil and its diesel blends are shown in Fig.3.2.1. It is observed from the figure that the brake thermal efficiency for cbm20% is 3% higher than diesel. And cbm40% is near to diesel. because it's an

oxidation fuel so that combustion takes place completely. So that brake thermal efficiency is increased. The decrease in brake thermal efficiency for higher blends may be due to the lower heating value and higher viscosity of blends with a higher proportion of methyl ester.

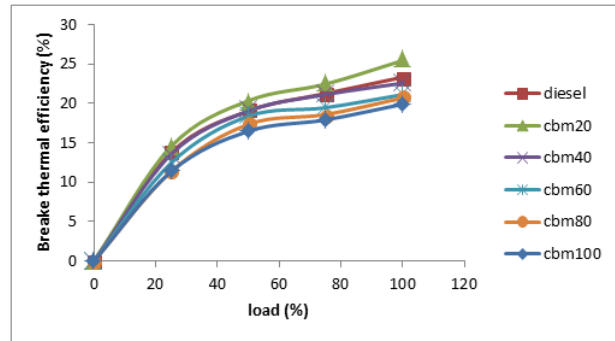


Fig. 3.2.1 Variation of brake thermal efficiency with load

3.3 EMISSION ANALYSIS

3.3.1 Carbon monoxide emissions

Carbon monoxide (CO) emission was increased in light and higher loads and decreased in medium load. Particulate matter vegetable oil and the blends are lower than that of diesel fuels at the full load, whereas the CO emissions are all slightly higher for lower loads. In no load high co because the cylinder temperature is very low. After that, the temperature is increased co is reduced. In high load due to insufficient oxygen. so fuel is not burned completely co emissions is high.

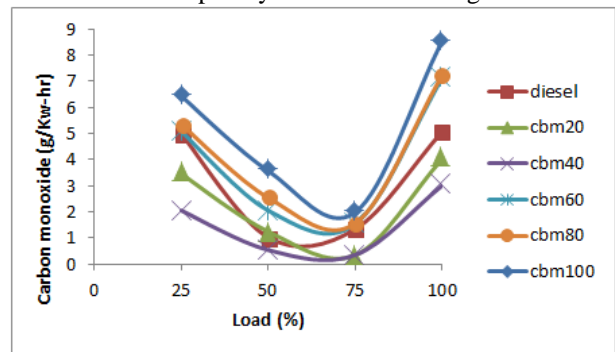


Fig.3.3.1 Variation of Carbon monoxide with a load

3.3.2 Hydro Carbon emissions

There was an increase in HC emissions by 12% and 8% cbm60, cbm80, cbm100 and blend respectively at full load compared to that of standard diesel. The effects of fuel viscosity on the fuel spray quality would be expected to produce some HC increase with vegetable oil fuels. The higher viscosity of cbm leads to poor combustion due to the large droplet size when it is injected. Another reason for higher HC emission for cbm and its diesel blend may be the fuel's physical properties such as

density and viscosity, which can have a greater influence on hydrocarbon emissions than the fuel chemical properties. However, the trend is different for methyl ester and its diesel blend. HC emissions are reduced over the entire range of loads for methyl ester and its diesel blend. Both cbm20 and cbm 40 produced lesser HC emissions by 33% and 31% respectively at full load compared to that of standard diesel. The reduction in HC emissions may be due to the presence of oxygen content in the biodiesel molecule, which leads to a more complete and cleaner combustion. The higher cetane number of bio-diesel reduces the combustion delay, and such a reduction has been related to decreases in hydrocarbon emissions

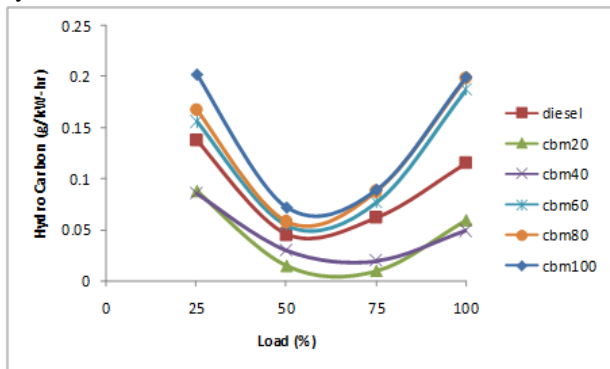


Fig.3.3.2. Variation of Hydro Carbon with a load

3.3.3 Oxides of nitrogen (NOx)

The variation of NOx emission with a load for methyl ester of country borage oil and its diesel blends. It was observed that NOx emission increases by 5% for cbm 50 and 8% for MEPS100 at full load. In spite of the slightly higher viscosity and lower volatility of the methyl ester, the ignition delay seems to be lower than that of diesel. Thus, a shorter ignition delay for biodiesel also may advance the start of combustion and contribute to higher NOx emissions. In addition, the oxygen present in the fuel may provide additional oxygen for NOx formation, thereby increasing its level of emission.

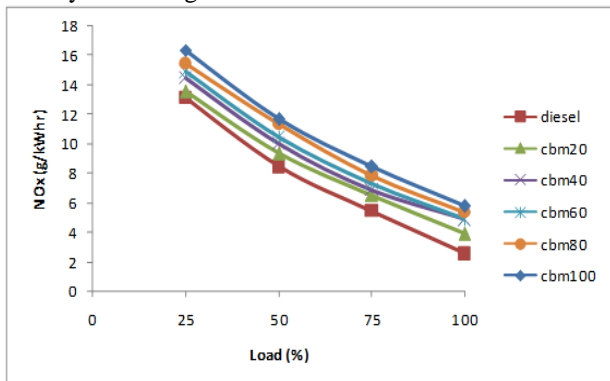


Fig 3.3.3 Variation of Oxides of nitrogen with a load

3.3.4 Smoke opacity

Smoke emission exhibited the same trend as HC emissions. However, the trend was different for methyl ester and its diesel. Variation of exhaust gas temperature with a load for various blends. The smoke is much lower for methyl ester of country borage oil 20 &40 blend compared to that of diesel. This is because of the better combustion characteristics of cbm and its diesel blends. A major reduction in smoke emission is observed with cbm and its diesel blend, especially at high loads. This may be due to the presence of oxygen molecule in the methyl ester, which enables more complete combustion even in regions of the combustion chamber with fuel rich diffusion flames and promotes the oxidation of the already formed soot Fig. 3.3.4 indicates a reduction in smoke by 28% in the case of cbm40 and a 34.5% reduction in the case of cbm40 at full load

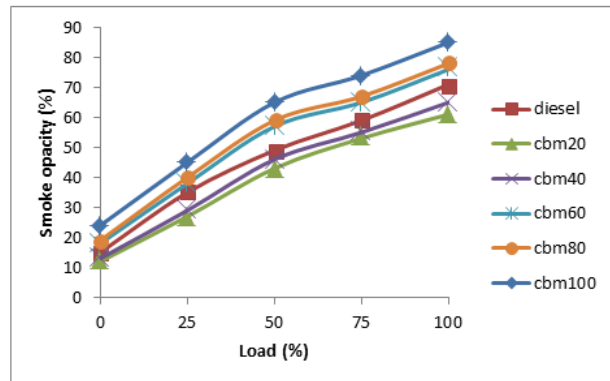


Fig 3.3.4 Variation of Smoke opacity with a load

3.3.5 Exhaust Gas Temperature

The variation of exhaust gas temperature with a load for methyl ester and its diesel blends and diesel. It is observed that as the proportion of methyl ester increases in the blend, exhaust gas temperature also increases for all the loads. This may be due to the oxygen content of CBM, which improves combustion and thus increases the exhaust gas temperature

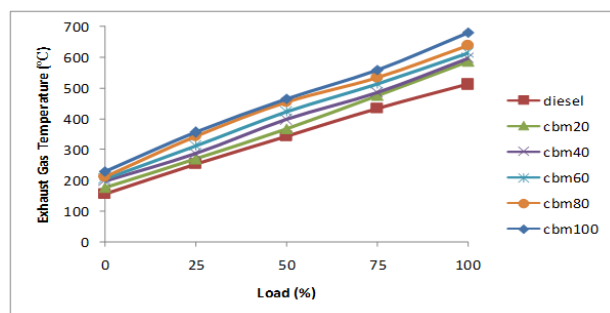


Fig.3.3.5 Variation of Exhaust gas temperature with a load

4. CONCLUSION

The performance, emission and combustion characteristics of a 4.4 kW DI compression ignition engine summer with cbm and its blends have been analyzed and compared to those of diesel fuel. The conclusion of the present work is summarized as follows.

- Brake thermal efficiencies of cbm20 blend were slightly higher 3% than that of std. diesel.
- A significant reduction in HC emissions by 22% and 33% respectively were recorded for cbm 20 blend and cbm40 blend
- A significant reduction in smoke emissions by 20% and 40% respectively were recorded for cbm 20 blend and cbm40 blend
- A slight increase of 5% and 8% Nox emissions were recorded for cbm20 and cbm40 respectively.
- Combustion characteristics of MEPS and its diesel blends are comparable with those of std. diesel.

REFERENCES

1. Deepak Agarwal A and Lokesh Kumar B., "Performance evaluation of a vegetable oil-fuelled compression ignition engine" *Renewable Energy* 33 (2008) 1147–1156
2. Devan P.K and Mahalakshmi N.V. "Study of the performance, emission and combustion characteristics of a diesel engine using poon oil-based fuels" *Fuel Processing Technology* 90 (2009) 513–519
3. Huang Z H, Lu H B and Jiang D M., "Engine performance and emissions of a compression ignition engine operating on the diesel–methanol blends" *D10903 Mech* 2004
4. Kajitani S. Chen Z.L Konno M. and RHEE K.T. "Engine performance and Exhaust characteristics of Direct-injection diesel engine operated with DME" *SAE Paper* (1997) No.972973, 156
5. Leenus Jesu Martin M. and Edwin Geo V. "A comparative analysis methods to improve the performance of cotton seed oil fuelled diesel engine" *Fuel* 102 (2012) 372–378
6. MandeepKaur and Amjad Ali., "Lithium ion impregnated calcium oxide as nano catalyst for the biodiesel production from karanja and jatropha oils" *Renewable Energy* 36 (2011) 2866 to 2871
7. Misra R.D. and Murthy M.S. "Performance, emission and combustion evaluation of soap nut oil-diesel blends in a compression ignition engine Fuel" *Biomass and Bio energy* (902011) 2514–2518
8. NezahatBoz, NebahatDegirmenbasi B, Dilhan M. and Kalyon C., "Conversion of biomass to fuel Transesterification of vegetable oil to biodiesel using KF loaded nano-g-Al₂O₃ as catalyst *Applied Catalysis*" *Environmental* 89 (2009) 590–596
9. Nwafor O.M.I, Rice G. and Ogbonna A.I "Effect of advanced injection timing on the performance of rapsed oil in diesel engines" *journal of renewable energy*, Vol.21, (2000) 433-444
10. Shengyang Hu, Yanping Guan, Yun Wang and Heyou Han "Nano-magnetic catalyst KF/CaO–Fe₃O₄ for biodiesel production *Applied Energy* 88 (2011) 2685–2690
11. SukumarPuhan A. and Vedaraman N., "Mahua oil methyl ester as biodiesel-preparation and emission characteristics" *Biomass and Bioenergy* 28 (2005) 87–93
12. Usta N. and Aydogan B., "Properties and quality verification of biodiesel produced from tobacco seed oil" *Energy conversion and Management* 52 (2011) 2031–2039
13. Ulf Schuchardta, RichardoSerchelia, and RogerioMatheus Vargas., 'Transesterification of crude oil: A Review', *J. Braz. Chem. Soc.*, Vol.9, pp.199-210 (1998)
14. Yusuf Ali, Milford A. Hannd, 'In-cylinder pressure characteristics of a DI heavy-duty diesel engine on Bio diesel Fuel', *SAE paper* No. 971683.199

Investigation of frequency dependent dielectric property of polysiloxane – TiO₂ nanocomposites

[¹]Md Nasir Ali, [²] Mir Safiulla

[¹] Research Scholar, Department of Mechanical engineering, Shri Jagdishprasad Jhabarmal Tibrewala University, Jhunjhunu, Rajasthan, India.

[²] Department of Mechanical Engineering, Ghousia College of Engineering, Ramanagram, Karnataka, India

Abstract:-- The polysiloxane – TiO₂ nanocomposites were prepared by a solvent casting method in triethanolamine and tetrahydrofuran solvents. Fourier transform infrared spectroscopy for structural analysis and surface morphology was carried by scanning electron microscopy. The amorphous nature of polysiloxane observed in the amorphous nature of polysiloxane observed in XRD spectra. The surface morphology was studied by employing scanning electron microscopy and it is found that the nanoparticles are completely embedded in the polysiloxane. Further, the dielectric spectroscopy study reveals that the 0.3 wt % shows low dielectric constant and dielectric loss, as a result, it shows high conductivity of 1.35×10^{-4} S/cm. Among all the nanocomposites, 0.3 wt % shows the lowest tangent loss value of 0.1 due to the non-debye's type of relaxation process where the charge carriers are relaxed at the higher energy state for a longer time. The quality factor confirms that there is a small damping loss for 0.3 wt % of nanocomposites which is favorable for the high conductivity. Therefore, these nanocomposites can be potential candidates for many high dielectrics engineering applications.

Keywords: Polysiloxane, Titanium dioxide, Nanocomposites, Dielectric

1. INTRODUCTION

The large scientific community have been attracted to the inorganic nanoparticle doped polysiloxane (PS) nanocomposite because of its unique properties such as absorption of heavy metal ions from aqueous and organic solvents [1], corrosion resistance [2], chemical inertness [3], anti-grafting [4] and high permeability of gases [5] made a potential candidate in many different technological applications. It is well known that the polysiloxane has low surface energy, high dielectric [6] and high-temperature resistance [7] up to 760 °C made suitable for insulation, electronic coating, automobile gaskets, sealing and lubricating greases [8]. Besides chemical (in the presence of hydrochloric acid, thionyl chloride, ammonia or organic amines) or thermal (300–400 °C) activation of polysiloxanes, the polymeric modified layer can be obtained by polymerization of precursors with different amount of functional groups, which was realized via utilizing oligomers (tri-, penta- and hexamethylcyclotrisiloxane) with siliconhydride groups [9] or siloxanes [10] as precursors. Such approach allows one to compose polysiloxane layer with well-defined structure having various topologies (linear, comb-branched and dendritic-branched). The multi-step process of modification by oligomers with different amount of chemically active groups also allows one to build comb-branched and dendritic-branched polymers. However, there is a great challenge in maintaining the transparency which depends on the concentration of

filler, a solvent used, preparation methods and curing temperature [9].

The investigation of dielectric properties of the polysiloxane nanocomposites is important to realize the several factors such as surface charge density, polarization effect, charge carrier mobility, damping loss and change in bulk resistance with a small doping of inorganic nanoparticles to determine the suitability of the electronic device packing application. The inorganic oxides dope in the polysiloxane nanocomposite may change the surface energy due to the presence of oxygen vacancies which are predominant at the higher temperature. It is reported that the addition of inorganic oxide nanoparticles may fill the interfacial cracks and improve significantly its electrical properties [10 -12].

It is often find difficulties to have transparent nanocomposite with homogenous distribution of inorganic nanoparticles in polysiloxane matrix which affects the refractive index (RI) of the nanocomposite. The formation of nods, twists and micro-cracks at the interface of the polymer and nanostructured inorganic oxide may be causes multiple scattering or diffraction at the interplanar space causes higher damping loss and high impedance value.

In either case, the stability of heterometallic bonds affects the structural features of the resulting materials. As a matter of fact, the multinuclear NMR study of these hybrid materials pointed out the different lability of Si O Me (Me = metal) bonds in solution, depending on the nature of the metal alkoxide [13]. In general, polydimethylsiloxane-oxide gels have been described as nanocomposites based on long and mobile

polydimethylsiloxane chains and oxide particles that are nanometric in size [14]. From the literature, it owes that the TiO₂ nanoparticles doped in polysiloxane nanocomposite films may have a smooth surface and low surface scattering which may be reduce the damping loss and impedance value. Therefore, the author made an attempt to investigate the temperature dependent electrical conductivity and dielectric properties of TiO₂ nanoparticles doped polysiloxane nanocomposites.

The nanocomposites of polysiloxane have been prepared by high intense ultra-sonication in tetrahydrofuran (THF) media. Further, the prepared nanocomposites were characterized by X-ray's diffraction (XRD) method and scanning electron microscopy (SEM) for structural and surface morphology analysis. The temperature dependent DC conductivity was carried out by two probes method.

2. MATERIALS AND METHOD

2.1 Materials

All chemicals used for the preparation of nanocomposites were analytical grade. The polysiloxane (99.99 % pure), titanium dioxide (TiO₂), triethanolamine (TOEA) and tetrahydrofuran (THF) was purchased from Sigma Aldrich, India.

2.2 Synthesis of polysiloxane – TiO₂ nanocomposites

The nanocomposite films were prepared by a solvent casting method. 5 gm of polysiloxane was dissolved in 150 ml of tetrahydrofuran (THF) and stirred for 72 hrs to obtain a clear solution. Then 0.1, 0.3 and 0.6 wt % of TiO₂ and 0.25 ml of triethanolamine (TOEA) were mixed with the above solution with high intense ultra-sonication until dissolution takes place. The homogeneous mixture then poured into a round Teflon mould and dried in room temperature to remove the solvent and later heated with 50 °C to form a dried thin film of nanocomposites. In a similar procedure, pure polysiloxane thin film was prepared as following in preparation of nanocomposites [16, 17].

3. CHARACTERIZATION

The X-ray crystallography was carried out by using Philips X-ray diffractometer for the range of 10° to 80° at the rate of 2° per second with CuK α radiation of wavelength $\lambda = 1.5406 \text{ \AA}$. The functional group of the polysiloxane and its nanocomposites were studied by using PerkinElmer1600 spectrophotometer in KBr medium. The nanocomposite was mixed with KBr crystals in the ratio of 1:5 and grounded the mixture to obtained homogeneous compound. The surface morphology of the nanocomposite was characterized by Scanning electron microscopy model of Philips XL 30 ESEM spectroscopy. The nanocomposites films were fixed onto the carbon-coated copper grid and introduce into the microscopic sample holder for the image

scanning. Further, the impedance spectroscopy of the nanocomposite was carried out by Hoki LCR-Q meter from the frequency range of 50 Hz to 5 MHz.

4. RESULTS AND DISCUSSION

4.1 X-ray crystallography

Figure 1 shows the X-ray diffraction pattern of pure polysiloxane and polysiloxane – TiO₂ nanocomposites for different weight percentages (0.1, 0.3 and 0.6 wt %). The pure polysiloxane (PS) show a broad peak around 14.73° and 23° may be due to the diffraction occurs at the interplanar spacing of the polymer and it indicates the amorphous nature of polysiloxane. The polysiloxane – TiO₂ nanocomposites for different weight percentage show the characteristic peaks of TiO₂ in polysiloxane at 26.30°, 33.22°, 37.62°, 45.02°, 42.12°, 56.34° and 68.21° 42.12° corresponding to the plan of (110), (101), (111), (210), (211), (220) and (301) respectively, which is matched with reported data [14]. The crystallite size of the polysiloxane – TiO₂ nanocomposite is calculated by using the Debye Scherrer equation and it is found to be 13 nm. It is also important to note that the TiO₂ structure is not distracted even after incorporating into the polysiloxane matrix.

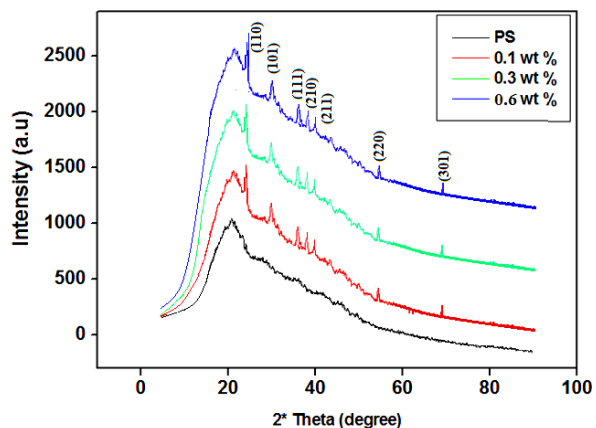


Figure 1 XRD pattern of polysiloxane and polysiloxane – TiO₂ nanocomposites

4.2 Scanning electron microscopy

Figure 2 (a – c) shows the SEM image of pure polysiloxane, TiO₂, and 0.3 wt % of polysiloxane - TiO₂ nanocomposites. From the image of pure polysiloxane (a), it is observed the polysiloxane film have a smooth surface without any crack or agglomeration at the polymer film interface. It is also interesting to note that the solvent aging effect does not appear on its surface and therefore its surface is very smooth. Figure (b) shows that the pure TiO₂ spherical bits are form aliened indusial nanoparticles and which are well connected at the boundary without any agglomeration. When these

titanium dioxide nanoparticles doped in polysiloxane matrix in tetrahydrofuran solvent, the nanoparticles embedded into the matrix without any formation of crack as shown in figure (c). The nanocomposite films are dried at 50 °C for an hour in presence of helium gas the solvent aging effect almost negligible as a results surface of the nanocomposites appeared very smooth with embedded of TiO₂ in nanocomposites.

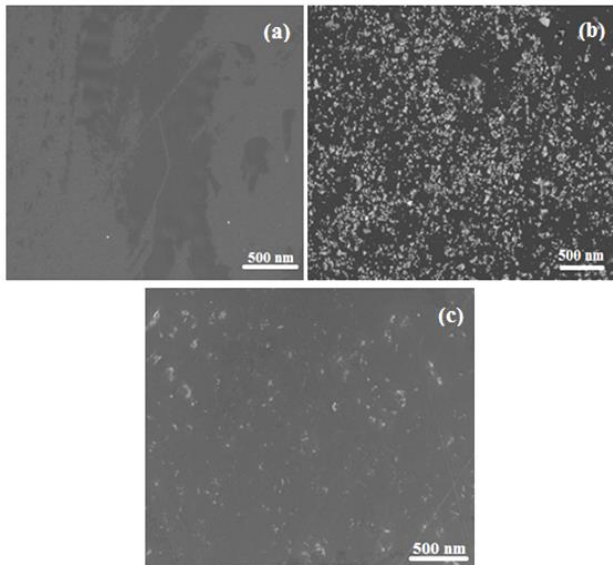


Figure 2 SEM image of polysiloxane, TiO₂ and 0.3 wt % of polysiloxane – TiO₂ nanocomposites

5. DIELECTRIC STUDY

Figure 3 shows the real part of permittivity of polysiloxane and polysiloxane - TiO₂ nanocomposites as a function of applied frequency from 50 Hz to 5 MHz. It is observed that the real permittivity value decreases with increase in applied frequency up to 10³ Hz after that its almost remains constant which is may be due to the dipole polarization where the polarization occurs due to the Si – O and Ti – O – Ti along with symmetry axis. The titanium dioxide nanoparticles have many hydroxyl ions due to the hydrophilic nature of nanoparticles and high surface area to the volume ratio causes high surface energy [17]. Among all the nanocomposites, 0.3 wt % of polysiloxane - TiO₂ nanocomposite shows lowest real permittivity of 1200 F/m may be due to the two reason i.e., homogeneous distribution of TiO₂ nanoparticles in polysiloxane matrix and negligible solvent aging effect causes smooth surface. However, after 0.3 wt % of TiO₂ in the polysiloxane matrix dramatically increase the real permittivity value due to the blocking of charge carriers at the interface. Figure 6 shows the imaginary part of permittivity of polysiloxane and polysiloxane - TiO₂ nanocomposites with different weight percentages as a

function of applied frequency from 50 Hz to 5 MHz. The similar behaviour is observed like a real part of permittivity for polysiloxane and polysiloxane - TiO₂ nanocomposites except have a smaller in a magnitude of imaginary permittivity. Among all the nanocomposites, 0.3 wt % of shows the low imaginary permittivity value of 584 F/m due to the dipole polarization effect and distribution of TiO₂ nanoparticles in polysiloxane.

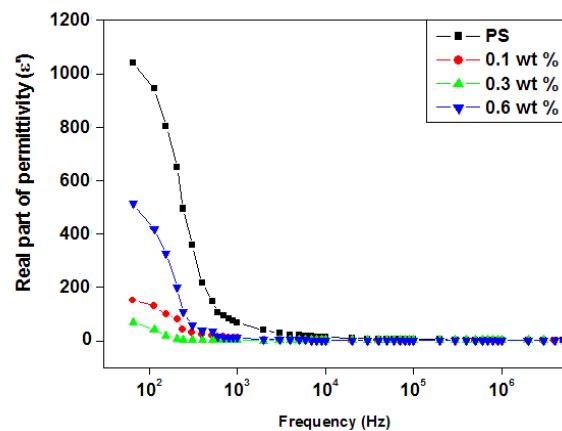


Figure 3 shows the real part of permittivity as a function of applied frequency for polysiloxane and polysiloxane – TiO₂ nanocomposites

Figure 4 shows the variation of quality factor (Q) as a function of applied frequency for different weight percentages of polysiloxane and its nanocomposites. The damping loss of nanocomposite at the mid frequency range is may be due to the different types of energy loss such as vibrational energy, translation energy and kinetic energy at the higher frequency range. It is observed that the damping loss of polysiloxane and polysiloxane – TiO₂ nanocomposites of all compositions have the value less than 0.5 indicates that the vibrational energy and translation energy loss is almost zero is due to the embedded TiO₂ in polysiloxane [18]. For all the nanocomposites, the hump are formed at the mid-frequency range between 10⁴ to 10⁵ Hz is due to the steady state of electron flow at the equilibrium. Among all the nanocomposites, 0.3 wt % of polysiloxane – TiO₂ nanocomposites show the lowest value of 2 because of the fact that there is no free space in between the nanoparticles and polymer matrix results in no oscillation at all.

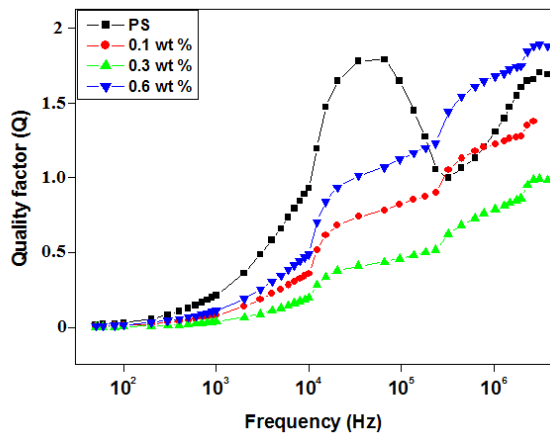


Figure 4 shows the quality factor as a function of applied frequency for polysiloxane and polysiloxane – TiO₂ nanocomposites.

Figure 5 shows the real part of electric modulus of polysiloxane and polysiloxane - TiO₂ nanocomposites with different weight percentages. It is observed that the real electric modulus value initially at the lower frequency almost constant for all the compositions and after 10⁴ Hz the electric modulus increase due to independent dipole formation. It also indicates that the lower frequency associated with magnetic field perpendicular to the electrical field. However, it is found that with a magnetic field decreases with increase in the frequency range may result gradually increase in electric modulus. Among all the nanocomposites, 0.3 wt % shows higher electric modulus of 0.0392 which is followed by other compositions and pure polysiloxane. Another reason could be for higher electric modulus is due to the formation of permanent dipole of Si – OH and Ti – O – Ti along with symmetry axis due to the hydrophilic nature of TiO₂ and high surface energy [19].

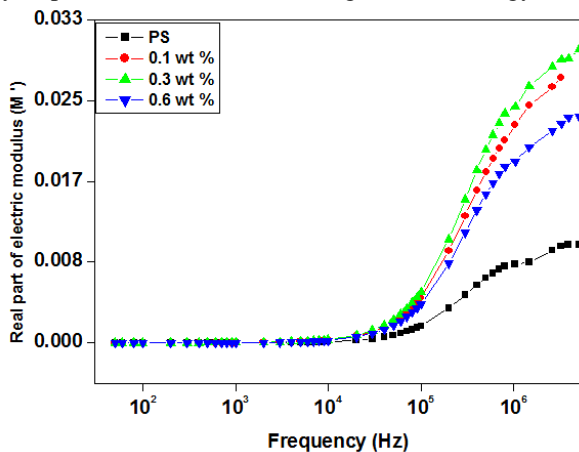


Figure 5 shows the real part of electric modulus as a function of applied frequency for polysiloxane and polysiloxane – TiO₂ nanocomposites

Figure 6 shows the imaginary part of electric modulus of polysiloxane and polysiloxane - TiO₂ nanocomposites with different weight percentages as a function of applied frequency from 50 Hz to 5 MHz. The similar behaviour is observed like the real part of electric modulus for polysiloxane and polysiloxane - TiO₂ nanocomposites except higher in a magnitude of the imaginary electric modulus. Among all the nanocomposites, 0.3 wt % of shows the highest value of imaginary electric modulus of 0.0492 due to the formation of permanent dipole polarization and distribution of TiO₂ nanoparticles in the polysiloxane [20].

Figure 10 shows the variation of tangent loss as a function of applied frequency for different weight percentages of TiO₂ in polysiloxane. It is observed that the tangent loss value decreases with increase in frequency up to 10⁴ Hz after that it's almost constant for all compositions. Among all the nanocomposites, 0.3 wt % of shows the lowest tangent loss value of 0.1 due to the non-debye's type of relaxation process where the charge carriers are relaxed at the higher energy state for a longer time. Hence, 0.3 wt % of polysiloxane – TiO₂ nanocomposite can be used as low k – dielectric materials electrochromic and electrochemical device, capacitor, varistor etc [21].

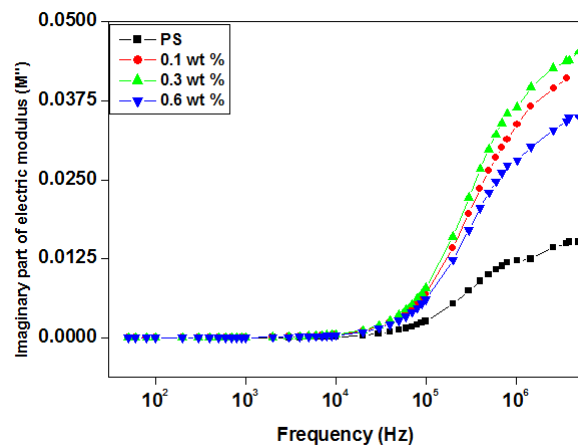


Figure 6 shows the imaginary part of electric modulus as a function of applied frequency for polysiloxane and polysiloxane – TiO₂ nanocomposites

Figure 7 shows the variation of σ_{ac} conductivity for different weight percentages of TiO₂ in polysiloxane as a function of frequency. It is observed that the conductivity of pure polysiloxane and its nanocomposites increase with an increase in frequency. The conductivity of the nanocomposites depends on the several factors such as size and shape of the nanoparticles, distribution factor, the orientation of nanoparticles in a polymer matrix, surface morphology, grain boundary which define the bulk resistance of the samples. Therefore, it is very

carefully illustrated the solvent casting process without any aging effects results in smooth surface morphology that influences the conductivity [22]. Among all the nanocomposites, 0.3 wt % shows the high conductivity of 1.35×10^{-4} S/cm due to the low dielectric constant and tangent loss due to the favorable surface morphology without any agglomeration or cracking on the surface and also null solvent aging effect [23]. Therefore, these nanocomposites can be potential candidates for the self-cleaning coating materials in superhydrophobic glass, capacitors, varistor etc.

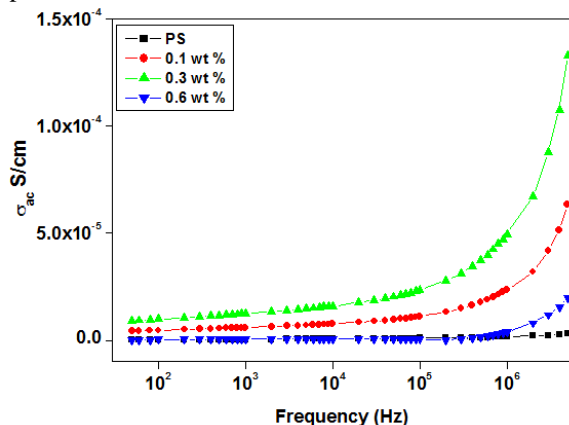


Figure 7 shows the variation in AC conductivity as a function of applied frequency for polysiloxane and polysiloxane – TiO₂ nanocomposites

7. CONCLUSION

The polysiloxane – TiO₂ nanocomposites have been prepared by a solvent casting method in triethanolamine and tetrahydrofuran solvents. The structural study was carried out by X-ray diffraction and Fourier transmission infrared spectroscopy. The dielectric spectroscopy study reveals that the 0.3 wt % shows low dielectric constant and dielectric loss, as a result, it shows high conductivity of 1.35×10^{-4} S/cm. Among all the nanocomposites, 0.3 wt % of shows the lowest tangent loss value of 0.1 due to the non-debye's type of relaxation process where the charge carriers are relaxed at the higher energy state for a longer time. The quality factor confirms that there is a small damping loss for 0.3 wt % of nanocomposites which is favorable for the high conductivity. Therefore, these nanocomposites can be potential candidates for many high dielectrics engineering applications.

REFERENCES

- [1] Tabakci M, Ersoz M, Yilmaz M, A Calix[4]arene-Containing Polysiloxane Resin for Removal of Heavy Metals and Dichromate Anion. *J. Macromol Sci A: Pure & App Chem.* 2006; 43: 57
- [2] Hammer P, Schiavetto M.G, Dos Santos F.C, Benedetti A.V, Pulcinelli S.H, Santilli C.V, Improvement of the corrosion resistance of polysiloxane hybrid coatings by cerium doping. *J. Non-Cryst. Solids.* 2010; 356: 2606
- [3] Barletta M, Rubino S V G, Puopolo M, Venettacci S, Functionalized polysiloxane coatings on hot-rolled and high-strength Fe 430 B steel: Analysis of mechanical response and resistance to chemicals. *Appl. Polym. Sci.* 2014; 131: 40624
- [4] Dewasthale S, Andrews C, Graiver D, Narayan R, Water Soluble Polysiloxanes. *Silicon.* 2017; 9: 619
- [5] Jodeh S, Khalaf B, Radi S, Tighadouini S, Salghi R, Samhan S, Warad I, Jodeh D, New Polysiloxane Surfaces Modified with Ortho-, Meta-, or Para-Nitrophenyl Moieties for Cadmium Removal from Water. *J Surf Eng Mat & Adv Tech.* 2016; 6: 18
- [6] Dünki S. J, Reyes E. C, Opris D. M, A facile synthetic strategy to polysiloxanes containing sulfonyl side groups with high dielectric permittivity. *Polym. Chem.* 2017; 8: 715
- [7] Racles C, Cozan V, Bele A, Dascalu M, Polar silicones: structure-dielectric properties relationship. *Designed Monomers and Polymers,* 2016; 19: 496
- [8] Giaveri S, Gronchi P, Barzoni A, IPN Polysiloxane-Epoxy Resin for High-Temperature Coatings: Structure Effects on Layer Performance after 450 °C Treatment. *Coatings.* 2017; 7: 213
- [9] Riehle N, Thude S, Götz T, Kandelbauer A, Thanos S, Tovar G.E.M, Lorenz G, Influence of PDMS molecular weight on transparency and mechanical properties of soft polysiloxane-urea-elastomers for intraocular lens application, *Eur. Polym. J.* 101 (2018) 190
- [10] Lu K, Erb D, Liu M, Phase transformation, oxidation stability, and electrical conductivity of TiO₂-polysiloxane derived ceramics. *J Mater Sci.* 2016; 51: 10166
- [11] Huang P, Shi H.Q, Xiao H.M, Li Y. Q, Hu N, Fu S.Y, High performance surface-modified TiO₂/silicone nanocomposite. *Scientific Reports.* 2017; 7: 5951
- [12] Roy A.S, Gupta S, Seethamraju S, Madras G, Ramamurthy P.C, Impedance spectroscopy of novel hybrid composite films of polyvinylbutyral(PVB)/functionalized mesoporous silica, *Composites Part B* 2014; 58:134
- [13] Roy A.S, Gupta S, Sindhu S, Parveen A, Ramamurthy P.C, Dielectric properties of novel PVA/ZnO hybrid nanocomposite films, *Compos. Part B Eng.* 2013; 47: 314
- [14] Li W, Liang R, Hu A, Huang Z, Zhou Y N, Generation of oxygen vacancies in visible light-activated

one-dimensional iodine TiO₂ photocatalysts, RSC Adv., 2014; 4: 36959

[15] Shen Y, Wang L, Zhang H, Wu T, Pan H Y, Preparation and characterization of titania/silicone nanocomposite material. Mat. Sci. Engg. 2015; 87: 012021

[16] Roy. AS. Antistatic and dielectric properties of one-dimensional Al₂O₃:Nd₂O₃ nanowire doped polyaniline nanocomposites for electronic application. Sensors and Actuators A 2018; 280: 1

[17] Lee J W, Cho H. B, Nakayama T, Suzuki T, Suematsu H, Niihara K, Internal structure control of the TiO₂ nanotubes and polysiloxane nanocomposites by nanosecond pulsed electric field. Journal of Asian Ceramic Societies. 2014; 2: 97

[18] Chiu Y C, Huang C C, Tsai H C. Synthesis, characterization, and thermomechanical properties of siloxane-modified epoxy-based nanocomposite. J. Appl. Polym. Sci. 2014; 131: 40984

[19] Ma T, Yang R, Zheng Z, Song Y. Rheology of fumed silica/polydimethylsiloxane suspensions. Journal of Rheology 2017; 61: 205

[20] Cassagnau, P. Melt rheology of organoclay and fumed silica nanocomposites, Polymer 2008; 49: 2183

[21] Kirst, K. U., F. Kremer, and V. M. Litvinov, Broad-band dielectric spectroscopy on the molecular dynamics of bulk and adsorbed poly(dimethylsiloxane). Macromolecules 1993; 26: 975

[22] Roy AS, Gupta S, Seethamraju S, Ramamurthy PC, Madras G. Fabrication of Poly(Vinylidene Chloride-Co-Vinyl Chloride)/TiO₂ Nanocomposite Films and Their Dielectric Properties. Science of Advanced Materials. 2014; 6: 946

[23] Ansari JN, Khasim S, Parveen A, Hartomy O AA, Khattari Z, Badi N, Roy AS. Synthesis, characterization, dielectric and rectification properties of PANI/Nd₂O₃:Al₂O₃ nanocomposites. Polymers for Advanced Technologies. 2016; 27: 1064

Electronic Toll Collection System Using RF Transceiver and IoT

^[1] Dr. Chitra kiran N, ^[2] Abhilash reddy S, ^[3] Diliipgowda B.M, ^[4] Bhargav saiTeja GS, ^[5] Meghana.A
^[1] Professor and Head

^{[1][2][3][4][5]} Dept of ECE, Alliance University, Bangalore, Karnataka, India

Abstract:-- This Project mainly focused on how the electronic toll collection system reduces manual work load using RF Transceiver. Ultimately, this system reduces environment pollution due to the burning of fuel as well as reduces the waiting time of users in toll queue. Users can access the website and may perform their toll transaction. Their transaction will reflect in the centralized database. Due to the use of online transaction, users do not need to carry cash with them. This leads in the reduction of human error occurring at the toll booths. Cashless transaction gives the transparency to this system. This design of the system includes an IOT module which will help to send a confirmation text to the vehicle owner about the toll deduction. With the significant development in Roadways, there is an increase in the number of toll plazas. These toll plazas have long queues and the time consumed in paying cash and returning change causes all the more delay. We have designed an IOT based Toll booth Manager System in which a person can easily pay the Toll charge with the help of RF Transceiver which has been set up in both the user vehicle and the toll gate. When the vehicle come in front of the toll gate, with the help of RF Transceiver the system would check if that particular vehicle has sufficient balance and then deduct the toll charge and update the balance through IOT.

Keywords: Arduino Uno, Apache, JSP, MySQL, Navicat, NetBeans, RF Transceivers

INTRODUCTION

India, the second most popular country in the world, and a fast-growing economy, is seeing terrible road congestion problems in its cities. The problem is often felt in almost all major cities. This is primarily because infrastructure growth is slow compared to growth in number of vehicles, due to space and cost constraints. Roads or highway are one form of the means of transporting men and material from one place to another. At present, revenue collection procedures at most toll facilities require a driver to stop his/her car, open the window or door, and find correct coins or a valid card before continuing his/her journey. As the use of tolls becomes more widely accepted, the drawbacks of this conventional toll collection method will be emphasized. Tollbooths suffer from being land intensive, labor-intensive (owing to the hiring of toll operators), and time-intensive and fuel consumption will be more. Electronic toll collection (ETC) systems are superior to manual methods from the perspective of both the toll agency and the user. ETC toll collection is a technology enabling the electronic collection of toll payment. This system can determine if the car is registered or not, and then informing the authorities of toll payment violation, debits and participating accounts. The most advantage of this technology is the opportunity to eliminate congestion in toll booths, especially during festive seasons when traffic trends to be heavier than normal. Other general advantages for the motorists include fuel savings and

reduced mobile emissions by reducing or eliminating deceleration, waiting time, and acceleration.

Electronic toll collection system based on Radio Frequency transceiver and IOT is mainly used in India. As time and efficiency are a matter of priority nowadays, the traditional method as to be reformed. Ultimately, this system reduces environment pollution due to the burning of fuel as well as reduces the waiting time of users in toll queue. Due to the use of online transaction, users do not need to carry cash with them. This leads in the reduction of human error occurring at the toll booths. Cashless transaction gives the transparency to this system. This design of the system includes an IoT module which will help to send a confirmation text to the vehicle owner about the toll deduction. When the vehicle come in front of the toll gate, with the help of RF Transceiver the system would check if that particular vehicle has sufficient balance and then deduct the toll charge and update the balance through IOT.

Prior Work:

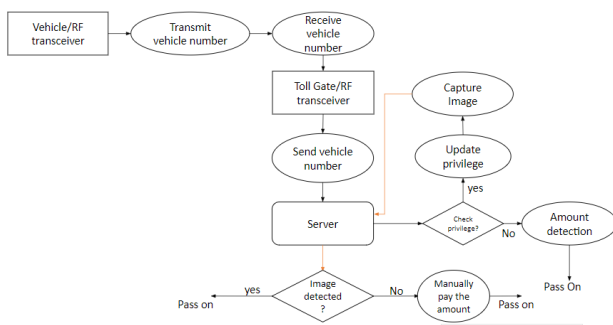
Sl. No	Early Work	Remarks	Year and Place
1.	Automated toll system for number plate detection and collection	Detection of number plate was not feasible	October 2016, Nagpur, India
2	Automated toll gate system using RFID and GSM technology	RFID tags were not easily detecting due to rainfall and dust	January 2018, Tamil Nadu, India
3	Automated toll collection using satellite navigation	The location of vehicles were not detecting due to low signals	April 2014, Maharashtra, India

PROPOSED WORK

The proposed system gives the simplified procedure to passengers to pay the tolls by making them automated and also provides intimation about vehicle. All these activities are carried using RF transceiver thus saving the efforts of carrying money and records manually.

The RF transceiver mounted at toll booth will read the RF Transceiver fixed on vehicles and automatically respective amount will be detected. When the vehicle is going to enter into the toll plaza, the first aim is to detect the type and no. of the vehicle. Whenever the vehicle come in front of the toll gate, both the transceiver of the user vehicle and the one mounted in the toll gate gets activated. The transceiver check for the vehicle number and then send it to the server. Since every vehicle registration ID is linked to user account, toll can be deducted from the account bank directly. Admin adds the vehicle details and according to that it sets the priority for the privileged person by adding some premium privileges. Whenever the vehicle comes in front of the toll gate, the software installed in the toll gate system gets activated and as a result it takes the picture of the person and send it to the server and as a result of that face recognition is done and then it detects the face. If the person face matches with the one saved in the server, then the respected person can pass the toll gate and there is no need for that very person to make any payment.

Block diagram



CONCLUSION

After doing study on this project it is found that introduction of ETC system can be beneficial for the country and its people. The main benefits are time consuming, fuel savings and traffic reducing, illegal use of privileged vehicles. It has also the best benefit which is government is not losing any revenue from toll collection. The traffic free toll system will add a good impression to those people and they can enjoy the travel on this road by short time. GSM module will send message to the phone, so the passenger will know how much he has paid for toll and no chance of charging extra money. The main objective of this project is dealing with

RF and IoT technology and keeping all the vehicles under registration, so that no unregistered car can be used and do unethical works against law.

FUTURE SCOPE

1. Develop a dynamic system for ETC conversion: In our research the number of ETC lanes and their time of implementation are decided based on the delays at the ETC lane and the value of the benefits. Thus an algorithm can be developed to decide upon the optimum number of ETC lanes as compared to the manual and automatic lanes and also take into account the lane type that needs to be converted in order maximize the benefits and reduce the delays at the toll plaza.

2. A full database and image processing system: All the data can be stored in a full database system with all the respective records of each vehicles with image processing then it can give a biggest security to the government. This record can help government to trace any culprit using this road.

Time consumption at the toll plaza can reduce pollution

3. Automated toll collection system using GPS and GPRS: The toll collection system, especially in India faces some problems such as long queue lines, escaping from toll plazas etc. These systems can service only 300 vehicles per hour, and if more than that number of vehicles arrive at that plaza, server traffic jams may occur. To solve this we are proposing to create ge-fences using GPS by giving latitude and longitude of the corner of the toll plaza. By comparing the position of the vehicle and toll plaza, the owner of the vehicle can be charged from the account.

4. Automated Toll Collection Using Satellite Navigation: The system is to do the tasks remotely on the client machine through server. The aim is to develop Toll Collection System on express highway in such a way that, so the user have no need to keep money with him to pay toll and without the vehicle even having to slow down or stop at a toll. As soon as the vehicle enters the toll road, the vehicle number, vehicle type is detected and automatically these data is transferred to toll booths. The toll charge is automatically deducted in the owners account and message details are sent to their respective mobiles. This system can be implemented using CDMA(code division for multiple access), GSM technology.

Wang Landau - Adaptive Monte Carlo Approach to Monomodal Brain Image Registration

^[1] D.Sasikala, ^[2] K.Venkatesh Sharma

^{[1][2]} Professor, Department of CSE, CVR College of Engineering, Hyderabad, India
^[1]anjasasikala@gmail.com, ^[2]venkateshsharma.cse@gmail.com

Abstract:-- An advanced method to get the better of the challenges of medical image registration is anticipated, using Wang Landau Adaptive Monte Carlo (WLAMC) approach. The Wang-Landau (WL) algorithm is a distinct Monte Carlo (MC) method that has generated much curiosity in the medical image registration technique owing to some remarkable simulation implementations. The multiresolution centered process for registering multimodal imageries by using MC structure is the efficient existing approach for image registration anywhere random solution aspirants are generated from a multidimensional solution space of possible geometric transformations at each of the repetition by using a sampling approach. The solution applicants generated are evaluated based on the Pearson type-VII error between the phase instants of the images to determine the solution candidate with the deepest error residual. Even the Monte Carlo approach is efficient, it has some drawbacks and it can be eliminated with this proposed Adaptive Monte Carlo approach. The experiments are performed on the real time medical images and the comparison of results illustrate that the proposed approach performs much better for monomodal brain images than the previous image registration techniques.

Keywords: Adaptive Monte Carlo, Image registration, Monomodal, Multimodal, Pearson error, Phase, Wang Landau algorithm.

INTRODUCTION

Image registration is a ubiquitous involving medical imaging and many other purposes of image analysis including but not limited to geo-spatial imaging, satellite imaging, movie editing, archeology etc. In medical imaging, non-rigid registration is common in longitudinal studies such as in child development, ageing studies and also in comparisons between controls and pathologies to assess progress or remission of disease. There is a more volume of non-rigid registration procedures in sources, the most general approaches come in two varieties, those that assume brightness constancy in their cost task being optimized and others that use information theory-based cost functions that don't require the abovementioned restrictive assumption. The first type is applicable only to same modality data sets while the second can be applied to both mono and multimodal data sets. There are several applications wherein use of these data sets is desired e.g., image-guided neurosurgery where an MR (Magnetic Resonance) is used to locate the tumor region and a registered high-resolution CT is used for guidance. Another application that was present in cognitive studies where, MRI and fMRI registrations are sought.

The multimodal image registration [1] is the emerging technique for the automated diagnosis system. The geometric arrangement or registration of multimodality images is a fundamental task in numerous applications in three-dimensional (3-D) medical image processing. Medical diagnosis, for instance, often benefits from the

complement of the information in images of different modalities. Quantity calculation is based on the computed tomography (CT) data in radiotherapy planning, while tumor outlining is often better performed in the corresponding magnetic resonance (MR) scan. For brain function analysis, MR images provide anatomical information while functional information may be obtained from positron emission tomography (PET) images, etc. Hence Multimodal image registration leads to complexities.

Monomodal image registration is also a very difficult problem for several reasons. The same scene obtained by same imaging modalities at different time are represented by different intensity values making it very complicated to align images based on their intensity values. This disproportion in intensity mappings is further complicated by the presence of local image nonuniformities such as static field and RF nonhomogeneities for MRI [2], [3] and noise. In addition, such differences can result in local minima along the convergence plane if evaluated in a direct manner, thereby affecting the ability of iterative optimization techniques, for instance conjugate gradient [4] and Nelder-Mead simplex [5] to converge to the global optima. Lastly, solving the registration problem can be very computationally expensive, predominantly for large images. Therefore, monomodal image registration techniques that can address all of these issues are highly desired.

In this paper, a monomodal non-rigid registration technique is developed from multimodalities with the use

of WL algorithm scheme. Nick Metropolis coined the name “Monte Carlo” which is the base algorithm for this WL method. The WL algorithm has been successfully applied to some complex sampling problems in physics firstly. The algorithm is closely related to multicanonical sampling, a method due to [6]. Briefly if π is the probability measure of interest, the idea behind multicanonical sampling is to obtain an importance sampling distribution by partitioning the state space along the energy function $(-\log \pi(x))$ and re-weighting appropriately each component of the partition so that the modified distribution π^* spends equal amount of time in each component, i.e., uniform in the energy space. The method is frequently criticized for the difficulty involved in computing the weights. The main contribution of the WL algorithm is to propose an efficient algorithm that simultaneously computes the balancing weights and samples from the re-weighted distribution. The main drive of using a Wang Landau Adaptive Monte Carlo (WLAMC) method for the determination of monomodal image registration is that it permits for efficient optimization while avoiding convergence issues under situations categorized by many local optima along the convergence plane and small cost gradients toward the global optima.

The document is organized as follows. Introduction in Section I followed by Literature survey in image registration deliberated in Section II. The Monte Carlo procedures for image registration is defined in detail in Section III. The anticipated method is obtainable in Section IV. The experimental results are conferred in Section V. Finally, conclusions and future work is discussed in Section VI.

II. LITERATURE REVIEW

There are a lot of previous works available on the image registration. The most recent and maximum related works are presented below for better understanding of the discussing techniques. Among the most popular monomodal image registration techniques, mutual information and entropy-based methods [9]–[14] are found to be better performing. The underlying goal of entropy-based techniques is to minimize the joint intensity entropy among the images being registered. These methods take advantage of the fact that correctly registered images correspond to tightly packed joint distributions and the transformation with minimum joint intensity entropy should theoretically be the optimal alignment. The main advantage of this is that it allows images acquired, using different imaging modalities to be compared in a direct manner. Presently, entropy-based

methods have been shown to be very efficient in monomodal registration too.

Entropy-based methods face several drawbacks. Primarily, entropy-based methods [15] are typically under-constrained with respect to intensity relationships. As such, the convergence planes related with this techniques acquire high nonmonotonicity with many local optima. This is challenging since most methods make use of iterative optimization methods to solve for the optimal alignment between images, which rely on the monotonicity of the convergence plane. In addition, entropy-based methods need the computationally costly calculation of marginal and joint entropies.

Feature-based methods are another set of image registration techniques [16]–[21]. In these techniques, the images are transformed into a common feature space proceeding to cost evaluation. Consequently, such methods attempt to find image correspondences in an indirect manner by finding correspondences among extracted features that exist in a common feature space. Intensity gradient information [16], [17], local frequency information [18]–[20], and shape properties [22] are the features used in these methods and there are several advantages in using this methods. First, since images are converted to a common feature space prior to comparison, objective functions that are more constrained than those used in entropy-based methods with respect to inter- image feature relationships can be used. As a result, the convergence planes related with feature-based methods typically have higher monotonicity with fewer local optima. Second, feature based techniques allow more computationally efficient objective functions, such as sum of squared distances and cross correlation to be employed. For this technique, proposed the functions [17] for possible translations and rotations on a pixel level.

Feature-based methods faced several important drawbacks that need to be addressed. 1) While methods exist for performing objective function evaluation exhaustively on a pixel level for simple transformations, this type of exhaustive evaluation becomes intractable to perform on a subpixel level and/or more complex transformations due to high computational costs. 2) While the convergence plane for this method are generally more monotonic than entropy-based methods, whether the global optima corresponds to the optimal alignment depends heavily on the selection of appropriate features as well as objective functions.

Correlation based measures [23], [24], [25] are the other image registration techniques found in the literature. Such techniques assume that the relationship between intensity values from the images being

registered can be represented as a function. The functional assumptions are often not true and are not easily customizable to handle scenarios with different intensity relationships [26] that are the considerable problem with these methods.

All the previously presented image registration methods, encounter difficulties when faced with situations characterized by: 1) large misregistration's; and 2) little to no initial region overlap between the images. Methods that make use of iterative optimization methods, such as gradient descent, conjugate gradient [7], Nelder–Mead simplex [8], Levenberg–Marquardt method, Powell's method, and quadratic programming are often unable to converge under such situations due to local optima along the convergence plane and small cost gradients toward the global optima (i.e., moving toward the global optima yields little to no decrease in cost), even when multiresolution methods are used. The consequences of local minima on the convergence to the global optima by initializing local optimizations at multiple starting points is attempted to reduce by the Multistart methods. However, this can become computationally expensive for large search spaces where many local optimizations must be performed at different starting points and choosing such starting points can also be a challenging task. Methods that utilize exhaustive search over all possible transformations are able to avoid the issue of local optima along the convergence plane, but at the cost of high-computational complexity that is only tractable for simple transformations and pixel-level accuracy.

Image registration using a MC scheme was presented in [1]. The method utilizes a sampling scheme to draw increasingly more plausible solution candidates from a multidimensional solution space. Solution candidate evaluation is performed based on the Pearson type-VII error between the phase moments of the images to determine the alignment between the multimodal images. The author mentioned that there are currently no methods that utilize the concept of MC method for the purpose of multimodal image registration. The key motivation of using this MC method for the purpose of image registration is that it allows for efficient optimization while avoiding convergence issues under situations characterized by many local optima along the convergence plane and small cost gradients toward the global optima.

The goal of the proposed study is to introduce a feature-based image registration method that addresses image registrations and the convergence and computational complexity issues associated with large misregistration's as well as situations where there is little

to no initial region overlap between the images through the use of WLAMC scheme.

III. THE MONTE-CARLO METHODOLOGIES

3.1 The Existing Monte Carlo Methodology

If two different images f and g acquired using different imaging modalities need to be registered, then the optimal transformation \hat{T} that bring f and g into alignment can be formulated as an optimization problem.

$$\hat{T} = \arg \min_T [C(f(T(\underline{x})), g(\underline{x}))] \quad (1)$$

In the equation the \underline{x} represents a point in image space and C is the objective function that estimates the dissimilarity between the images. The goal is to find a feasible solution from the solution space of possible geometric transformations that reduces the objective function based on this formulation.

For finding the optimal solution many iterative optimization schemes have been suggested [7], [8]. Based on the assumption that the convergence plane is monotonic in nature such methods work. Though, this idea of monotonicity is often not the case, mostly for states considered by high-dimensional solution spaces. So, such methods often become trapped in local optima along the convergence plane. This issue is specifically problematic in conditions, where categorized by large misregistration's and little region overlap between the images. In such cases, moving on the way to the global optima bring forth little to no decrease in cost, and hence, iterative methods would fail to discover the global optima in such cases. A technique to alleviate this problem is to weigh up all feasible solutions in the solution space. While methods exist to perform such exhaustive solution evaluation efficiently for low-dimensional solution spaces on a pixel level [17], it is intractable to evaluate \hat{T} in such a manner for high-dimensional solution spaces or on a subpixel level from a computational view. For example, to profoundly weigh up solutions from the solution space of all possible integer 2-D translations and rotations for two 256×256 images, the evaluation of over 23 million solution candidates would need.

3.2 The Proposed Adaptive Monte Carlo Methodology

To solve this problem, as an alternative engendering arbitrary solution candidate for \hat{T} from the solution space of possible geometric transformations in an efficient manner, adaptive Monte Carlo scheme is used. An m -D random field is considered, where S represents the solution space of all possible geometric transformations as defined by m model parameters, T be a random variable in S , and p be an arbitrary probability density function on S . If n random solution candidates $T_1, \dots,$

Tn based on p need to be taken, then the Monte Carlo estimate of \hat{T} that can be given as equation 2.

$$\hat{T} = \arg \min_{T \in \{T_1, \dots, T_n\}} [C(f(T(\underline{x})), g(\underline{x}))] \quad (2)$$

The use of Adaptive Monte Carlo method for the purpose of image registration leads to numerous returns. First, it avoids the issues associated with local optima along the convergence plane faced by iterative optimization methods, since it does not rely on local cost gradients to guide it toward the global optima. Thus, such a method would not have need of manual initialization since the initial alignment of the images does not affect its ability to determine the global optima. Second, the use of Adaptive Monte Carlo techniques consents optimization problems that are infeasible to estimate exhaustively to be solved in an efficient method. The second problem may be complications involving high-dimensional solution spaces.

The problem with the Monte Carlo (MC) approach to image registration is that it causes too many solution candidates that are either infeasible or far from the desired global optima. This leads to an unnecessary increase in computational overhead from too many irrelevant solution candidates being evaluated. The reason that the conventional Monte Carlo method produces a lot of irrelevant solution candidates is that it generates solution candidates from the solution space based on an arbitrary probability density function p. Consequently, the probability density function used to generate the solution candidates may differ considerably from that of solution candidates that are more plausible to be the global optima. An effective technique for handling this issue of solution candidate irrelevancy is adaptive sampling, where the underlying concept is that random variables with greater impact on the estimate should be sampled more frequently. In an attempt to significantly reduce irrelevant solution candidates and improve computational performance p* is a sampling density function which is used to emphasize important regions in the solution space.

Selection of sampling density function p* is the fundamental issue associated with adaptive sampling is the, which is critical to the computational performance of the Adaptive Monte Carlo method. The probability density that describes whether a given solution candidate is close to the desired solution is generally unknown, in the case of image registration. As such, it is very difficult to select a good sampling density for the image registration problem, particularly in situations where the solution exists in a high-dimensional solution space. To handle this problem an adaptive sampling scheme, where an initial sampling density is corrected and refined with each of the iteration to produce increasingly more plausible solution candidates for the optimal alignment.

The adaptive sampling scheme is given as follows. Let $T = (t_1, t_2, \dots, t_n)$ be a solution candidate in the n-dimensional solution space of possible transformations for 2-D image alignment, where t_i is the i th parameter of the transformation model, and t_1 and t_2 correspond to the translation along the x- and y-axis, respectively. First, an initial sampling density p_* is used to generate an initial set of random solution candidates T_1^1, \dots, T_n^1 . The initial sampling density p_* is defined as follows:

$$p_*^1(t_1) = \frac{1}{\sigma_1 \sqrt{2\pi}} \exp\left(-\frac{(t_1 - m_1)^2}{2\sigma_1^2}\right) t_1^{max} > t_1 > t_1^{min} \quad (3)$$

$$p_*^1(t_2) = \frac{1}{\sigma_2 \sqrt{2\pi}} \exp\left(-\frac{(t_2 - m_2)^2}{2\sigma_2^2}\right) t_2^{max} > t_2 > t_2^{min} \quad (4)$$

$$p_*^1(t_i) = \frac{1}{t_i^{max} - t_i^{min}}, t_i^{max} > t_i > t_i^{min} \text{ and } i > 2 \quad (5)$$

In the equations σ_1 and σ_2 are the base standard deviations of p_* for t_1 and t_2 , respectively, m_1 and m_2 represent the translation along the x- and y-axis, respectively that aligns the center of masses of f and g, and t_i^{min} and t_i^{max} represent the minimum and maximum allowable values for parameter t_i . The objective function C is used to test each solution candidate to determine the solution \hat{T}^{k-1} that minimizes the objective function from the set of solution candidates. The sampling density p_*^k is adaptively refined based on the cost gradient ΔC_k between iteration $k - 1$ and $k - 2$ at each iteration k, and solution candidate \hat{T}^{k-1} can be formulated as equation 6:

In the equations σ_1 and σ_2 are the base standard deviations of p_* for t_1 and t_2 , respectively, m_1 and m_2 represent the translation along the x- and y-axis, respectively that aligns the center of masses of f and g, and t_i^{min} and t_i^{max} represent the minimum and maximum allowable values for parameter t_i . The objective function C is used to test each solution candidate to determine the solution \hat{T}^{k-1} that minimizes the objective function from the set of solution candidates. The sampling density p_*^k is adaptively refined based on the cost gradient ΔC_k between iteration $k - 1$ and $k - 2$ at each iteration k, and solution candidate \hat{T}^{k-1} can be formulated as equation 6:

$$p_*^1(t_i) = \frac{1}{\sigma_i(\Delta C_k / \Delta C_3) \sqrt{2\pi}} \exp\left(-\frac{(t_i - t_i^{k-1})^2}{2(\sigma_i(\Delta C_k / \Delta C_3))^2}\right), \quad (6)$$

$$t_i^{max} > t_i > t_i^{min} \quad (7)$$

In the equation σ_i is the base standard deviations of p_* for t_i and can be defined as follows:

$$\sigma_i = \frac{t_i^{max} - t_i^{min}}{4} \quad (8)$$

The i th parameter of \hat{T}^{k-1} is t_i^{k-1} , and ΔC_k and ΔC_3 are the cost gradients at iterations k and 3 as defined as follows:

$$\Delta C_k = C(\hat{T}^{k-1}) - C(\hat{T}^{k-2}) \quad (9)$$

$$\Delta C_3 = C(\hat{T}^2) - C(\hat{T}^1) \quad (10)$$

The mean and variance of sampling density p^* are refined at each iteration which can be observed from equation (6) relative to the parameters of the optimal solution from the previous iteration \hat{T}^{k-1} and the reduction in cost between the previous two iterations ΔC_k . This adaptive sampling density estimation is based on the theory that as the algorithm converges to the global optima, the most plausible solutions for the optimization problem should be found in regions in the solution space that is increasingly closer to the previous best solution. Based on this assumption, Gaussian distribution model would be a good solution candidate distribution model where the sampling density of solution candidates is concentrated near the previous best solution, and steadily declines as moved away from the previous best solution.

3.3 Solution Candidate Evaluation

T generated by the adaptive sampling scheme for each solution candidate, it is necessary to test the solution candidate, with the use of an objective function C to determine the associated cost. Consequently, registration accuracy depends heavily on the objective function being used. To allow for well-constrained similarity evaluation between images acquired under different modalities, used an approach that each generated solution candidate is evaluated, using an objective function based on the Pearson type-VII [26] error between the phase moments of the images being registered. The solution candidate evaluation process can be described in the following manner. Upon initialization, the phase moments ρ associated with each point in f and g are calculated depends on the iterative estimation scheme which is in [28], which was shown to be highly robust to image nonuniformities and noise. Given an image f_0 , using the following expression taken from [29] the initial local phase coherence estimate P_0 at orientation θ is obtained at iteration $t = 0$:

$$P(\underline{x}, \theta) = \frac{\sum_n W(\underline{x}, \theta) |A_n(\underline{x}, \theta) \Delta \Phi(\underline{x}, \theta) - T|}{\sum_n A_n(\underline{x}, \theta) + \epsilon} \quad (11)$$

$$\Delta \Phi(\underline{x}, \theta) = \cos(\Phi_n(\underline{x}, \theta)) - \bar{\Phi}(\underline{x}, \theta) - |\sin(\Phi_n(\underline{x}, \theta)) - \bar{\Phi}(\underline{x}, \theta)| \quad (12)$$

From the equation W is the frequency-spread weighting factor (coherence across a wide frequency spread is weighted more than coherence across a narrow frequency spread), $\bar{\Phi}$ is the weighted mean phase, T is a noise threshold, and ϵ is a small constant used to avoid division by zero. In [29] the parameters used during implementation were those described.

At each iteration t, phase moments ρ_t are computed based on P_{t-1} as follows:

$$\rho_t(\underline{x}) = \frac{1}{2} \sum_{\theta} \rho_{t-1}(\underline{x})^2 + \frac{1}{2} [4(\sum_{\theta} \rho_{t-1}(\underline{x}, \theta) \sin(\theta) (\rho_{t-1}(\underline{x}, \theta) \cos(\theta)))^2 +$$

$$(\sum_{\theta} [\rho_{t-1}(\underline{x}, \theta) \cos(\theta)]^2 - (\rho_{t-1}(\underline{x}, \theta) \sin(\theta))^2)]^{1/2} \quad (13)$$

$$f_t(\underline{x}) = \frac{\sum_{\psi} \omega(\underline{x}, \psi, \rho_t(\underline{x})) f_{t-1}(\psi)}{\sum_{\psi} \omega(\underline{x}, \psi, \rho_t(\underline{x}))} \quad (14)$$

A new estimate of f_t is then figured out based on a moment adaptive bilateral estimation scheme. In the equation 14 ψ is a local neighborhood around \underline{x} , and the estimation weighting function w consists of a spatial weighting function w_s , and an amplitudinal weighting function w_a

$$\omega(\underline{x}, \psi, \varpi_t(\underline{x})) = \omega_a(\underline{x}, \psi, \varpi_t(\underline{x})) \omega_s(\underline{x}, \psi, \varpi_t(\underline{x})) \quad (15)$$

$$\omega_s(\underline{x}, \psi, \varpi_t(\underline{x})) = e^{-1/2(\|\underline{x}, \psi\|/\sigma_s(\varpi_t(\underline{x})))^2} \quad (16)$$

$$\omega_a(\underline{x}, \psi, \varpi_t(\underline{x})) = e^{-1/2(\|I(\underline{x}) - I(\psi)\|/\sigma_a(\varpi_t(\underline{x})))^2} \quad (17)$$

The basis for estimating phase coherence P_{t+1} during the next iteration is the estimated image f_t . For f and g the iterative estimation scheme is performed to determine the phase moments ρ_f and ρ_g . In [28] the parameters used during implementation were described.

The objective function is defined as the cumulative Pearson type-VII error [27] between the phase moments ρ_f and ρ_g to evaluate the cost associated with solution candidate T.

$$C(f(T(\underline{x}), g(\underline{x}))) = \sum_{\underline{x}} \ln(1 + (\rho_f(T(\underline{x})) - \rho_g(\underline{x}))^2)^{1/2} \quad (18)$$

It is highly robust to outlier which is the main advantage of using the Pearson type-VII error metric. Common methods for evaluating error, such as Manhattan and quadratic error metrics are highly sensitive to outliers. To demonstrate this, the influence of outliers on an error metric can be studied based on its derivative. For example, the derivative of the quadratic error metric e^2 is $2e$. The influence of outliers on quadratic error metric increases linearly and without bound. The derivative of the Pearson type-VII error metric $\ln((1 + e^2)^{1/2})$, on the other hand, is $e/(1 + e^2)$. Consequently, the influence of outliers on Pearson type-VII error is bounded.

IV. PROPOSED WL ADAPTIVE MONTE

CARLO APPROACH

4.1 The WL Method

In multicanonical sampling, a state space χ is given and a probability measure π . χ is then partitioned as $\chi = \cup \chi_i$, where $\chi_i \cap \chi_j = \emptyset$ and π is re-weighted in each component χ_i . An conceptual way to do the same

and much more is the following. With $(\chi_i, \mathcal{B}_i, \lambda_i)$ $i = 1, \dots, d$, a finite family of measure spaces λ_i here it is started λ_i is a σ -finite measure. The union space $\chi = \cup_{i=1}^d \chi_i \times \{i\}$ is introduced. χ is equipped with the σ -algebra \mathcal{B} generated by $\{(A_i, i), i \in \{1 \dots d\}, (A_i \in \mathcal{B}_i)\}$ and the measure λ satisfying $\lambda(A, i) = \lambda_i(A) 1_{\mathcal{B}_i}(A)$. Let $h_i: X_i \rightarrow \mathbb{R}$ be a nonnegative measurable function and define $\theta^*(i) = \int \chi_i^{h_i}(x) \lambda_i(dx) / Z$.

In the equation $Z = \sum_{i=1}^d \int \chi_i^{h_i}(x) \lambda_i(dx)$. It is assumed that $\theta^*(i) > 0$ for all $i = 1 \dots d$ and consider the following probability measure on (χ, \mathcal{B}) :

$$\pi^*(dx, i) \propto \frac{h_i(x)}{\theta^*(i)} 1_{\chi_i}(x) \lambda_i(dx) \quad (19)$$

The main objective is to sample from π^* . The problem of sampling from such a distribution arises in a number of different Monte Carlo strategies. For an example and as explained before, if π is a probability measure of interest on some space $(\chi, \mathcal{B}, \lambda)$, X can be partitioned along the energy function $-\log(\pi)$ and re-weight π by $\pi(X_i)$ in each component X_i . The sampling problem then becomes of the form (1).

Sampling from (19) also arises naturally when optimizing the simulated tempering algorithm. The states space X is not partitioned in simulated tempering but, instead, some auxiliary distributions $\pi_1 \dots \pi_d$ are introduced (take $\pi_1 = \pi$). These distributions are chosen close to π but easier to sample from. For good performances, one typically imposes that all the distributions have the same weight. Taking each of the probability space (X, \mathcal{B}, π_i) as a component in the formalism above leads to a sampling problem of the form (1). Multicanonical sampling and simulated tempering have been combined in [31] giving an algorithm which can also be framed as (19). Sampling from (1) can also be an efficient approach to improve on trans-dimensional Markov Chain Monte Carlo (MCMC) samplers for Bayesian inference with model uncertainty.

The major obstacle in sampling from π^* is that the normalizing constants θ^* are not known. The contribution of the Wang-Landau algorithm [30] is an efficient algorithm that simultaneously estimates θ^* and sample from π^* . In a discrete setting the algorithm was introduced with the π^* being uniform in i . In this work the algorithm is used to overcome the problem in the Monte Carlo approach of image registration. To carry on the discussion in the general framework, the family of probability measures introduced $\pi_\theta, \theta \in (0, \infty)^d$ on $(X, \mathcal{B}, \lambda)$ is defined by:

$$\pi_\theta(dx, i) \propto \frac{h_i(x)}{\theta(i)} 1_{\chi_i}(x) \lambda_i(dx) \quad (20)$$

It is assumed that for all $\theta \in (0, \infty)^d$, a transition kernel P_θ present at the disposal on (X, \mathcal{B}) with invariant distribution π_θ . Note that π_θ and P_θ remain unchanged if

the vector θ by a positive constant is changed. How to build such Markov chain P_θ typically depends on the particular instance of the algorithm.

The structure of the WL algorithm is as follows. It is started with some initial value $(X_0, I_0) \in X, \phi_0 \in (0, \infty)^d$ and set $\theta_0(i) = \phi_0(i) / \sum_{j=1}^d \phi_0(j), i = 1, \dots, d$. Here θ_0 serves as an initial guess of θ^* . At iteration $n+1, (X_{n+1}, I_{n+1})$ is generated by sampling from $P_{\phi_n}(X_n, I_n; \cdot)$ and update ϕ_n to ϕ_{n+1} , which is used to form $\theta_{n+1}(i) = \phi_{n+1}(i) / \sum_j \phi_{n+1}(j)$. The updating rule for ϕ_n is fairly simple. For $i \in \{1 \dots d\}$, if $X_{n+1} \in X_i$ (equivalently, if $I_{n+1} = i$), then $\phi_{n+1}(i) = \phi_n(i) (1 + \rho)$ for some $\rho > 0$; otherwise $\phi_{n+1}(i) = \phi_n(i)$. This lead to the WL algorithm presented below.

The Wang-Landau algorithm

Let $\{\rho_n\}$ be a sequence of decreasing positive numbers. Let $(X_0, I_0) \in X$ be given. Let $\phi_0 \in \mathbb{R}^d$ be such that $\theta_0(i) > 0$ and set $\theta_0(i) = \phi_0(i) / \sum_j \phi_0(j), i = 1, \dots, d$. At some time $n \geq 0$, given $(X_n, I_n) \in X, \phi_n \in \mathbb{R}^d, \theta_n \in \mathbb{R}^d$:

- (i) Sample $(X_{n+1}, I_{n+1}) \sim P_{\theta_n}(X_n, I_n; \cdot)$.
- (ii) For $i = 1 \dots d$, set $\phi_{n+1}(i) = \phi_n(i) (1 + \rho_n 1_{\{I_{n+1}=i\}})$ and $\theta_{n+1}(i) = \phi_{n+1}(i) / \sum_j \phi_{n+1}(j)$.

It remains to choose the sequence $\{\rho_n\}$. As shown below, $\{\theta_n\}$ as defined by Algorithm is a stochastic approximation process driven by $\{(X_n, I_n)\}$. The general guidelines in the literature to choose $\{\rho_n\}$ are: $\rho_n > 0, \sum \rho_n = \infty$ and $\sum \rho_n \epsilon + \epsilon < \infty$ for some $\epsilon > 0$, often $\epsilon = 1$. The typical choice is $\rho_n \propto n^{-1}$. In practice, more careful choices are often necessary for good performances. To the best of knowledge, there is no general, satisfactory way of choosing the step-size in stochastic approximation. Interestingly, Wang-Landau came up with a clever, adaptive way of choosing $\{\rho_n\}$ which works very well in practice.

Let $v_{n,k}(i)$ denote the proportion of visits to $X_i \times \{i\}$ between times $n + 1$ and k . That is, $v_{k,n}(i) = 0$ for $k \leq n$ and for $k \geq n + 1, v_{n,k}(i) = \frac{1}{k-n} \sum_{j=n+1}^k 1_{\{I_j = i\}}$. Let $c \in (0, 1)$ be a parameter to be specified by the user. Two additional random sequences $\{k_n\}$ and $\{a_n\}$ are introduced. Initially, $k_0 = 0$. For $n \geq 1$, define

$$k_n = \inf \left\{ k > k_{n-1} : \max_{1 \leq i \leq d} \left| v_{k_{n-1}, k}(i) - \frac{1}{d} \right| \leq \frac{c}{d} \right\} \quad (21)$$

with the usual convention that $\inf \emptyset = \infty$. Another sequence is needed $\{\gamma_n\}$ of positive decreasing numbers, representing “stepsizes”. Then, $\{a_n\}$ represents the index of the element of the sequence $\{\gamma_n\}$ used at time n : $a_0 = 0$, if $k = k_j$ for some $j \geq 1$, then $a_k = a_{k-1} + 1$ otherwise $a_k = a_{k-1}$. In other words, start the algorithm with a step-size equal to γ_0 and continue using it until time k_1 when all

the components are visited equally well. Only then the step-size is changed to γ_1 and keep it constant until time k_2 etc.

The algorithm presented above is used for the proposed image registration method. The problems associated with the previous approach Monte Carlo is completely eliminated using the proposed image registration method.

V. EXPERIMENTAL RESULTS

A series of experiments is performed using medical images. The tests are performed using different images of different sizes. A set of CT and magnetic resonance (MR) medical images that represent the head of the same patient is considered. The original size of these images is given as pixels. In order to eliminate the background parts and the head outline, the original images are cropped, creating sub-images of different dimension pixels.

In probability theory and information theory, Mutual Information (sometimes known as transinformation) between two discrete random variables is termed as the amount of information shared between the two random variables. It is a dimensionless quantity measured in units of bits and can be the reduction in uncertainty. High Mutual information (MI) points out a large reduction in uncertainty; low MI indicates a small reduction; and zero MI between two random variables means the variables are independent.

$$(X; Y) = \sum_{y \in Y} \sum_{x \in X} p(x, y) \log\left(\frac{p(x, y)}{p_1(x)p_2(y)}\right) \quad (22)$$

- X and Y - Two discrete random variables.
- $p(x, y)$ - Joint probability distribution function of X and Y .
- $p_1(x)$ and $p_2(y)$ - Marginal probability distribution functions of X and Y respectively.

The Correlation Coefficient (CC) is from statistics, is a measure of how well the predicted values from a forecast model “fit” with the real-life-data. If there is no relationship among the predicted values and actual values the CC is very low. As the strength of the relationship among the predicted values and actual values increases, so does the CC. Thus higher the CC the better is the CC. The formula to compute CC is equation 23.

$$C(t, s, \theta) = \frac{\sum_x \sum_y \{I_1^{new}(x, y) - \overline{I_1^{new}(x, y)}\} \{I_2^{new}(xcos\theta - ysin\theta - t, xsin\theta + ycos\theta - s) - \overline{I_2^{new}(x, y)}\}}{\sqrt{\sum_x \sum_y \{I_1^{new}(x, y) - \overline{I_1^{new}(x, y)}\}^2 \sum_x \sum_y \{I_2^{new}(xcos\theta - ysin\theta - t, xsin\theta + ycos\theta - s) - \overline{I_2^{new}(x, y)}\}^2}} \quad (23)$$

I_1^{new}, I_2^{new} Two new images that differ from each other by rotation and translation only.

t, s Shifting parameters between the two images.

θ Rotation angle.

$\overline{I_1^{new}(x, y)}, \overline{I_2^{new}(x, y)}$ Average structure value of the pixels in the overlapping parts of images $I_1^{new}(x, y), I_2^{new}(x, y)$ respectively.

The input MRI – T2 Sagittal image of size 37kB with resolution of 400 x 419 pixels given for experimentation is presented in Figure 1.

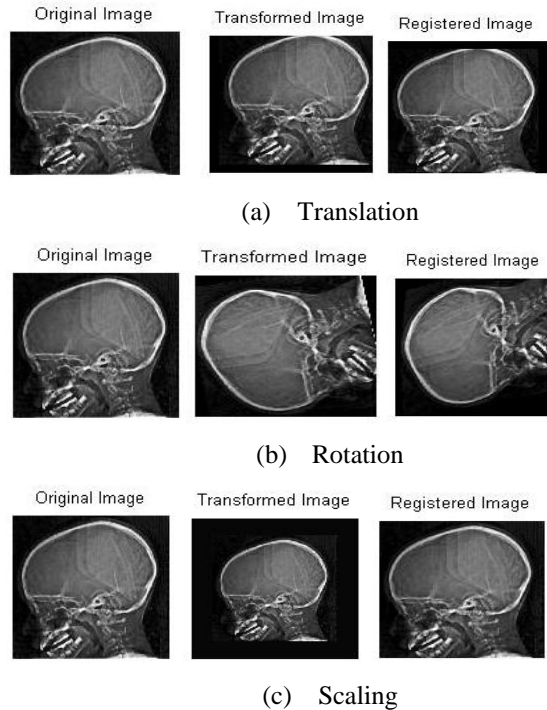


Figure 1. Images used for experimentation

The Mutual Information and Correlation Coefficient executions for the two approaches are specified in Table I. The outcomes obviously show that the MI & CC values for the purported WL Monte Carlo method is immense than the current method that displays the reliance among the CT and MRI image as input is high. This demonstrates that the approach put forward turn out image registration with better outcome. The attained MI and CC values are plotted in graph for the assessment of the two methods that is shown in Figure 2.

The outcomes obviously prove that the MI & CC values for the projected WL Adaptive Monte Carlo method is superior than the prevailing method that conclude that the insinuated Adaptive Monte Carlo Image Registration (AMCIR) approach accomplishes better outcomes than the current Monte Carlo Image Registration (MCIR) approach.

TABLE I
MUTUAL INFORMATION (MI) AND CORRELATION
COEFFICIENT (CC) OF WLMCIR AND WLAMCIR

S.No	Transformations performed	After registration for	
		WL-MC	WL-AMC
1	Translation X= 25, Y= -25	MI= 0.7928 CC=0.4005	MI=7.4400 CC=0.9727
2	Rotation 100 Degrees	MI=0.6874 CC=0.3240	MI=0.7101 CC=0.3842
3	Scaling 0.75	MI=0.8059 CC=0.4373	MI=0.8188 CC=0.4477

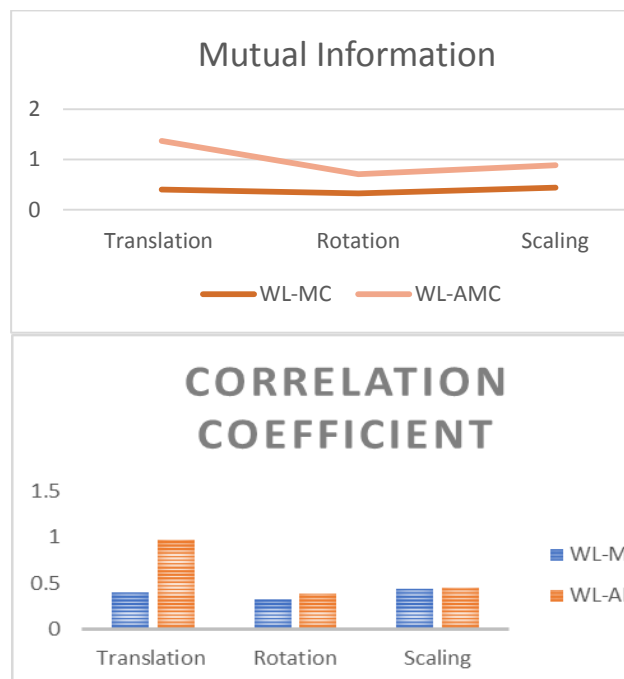


Figure 2. Comparisons of the MI & CC values for the two approaches- WL-MC & WL-AMC Approaches

The result illustrates that the anticipated method has the better efficiency than the present Monte Carlo method of Image registration.

VI. CONCLUSIONS AND FUTURE WORK

In this paper, a new method for registering images from same imaging modalities is put forward, using a Wang-Landau Adaptive Monte Carlo scheme. It is an extension with the Monte Carlo method that can be efficiently utilized for the image registration. A sampling scheme is used for generating reasonable solution candidates from the solution space of possible transformations. The objective function for solution candidate evaluation was

deployed, based on the Pearson type-VII error between the phase moments of the images being registered. The suggested WLAMC method produces better result than the earlier approach with the very high MI and CC value. Experimental results for the MRI medical image registration produce high registration accuracy. Since the approach produces result with maximum accuracy the system can be extended for the 3D image registration approach in future.

REFERENCES

[1] Alexander Wong, "An Adaptive Monte Carlo Approach to Phase-Based Multimodal Image Registration", IEEE Transactions on Information Technology in Biomedicine, Vol. 14, No. 1, January 2010, PP: 173-179

[2] A. Simmons, P. Tofts, G. Barker, and S. Arridge, "Sources of intensity nonuniformity in spin echo images at 1.5 T," Magn. Reson. Med., vol. 32, no. 1, pp. 121–128, 1994.

[3] M. Oghabian, S. Mehdipour, and N. Alam, "The impact of RF inhomogeneity on MR image nonuniformity," presented at the Proc. Image Vis.Comput., New Zealand, 2003.

[4] M. Hestenes and E. Stiefel, "Methods of conjugate gradients for solving linear systems," J. Res. Nat. Bureau Stand., vol. 49, pp. 409–436, 1952.

[5] J. Nelder and R. Mead, "A simplex method for function minimization," Comput. J., vol. 7, pp. 308–313, 1965.

[6] Berg, B. A. and Neuhaus, T. (1992). Multicanonical ensemble: A new approach to simulate first-order phase transitions. Phys. Rev. Lett. 68.

[7] M. Hestenes and E. Stiefel, "Methods of conjugate gradients for solving linear systems," J. Res. Nat. Bureau Stand., vol. 49, pp. 409–436, 1952.

[8] J. Nelder and R. Mead, "A simplex method for function minimization," Comput. J., vol. 7, pp. 308–313, 1965.

[9] Nemir Al-Azzawi1, Wan Ahmed K. and Wan Abdullah, "MRI Monomodal Feature-Based Registration Based on the Efficiency of Multiresolution Representation and Mutual Information", American Journal of Biomedical Engineering, vol. 2, no.3, pp. 98-104, 2012.

[10] P. Viola and W. Wells, "Alignment by maximization of mutual information," Int. J. Comput. Vis., vol. 24, no. 2, pp. 137–154, 1997.

[11] C. Studholme, D. Hill, and D. Hawkes, "An overlap invariant entropy measure of 3-D medical image alignment," Pattern Recogn., vol. 32, no. 1, pp. 71–86, 1999.

[12] J. Pluim, J. Maintz, and M. Viergever, "Mutual-information-based registration of medical images: A

- survey,” *IEEE Trans. Med. Imag.*, vol. 22, no. 8, pp. 986–1004, Aug. 2003.
- [13] M. Mellor and M. Brady, “Phase mutual information as a similarity measure for registration,” *Med. Image Anal.*, vol. 9, pp. 330–343, 2005.
- [14] G. Song, B. Avants, and J. Gee, “Multistart method with prior learning for image registration,” in *Proc. IEEE 11th Int. Conf. Comput. Vis. (ICCV)*, 2007, pp. 1–8.
- [15] A. Roche, G. Malandain, and N. Ayache, “Unifying maximum likelihood approaches in medical image registration,” *Int. J. Imag. Syst. Technol.*, vol. 11, no. 1, pp. 71–80, 2000.
- [16] Stefan Klein, Marius Starin, Keelin Murphy, Max A. Viergev and Josien P. W. Plu, “elastix: A Toolbox for Intensity-Based Medical Image Registration,” *IEEE Transactions on Medical Imaging*, vol. 29, no. 1, pp. 196–205, January 2010.
- [17] J. M. Sloan, K. A. Goatman and J. P. Siebert, “Learning Rigid Image Registration Utilizing Convolutional Neural Networks for Medical Image Registration,” in *Proceedings of the 11th International Joint Conference on Biomedical Engineering Systems and Technologies (BIOSTEC 2018) – vol. 2: BIOIMAGING, SCITEPRESS – Science and Technology Publications, Lda*, pp. 89-99, Funchal, Portugal, 19th to 21st January 2018.
- [18] Aristeidis Sotiras, and Nikos Paragios, “Deformable Image Registration: A Survey,” *A Research Report RR-7919 by Project-Team GALEN*, pp. 1–59, March 2012.
- [19] M. Hemmendorff, M. Andersson, T. Kronander, and H. Knutsson, “Phase based multidimensional volume registration,” *IEEE Trans. Med. Imag.*, vol. 21, no. 12, pp. 1536–1543, Dec. 2002.
- [20] A. Wong and D. Clausi, “ARRSI: Automatic registration of remote sensing images,” *IEEE Trans. Geosci. Remote Sens.*, vol. 45, no. 5, pp. 1483–1493, May 2007.
- [21] C. Florin, J. Williams, A. Khamene, and N. Paragios, “Registration of 3D angiographic and X-ray images using sequential Monte Carlo sampling,” in *Proc. CVBIA*, 2005, pp. 427–436.
- [22] M. Ali and D. Clausi, “Automatic registration of SAR and visible band remote sensing images,” in *Proc. IEEE IGARSS*, 2002, vol. 3, pp. 1331–1333.
- [23] D. Sasikala, and R. Neelaveni, “Monomodal Brain image registration Using Fast Walsh Hadamard Transform,” *CiiT International Journal of Fuzzy Systems*, 2010, vol. 2, no. 8, pp. 37–49.
- [24] F. Candocia, “Jointly registering images in domain and range by piecewise linear comparametric analysis,” *IEEE Trans. Image Process.*, vol. 12, no. 4, pp. 409–419, Apr. 2003.
- [25] Sasikala D and Neelaveni R, “Performance analysis of brain image registration technique using fast walsh hadamard transform and modified adaptive polar transform,” *Journal of Scientific and Industrial Research (JSIR)*, vol. 70, no.2, pp. 123–128, February. 2011.
- [26] Sasikala D and Neelaveni R, “Brain Image Registration Techniques using Wang Landau Adaptive Monte Carlo Approach,” *Journal of Scientific and Industrial Research (JSIR)*, vol. 72, no.2, pp. 114–121, February. 2013.
- [27] K. Pearson, “Mathematical contributions to the theory of evolution, XIX: Second supplement to a memoir on skew variation,” *Trans. Philos. R.Soc. Lond. Ser. A, Containing Papers Math. Phys. Character*, vol. 216, pp. 429–457, 1916.
- [28] A. Wong, “An iterative approach to improved local phase coherence estimation,” in *Proc. CRV*, 2008, pp. 301–307.
- [29] P. Kovesei, “Phase congruency detects corners and edges,” in *Proc. Aust. Pattern Recogn. Soc. Conf.*, 2003, pp. 309–318.
- [30] Wang, F. and Landau, D. P. (2001). Efficient, multiple-range random walk algorithm to calculate the density of states. *Physical Review Letters* 86 2050–2053.
- [31] Atchade, Y. F. and Liu, J. S. (2006). Discussion of the paper by kou, zhou and wong. *Annals of Statistics*.

ICT Impact in Modern Education

^[1] Vijaya Kumar A V, ^[2] Dr. Yogesh Kumar Sharma

^{[1][2]} Research Scholar, ^[2] Associate Professor, HOD/Research Coordinator

^{[1][2]} Department Of Computer Science and Engineering, Shri JTT University , Jhunjhunu, India

^[1] pdit.vijay@gmail.com, ^[2] dr.sharmayogeshkumar@gmail.com

Abstract:-- Information and Communication Technology (ICT) in education is that the mode of education that use information and engineering to support, enhance, and optimise the delivery of data. Worldwide analysis has shown that ICT will result in associate degree improved student learning and higher Quality teaching ways.

ICT covers any product that may store, retrieve, manipulate, transmit or receive data electronically in an exceedingly digital type. for instance, personal computers, digital tv, email, robots. Therefore ICT thinks about with the storage, retrieval, manipulation, transmission or receipt of digital information.

In today's world the communication is so speed that every information is obtained at the accurate levels with no time. The good things with the ICT is connecting the world and learning together. The platform that is created with the ICT is independent and diverse. The benefits of the ICT stay ideal in delivering the information reaching the millions in less time. Exclusively relying on the technology completely leads to the adverse effects on the Human values and quality of information exchange. The ICT impact on the today's education systems is extensively improved the performance of the learners. Making the learners completely depend on the latest technology The advantages of ICT includes anywhere any time, improves standards, usage of Limited resources, versatile and reliable information interchange. The Speed, time , Performance and money could be saved as it is much quicker to transfer the information around. Remarkable disadvantages would include difficulty in analysing the Reliable and Un reliable resources, Privacy cannot be maintained, can be easily cheated. In spite of the drawbacks the ICT expansion is creating the room Technological Development in the field of the Modern Education System. The Modern education system is digitalized and resulting in tremendous changeovers proving better results in the performance of the learners.

The impact of employee agility on the marketing team performance of pharmaceutical firms, India: A qualitative study

^[1] Venkateswarlu Nalluri

^[1] Da-Yeh University, No. 168, Dacun Township, Changhua County, Taiwan

Abstract:-- Although the marketing department is an emerging platform that can help organizations handle uncertainties. The concept of agility is underexplored in the marketing literature. Little is known about the ability of marketing to become agile and under what conditions agility can lead to better market performance. This study examines whether and how marketing team usage is positively associated with team performance. Firstly, the study tries to find that agility importance to marketing team performance when key employees have marketing knowledge, employee experience and sharing information. Secondly, we are trying to show that creativity and organization planning is the main decision-making drivers of agility in marketing team performance. In this qualitative research study was conducted using the data of seventeen face to face interviews with pharmaceutical marketing managers and experts in Hyderabad City, India. And also we are creating a great platform for future research towards agility in the marketing field.

Keywords: Marketing team, Sharing information, Employee experiences, Marketing knowledge, Agility conditions.
